



UNIVERSIDADE DE BRASÍLIA  
FACULDADE DE TECNOLOGIA  
DEPARTAMENTO DE ENGENHARIA MECÂNICA

Guillermo Alvarez Bestard

**Universidade de Brasília - UnB**

SENSOR FUSION AND EMBEDDED DEVICES TO  
ESTIMATE AND CONTROL THE DEPTH AND WIDTH OF  
THE WELD BEAD IN REAL TIME

Brasilia  
2017

Guillermo Alvarez Bestard

**Universidade de Brasília - UnB**

Tese apresentado ao Programa de Pós-graduação em Sistemas Mecatrônicos, como parte dos requisitos necessários à obtenção do título de Doutor.

Orientador: Sadek C. Absi Alfaro, PhD

Brasilia  
2017

Ficha catalográfica elaborada automaticamente,  
com os dados fornecidos pelo(a) autor(a)

BB561s Bestard, Guillermo Alvarez  
Sensor fusion and embedded devices to estimate and  
control the depth and width of the weld bead in real time /  
Guillermo Alvarez Bestard; orientador Sadek C. Absi Alfaro.  
-- Brasília, 2017.  
159 p.

Tese (Doutorado - Doutorado em Sistemas Mecatrônicos) --  
Universidade de Brasília, 2017.

1. arc welding process. 2. bead depth estimation. 3.  
bead width estimation. 4. neural network. 5. sensor fusion.  
I. Alfaro, Sadek C. Absi, orient. II. Título.

Faculdade De Tecnologia

TESE DE DOUTORADO

**SENSOR FUSION AND EMBEDDED DEVICES TO ESTIMATE  
AND CONTROL THE DEPTH AND WIDTH OF THE WELD BEAD  
IN REAL TIME**

Guillermo Alvarez Bestard

Relatório submetido ao Departamento de Engenharia  
Mecatrônica como requisito parcial para obtenção do  
grau de Doutor em Sistemas Mecatrônicos

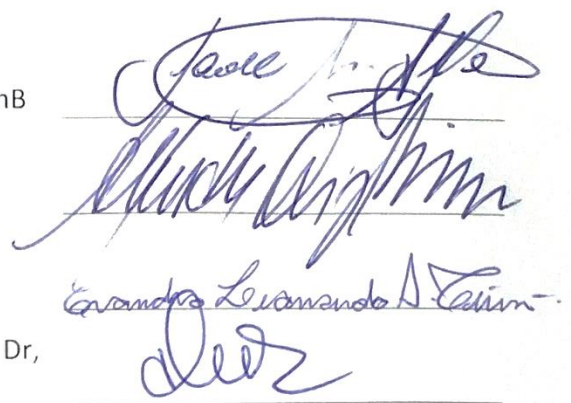
Banca Examinadora

Prof. Sadek C. Absi Alfaro, Orientador, PhD, ENM/UnB

Prof. Alexandre Queiroz Bracarense, Examinador  
Externo, PhD, DEMEC/UFMG

Prof. Evandro Leonardo Silva Teixeira, Examinador  
Externo, Dr., Gama/UnB

Prof. José Alfredo Ruiz Vargas, Examinador Interno, Dr,  
ENE/UnB



The image shows three handwritten signatures in blue ink, each written over a horizontal line. The top signature is for Prof. Sadek C. Absi Alfaro, the middle for Prof. Alexandre Queiroz Bracarense, and the bottom for Prof. Evandro Leonardo Silva Teixeira. The bottom signature is partially obscured by the text 'Evandro Leonardo A. Teixeira' written below it.

## Dedictory

*To my grandparents for your example, dedication and infinite love*

*“A mis abuelos por su ejemplo, dedicación y amor infinito”*

*“A meus avós por seu exemplo, dedicação e amor infinito”*

*To my mother for staying with me every moment whether sad or happy.*

*“A mi madre por estar a mi lado en cada momento de felicidad y tristeza”*

*“A minha mãe por ficar ao meu lado em cada momento de felicidade e tristeza”*

*To my father for inspiring me in this profession*

*“A mi padre por inspirarme en estas labores”*

*“A meu pai por inspirar-me nesta profissão”*

*To my wife for communicating her trust and love across thousands of kilometers*

*“A mi esposa por transmitirme su confianza y amor a miles de kilómetros de distancia”*

*“A minha esposa por transmitir sua confiança e amor a milhares de quilômetros de distância”*

*To my princess because your smile is the best prize for this effort*

*“A mi princesita porque su sonrisa es la mejor recompensa a todo este esfuerzo”*

*“A minha princesa porque seu sorriso é a melhor recompensa a todo este esforço”*

# Acknowledgements

*Many peoples helped me in different ways in this work which were all important.*

*“Muchas personas me ayudaron de diferentes maneras en este trabajo, todas importantes”*

*“Muitas pessoas ajudaram-me de diferentes maneiras neste trabalho, todas importantes”*

*To professor Sadek by his great help and his trust on me throughout this adventure.*

*“Al profesor Sadek por su gran ayuda y confianza en esta aventura”*

*“Ao professor Sadek por sua grande ajuda e confiança nesta aventura”*

*To Luis Miguel in memoriam for advancing this project.*

*“A Luis Miguel in memoriam por impulsar este proyecto”*

*“A Luis Miguel in memoriam por impulsar este projeto”*

*To Carlos Llanos and Armando for their unconditional support from both sides of the world.*

*“A Carlos Llanos e Armando por su apoyo incondicional en cada lado del mundo”*

*“A Carlos Llanos e Armando por seu suporte incondicional em cada lado do mundo”*

*To my mom and Michael Rivas for their wonderful help in reviewing the text.*

*“A mi mamá y a Michael Rivas por su maravillosa ayuda en la revisión de los textos”*

*“A minha mãe e a Michael Rivas pela maravilhosa ajuda na revisão dos textos”*

*To José Vargas and Alysson Martins for their friendship and valuable ideas and suggestions.*

*“A José Vargas y Alysson Martins por su amistad, sus valiosas ideas y consejos”*

*“A José Vargas e Alysson Martins por sua amizade, suas valiosas ideias e dicas”*

*To my family and my wife’s family for taking care of my paternal responsibilities while I was away.*

*“A mi familia y la de mi esposa por ocuparse de mis tareas paternas mientras estuve lejos”*

*“A minha família e a de minha esposa por cuidar de minhas tarefas paternas enquanto eu estava ausente”*

*To CAPES, PPMEC, Osmel and Michael Rivas for the resources for the thesis project and my stay in Brazil.*

*“A CAPES, PPMEC, Osmel y Michael Rivas por los recursos para el proyecto de tesis y la estadia en Brasil”*

*“A CAPES, PPMEC, Osmel e Michael Rivas pelos recursos para o projeto de teses e a estadia no Brasil”*

*To one and all who contributed to this effort, especially the colleagues of the Institute of Mathematics, Cybernetics and Physics and University of Brasilia.*

*“A todos aquellos que contribuyeron con este trabajo, en especial a los colegas del Instituto de Cibernética, Matemática y Física y de la Universidad de Brasilia”*

*“A todos aqueles que contribuíram neste trabalho, em especial aos colegas do Instituto de Cibernética, Matemática e Física e a Universidade de Brasília”*

SENSOR FUSION AND EMBEDDED DEVICES TO ESTIMATE AND CONTROL  
THE DEPTH AND WIDTH OF THE WELD BEAD IN REAL TIME

## Abstract

The GMAW process is widely used in industry, but the automatic control is limited by the difficulty in the process for measuring the main magnitudes and for closing the control loop. Adverse environmental conditions in the process make it harder to use conventional measurement systems to obtain information about the weld bead geometry. Under these conditions, the control system design is complex and good performance is not guaranteed. In this research, systems and tools were developed to collect the values of the welding variables and send stimuli to the GMAW conventional process with constant voltage power source, which us allows to estimate the geometry of the weld bead in an open-loop control. The depth and width estimates of the weld bead are implemented based on the fusion of the thermographic data, the welding current and the welding voltage in a neural network. An algorithm was developed to extract the features of the infrared image and deliver this information to the estimators. To validate the estimator models, a laser profilometer was implemented to measure the external dimensions of the bead and an image processing algorithm to measure the depth by making a longitudinal cut in the weld bead. The results obtained are documented and discussed in the text. This work also includes a design proposal for a robotic orbital welding emulator and its multivariable control system to control the geometry of the weld bead using the developed estimators. The algorithms are optimized for embedded devices and real-time processing.

FUSÃO SENSORIAL E DISPOSITIVOS EMBARCADOS PARA ESTIMAR E CONTROLAR A  
PENETRAÇÃO E A LARGURA DO CORDÃO DE SOLDA EM TEMPO REAL

## Resumo

O processo GMAW é amplamente utilizado na indústria, mas seu controle automático está limitado pela dificuldade existente em medir as principais grandezas do processo e fechar a malha de controle. As condições ambientais adversas dificultam o uso dos sistemas de medição convencionais para obter informações da geometria do cordão de solda. Nestas condições o desenvolvimento do sistema de medição é complexo e o correto desempenho não é garantido. Neste trabalho desenvolvem-se sistemas e ferramentas para coletar os valores das variáveis e fornecer estímulos ao processo de soldagem GMAW convencional com fonte de soldagem de tensão constante, permitindo a estimação da geometria do cordão de solda em um sistema de controle em malha aberta. Os estimadores da penetração e a largura do cordão são implementados baseados na fusão dos dados termográficos, a intensidade da corrente e a tensão de soldagem em uma rede neural. Desenvolveu-se um algoritmo para extrair as características da imagem infravermelha e para fornecer essas informações aos estimadores. Para validar os modelos dos estimadores foi implementado um perfilômetro a laser para obter as dimensões externas do cordão de solda e um algoritmo de processamento de imagem para medir a penetração fazendo um corte longitudinal no cordão. Os resultados obtidos são documentados e discutidos no texto. Este trabalho também inclui uma proposta de projeto para um emulador robótico de soldagem orbital e seu sistema de controle multivariável para controlar a geometria do cordão de solda utilizando os estimadores desenvolvidos. Os algoritmos são otimizados para dispositivos embarcados e processamento em tempo real.

## Table of contents

Dedicatory .....	18
Acknowledgements .....	19
Abstract .....	20
Resumo .....	20
Table of contents .....	21
Figures index.....	25
Tables index .....	29
Abbreviations list .....	30
Symbols list .....	31
<b>1 Introduction.....</b>	<b>19</b>
1.1 General objective. ....	19
1.2 Specific objectives. ....	19
1.3 Summary of contributions.....	20
1.4 Potential applications.....	20
1.5 Summary of results. ....	20
1.6 Work organization.....	21
<b>2 Literature review. ....</b>	<b>23</b>
2.1 GMAW process.....	23
2.2 Measurements in the GMAW process. ....	27
2.2.1 Measurement of arc welding variables.....	27
2.2.2 Measurement of contact tip to work distance. ....	28
2.2.3 Measurement of welding joint and weld bead geometry. ....	29
2.2.4 Estimation of weld bead depth. ....	31
2.2.5 Sensor fusion in welding process. ....	38
2.2.6 Chronological evolution of the research in geometry sensing and estimators. .	40
2.3 Control of the weld bead geometry in arc welding process. ....	42
2.3.1 Chronological development of the geometry control in arc welding process....	45
2.4 Embedded devices in welding process control. ....	51
2.5 Chapter considerations. ....	52



<b>3</b>	<b>Methods and tools.....</b>	<b>53</b>
3.1	Data acquisition system .....	54
3.1.1	Measurement of the welding voltage and welding electric current.....	54
3.1.2	Measurement of the welding speed. ....	54
3.1.3	Measurement of the weld bead profile. ....	55
3.1.4	Feature extraction of the bead profile. ....	56
3.1.5	Infrared measurement. ....	57
3.1.6	Feature extraction of the infrared image.....	57
3.1.7	Image processing for offline measuring of the weld bead depth. ....	59
3.1.8	Sensor fusion for estimating the depth and width of the weld bead. ....	59
3.2	Actuator system. ....	61
3.2.1	Welding power source .....	61
3.2.2	Flat welding table. ....	63
3.3	Open loop control system. ....	63
3.4	User interface. ....	65
<b>4</b>	<b>Experimental results. ....</b>	<b>67</b>
4.1	Experiments with argon and oxygen as the shielding gas. ....	67
4.1.1	Experiment 1: Process response to the steps in the welding speed and wire feed speed using 98% argon and 2% oxygen as the shielding gas. ....	68
4.1.2	Experiment 2: Process response to the steps in the welding voltage using 98% argon and 2% oxygen as the shielding gas. ....	73
4.1.3	Modeling and validation of the weld bead depth estimator with data from experiments with argon and oxygen as the shielding gas. ....	78
4.1.4	Modeling and validation of the weld bead width estimator with data from experiments with argon and oxygen as the shielding gas. ....	80
4.2	Experiments with argon and carbon dioxide as the shielding gas. ....	83
4.2.1	Experiment 3: Process response to the steps in the welding speed and wire feed speed using 96% argon and 4% carbon dioxide as the shielding gas.....	83
4.2.2	Experiment 4: Process response to the steps in the welding voltage using 96% argon and 4% carbon dioxide as the shielding gas. ....	87
4.2.3	Modeling and validation of the weld bead depth estimator with data from experiments with argon and carbon dioxide as the shielding gas. ....	91
4.2.4	Modeling and validation of the weld bead width estimator with data from experiments with argon and carbon dioxide as the shielding gas. ....	93
4.3	Chapter considerations. ....	96
<b>5</b>	<b>Conclusions.....</b>	<b>98</b>

6	Future works.....	98
	Bibliographic references.....	99
Apendix 1	Representative information about measurement and estimation of the bead weld geometry found in literature. ....	114
Apendix 2	Representative information about control systems found in welding research literature. ....	129
Apendix 3	Design proposal of a multivariable control system to GMAW orbital process.....	137
A 3.1	The measuring system.....	137
A 3.1.1	Measurement of the orbital angle and the welding speed.....	138
A 3.1.2	Measurement of the joint profile and weld bead profile. ....	138
A 3.1.3	Measuring the contact tip to work distance. ....	139
A 3.1.4	Calculation of the volume deposited by length unit. ....	140
A 3.1.5	Infrared measurement. ....	141
A 3.1.6	Sensor fusion for estimating the depth and width of the weld bead in orbital welding position.....	141
A 3.1.7	Data acquisition.....	141
A 3.2	The actuator system.....	142
A 3.2.1	Robotic emulator of orbital welding process.....	142
A 3.2.1.1	Relationship between the torch speed and the base orbital movement. ....	144
A 3.3	The multivariable control system.....	144
A 3.3.1	Control of seam tracking. ....	146
A 3.3.2	Control of contact tip to work distance. ....	146
A 3.3.3	Control of welding speed and welding angle. ....	146
A 3.3.4	Control of depth and width of weld bead. ....	147
A 3.3.4.1	Professional version of the PID controller.....	149
A 3.3.4.2	Smith Predictor variation for the weld bead width control loop.....	151
A 3.3.4.3	Fuzzy self-adaptive PID controller. ....	152
A 3.3.4.4	Decoupling the control loops. ....	154
A 3.3.4.5	Fuzzy logic for manipulated the CTWD. ....	156
A 3.3.5	Estimation of the initials control parameters. ....	156
A 3.3.6	Sequential controller.....	157

A 3.3.7	Task distribution.....	158
A 3.4	Web user interface for process monitoring and parameter configuration. ....	159

# Figures index

Figure 1 Number of documents relevant to the work published between 2007 and 2017 (Total=119).....	23
Figure 2 Number of documents relevant to the work that were published before and after 2007 (Total=228) .....	23
Figure 3 Process arc welding. Adapted from (NIT, 2015) .....	24
Figure 4 Equipment for constant voltage GMAW process (MILLER ELECTRIC MFG. CO., 2012).....	24
Figure 5 GMAW torch cutaway (LINCOLN ELECTRIC, 2017) .....	25
Figure 6 Contact tip to work distance and electrical stick out (or electrode extension) differences (LINCOLN ELECTRIC, 2017).....	28
Figure 7 Time of flight measurement principle (MICRO-EPSILON, 2017b). .....	28
Figure 8 Phase-comparison measuring principle (MICRO-EPSILON, 2017b). .....	29
Figure 9 Triangulation measuring principle (MTI INSTRUMENTS, 2017).....	29
Figure 10 Geometric dimensions of the weld bead. ....	29
Figure 11 Two-dimensional laser triangulation principle. ....	30
Figure 12 Weld pool and penetration: (a) partial penetration; (b) total penetration. ....	31
Figure 13 Analysis method used to measurement or estimate the weld bead geometry found in the documents analyzed.....	32
Figure 14 Type of model used to estimate the weld bead depth in documents analyzed.....	32
Figure 15 Welding position used in documents analyzed.....	33
Figure 16 Technologies of indirect monitoring used to estimate the bead geometry found in the documents analyzed.....	34
Figure 17 Infrared emission in welding process (a). Discontinuities caused by oil (b) and lack of penetration (c) (NIT, 2015). ....	38
Figure 18 Set up and functional main units of the multi-sensor welding system (a). Multi-sensor information flow (b) Adapted from (ALFARO, SADEK C. A; DREWS, 2006).....	39
Figure 19 Evolution of number of documents relevant to the work, published in the last fifty years. ....	40
Figure 20 Evolution of main measuring technologies used to obtain the information to estimate the bead geometry. ....	41
Figure 21 Evolution of main methods de analysis used to estimate the bead geometry. ....	41
Figure 22 Welding position used in control systems of the weld bead geometry, found in the analyzed documents: (a) Control in flat and orbital welding; (b) Control of the GMAW orbital process. ....	42
Figure 23 Model type (a) and quantity of variables controlled (b) in the control systems of the weld bead geometry found in the analyzed documents. ....	42
Figure 24 Graphic summary of the main methods or techniques used for control the geometry of weld bead.....	43
Figure 25 Main variables used in the bead geometry control in arc welding process.....	45
Figure 26 Control loop proposed for Andersen process (Anderson et al. 1990) when the initial set point condition are defined by neural network and the penetration are estimated (COOK, GEORGE E; BARNETT; STRAUSS, 1999) .....	46
Figure 27 SISO (a) and DIDO (b) control loops that employ infrared information.....	47
Figure 28 Neural network for determining weld parameters (YANG, SANG-MIN et al., 2007) .....	48
Figure 29 Block diagram of the weld pool controller (SHEN et al., 2008).....	48
Figure 30 Model-based predictive control to orbital GTAW process (YU KANG LIU; YU MING ZHANG, 2014).....	50
Figure 31 Embedded devices in welding process.....	51
Figure 32 Block diagram of the data acquisition and closed loop control system architecture. ....	53
Figure 33 Block diagram of the data acquisition and open loop control system architecture. ....	53
Figure 34 Data acquisition and open loop control system: (a) Main components and data flow; (b) Flat welding table and instruments support; (c) Schematic side view.....	54
Figure 35 Low cost laser profilometer components.....	55
Figure 36 Laser scanner software and profile data stored in a text file. ....	56

Figure 37 Curves of the bead profile (above) and from its second derivative (below). .....	56
Figure 38 Infrared feature extraction block.....	57
Figure 39 Features extracted of the infrared images. ....	58
Figure 40 Longitudinal cut of the weld bead (above). Weld bead depth profile (yellow line) and base surface (red line) on the same picture (below), obtained using image processing algorithms. ....	59
Figure 41 Neural network structure for estimate the depth and width of the weld bead.....	59
Figure 42 Estimator of depth and width of the weld bead that uses the thermographic features with welding current or voltage in cooperative mode.....	60
Figure 43 Welding power source operation sequence for the process control and data acquisition. ....	62
Figure 44 Data acquisition and control interface. ....	63
Figure 45. Electronic circuit of the data acquisition and control interface. ....	64
Figure 46 Main loop of the data acquisition and control interface. ....	64
Figure 47. Data acquisition and stimulus sequence design software.....	65
Figure 48. Examples of configuration, stimulus and data files. ....	66
Figure 49 Three-dimensional reconstruction of the weld bead obtained with the low-cost laser scanner in the experiment 1. ....	69
Figure 50 Weld bead obtained in the experiment 1: (a) Top view of the weld bead; (b) Weld bead depth profile (yellow line) and surface of the workpiece (red line) obtained by the macrographic analyses algorithm. ....	69
Figure 51 Unfiltered measurements obtained with the data acquisition and open-loop control system in the experiment 1. ....	70
Figure 52 Filtered measurements obtained with the data acquisition and open-loop control system in the experiment 1.....	71
Figure 53 Sample of the thermographic data and feature extraction process in the experiment 1.....	72
Figure 54 Three-dimensional reconstruction of the weld bead obtained with the low-cost laser scanner in the experiment 2. ....	74
Figure 55 Weld bead obtained in the experiment 2: (a) Top view of the weld bead; (b) Weld bead depth profile (yellow line) and surface of the workpiece (red line) obtained by the macrographic analyses algorithm. ....	74
Figure 56 Unfiltered measurements obtained with the data acquisition and open-loop control system in the experiment 2. ....	75
Figure 57 Filtered measurements obtained with the data acquisition and open-loop control system in the experiment 2.....	76
Figure 58 Example of the thermographic data and feature extraction process in the experiment 2.....	77
Figure 59. Results in the training of the weld bead depth model for experiments with argon and oxygen: (a) Regression curve between the model output and the real depth (target); (b) Performance curve in training, validation and test. ....	78
Figure 60 Comparison between the response of the weld bead depth model (outputs) and the measurements obtained in the experiment 1 (targets). In the time axis, each time value corresponds with a position in the piece.....	79
Figure 61 Regression curve between the measurements of the weld bead depth (target) obtained in experiment 2 and the output of the weld bead depth model obtained from the data of experiment 1. ...	79
Figure 62 Comparison between the measurements of the weld bead depth (target) obtained in experiment 2 and the output of the weld bead depth model obtained from the data of experiment 1. In the time axis, each time value corresponds with a position in the piece.....	80
Figure 63. Results in the training of the weld bead width model for experiments with argon and oxygen: (a) Regression curve between the model output and the real depth (target); (b) Performance curve in training, validation and test. ....	81
Figure 64 Comparison between the response of the weld bead width model (outputs) and the measurements obtained in the experiment 2 (targets). In the time axis, each time value corresponds with a position in the piece.....	81
Figure 65 Regression curve between the measurements of the weld bead width (target) obtained in experiment 1 and the output of the weld bead depth model obtained from the data of experiment 2. ...	82

Figure 66 Comparison between the measurements of the weld bead width (target) obtained in experiment 1 and the output of the weld bead width model obtained from the data of experiment 2. In the time axis, each time value corresponds with a position in the piece.....	82
Figure 67 Three-dimensional reconstruction of the weld bead obtained with the low-cost laser scanner in the experiment 3. ....	83
Figure 68 Weld bead obtained in the experiment 3: (a) Top view of the weld bead; (b) Weld bead depth profile (yellow line) and surface of the workpiece (red line) obtained by the macrographic analyses algorithm. ....	84
Figure 69 Unfiltered measurements obtained with the data acquisition and open loop control system in the experiment 3. ....	85
Figure 70 Filtered measurements obtained with the data acquisition and open loop control system in the experiment 3.....	86
Figure 71 Three-dimensional reconstruction of the weld bead obtained with the low-cost laser scanner in the experiment 4. ....	87
Figure 72 Weld bead obtained in the experiment 4: (a) Top view of the weld bead; (b) Weld bead depth profile (yellow line) and surface of the workpiece (red line) obtained by the macrographic analyses algorithm. ....	88
Figure 73 Unfiltered measurements obtained with the data acquisition and open-loop control system in the experiment 4. ....	89
Figure 74 Filtered measurements obtained with the data acquisition and open-loop control system in the experiment 4.....	90
Figure 75. Results in the training of the weld bead depth model for experiments with argon and carbon dioxide: (a) Regression curve between the model output and the real depth (target); (b) Performance curve in training, validation and test.....	91
Figure 76 Comparison between the response of the weld bead depth model (outputs) and the measurements obtained in the experiment 3 (targets). In the time axis, each time value corresponds with a position in the piece.....	92
Figure 77 Regression curve between the measurements of the weld bead depth (target) obtained in experiment 4 and the output of the weld bead depth model obtained from the data of experiment 3. ....	92
Figure 78 Comparison between the measurements of the weld bead depth (target) obtained in experiment 4 and the output of the weld bead depth model obtained from the data of experiment 3. In the time axis, each time value corresponds with a position in the piece.....	93
Figure 79. Results in the training of the weld bead width model for experiments with argon and oxygen: (a) Regression curve between the model output and the real depth (target); (b) Performance curve in training, validation and test. ....	94
Figure 80 Comparison between the response of the weld bead width model (outputs) and the measurements obtained in the experiment 4 (targets). In the time axis, each time value corresponds with a position in the piece.....	94
Figure 81 Regression curve between the measurements of the weld bead width (target) obtained in experiment 3 and the output of the weld bead depth model obtained from the data of experiment 4. ....	95
Figure 82 Comparison between the measurements of the weld bead width (target) obtained in experiment 3 and the output of the weld bead width model obtained from the data of experiment 4. In the time axis, each time value corresponds with a position in the piece.....	95
Figure 83 Data acquisition and control system proposed for the orbital welding process.....	138
Figure 84 Sensors for measure the orbital angle and the welding speed (a) Encoder for welding angle measurement; (b) Optical sensor for detect the start position. ....	139
Figure 85 Profilometer laser. Adapted from (RIFTEK, 2015).....	139
Figure 86 Calculus of the contact tip to work distance using the bead profile.....	140
Figure 87 Area of the weld bead and joint. ....	140
Figure 88 Infrared camera. Adapted from (NIT, 2014).....	141
Figure 89 Estimator of depth and width of the weld bead for orbital welding position.....	142
Figure 90 Mechanic structure for robotic emulator of orbital welding process. ....	143
Figure 91 Degrees of freedom of the robotic emulator. ....	143

<i>Figure 92 Motor and gearbox: (a) Stepper motor and gearbox to linear movement; (b) Stepper motor and gearbox to CTWD movement; (c) DC motor, encoder and gearbox to orbital movement. ....</i>	<i>144</i>
<i>Figure 93 General diagram of the multivariable control system. ....</i>	<i>145</i>
<i>Figure 94 Blocks diagram of the seam tracking control loop. ....</i>	<i>146</i>
<i>Figure 95 Blocks diagram of the contact tip to work distance control loop. ....</i>	<i>146</i>
<i>Figure 96 Blocks diagram of welding speed and orbital welding control loop. ....</i>	<i>147</i>
<i>Figure 97 Welding process represented as a multiple input-multiple output process. ....</i>	<i>147</i>
<i>Figure 98 Diagram of the weld bead width and depth control loops. ....</i>	<i>148</i>
<i>Figure 99 Professional version of the Proportional-Integral-Derivative controller. ....</i>	<i>149</i>
<i>Figure 100 Controller of depth and width of the weld bead based on the Professional PID algorithm. ..</i>	<i>151</i>
<i>Figure 101 Typical control loop with Smith Predictor. ....</i>	<i>151</i>
<i>Figure 102 Weld bead width controller with modified Smith Predictor. ....</i>	<i>152</i>
<i>Figure 103 Fuzzy self-adaptive professional PID controller. Adapted from (LIU, WEN HONG; XIE, 2011)</i>	<i>152</i>
<i>Figure 104 The membership functions for the inputs (<math>e</math> and <math>\Delta e</math>) and outputs (<math>B_p</math>, <math>T_i</math> and <math>T_d</math>) of the fuzzy system. ....</i>	<i>153</i>
<i>Figure 105 Weld bead width and depth controller with Fuzzy Self-Adaptive Professional PID algorithm. ....</i>	<i>154</i>
<i>Figure 106 Typical feed forward control in a single control loop. ....</i>	<i>154</i>
<i>Figure 107 Weld bead width and depth penetration controller with decouples. ....</i>	<i>155</i>
<i>Figure 108 Weld bead width and depth penetration controller with Fuzzy and P-PID controllers. ....</i>	<i>156</i>
<i>Figure 109 Estimator of the initials control parameters executed in three steps by the same neural network structure. ....</i>	<i>157</i>

## Tables index

<i>Table 1 Main variables of automatic GMAW process to constant voltage. ....</i>	<i>26</i>
<i>Table 2 Methods or techniques used for modeling and control of the geometry of weld bead. ....</i>	<i>44</i>
<i>Table 3 Inversal 450 welding power source characteristics (IMC-SOLDAGEM, 2005). ....</i>	<i>61</i>
<i>Table 4 Sequence of stimulus applied during the experiment 1 ....</i>	<i>68</i>
<i>Table 5 Sequence of stimulus applied during the experiment 2 ....</i>	<i>73</i>
<i>Table 6 Sequence of stimulus applied during the experiment 3 ....</i>	<i>83</i>
<i>Table 7 Sequence of stimulus applied during the experiment 4 ....</i>	<i>87</i>
<i>Table 8 Results obtained in train and test of estimators with argon and oxygen as protection gas. ....</i>	<i>96</i>
<i>Table 9 Results obtained in train and test of estimators with argon and carbon oxide as protection gas. ....</i>	<i>96</i>
<i>Table 10 Fuzzy matrix to <math>B_p</math>, <math>T_i</math> and <math>T_d</math>. ....</i>	<i>153</i>
<i>Table 11 Task distribution between the three logics components of the system. ....</i>	<i>158</i>



## Abbreviations list

3D	Tree-dimensional
ANFIS	Nonlinear neuro-fuzzy
ANFIS	Adaptive Neuro-fuzzy Inference System
ARMA	Auto-regressive Moving Average
Bp	Proportional band
CCD	Charge coupled device
DARMA	Deterministic Auto-regressive Moving Average
DC	Direct current
DIDO	Double-input and double-output
D-S	Dempster-Shafer evidence theory
FCAW	Flux-Cored Arc Welding
FFT	Fast Fourier Transform
FL-PID	Feedback linearization based PID
FPGA	Field Programmable Gate Array
GMAW	Gas Metal Arc Welding
GMAW-P	Gas Metal Arc Welding – Pulsed mode
GMAW-S	Gas Metal Arc Welding – Short Circuit Mode
GPC	Generalized predictive control
GTAW	Gas Tungsten Arc Welding
IGBT	Isolated gate bipolar transistor
LAN	Local Area Network
MA	Moving-average
MAG	Metal Active Gas
MFC	Model-free adaptive control
MIG	Metal Inert Gas
MIMO	Multi-Input-Multi-Output
MIMO	Multiple Input, Multiple Output
MISO	Multiple Input, Single Output
MLP	Multilayer perceptron artificial neural network
MPC	Model Predictive Control
MSE	Median square error
P	Proportional controller
PAW	Plasma Arc Welding
PI	Proportional-Integral controller
PID	Proportional-Integral-Derivative controller
PID	Proportional-Integral-Derivative controller
P-PID	Proportional-Integral-Derivative Professional controller
PWM	Pulse width modulation
RAM	Random Access Memory
RTOS	Real-time operating system
SAW	Submerged Arc Welding
SISO	Single-Input-Single-Output
SMAW	Shielded Metal Arc Welding
SoC	System on Chip
SPOT	Spot welding
SPSS	Statistical Package for the Social Sciences
SQL	Structured Query Language

## Symbols list

$A$	Area of the weld bead
$\alpha$	Angle between the camera and the laser diode or welding angle
$CTWD$	Contact tip to work distance
$\theta$	Delay time
$d_i$	Weld bead depth or weld bead reinforcement value supplied by the scanner profile
$\hat{D}$	Weld bead depth
$\hat{DW}$	Weld bead depth or weld bead width
$i$	Welding current
$iu$	Welding current or welding voltage
$n$	Sample number
$R$	Weld bead reinforcement
$r$	Step or scanner resolution in the horizontal axis
$R_{SP}$	Weld bead reinforcement set point
$SM$	Step motor signal
$T$	Sample time
$T_a$	Thermographic area
$T_b$	Thermographic base plane
$Tc$	Control time
$Td$	Derivative time
$Ti$	Integration time
$T_p$	Thermographic peak
$TP$	Torch position
$TP_{SP}$	Torch position set point
$ts$	Longitude of the torch step
$T_v$	Thermographic volume
$T_w$	Thermographic curve width
$u$	Welding voltage
$WD$	Volume deposited by length unit
$WS$	Welding speed
$WSO$	Orbital welding speed
$W_{sp}$	Weld bead width set point
$\hat{W}$	Weld bead width

## 1 Introduction.

The Gas Metal Arc Welding (GMAW) is a versatile process and allows us to obtain weld beads of high quality. It is a very important welding process in automobile, naval and aeronautic industries; the production of machines, instruments and tools for the industrial, scientific, domestic and medical sectors; the manufacture of power plants such as thermoelectric, hydroelectric, nuclear and wind farms; the transportation of fluids such as water, oil and gas; and in the construction of civil and military buildings.

In the process, the geometry of the weld bead is very important and it is commonly used to quality validation, but an online measurement is very difficult due to extreme environmental conditions imposed on the welding arc (BESTARD; ALFARO, 2016). Although its applications are extensive, the use in automatic forms is limited by the difficulty in closing the control loop. The existing conditions in the arc zone and close to it, make it impossible to use conventional measurement systems for obtaining information of the bead geometry and other significant variables. The use of non-contact measuring techniques is expanding more and more, for example: in video or thermographic cameras, microphones, spectrometers, x-rays, and ultrasound, among others. The weld bead depth (or bead penetration) is very important for obtaining good results in this process, but the online measurement of this geometry variable is very difficult or impossible with the current technology. In this case, the design of a control system is complex and involves many criteria and decisions.

The sensor fusion techniques are used to describe the static or dynamic behaviors of variables of process. These techniques are strongly used to estimate magnitudes that are impossible to measure directly. The sensor fusion is based on several others areas of knowledge, such as statistic and artificial intelligence, but it finds new applications in this field. This notion suggests the use of these methods to estimate the weld bead depth and other variables in the welding process.

Nowadays, the electronic component manufacturing technology increasingly reduces the devices size. The control systems do not escape this trend and embedded devices are at the forefront. Among them are the microcontrollers and more recently the Field Programmable Gate Array (FPGA), which are already part of many control systems and has to demonstrate excellent performance.

The combination of FPGA and sensor fusion system can be a solution close to the optimum for the control of welding processes, resulting in high performance, low power consumption, reducing size and weight. In addition, the selection and design of suitable control strategies can help obtain high quality weld beads and reduce the exposure of the welder to this harmful environment.

### 1.1 General objective.

The main objective of this work is to develop techniques to estimate the depth and width of the weld bead in real time, using sensor fusion and embedded devices. These techniques must be optimized for use in monitoring and control systems of the weld bead geometry in GMAW conventional process with constant voltage source.

### 1.2 Specific objectives.

1. Develop an estimator of the weld bead depth, based on the fusion of thermographic images information and welding current intensity, for use in real-time.

2. Develop an estimator of the weld bead width, based on the fusion of thermographic images information and welding voltage, for use in real-time.
3. Develop a data acquisition and real-time open loop control system of the bead geometry for GMAW conventional process with constant voltage source, using embedded devices.
4. Develop an algorithm of image processing, tools and methodology to measure the weld bead depth in longitudinal cuts of the weld bead.

### 1.3 Summary of contributions.

The expected contributions are summarized thus:

1. The estimator of the weld bead depth, based on the fusion of thermographic images information and welding current intensity, for use in real-time.
2. The estimator of the weld bead width, based on the fusion of thermographic images information and welding voltage, for use in real-time.
3. The algorithm of image processing, tools and methodology to measure the weld bead depth in longitudinal cut of the weld bead.

### 1.4 Potential applications.

This work develops an open loop control system that can be applied in welding manufacture processes, fill of joint, metal structure repair and researches in welding and automatic control. It is useful for testing the parameters in orbital and flat welding position, research the fusion weld and arc thermal behavior, and the modeling of the process. Also, if other sensors are added, it is possible to extend the application of this system to other research fields.

The estimators are an important application of this work because they allow the monitoring and control of the process in many ways: open loop control, closed loop control, quality control, among others.

The algorithm to measure the weld bead depth in longitudinal cut of the weld bead is an inexpensive solution to weld bead depth research, which can achieve good precision and capture the dynamics of the process.

The proposed robotic emulator of the orbital welding process can be useful for orbital welding research, and the education and training of welding operators in the industry.

Finally, the proposed multivariable control system is the first step in a project that can help improve the quality of automatic welding in industrial processes.

### 1.5 Summary of results.

The main results of the work are described below.

- Methodology for developing an estimator of the weld bead depth, based on the fusion of thermographic images information and welding current intensity, for use in real-time.
- Methodology for developing an estimator of the weld bead width, based on the fusion of thermographic images information and welding voltage, for use in real-time.
- The data acquisition and real-time open loop control system of the bead geometry for GMAW conventional process with constant voltage source, using embedded devices.
- The algorithm, tools and methodology to measure the weld bead depth in longitudinal cuts of the weld bead.
- The CNPQ project and resources for developing the design proposal of robotic emulator of orbital welding process and its multivariable real-time control system (ALFARO, SADEK CRISÓSTOMO ABSI, 2016)

Five papers were published and two were submitted to scientific journals. Two documents being reviewed for submission. The following describes the results:

- Four papers were presented in conferences and published in conference proceedings.
  - 1) Bestard, G. A. and Alfaro, S. C. A. (2015) 'Sensor fusion: theory review and applications', in *23rd ABCM International Congress of Mechanical Engineering COBEM 2015*. Rio de Janeiro, Brazil. doi: 10.20906/CPS/COB-2015-0365.
  - 2) Bestard, G. A. and Alfaro, S. C. A. (2016) 'Propuesta de diseño de un sistema de control de la geometría del cordón en procesos de soldadura orbital', in *Taller de Cibernética Aplicada TCA 2016*. La Habana, p. 9.
  - 3) Bestard, G. A. and Alfaro, S. C. A. (2017) 'Sistema de adquisición de datos y control en lazo abierto para procesos de soldadura GMAW', in *Taller Internacional de Cibernética Aplicada TCA 2017*. La Habana, ISBN 2312-5276, pp. 1–7.
  - 4) Bestard, G. A., Martínez, R. T. and Alfaro, S. C. A. (2017) 'Open loop control system and tools for data acquisition and feature extraction of the weld bead geometry in GMAW process', in *24th ABCM International Congress of Mechanical Engineering COBEM 2017*, pp. 1–5.
- One paper was published in scientific journals.
  - 5) Bestard, G. A. and Alfaro, S. C. A. (2016) 'Propuesta de diseño de un sistema de control de la geometría del cordón en procesos de soldadura orbital', *Revista Control, Cibernética y Automatización*, IV(1). ISSN 2312-5276. Available at: <http://revista.icimaf.cu/?q=content/propuesta-de-dise%C3%B1o-de-un-sistema-de-control-de-la-geometr%C3%ADa-del-cord%C3%B3n-en-procesos-de-solda>
- Two papers were submitted to scientific journals.
  - 6) Bestard, G. A. and Alfaro, S. C. A. (2017) 'Measurement and estimation of weld bead geometry in arc welding process: the last fifty years of development', *Journal of the Brazilian Society of Mechanical Sciences and Engineering*. B1 journal. Submitted at 9/22/2017.
  - 7) Bestard, G. A., Sampaio, R. and Alfaro, S. C. A. (2017). 'Sensor fusion to estimate the depth and width of the weld bead in real time', *Sensors*. A1 journal. Submitted at 11/25/2017.
- Two papers are being reviewed for submission to scientific journals.
  - 8) Sensor fusion and embedded devices to estimate the depth and width of the weld bead in real time: two different implementations in FPGA.
  - 9) Control of weld bead geometry in arc welding process: the last fifty years of development.

## 1.6 Work organization.

This work is organized in six chapters, the bibliography references and appendix.

The first chapter shows the introduction, the objectives of the work, the foreseen contributions, the potential applications and the results summary.

The second chapter discusses the literature review about the GMAW process, the measurement and the control systems related to the bead geometry and weld bead depth. Several sensing technologies and sensor fusion algorithms are described in this chapter. A summary at the end shows the sensing and control of the geometry of the weld bead and also its chronological development. The use of embedded systems in this process is also discussed.

Chapter three describes the data acquisition and open-loop control system developed for the experimental work. This chapter is subdivided in four parts: the measuring system, the actuator system, the control system and the user interface. It includes an exhaustive description of the whole system components and the algorithms used in its operation is shown.

Chapter four describe and analyzes several results obtained in this work, based on four experiments developed under different process conditions.

The last chapter shows the conclusions of the work and analyzes in a global way the results obtained and the fulfillment of the objectives of the work.

The bibliographic reference lists the papers, books, thesis, patents and other consulted materials.

The appendix 1 and 2 has a summary of the measurement, estimation control strategies of the bead geometry founded in literature review.

The appendix 3 describes a design of the data acquisition and real-time control system proposed for the control of the bead geometry in GMAW orbital process.

## 2 Literature review.

The literature review on the topic of work shows a great research activity in the last ten years, as shown in Figure 1. The number of documents relevant to the work found in the last decade is similar to the number of documents found between 1971 and 2006, as shown in Figure 2. Of the 244 references cited in the text, only 228 were considered for this comparison.

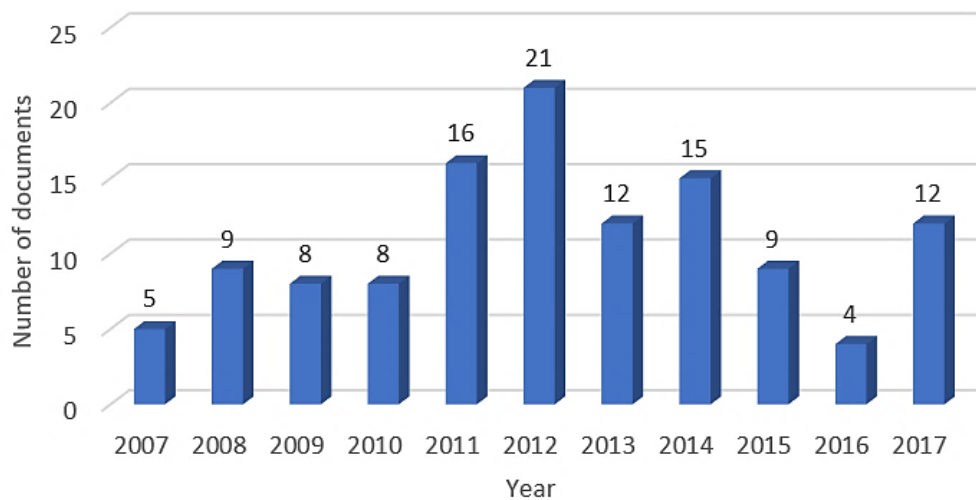


Figure 1 Number of documents relevant to the work published between 2007 and 2017 (Total=119)

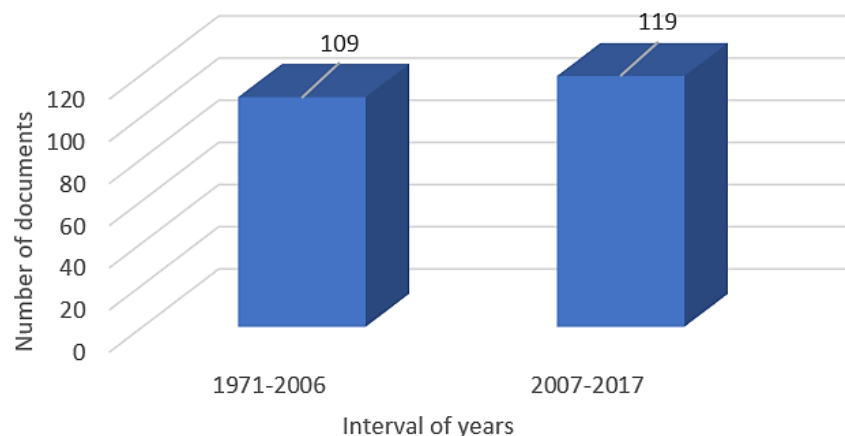


Figure 2 Number of documents relevant to the work that were published before and after 2007 (Total=228)

The following describes the main characteristics of the GMAW process, the ways to measure of the main variables, the most common methods of automatic control found in the literature and the embedded devices in welding process applications.

### 2.1 GMAW process.

The Gas Metal Arc Welding (GMAW) process, also referred by its subtypes Metal Inert Gas (MIG) welding or Metal Active Gas (MAG) welding, employs a consumable electrode, which is supplied by a feed system continuously, and a shielding gas which reduces the incorporation of impurities and defect formation (AMERICAN WELDING SOCIETY STAFF, 2002; KIELHORN *et al.*, 2002). The electric arc created between the electrode and the base metal, causes the fusion of both and the molten weld pool is formed, containing the metal in liquid state. The movement of the torch over the weld joint and the deposition of addition material, form the weld bead, as shown in Figure 3.

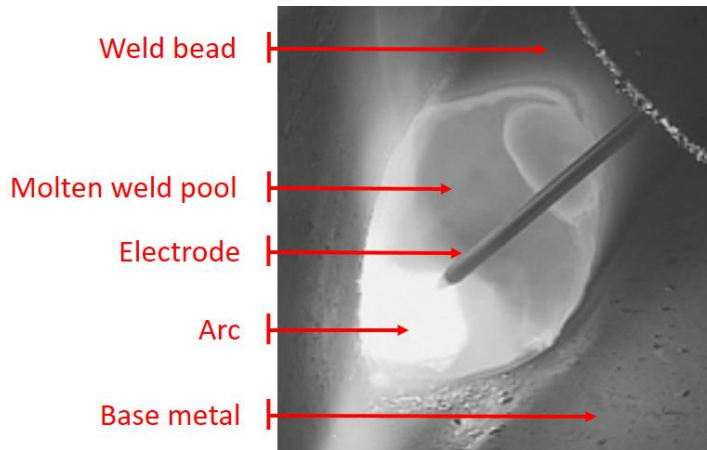


Figure 3 Process arc welding. Adapted from (NIT, 2015)

A constant voltage and direct current power source is the most commonly used in GMAW process, but constant and alternating current systems can also be used (KIELHORN *et al.*, 2002). The principal technological equipment for the constant voltage GMAW process is shown in the Figure 4.

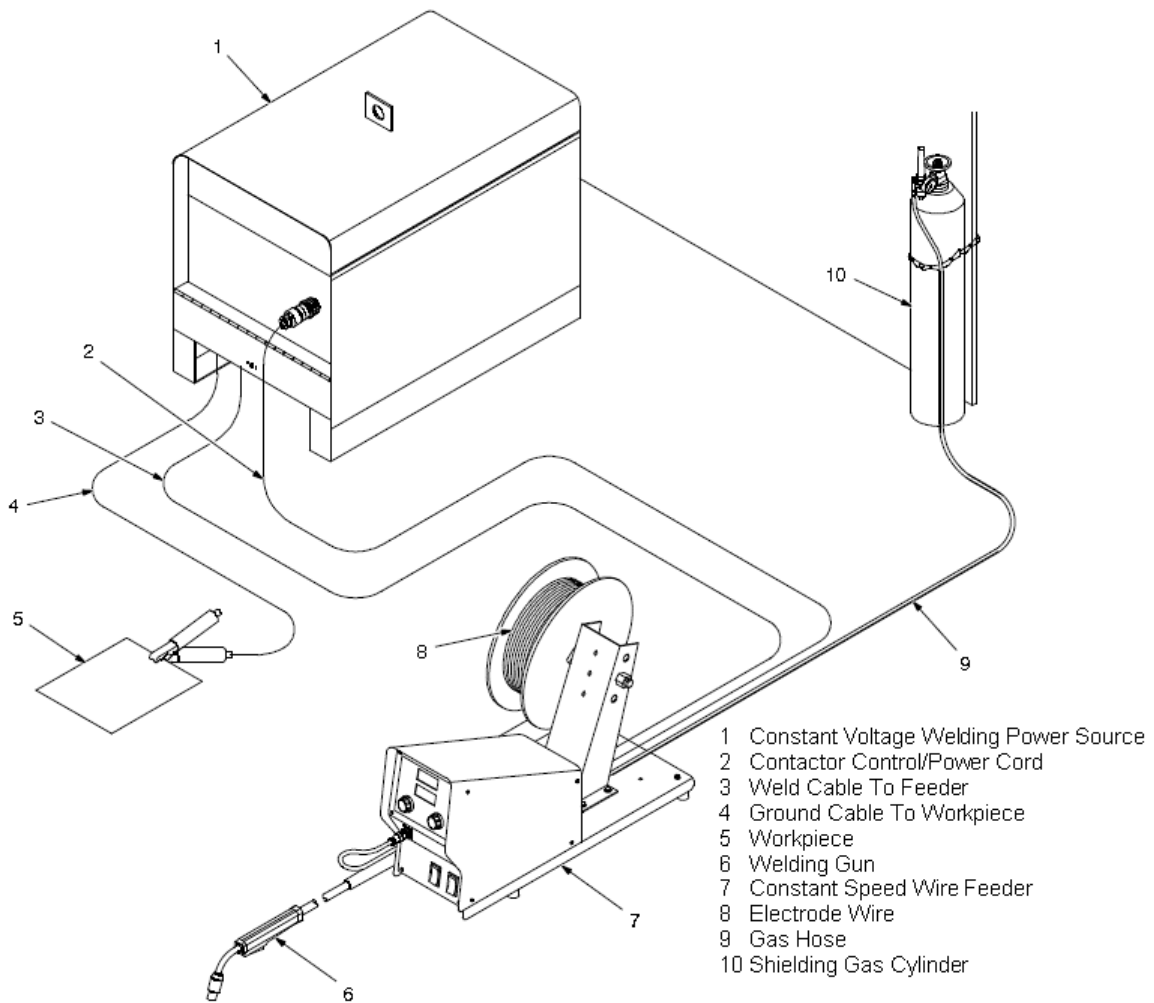


Figure 4 Equipment for constant voltage GMAW process (MILLER ELECTRIC MFG. CO., 2012).



Shielding gases are necessary for gas metal arc welding to protect the welding material from atmospheric gases such as nitrogen and oxygen, which can cause fusion defects, porosity, and weld metal embrittlement if they come in contact with the electrode, the arc, or the welding metal.

The choice of a shielding gas depends on several factors, most importantly the type of material being welded and the process variation being used. Pure inert gases such as Argon and Helium are only used in nonferrous welding, but the first is the most used mixed with other gases (Oxygen, Helium, Hydrogen and Nitrogen). The addition of up to 5% Oxygen can be helpful in welding stainless steel, however, in most applications Carbon Dioxide is preferred.

The desirable rate of shielding-gas flow depends primarily on weld geometry, speed, current, the type of gas, and the metal transfer mode. Welding flat surfaces requires higher flow than welding grooved materials, since gas disperses more quickly. Faster welding speeds, in general, mean that more gas must be supplied to provide adequate coverage.

The electrode selection is based on the composition of the base metal, the process variation being used, the joint design and the material surface conditions. This has a significant influence on the mechanical properties of the weld and is a key factor of weld quality. Depending on the process variation and base material, the typical diameters of the electrodes used in GMAW have a range from 0.7 to 2.4 mm.

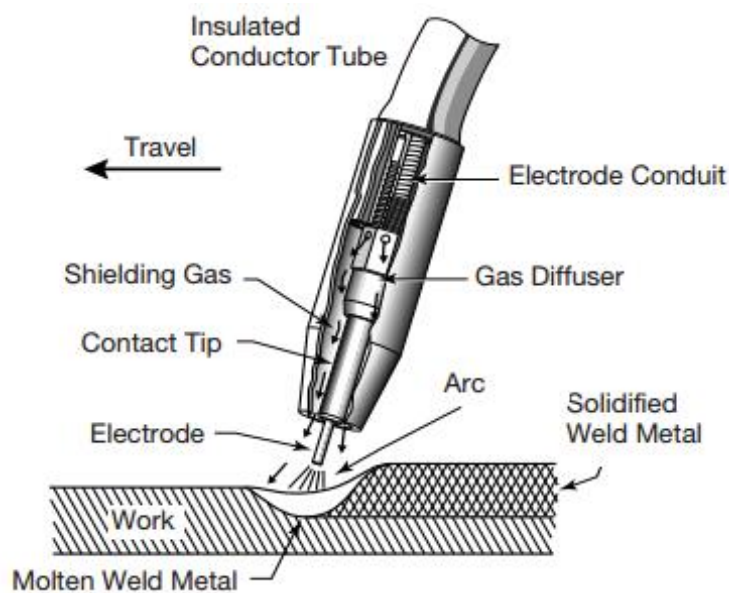


Figure 5 GMAW torch cutaway (LINCOLN ELECTRIC, 2017)

The main process variables of GMAW orbital welding process to constant voltage can be divided in five basic groups:

- Fixed, that can't be modified by the operator and it is defined in the process design.
- Adjustable online, that can be modified during the process.
- Adjustable offline, that can be modified only before starting the process.
- Quantifiable online, that is measurable during the process.
- Quantifiable offline, that is measurable only after the process ended.

The variables and groups are shown in Table 1.

Table 1 Main variables of automatic GMAW process to constant voltage.

<p><b>Fixed</b></p> <ul style="list-style-type: none"> <li>•Shielding gas composition.</li> <li>•Position of the piece or pipe.</li> <li>•Electrode characteristics (<math>\emptyset</math>, composition material, among others)</li> <li>•Thickness of the base metal.</li> <li>•Physic properties of the base metal.</li> <li>•Polarity of the weld electric current.</li> </ul>
<p><b>Adjustable online</b></p> <ul style="list-style-type: none"> <li>•Welding voltage.</li> <li>•Inductance of the welding power source. *<sup>1</sup></li> <li>•Wire-feeding speed, wire speed or wire feed rate.</li> <li>•Welding speed or torch speed</li> <li>•Orbital angle (torch angle relative to pipe center)</li> <li>•Gun angle or attack angle (torch angle side view relative to base metal surface)</li> <li>•Work angle (torch angle end view relative to base metal surface)</li> <li>•Contact tip to work distance (CTWD)</li> <li>•Electrical stick out (ESO) or electrode extension.</li> <li>•Nozzle to plate distance.</li> <li>•Shielding gas flow rate. *<sup>2</sup></li> </ul>
<p><b>Adjustable offline</b></p> <ul style="list-style-type: none"> <li>•Inductance of the welding power source.</li> <li>•Shielding gas flow rate.</li> </ul>
<p><b>Quantifiable online</b></p> <ul style="list-style-type: none"> <li>•Welding voltage.</li> <li>•Welding electric current intensity.</li> <li>•Width of weld bead or bead width.</li> <li>•Weld buildup or reinforcement of the weld bead.</li> </ul>
<p><b>Quantifiable offline</b></p> <ul style="list-style-type: none"> <li>•Weld bead depth, depth of penetration or weld depth of fusion.</li> <li>•Width of weld bead or bead width.</li> <li>•Weld buildup, reinforcement of weld bead or bead reinforcement.</li> </ul>

<sup>1</sup>Only in sources where the inductance is simulated with semiconductors.

<sup>2</sup>If a control valves are installed in the gas flow path

Many of these variables are strongly coupled and if you change one, the others are also modified. These correlation are mentioned in the literature but often they are not totality quantified (CHEN, S B; WU, 2008; KIELHORN *et al.*, 2002; MIGUEL *et al.*, 2012; SCOTTY; PONOMAREV, 2008; ZHANG, Y. M., 2008), indicating that there is still a wide open field of research in modeling these processes.

The process has three primary methods of metal transfer in GMAW process, called short-circuiting, globular and spray, but many variations of these have been defined (AMERICAN WELDING SOCIETY STAFF, 2002; KIELHORN *et al.*, 2002).

According to the form of use of the tools and control of process parameters, it can be classified into: manual, mechanized or automated welding (SCOTTY; PONOMAREV, 2008)

Another possible classification is based on the movement of the torch, where two types of weld are defined: flat and orbital. In the flat, the torch moves in a plane following the weld joint. In the orbital, the torch goes in a circular motion around of tubular work pieces. In this, the torch angle (position of the torch around the pipe), is a disturbance of great influence in the formation of the weld bead, due to the action of gravity force on the molten weld pool.

This process is characterized as inherently multivariable, nonlinear, time varying, with stochastic behavior and having a strong coupling among welding parameters. For this reason, it is very difficult to find a reliable mathematical model to design an effective control scheme for arc welding by conventional modeling and control methods. This issue will be discussed in the next section.

## 2.2 Measurements in the GMAW process.

In the GMAW process there are many variables, which need to have measurements, estimated or controlled, in order to obtain a weld bead with optimal quality. Some parameters can be measured directly from the welding power source, through any analog or digital interface, such as the voltage and electric current.

Other measurements need more complex techniques because the electric arc is a powerful radiation emitter, in a long range of the frequency spectrum, including high temperature and visible light. In the arc zone, you can find vapor and drops of melt metal to come from the electrode and base metal. This group includes parameters of the weld bead geometry.

Automatic welding is affected by variations that often occur in the production parameters, especially if the system lacks sensory abilities. For example, variations in positioning and dimensions of components, alignment of the weld joint, edge preparation and surface conditions. However, by adding measuring systems it is possible that the control system will have a better performance when disturbances is found.

Some of the techniques selected in this work to measure the main parameters of the welding process are described in the next sections. A total reference and important data are shown in Appendix 1.

### 2.2.1 Measurement of arc welding variables.

The most common measurement variables in the welding process are the electric voltage and electric current. But in many cases, it is necessary to know or modify other parameters of the process, in particular the welding power source, for example the wire feed speed, the gas flow, the pre-gas and post-gas time, the source impedance and the arc open or close actions.

The welding power sources with microcontroller or microprocessor control, usually have a serial interface to obtain or send this information from a control system (computer, programmable logic controller, among others), but not all have an open protocol. In this case, the user needs to buy and use a proprietary software. In both cases the information is obtained or sent in digital format. One example of the open protocol is the Brazilian welding power source Inversal 450, manufacturing for IMC-Soldagem (IMC-SOLDAGEM, 2005). The closed protocol is presented in the Fronius welding power sources, but it offers the analogic ROB5000 interface and specific cards with digital interface (FRONIUS, 2001).

The welding power sources without this interface, needs a data acquisition system dedicate at this work. This system converts the analog values in digital information and needs to add the test point in the welding power source or torch electric circuit.

### 2.2.2 Measurement of contact tip to work distance.

The contact-tip to work distance, the electrical stick out or electrode extension (see Figure 6), can be obtained from the robot control system related to torch or piece position, or it can be measured with a laser distance sensor.

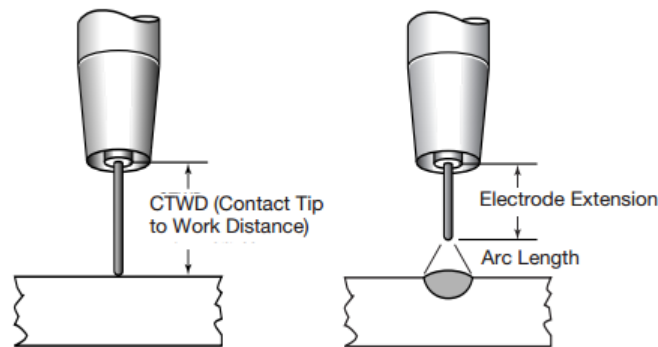


Figure 6 Contact tip to work distance and electrical stick out (or electrode extension) differences (LINCOLN ELECTRIC, 2017)

The first method is more economical but has low accuracy. The zero reference of the robotic system is calibrated with the work piece position, but the surface variations and thickness of the material can affect the accuracy of the value. In the GMAW process with constant voltage, any small variations in the CTWD can affect the electric resistance of the arc, the welding electric current and the heat input significantly (R. S. PARMAR, 1997). For example, the reduction of the arc length causes the increase of heat input (and more current because it reduces the equivalent resistance of the arc) which makes the wire electrode melt more quickly and thereby restore the original arc length (AMERICAN WELDING SOCIETY STAFF, 2002; LINCOLN ELECTRIC, 2017).

The laser sensor can be more accurate, but the measurement point needs to be selected correctly. It has three basic principles of operation: time of flight, phase comparison or triangulation method (ACUITY L, 2014; CHANG *et al.*, 2012; LAP LASER, 2017; MICRO-EPSILON, 2017a).

In the **time of flight** measurement principle, a laser diode produces short pulses which are projected onto the target. The light reflected from the target is recorded by the sensor element. The time of flight of the light pulse to the target and back determines the measured distance. The integrated electronics in the sensor compute the distance using the time of flight. Sensors using this principle are not sensitive to external light.

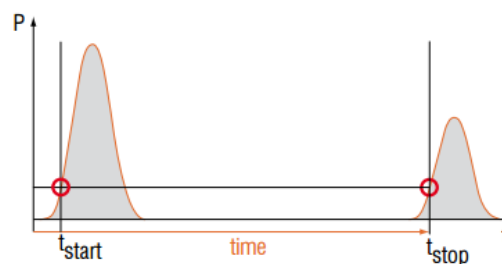


Figure 7 Time of flight measurement principle (MICRO-EPSILON, 2017b).

In the **phase-comparison** measuring principle, a high frequency modulated laser light with low amplitude is transmitted to the target. Depending on the distance of the object, it changes the

phase relationship between transmitted and received signal. Sensors using this principle operate with high accuracy for measurement distances up to 150 m.

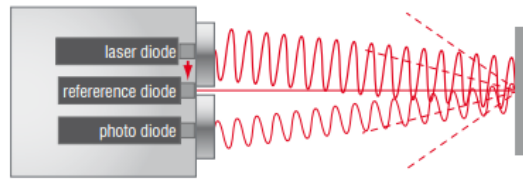


Figure 8 Phase-comparison measuring principle (MICRO-EPSILON, 2017b).

In the **triangulation** method, the laser beam is projected and is reflected from a target surface to a collection lens. The lens focuses an image of the spot on a linear array camera. The camera views the measurement range from an angle at the center of the measurement range. The position of the spot image on the pixels of the camera is then processed to determine the distance to the target. The camera integrates the light falling on it, so longer exposure times allow greater sensitivity to weak reflections.

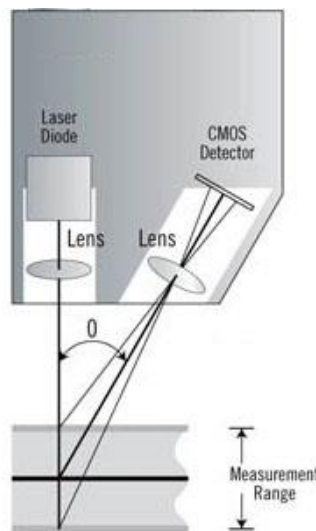


Figure 9 Triangulation measuring principle (MTI INSTRUMENTS, 2017).

Others researched methods use the voltage and current feedback signals from the welding process, computing the minimum resistance during the short circuit period, and uses this to estimate the CTWD after applying a correction factor for the duration of the short circuit. The effect of wire feed speed, actual CTWD and shielding gas on the correction factor, is determined experimentally (CUIURI, 2000).

### 2.2.3 Measurement of welding joint and weld bead geometry.

The geometry of the weld bead is a set of parameters defined in the design stage, and to achieve the required quality should be measured and controlled throughout the process. The parameters show in Figure 10 define the most important characteristics of the geometry of the weld bead.



Figure 10 Geometric dimensions of the weld bead.

The quality of arc welding is commonly described by the geometry of the molten weld pool. This is because the weld pool geometry affects directly the mechanical properties of the welding

joint. In this sense, is important to note that the expert operators can control the welding process using the molten weld pool visual information (KOVACEVIC; ZHANG, 1997; KOVACEVIC; ZHANG; LI, 1996; LIM; CHO, 1993).

The weld pool and the weld bead geometry include the width, the reinforcement and depth or penetration. These geometry parameters are governed by many factors, such as welding current, welding voltage, wire feed speed, welding speed and the contact tip to work distance.

The molten metal reaches very high temperatures (1500°C or more) and the arc even higher, which would damage most measuring instruments that require physical contact with the surface to be measured. This makes the measuring of the weld bead geometry a difficult task using conventional measuring principles. Instead, non-contact measurement techniques have been developed and employed successfully.

Among the methods proposed in available literature (BAE; LEE; AHN, 2002; HIRAI *et al.*, 2001; SAEED; ZHANG; JAYNES, 2005), vision sensing is one of promising solution. One common method is formed by a laser beam, which drawing one or more lines on the surface to be measured and a camera then captures the image that this line creates, filtering it for obtaining only the wavelength emitted by the laser. Subsequently, employing special lenses, image processing algorithms and triangulation techniques, a profile of the piece is obtained with the required information (BROSED *et al.*, 2011; LUO, HONG; CHEN, 2005).

This system, referred as laser scanners or profile sensors, is shown in Figure 11. In it, the optical system projects the diffusely reflected light of this laser line onto a highly sensitive sensor matrix. From this matrix image and angle between the camera and the laser diode ( $\alpha$ ), the controller calculates the distance information (z-axis) and the position alongside the laser line (x-axis). These measured values are then projected in a two-dimensional coordinate system that is fixed with respect to the sensor. In the case of moving objects or a traversing sensor, it is therefore possible to obtain three-dimensional (3D) measurement values. (MICRO-EPSILON, 2017a).

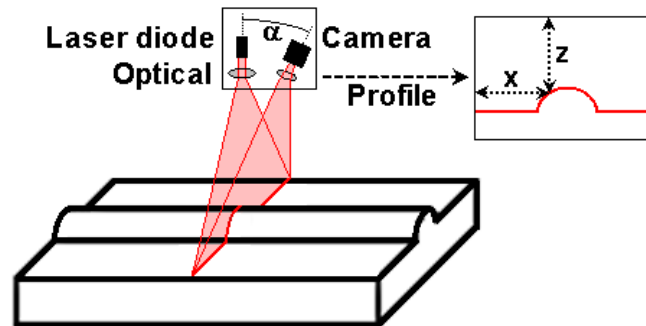


Figure 11 Two-dimensional laser triangulation principle.

It can also use the same principle to obtain a profile of the weld joint before joining the one. This allows to the implementation of algorithms to define or adjust the trajectory to be followed by the torch (DE; PARLE, 2003; HUANG, WEI; KOVACEVIC, 2012; LUO, HONG; CHEN, 2005; MOON, H S; KIM; BEATTIE, 2006; WEI *et al.*, 2011). Similarly, it is possible to calculate the amount of material required (deposition rate) for the formation of a bead with the desired dimensions.

Other way to obtain the 3D profile is using a laser dot matrix or laser line grill (KOVACEVIC; ZHANG, 1996, 1997; YU KANG LIU; YU MING ZHANG, 2014). With this two-dimensional information and using the same triangulation techniques is possible obtain the third dimension of the profile. The use of video cameras to measure the weld bead width and reinforcement is possible too, as is shown in (CHEN, SHANG-BEN; WU, 2009; CRUZ, 2014; FONT COMAS *et al.*, 2017; PINTO-LOPERA; S. T. MOTTA; ABSI ALFARO, 2016; TORRES, 2013) but these methods need optimal light conditions and are difficult to applicate in the industrial environment.

These principles cannot be applied to penetration measurement because the laser has no access to the inner of the workpiece. This variable could be estimated from others measurements if is necessary to process control.

#### 2.2.4 Estimation of weld bead depth.

The weld bead depth can be determined by nondestructive testing techniques such as ultrasound or x-ray, but the robustness of these traditional instruments is not sufficient to support the hard conditions of the process and allows the development of a practical system to be applied online.

The weld pool offers much information correlated with the penetration state; the information includes temperature, arc voltage, arc light, arc sound, geometry parameters, among others. For obtaining the information and estimate the weld penetration, indirect sensing technologies were used. But many works are oriented to detect the total or partial penetration (see Figure 12) and not for obtaining a value useful for the control system algorithm.

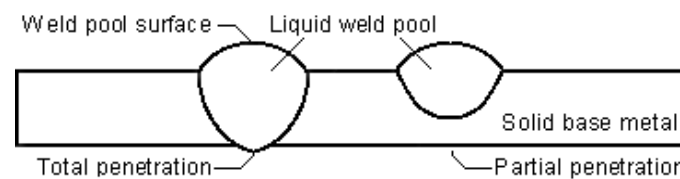


Figure 12 Weld pool and penetration: (a) partial penetration; (b) total penetration.

For obtaining an effective value, estimators have been successfully used under specific conditions. But it is imperative to create a model which can be programmed easily and fed to the control system. It should have a high degree of confidence in predicting the weld bead depth and the model should cover all welding positions. It is very helpful if it also represents a wide range of thicknesses of the material, but this is not always possible.

The research about modeling the weld bead depth, tries to relate this variable with the welding electric current intensity, welding voltage, wire feed speed and welding speed. It works mostly in **horizontal or flat welding** and obtains **static models** employing statistical techniques such as multiple regression analysis and least square (KIM, I. S.; BASU; SIORES, 1996; KIM, I S *et al.*, 2005; KIM, ILL-SOO *et al.*, 2001) or factorial design (MURUGAN; GUNARAJ, 2005), neural networks (AKKAS *et al.*, 2013; HIRAI *et al.*, 2001; KIM, I S *et al.*, 2005; KOVACEVIC; ZHANG; LI, 1996; NAGESH; DATTA, 2002, 2010; SUDHAKARAN *et al.*, 2011), fuzzy logic (NELE; SARNO; KESHARI, 2013; SUNG *et al.*, 2007; XUE *et al.*, 2005), neuro-fuzzy system (AKKAS *et al.*, 2013; SUBASHINI; VASUDEVAN, 2012) and others. A graphical summary of analysis techniques used to estimate the weld bead geometry is shown in Figure 13.

In the welding process, the thermal energy is supplied through electric current and stored in the material. In it there is thermal inertia and that is why dynamic models can be a better representation of the process. In these models, the historical values of welding parameters were also selected as inputs. The dynamic behavior is essential for estimating the current or future state from to the past state. Despite this, the minority report **dynamic models** (BEARDSLEY; ZHANG; KOVACEVIC, 1994; CHEN, BO; FENG, 2014; CHEN, BO; WANG; CHEN, 2010; CHEN, HUABIN *et al.*, 2009; CHEN, S B *et al.*, 2003; DOUMANIDIS, C.C.; HARDT, 1990; DOUMANIDIS, CHARALABOS; KWAK, 2002; LIU, YUKANG; ZHANG; ZHANG, 2015; LV *et al.*, 2014; SONG; HARDT, 1993; WU, CS; GAO, 2006; YAN, ZH; ZHANG; WU, 2011; YU KANG LIU; YU MING ZHANG, 2014; ZHANG, G J; CHEN; WU, 2005; ZHANG, Y. M.; KOVACEVIC; WU, 1996; ZHANG, YM Y.M.; KOVACEVIC, 1998; ZHAO *et al.*, 2001) as show the summary in Figure 14. One example of use of dynamic models are show in (CHEN, HUABIN *et al.*, 2009; CHEN, S B *et al.*, 2003), that employs neural networks

adding previous values of the interest variables and (LIU, YUKANG; ZHANG; ZHANG, 2015; YU KANG LIU; YU MING ZHANG, 2014) that develop an adaptive neuro-fuzzy inference system (AN-FIS) based human intelligence. Are both used for total penetration control in GTAW process.

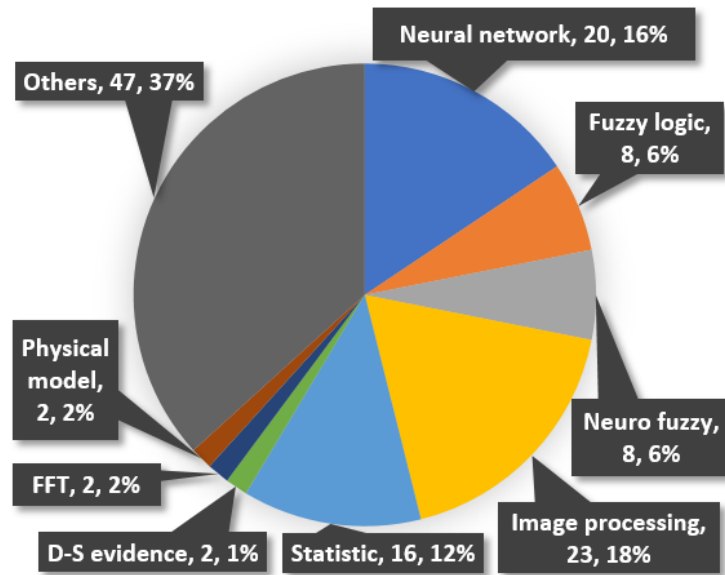


Figure 13 Analysis method used to measurement or estimate the weld bead geometry found in the documents analyzed.

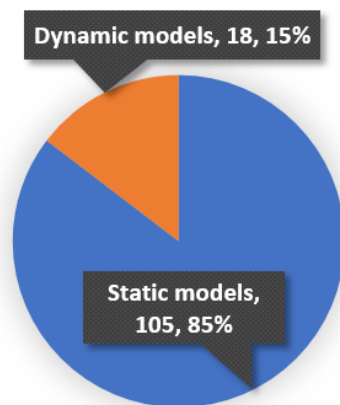


Figure 14 Type of model used to estimate the weld bead depth in documents analyzed.

Based on the literature review and the experience of the author of this work, we consider that the main cause of static model selection is the difficult to obtain a continuous data set of penetration. A way to obtain it is making longitudinal cut and macrographic analysis in the bead with an image processing algorithm. In the traditional transversal cut is not possible obtain enough information to make a dynamic model.

The arc welding process has various welding positions commonly used in industry (AMERICAN WELDING SOCIETY STAFF, 2002), but the researchers worked mostly in horizontal or flat welding positions (see Figure 15) and a few researchers work in **orbital welding** (BAE; LEE; AHN, 2002; CHEN, HUABIN *et al.*, 2009; DOUMANIDIS, CHARALABOS C., 1994; DOUMANIDIS, CHARALABOS; KWAK, 2002; FRANCOIS *et al.*, 1988; LIU, YUKANG; ZHANG; ZHANG, 2015; MOON, H S; KIM; BEATTIE, 2006; SREEDHAR *et al.*, 2012; YU KANG LIU; YU MING ZHANG, 2014). A cause of this is the sensory techniques did not have the robustness, portability and performance needed to move next to the torch. This will change in the next years with the increasing miniaturization of sensors. It is important to note that only 4 research (3.5%) used dynamic models in orbital welding and none of them applies longitudinal cutting in the macrographic analysis.



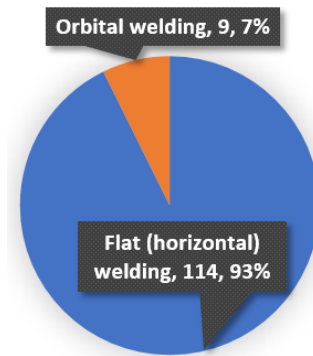


Figure 15 Welding position used in documents analyzed.

Some published papers about methods and technologies, used in this subject, are discussed as follows.

I. S. Kim et al. (KIM, I. S.; BASU; SIORES, 1996) presents in experimental data that the weld bead penetration is increased when the wire diameter, arc current and welding voltage are increased, whereas an increase in welding speed was found to decrease the weld bead penetration. Kim's results show that the gas flow rate does not have a significant effect on the weld bead penetration.

Similarly, Karadeniz studies the effects of various welding parameters on welding penetration (KARADENIZ, 2007). The result shows that increasing the welding current has increased the weld bead depth.

In (SUDHAKARAN *et al.*, 2011) a neural network is employed for estimating the weld bead depth, that the welding current, shielding gas flow rate, welding speed and welding gun angle have. The network used is a feedforward backpropagation network with 4 input neurons, 15 in the hidden layer and one in the output. The static model is obtained using experimental data of 125 tests for training the neural network with Levenberg-Marquardt algorithm. The data are normalized between slightly offset values such as 0.1 and 0.9 rather than between 0 and 1 to avoid saturation of the sigmoid function leading to slow or no learning. The results show similar effects to previous works, of process parameters on weld bead depth for welding current and welding speed but add the analysis of gas flow rate and gun angle. They concluded that welding speed is one of the main the factors that control heat input and weld bead width. The weld bead width and dimensions of the heat-affected zone decrease as welding speed is increased. This is because heat input is inversely proportional to welding speed. Due to the above facts, the weld bead depth decreases as welding speed is increased.

The **indirect sensing technologies** from topside of weld pool can be classified as **conventional sensing technology** where some parameters closely related with the weld pool geometry are monitored, **vision sensing technology** (ALFARO, SADEK C. A; DREWS, 2006; BAE; LEE; AHN, 2002; BESTARD; ALFARO, 2017; CHEN, BO; CHEN; FENG, 2014; CHEN, BO; FENG, 2014; CHEN, BO; WANG; CHEN, 2009, 2010; CHEN, HUABIN *et al.*, 2009; CHEN, S B *et al.*, 2003; CHENG *et al.*, 2004; CRUZ, 2014; FONT COMAS *et al.*, 2017; FRANCOIS *et al.*, 1988; HIRAI *et al.*, 2001; HUANG, WEI; KOVACEVIC, 2012; KOVACEVIC; ZHANG, 1997; KOVACEVIC; ZHANG; LI, 1996; LIN, M.; EAGAR, 1985; LIN, M. L.; EAGAR, 1984; LIU, YUKANG; ZHANG; ZHANG, 2015; LUO, HONG; CHEN, 2005; MOTA, CAROLINA PIMENTA *et al.*, 2011; MOTA, CAROLINA PIMENTO *et al.*, 2013; PINTO-LOPERA; S. T. MOTTA; ABSI ALFARO, 2016; SAEED; ZHANG; JAYNES, 2005; SFORZA; BLASIIS, 2002; SHI *et al.*, 2015; TORRES, 2013; WANG, XUEWU, 2014; WEI *et al.*, 2011; WU, CS; GAO, 2006; YAN, ZH; ZHANG; WU, 2011; YU; YE; CHEN, 2013; YU KANG LIU; YU MING ZHANG, 2014; ZHANG, G J; CHEN; WU, 2005; ZHANG, Y. M.; KOVACEVIC; WU, 1996; ZHANG, YM Y.M.; KOVACEVIC, 1998) where weld pool characteristic is monitored as skilled welders do, and **multi-sensor or sensor fusion technology** (ALFARO, SADEK C. A; DREWS, 2006; ALFARO, SADEK

CRISÓSTOMO ABSI; CAYO, 2012; CHEN, BO; CHEN; FENG, 2014; CHEN, BO; FENG, 2014; CHEN, BO; WANG; CHEN, 2009, 2010; MOON, H S; KIM; BEATTIE, 2006; PAL; PAL, 2011; SFORZA; BLASIIS, 2002; SONG; HARDT, 1993, 1991; YU; YE; CHEN, 2013) where various sensing technologies are fused in a sensing system.

The conventional sensing technologies include ultrasonic, infrared thermography, weld pool oscillation, arc sound, x-ray, among others. The vision sensing technologies comprehend two-dimensional and three-dimensional sensing technology. In the last 20 years, these technologies were applied to get the weld pool geometric shape with good results (WANG, XUEWU, 2014). A graphical summary is shown in Figure 16, where the vision, the infrared thermography (ALFARO, SADEK C ABSI *et al.*, 2015; ALFARO, SADEK CRISÓSTOMO ABSI, 2012; ALFARO, SADEK CRISÓSTOMO ABSI; CAYO, 2012; BANGS; LONGINOW; BLAHA, 1989; BEARDSLEY; ZHANG; KOVACEVIC, 1994; CAYO, EBER HUANCA; ALFARO, 2011; CHANDRASEKHAR *et al.*, 2015; CHEN, W.; CHIN, 1990; CHEN, W. H.; NAGARAJAN; CHIN, 1988; CHEN, ZIQIN; GAO, 2014; CHOKKALINGHAM; CHANDRASEKHAR; VASUDEVAN, 2012; CULLEN *et al.*, 2008; DE; PARLE, 2003; DOUMANIDIS, C.C.; HARDT, 1990; DOUMANIDIS, CHARALABOS C., 1994; DOUMANIDIS, CHARALABOS; KWAK, 2002; FAN *et al.*, 2003; GWEON, 1999; HKS PROZESSTECHNIK, 2017; HURTADO; ALFARO; LLANOS, 2012; ICELAND; MARTIN E. O'DOR, 1971; LIM; CHO, 1993; LLANOS; HURTADO; ALFARO, 2016; MOTA, CAROLINA PIMENTA *et al.*, 2011; MOTA, CAROLINA PIMENTO *et al.*, 2013; NAGARAJAN *et al.*, 1990; NAGARAJAN; CHEN H.; CHIN, 1989; NIT, 2015; NOMURA, H. *et al.*, 1980; PAL; PAL, 2011; PALACÍOS, 2010; PEÑA SANTOS, 2012; S. NAGARAJAN; CHIN; CHEN., 1992; SCHLICHTING *et al.*, 2012; SFORZA; BLASIIS, 2002; SONG; HARDT, 1993; SREEDHAR *et al.*, 2012; SUBASHINI; VASUDEVAN, 2012; WIKLE III *et al.*, 2001; WIKLEIII; ZEE; CHIN, 1999) and the sensor fusion techniques are the most used.

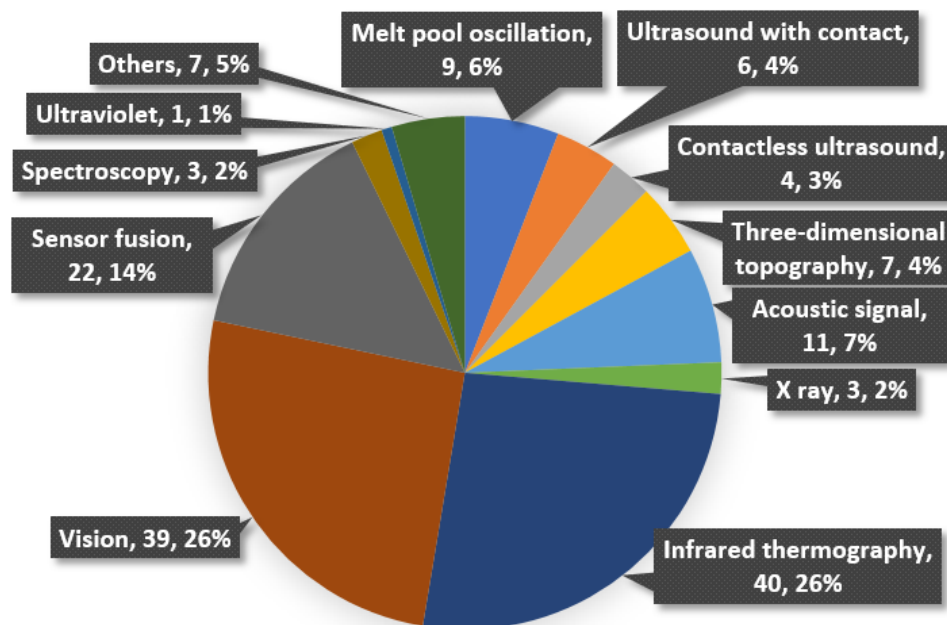


Figure 16 Technologies of indirect monitoring used to estimate the bead geometry found in the documents analyzed.

The total penetration in the welding process is important to ensure the weld quality. When the total penetration take place, the melt weld pool crosses to bottom side of the workpiece. In this moment, the metal in liquid state can drop out from workpiece because the solid metal support is not present. A method to ensure the total penetration is the measurement of backside width of the weld pool, but this method is difficult because the practical conditions of the process (such as space, movements, restrict access, among others) make impossible to place the sensors under the weld pool. The measurement of the weld pool (on front side) too offers information

about the total penetration state and some sensing technologies are used for this purpose (WANG, XUEWU, 2014).

In this sense, the **weld pool oscillation** methods have been used innovatively by Renwick (RENWICK; RICHARDSON, 1983), Zacksenhouse and their coworkers (ZACKSENHOUSE; HARDT, 1983). Wang, et. al. (WANG, Q. L.; YANG; GENG, 1993) found a relation between the weld pool resonance frequency and the width of a stationary weld pool, in total penetration conditions, and distinguish between the partial penetration and total penetration using the resonance frequencies. In (XIAO; OUDEN, 1990, 1993; YOO, 1990) the authors shown that the oscillation frequency decreases when the penetration state changes from partial to total penetration. For the measurement of the weld pool oscillation, both arc voltage and arc light fluctuations have been used (RENWICK; RICHARDSON, 1983; YOO, 1993). Aendenroomer and den Ouden (AENDENROOMER; DEN OUDEN, 1998) detect under-penetration, optimal penetration or over-penetration states using the oscillation frequency of the weld pool. The oscillation frequency is calculated from the measured voltage variations using a Fast Fourier Transform (FFT) algorithm. Shi et. al. (SHI *et al.*, 2015) develop an image processing algorithm to extracting the weld pool oscillation frequency in real time and proved that of frequency of partial penetration is higher than the frequency of complete penetration, along with an abrupt transition. But these methods only detect discrete states, it is not possible to estimate the weld bead depth value.

The **contact ultrasonic** testing has become a standard off-line technique for locating cracks, incomplete fusion, porosity and other discontinuities in fusion welds (HARDT; KATZ, 1984). A direct method was developed to measure the depth of weld pool by detecting solid-liquid interface, using ultrasonic reflection techniques (CARLSON, N.M. ET AL., 1992; CARLSON, N.M.; JOHNSON, 1988; FENN, 1985; HARDT; KATZ, 1984; LOTT, 1984). However, in on-line applications, the hard conditions of the process can damage the contact transducer or make very difficult its use.

But the **contactless ultrasound** is generated by a pulsed laser and eliminated the contact transducer (CARLSON, N.M. ET AL., 1992). The sensing system used a laser phased array technique to generate focused and steered ultrasound, and an electromagnetic acoustic transducer (EMAT) as a receiver. Both were non-contact, which could thus eliminate the need for a coupling medium (MILLER *et al.*, 2002; WANG, XUEWU, 2014; YANG, J. ET AL, 1994). The ultrasonic data, too, is employed combined with other information.

The **three-dimensional topography** of the weld pool surface may also be used to determine the weld penetration. Previous research shows that the pool sag or the pool depression is correlated to the weld penetration (LIN, M. L.; EAGAR, 1984; ROKHLIN; GUU, 1993) and develops a specular reflection-based vision system to directly monitor, the three-dimensional topography of the weld pool surface (KOVACEVIC; ZHANG, 1996, 1997; YU KANG LIU; YU MING ZHANG, 2014). However, sensing the three-dimensional pool surface was difficult and employed complex algorithms.

The **acoustic signal** was employed for detecting defects in many research efforts (ALFARO, SADEK CRISÓSTOMO ABSI; CAYO, 2012; CAYO, EBER H.; ALFARO, 2009; GRAD *et al.*, 2004; LV *et al.*, 2013; PAL; PAL, 2011; VAN BOHEMEN; HERMANS; DEN OUDEN, 2001) or for identify the transfer mode (CAYO, EH, 2008). Na Lv et al. presents a method for real-time arc length monitoring and sag-depression prediction through arc sound signal in GTAW (LV *et al.*, 2014)

The **X-ray** was used by (GUU; ROKHLIN, 1989; ROKHLIN; GUU, 1993; ROKHLIN; CHO; GUU, 1989) to measure the surface shape of the weld pool. The depression depth of the weld surface makes the thickness decrease, so that the X-ray radiation penetrated and received in the other face are increased. Many valuable results have been obtained based on pool surface measurements by using this approach. However, the imaging device and X-ray source could not both be easily attached to the torch and therefore its application is restricted.

The modern ***infrared thermograph*** equipment provides a non-contact feasible means to measure the temperature field. The infrared sensing of arc welding processes has been extensively investigated by Nagarajan, Chen and coworkers (CHEN, W.; CHIN, 1990; CHEN, W. H.; NAGARAJAN; CHIN, 1988; NAGARAJAN *et al.*, 1990; NAGARAJAN; CHEN H.; CHIN, 1989; S. NAGARAJAN; CHIN; CHEN., 1992). The temperature distribution is measured in gas metal arc welding (CHEN, W.; CHIN, 1990) and it was found that the weld bead depth can be determined using the characteristics of the temperature profiles. In (CHEN, W. H.; NAGARAJAN; CHIN, 1988) the thermal volume was obtained and was observed to be proportional to penetration depth. Beardsley, et al. (BEARDSLEY; ZHANG; KOVACEVIC, 1994), found that the root surface weld bead width of the total joint penetration welds can be determined in GTAW using the pool area and a ratio between a surrounding area (600°C isotherm area) of the weld pool and the weld pool area. The research in (WIKLEIII; ZEE; CHIN, 1999) shows the direct correlation between the welding current and infrared emission.

Since 1971 several patents have been registered on the use of infrared emission information to total penetration detect and control (BANGS; LONGINOW; BLAHA, 1989; ICELAND; MARTIN E. O'DOR, 1971; NOMURA, H. *et al.*, 1980)

In 1989 Edmund R. Bangs and others (BANGS; LONGINOW; BLAHA, 1989), registered a patent that described a system for real-time welding adaptive control using infrared images, artificial intelligence (expert system) and distributed processors. The point infrared sensor, used in (FAN *et al.*, 2003; WIKLE III *et al.*, 2001) to weld bead depth monitoring in GTAW and SWA process, proves that it is useful for compensating the process perturbations and is a low cost system. In (SONG; HARDT, 1993) the thermally information is used to closed loop control of the weld pool depth and the experimental tests in (CAYO, EBER HUANCA; ALFARO, 2011) prove that the behavior of infrared emission is representative of the arc power dynamics.

Ghanty et al. (GHANTY *et al.*, 2008) using an artificial neural network to predict weld bead geometry. The inputs of the neural network are the features derived from the infrared thermal video of a GTAW welding process. These features are extracted using line scan analysis and image processing techniques corresponding to particular locations of the weld joint. The depth and width data of the weld bead are obtained by the traditional procedure (transversal cut and macrographic image). The data points were generated from eleven welding experiments, each with 5 cut sections. A set of 55 samples is obtained and is used to train and validate the neural network. This procedure has some limitations discussed below.

Four years later, two members of the previous research team and Chokkalingham (CHOKKALINGHAM; CHANDRASEKHAR; VASUDEVAN, 2012) used a similar experimental and feature extraction procedure to estimate the width and depth of the weld bead in A-TIG welding process. They used the infrared images of the weld pool and a static model obtained with an artificial neural network. Real time infrared images were captured using an infrared camera for the entire weld length at various current values. The image features such as the length and width of the hot spot, the peak temperature, the mean and the standard deviation of the Gaussian temperature profile, the thermal area under the Gaussian temperature profile, the full width half maximum of the Gaussian temperature curve and the weld bead width (computed from the first derivative curve of the Gaussian temperature curve) are obtained. These features are extracted using line scan analysis and image processing techniques corresponding to particular locations of the weld joint.

These parameters along with their respective current values are used as inputs while the measured of width and depth of the weld bead are used as output of the neural network models. The two neural network models have the same structure 9-11-1 (9 input nodes, 11 hidden nodes and one output node) and are static models. The weld bead penetration and weld bead width

data are obtained by the traditional procedure (transversal cut and macrographic image). A set of 90 samples is obtained in several experiments and is used to train and validate the neural network. The correlation coefficient obtained between the predicted and measured weld bead depth was 0.99184 for the test dataset and 0.92255 for validation data set. Similarly, the correlation coefficients obtained in the test and validation of the weld bead width model were 0.98862 and 0.95525 respectively.

The previous results are very good, but the authors assume that the thermographic curve has a Gaussian behavior and use this curve to obtain several parameters. The measures obtained in this doctoral work for the GMAW process, prove that the thermographic curve can be approximated to Gaussian behavior using a median or average filter (with a wide filter window), but it should show several peaks and irregular contour that makes a first derivative very different from the Gaussian theoretical curve. The static model does not represent the dynamic of the process because it did not consider the previous states. This model type has a limited use in control algorithms that need a quick response and an understanding of the process dynamic.

In (CHANDRASEKHAR *et al.*, 2015) a predictive methodology is developed for the A-TIG welding process, using hybrid soft computing techniques for estimating the weld bead width and weld bead depth from the infrared thermal image of the weld pool. The adaptive neuro fuzzy inference system and artificial neural network based models are used. The image features extraction and estimator algorithm are similar to the previous work (CHOKKALINGHAM; CHANDRASEKHAR; VASUDEVAN, 2012) and the model has the same limitations. The algorithm is programming in Matlab environment and analytical results were processed in the Origin software, therefore it is not optimized for embedded systems.

A adaptive neuro-fuzzy inference system (ANFIS) is used in (SUBASHINI; VASUDEVAN, 2012) for predicting the weld bead width and weld bead depth using the infrared thermal image of the weld pool and the welding current. The extracted features from the thermal image such as length and width of hot spot (using k-means algorithm), thermal area (using the Gaussian fit) and thermal bead width (using the first derivative of the thermal curve) were used as inputs for models.

A weld inspection sensor based on a scanning thermal profile called ThermoProfilScanner (TPS) was developed by HKS Prozesstechnik GmbH for evaluation of weld quality and misalignment of welds during cooling. As the characteristics of the thermal profile (symmetry, width of a thermal zone, maximum temperature, among others) and the seam quality are directly correlated, the abnormalities like weld seam offset, holes, lack of fusion, insufficient weld penetration, among others, can be detected by TPS. The correlations between thermal profile and weld quality from previous experience can be used to compare the desired values and tolerances. If tolerance limits are exceeded, an alarm is trigger and marking the defective point (HKS PROZESSTECHNIK, 2017).

Several research detects on-line the most common defects with the infrared information (ALFARO, SADEK C ABSI *et al.*, 2015; ALFARO, SADEK CRISÓSTOMO ABSI; CAYO, 2012; GWEON, 1999; HURTADO; ALFARO; LLANOS, 2012; LLANOS; HURTADO; ALFARO, 2016; MOTA, CAROLINA PIMENTO *et al.*, 2013; NIT, 2015; PALACÍOS, 2010; PEÑA SANTOS, 2012; RODRIGUEZ-COBO *et al.*, 2013; SCHLICHTING *et al.*, 2012; SREEDHAR *et al.*, 2012), with the analysis of the differences in the spatial and temporal surface temperature distributions, joint strength, Kalman filter, cumulative sum, among others, or combined with other information (see section 2.2.5). This shows that the infrared emission offers much information, not only for the weld bead depth, but also other aspects of welding. The Figure 17b and c, has an example of it.

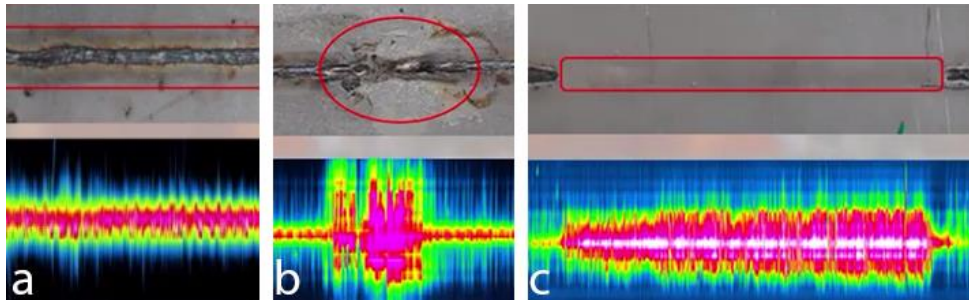


Figure 17 Infrared emission in welding process (a). Discontinuities caused by oil (b) and lack of penetration (c) (NIT, 2015).

Illuminating the weld pool with infrared light is another way for obtaining a good image of it. The research in (CHEN, ZIQIN; GAO, 2014; MOTA, CAROLINA PIMENTA *et al.*, 2011; MOTA, CAROLINA PIMENTO *et al.*, 2013) are examples of this.

It is important to note that the temperature measurements of the weld pool using a thermographic camera should be considered approximate measurements because of the uncertainty or variable emissivity of it, which oscillates with the temperature, surface finish and type of work material. The weld pool is in a liquid phase with its surface almost a mirror, which results in a low emissivity (ALFARO, SADEK C ABSI *et al.*, 2015).

### 2.2.5 Sensor fusion in welding process.

The use of magnitudes obtained by various sensors or measuring systems and compiled to obtain a value or values that describe the static or dynamic behavior of process or variables, have been popularized in the scientific community with the expression “sensor fusion” or “fusion sensory data” (ALFARO, SADEK CRISÓSTOMO ABSI, 2012; BESTARD; ALFARO, 2015; HENDERSON, THOMAS C. *et al.*, 1998).

If some different sensing technologies are combined, better sensing results may be found. For example, you can combine the weld pool information obtained from a vision system and infrared camera for obtaining the weld pool dimensions, with more accuracy and more information, or combine the weld bead width (from vision system) and back bead temperature (from pyrometer) to estimate the bead penetration value on-line (SONG; HARDT, 1991, 1993). Because of these and other advantages, multi-sensor systems were studied in recent years to realize effective weld pool and weld bead sensing.

There are applications in different spheres such as the aerial and ground navigation of mobile robots (INVENSENSE, 2014; MURATA MANUFACTURING CO., 2014; SANTIAGO MARTÍNEZ, 2009), the systems for environmental monitoring (BARRON ADAME, 2010; REGUEIRO *et al.*, 2017) and visual sensor networks (CASTANEDO SOTELA, 2010; MALDON, 2002; RODRÍGUEZ MUÑOZ, 2003). This grows daily and the continuing research has envisioned many others applications in fields such as medicine, security, fault detection, quality control, among others. This relatively young research area has few but important results in the welding process. Below we will comment on some.

Sforza and Blasiis combined the visible, infrared and ultraviolet emission of the plasma in a system for detecting the bad welds. For this they employed the Fourier frequency monitoring rules and statistical analysis (SFORZA; BLASIIS, 2002).

Chen *et al.* (CHEN, BO; WANG; CHEN, 2009) employed an arc sensor and visual sensor to acquire welding current, welding voltage, and weld pool image of pulsed GTAW. Then electronic signal features and weld pool image features were extracted. Based on the data acquired in a random experiment, a back-propagation neural network was used to fuse the information and predict the backside width of weld pool. Comparison results showed that more precise predicting result was presented by the multi-sensor information model.

The information of welding current, voltage, weld pool image, and welding sound information, about the pulsed GTAW process, and special algorithms was used in (CHEN, BO; WANG; CHEN, 2010) to features extraction of different sensors information. Then Dempster-Shafer (D-S) evidence theory was used to fuse the different signal features to predict the penetration state (incomplete penetration) about the welding process. Neural network was used to obtain the basic probability assignment for D-S algorithm. The experiments with fusion demonstrated that the information of different sensors obtained better prediction result than a single sensor. In other similar research (CHEN, BO; FENG, 2014), fuzzy logic was used to obtain the basic probability assignment for D-S algorithm and predict the penetration status.

In the reference work (ALFARO, SADEK C. A; DREWS, 2006) show in Figure 18, a video system was coupled to the torch to observe the welding pool directly, and a sensor for optical seam tracking was put in front of the torch. The sensor fusion was implemented using specialized distributed processing units, artificial neural networks, pattern recognition and fuzzy logic supervision.

For spot welding, in (CULLEN *et al.*, 2008), ultrasonic, infrared and force sensors are combined with voltage, weld current and dynamic resistance measurement for monitoring the integrity of the weld parameters. They use a neural network that predicts the quality and nugget size of each spot weld in real time.

A sound sensor and infrared pyrometer were used to monitor the weld bead depth in pulsed MIG welding in (PAL; PAL, 2011).

In (YU; YE; CHEN, 2013), a spectrometer and a visual sensor were used simultaneously to collect the arc spectral and visual information in pulsed GTAW process. A fuzzy system was developed to estimate the weld penetration status.

Chen *et al.* (CHEN, BO; CHEN; FENG, 2014) study the multi-sensor information fusion technology in welding process, and used the choquet fuzzy integral method to fuse the information obtained by arc, sound, and visual sensors in pulsed GTAW process.

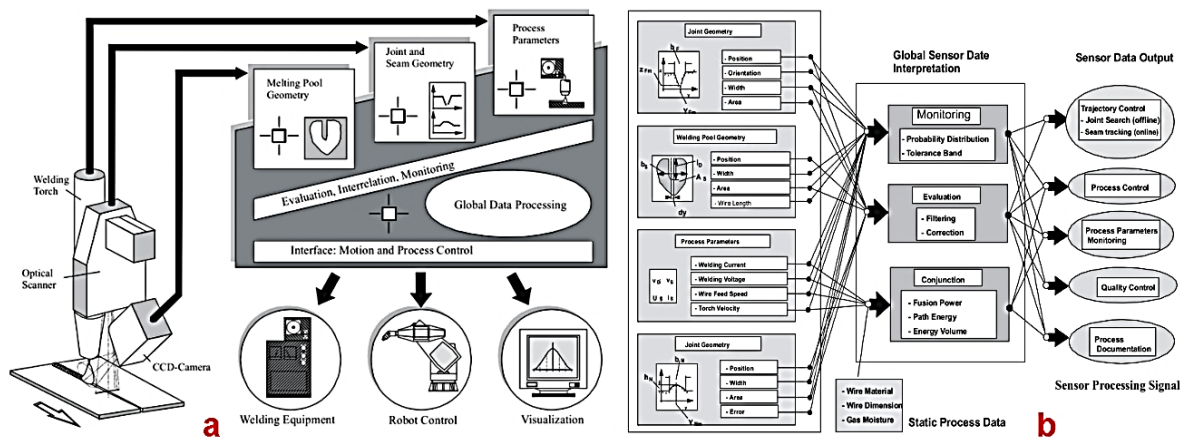


Figure 18 Set up and functional main units of the multi-sensor welding system (a). Multi-sensor information flow (b) Adapted from (ALFARO, SADEK C. A; DREWS, 2006)

From the above research, it can be noticed that more accurate sensing results were obtained based on multi-sensor information fusion technology, due to more weld pool information and effective information fusion techniques.

### 2.2.6 Chronological evolution of the research in geometry sensing and estimators.

Although the objective of this work was not to investigate the evolution of the studied theme and the number of publications found is not representative of this evolution, it was interesting to note some tendencies that we share next.

Despite the existence of some publications on how to estimate the penetration in the weld bead since 1971, it is not until the decade of the 80s that a greater interest in this subject is observed. In the last 12 years the number of published documents is greater than to published in the previous time, as show the Figure 19. This prove a grown interest in improve the welding process, in special the bead penetration control.

The increase in the number of scientific works was propelled by the technological develop of sensors, the need of welding process control in industrial environment (robotic welding) and the sensors cost reduction. The infrared sensor is a good example.

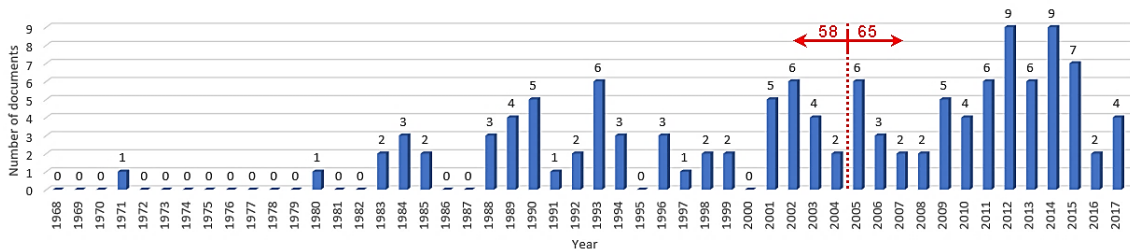


Figure 19 Evolution of number of documents relevant to the work, published in the last fifty years.

Since the 1970s infrared sensors (pyrometer) were available and during the 80's the Department of Defense gave both Honeywell and Texas Instruments classified contracts to develop uncooled infrared sensor technology. In 1992 the US Government de-classified the use of this technology for commercial products and the use of infrared was moving towards civil use. The U.S. government allowed to sell their devices to foreign countries, but not to divulge manufacturing technologies. In the first decade of this century, several countries developed their own uncooled imaging systems (ROGALSKI, 2003). There was a dramatic lowering of costs for uncooled arrays and in the Figure 20 can be observed a signify increase of scientific publications in this decade.

The use of acoustic signal and vision techniques to geometry estimation show mayor activity in the last twenty years. The development of high speed, little size and low-cost cameras, high-quality audio systems and digital signal processors helped in this trend. The weld pool oscillation had a peak in 90's but has others publications more recently.

In other way, the analysis techniques evolved from the statistic to artificial intelligence. In the last century was intensely used the regression models, the least mean square, the Kalman filter and others statistical methods. The principal techniques used in the last 10 years are the neural network, fuzzy logic and both combinations. The development of vision system and high processing capabilities was accompanied by the intense research of image processing algorithms in the last twenty years. The Figure 21 shows the evolution of main methods of analysis used to estimate the bead geometry in the found publications.



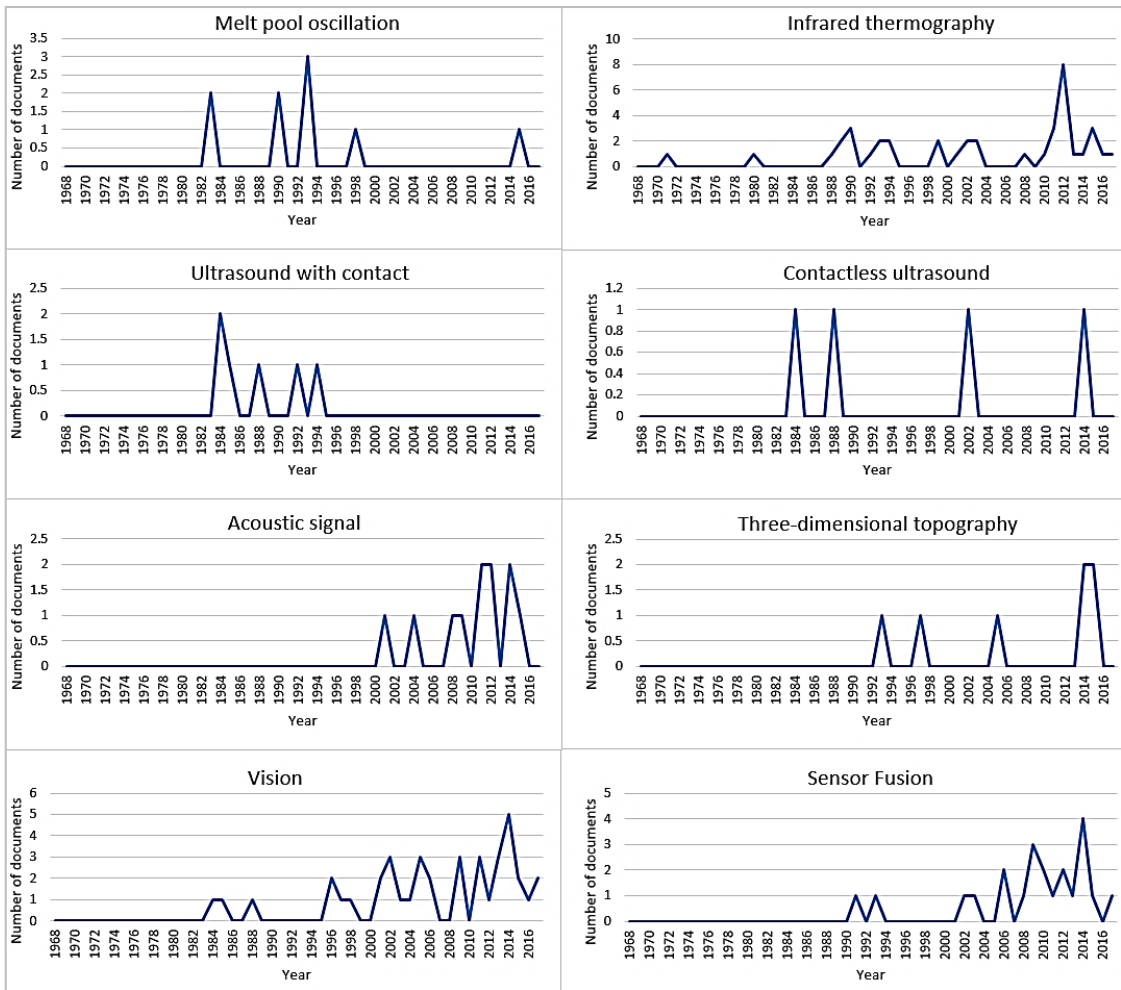


Figure 20 Evolution of main measuring technologies used to obtain the information to estimate the bead geometry.

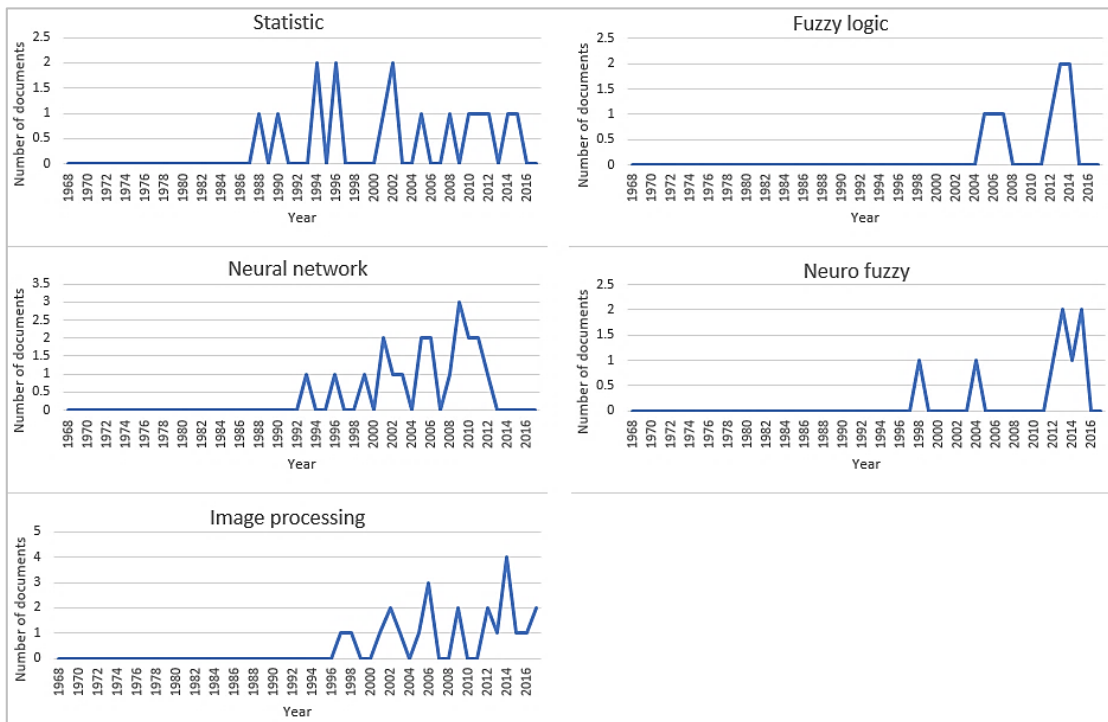


Figure 21 Evolution of main methods de analysis used to estimate the bead geometry.

### 2.3 Control of the weld bead geometry in arc welding process.

All fusion welds involve the melting and subsequent solidification of the base metal. The geometry of the weld bead is a good indicator of the melting and solidifying process. Generally, weld inspection starts by evaluating this weld bead geometry and is followed by further inspection of the mechanical properties and metallurgical structures (JOU, 2002). This is one of the reasons why the control of the weld pool geometry is imperative for obtaining good quality in the weld.

Research and development in this area has increased in the last five decades, starting from simple control methods and analogical devices (ICELAND; MARTIN E. O'DOR, 1971), to complex algorithms and digital devices and computers (LIU, YUKANG; ZHANG; ZHANG, 2015; LIU, YUKANG; ZHANG, 2015) But the most of cases (90%) work in a horizontal position and only the 10% work in orbital welding, as shown in Figure 22a. Of this 10% that works in orbital welding, only 14% do it in GMAW processes (see Figure 22b). That is, only one (1.6%) of the control systems found in the analyzed documents, work in orbital GMAW processes.

In this work we considered the GMAW orbital welding process for a design proposal. Only a few researchers (in the literature review) are working in this important area. For example (CHEN, HUABIN *et al.*, 2009; DOUMANIDIS, CHARALABOS; KWAK, 2002; LIU, Y. K.; ZHANG; KVIDAHL, 2014a, b; LIU, YUKANG; ZHANG; ZHANG, 2015; LIU, YUKANG; ZHANG, 2015; YU KANG LIU; YU MING ZHANG, 2014). Of these only one (DOUMANIDIS, CHARALABOS; KWAK, 2002) worked in the GMAW process.

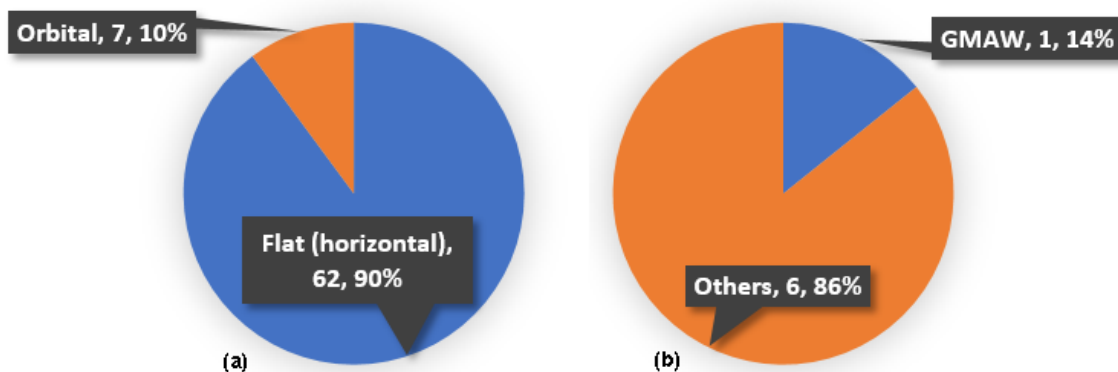


Figure 22 Welding position used in control systems of the weld bead geometry, found in the analyzed documents: (a) Control in flat and orbital welding; (b) Control of the GMAW orbital process.

In addition, most cases apply static models, do not control all parameters of the bead geometry and do not apply multivariable techniques, as shown in Figure 23. The black box model approach is widely used. Because the complex characteristics of the process, a physic model approach is very difficult and needs an extensive research and resources.

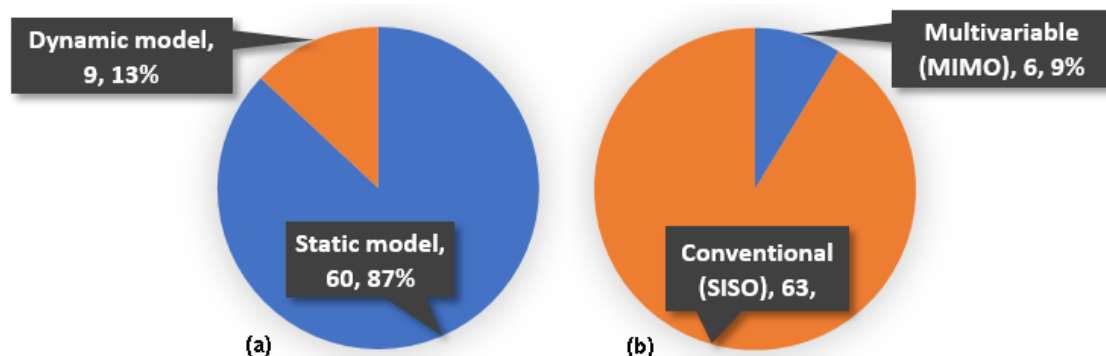


Figure 23 Model type (a) and quantity of variables controlled (b) in the control systems of the weld bead geometry found in the analyzed documents.

The dynamic models can be a better representation of the process producing best prediction results (see section 2.2.3). The research where these models were used represent only 13% of the total (BROWN; MEYN; WEBER, 1998; CHEN, S.B. *et al.*, 2000; DOUMANIDIS, CHARALABOS C., 1994; DOUMANIDIS, CHARALABOS; KWAK, 2002; JOU, 2002; LU, WEI *et al.*, 2005; MOUSAVI; HAERI, 2011; XIONG; ZHANG, 2014; ZHANG, YM; KOVACEVIC; WU, 1996)

With the multivariable techniques, it is possible to consider the interactions between variables in the process and reduce their effect in the control loop. Only a few works (9%) used multivariable control loops, for example, in (CHEN, S.B. *et al.*, 2000; DOUMANIDIS, C.C.; HARDT, 1990; DOUMANIDIS, CHARALABOS; KWAK, 2002; LÜ *et al.*, 2010; MASMUDI; HARDT, 1992; SONG; HARDT, 1991)

Due to the characteristics of this process (see section 2.1), the use of adaptive techniques has spread in the last decades with favorable results, only overcome by Proportional-Integral-Derivative (PID) controller. The adaptive control has been implemented in some researchers to cope with the problem of the high dependence of process parameters to its operating condition. The main drawback of this method is that it requires online estimation or tuning of the parameters, which is usually a time-consuming operation. The single implementation of PID and low computational resources, make it still the most used, as in the rest of industrial applications. A graphic summary is shown in Figure 24 and Table 2 shows the documents found.

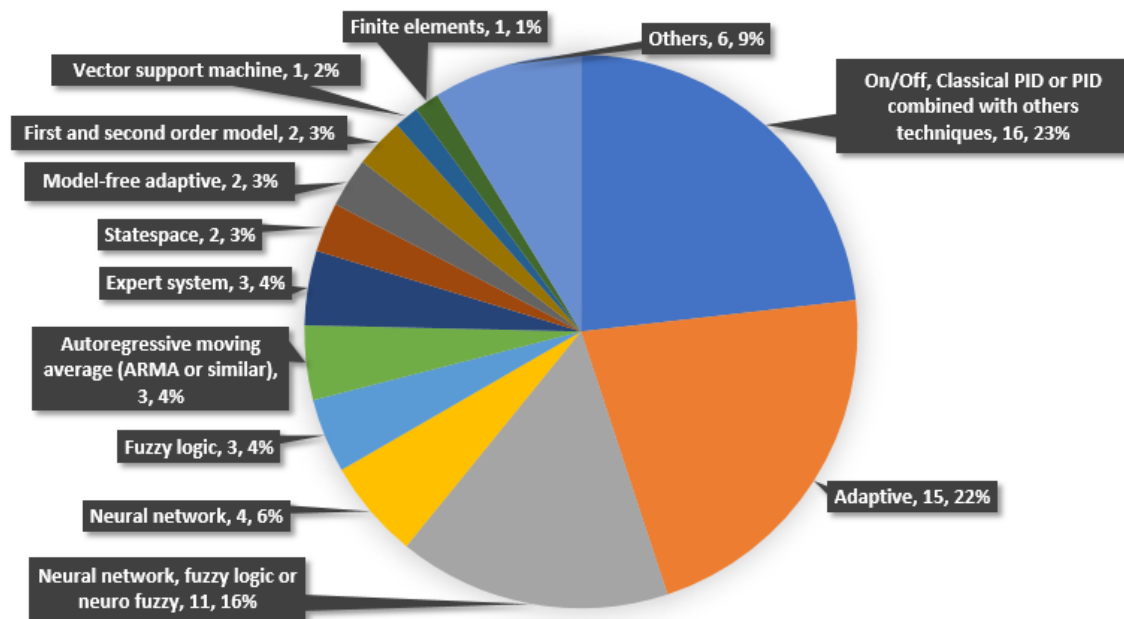


Figure 24 Graphic summary of the main methods or techniques used for control the geometry of weld bead.

Neural-networks, fuzzy methods and their combinations also stand out. Note that the magnificent behavior of the neural network can be clouded by a slow convergence because the excessive quantity of neurons or hidden layers. Many research efforts use this approach but neglected the need of quickly response of the control system.

Statistical methods, as the classic autoregressive moving average (ARMA) and expert systems, are represented too. Other less used techniques include: state space, model-free adaptive, first and second order model, support vector machine and finite elements.

Table 2 Methods or techniques used for modeling and control of the geometry of weld bead.

Model type or control technique	References	Quantity of references
<b>On/Off, classic PID or PID combined with other method</b>	(ANDERSEN <i>et al.</i> , 1990; BOUGHTON; RIDER; SMITH, 1978; BROWN; MEYN; WEBER, 1998; CHENG <i>et al.</i> , 2004; CHIN, 2001; DOUMANIDIS, CHARALABOS C., 1994; ICELAND; MARTIN E. O'DOR, 1971; LV <i>et al.</i> , 2014; MOORE; NAIDU; OZCELIK, 2003; NOMURA, H. <i>et al.</i> , 1980; SMITH, C.J., 1974; SMITH, JEREMY S.; BALFOUR, 2005; VORMAN; BRANDT, 1978; WIKLE III <i>et al.</i> , 2001; ZI <i>et al.</i> , 2012)	16
<b>Adaptive</b>	(BANGS; LONGINOW; BLAHA, 1989; BROWN; MEYN; WEBER, 1998; CHEN, HUABIN <i>et al.</i> , 2009; DOUMANIDIS, C.C.; HARDT, 1990; DOUMANIDIS, CHARALABOS C., 1994; HENDERSON, D E <i>et al.</i> , 1993; KOVACEVIC; ZHANG; RUAN, 1995; LU, WEI <i>et al.</i> , 2005; LV <i>et al.</i> , 2014; MOON, H.; BEATTIE, 2002; NIED; BAHETI, 1986; OZCELIK; MOORE; NAIDU, 1998; SUZUKI; HARDT; VALAVANI, 1991; WANG, ZHIJIANG; ZHANG; WU, 2012; ZHANG, Y. M.; LIU, 2003)	15
<b>Neural network and fuzzy logic, or neuro-fuzzy</b>	(BANERJEE; CHIN, 1992; CASALINO; HU; HOU, 2003; CHEN, S.B. <i>et al.</i> , 2000; CRUZ, 2014; DI <i>et al.</i> , 2001; LIU, Y. K.; ZHANG; KVIDAHL, 2014a, b; LIU, YUKANG; ZHANG; ZHANG, 2015; LIU, YUKANG; ZHANG, 2015; LUO, H <i>et al.</i> , 2002; WU, CS; GAO, 2006; YU KANG LIU; YU MING ZHANG, 2014)	11
<b>Neural network</b>	(CHENG <i>et al.</i> , 2004; TORRES, 2013; YAN, JUN RONG <i>et al.</i> , 2011; YANG, SANG-MIN <i>et al.</i> , 2007)	4
<b>Fuzzy logic</b>	(CHEN, HUABIN <i>et al.</i> , 2009; HUANG, XIXIA <i>et al.</i> , 2009; SHEN <i>et al.</i> , 2008)	3
<b>Autoregressive moving average (ARMA or similar)</b>	(DOUMANIDIS, CHARALABOS C., 1994; DOUMANIDIS, CHARALABOS; KWAK, 2002; XIONG; ZHANG, 2014)	3
<b>Expert systems</b>	(BANGS; LONGINOW; BLAHA, 1989; CHEN, S.B. <i>et al.</i> , 2000; DOUMANIDIS, C.C.; HARDT, 1990)	3
<b>State space</b>	(JOU, 2002; MOUSAVI; HAERI, 2011)	2
<b>Model-free adaptive</b>	(LÜ <i>et al.</i> , 2010; MOUSAVI; HAERI, 2011)	2
<b>First or second order model</b>	(DOMFELD; TOMIZUKA; LANGARI, 1982; HALE, 1990)	2
<b>Support vector machine</b>	(HUANG, XIXIA <i>et al.</i> , 2009)	1
<b>Finite elements</b>	(CASALINO; HU; HOU, 2003)	1

A generic diagram of a multivariable control loop of the weld bead geometry for GMAW process, are shown in the Figure 25. It used the main variables that affect the process, to control the bead geometry, but it should be noted that due to the interdependence between them, setting the controller parameters and the use of uncoupling becomes difficult.

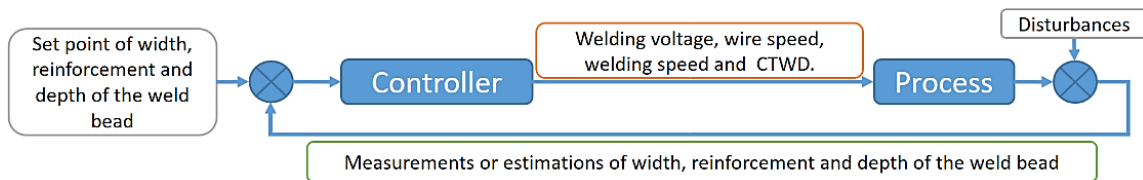


Figure 25 Main variables used in the bead geometry control in arc welding process.

It is important to note that the orbital welding adds more complexity to control, due to the effect of gravity on the transfer of material, the weld pool and the weld bead formation (SCOTTY; PONOMAREV, 2008), in addition to other requirements (DE GARCIA *et al.*, 2010). So, it is important to consider the orbital angle as a measurable disturbance.

### 2.3.1 Chronological development of the geometry control in arc welding process.

Developments in the field of automatic control of the geometry in the arc welding process have been intense in the last four decades. The most representative research efforts found in the literature in this area at the last two decades (and exceptions) will be discussed below and the rest are listed in Appendix 2.

In 1986 Nied (NIED; BAHETI, 1986) registered a patent where a robotic welding system has an integrated vision sensor to image and analyze the weld scene in real time. It used an adaptive feedback control to assure the full penetration, the weld puddle area and maximum width in TIG process. The adaptive control system determines a puddle geometry error and a correction to nominal welding current to change the heat input to the weld pool, regulating a combination of puddle area and width. Arc voltage is modulated to reflect changes in welding current and maintain constant arc length.

In 1989 Edmund R. Bangs and others (BANGS; LONGINOW; BLAHA, 1989), registered a patent that described a system for real-time welding adaptive control using infrared images, artificial intelligence (expert system) and distributed processors.

Already in 1990 Andersen designed an interesting control system for GMAW process (Anderson *et al.* 1990). A neural network set-point selector defines the start parameters of welding speed (V), current (I) and arc length (L). Other neural network estimates the width (W) and penetration (P). Two independently closed-loops PI adjust continuously the start parameters in function of weld bead width and depth penetration control error (see Figure 26). The experimental results are satisfactory. In (TORRES, 2013) a similar structure was proposed for the control of weld bead width, without the estimator and using a fuzzy controller. The same philosophy is used in (CRUZ, 2014) for width and reinforcement control in independent control loops.

Zhang *et al.* in (ZHANG, YU. M.; KOVACEVIC; LI, 1996) developed an adaptive control of full penetration for GTAW processes, based on the generalized predictive control (GPC) algorithm presented by Clarke in (CLARKE; MOHTADI, 1989; CLARKE; MOHTADI; TUFFS, 1987a, b). The controlled variables are the sag width and reinforcement of the weld bead, measured by a vision system and laser strip. The control variables are the welding current and arc length. The sampling interval of the control system is 0.5 s. The process has been described by a moving-average (MA) model with a predictive decoupling algorithm. The system is not controlling the penetration directly but has a good performance in the weld quality control.

Brown *et al.* (BROWN; MEYN; WEBER, 1998) designed a control loop with PID and an adaptive dead-time compensator for GMAW processes in a horizontal position. The controlled variable is the weld pool width and while the welding speed is manipulated. The simulation results show a good response.

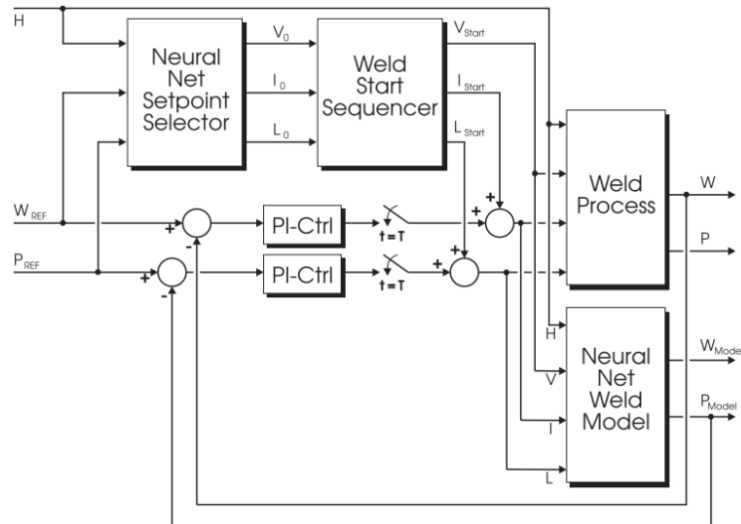


Figure 26 Control loop proposed for Andersen process (Anderson et al. 1990) when the initial set point condition are defined by neural network and the penetration are estimated (COOK, GEORGE E; BARNETT; STRAUSS, 1999)

A neural network dynamic model was designed in (CHEN, S.B. et al., 2000) to predict the maximum backside width in pulsed GTAW processes. Also, a self-learning fuzzy neural network controller was developed for control of the maximum backside width and the fuzzy rules were modified on-line. Based on the neuro-fuzzy, and combined with an expert system, a double-input and double-output (DIDO) intelligent controller was developed for controlling the maximum backside width and the shape of the weld pool. Experiment results showed the best behavior in the DIDO intelligent controller.

In (DI et al., 2001) a neuro-fuzzy controller is designed for the GTAW process. This technique overcomes limitations such as the dependency on the experts for fuzzy rule generation and non-adaptive fuzzy set. The adaptation of membership function as well as the self-organizing of fuzzy rule are realized by the self-learning and competitiveness of the neural network of 3 hidden layers. The simulation test obtained a good behavior.

Chin (CHIN, 2001) development a system for infrared image sense and PID control of the SAW process. He executed various tests with diverse conditions in the control variables. Similarly a point infrared sensor is used in (WIKLE III et al., 2001) to estimate the weld bead depth in GTAW and SAW process. The penetration is controlled indirectly (through infrared emission) by a PI regulator, that changes the welding current in the GTAW process and the welding voltage and speed in the SAW process. A good result is obtained under laboratory conditions.

Moon and Beattie (Moon & Beattie 2002) developed an adaptive fill control for the multi-torch multi-pass SAW process. The system measures the joint geometry with laser seam tracking and calculates the total area of the joint, computing by a numerical integration based on the actual joint profile and not one based on any idealized profile. With the area ratio of the joint the welding current/voltage combination is obtained and the welding speed is adjusted inversely in proportion to the area to be filled. The control improves the bead quality significantly. This technology has been used in longitudinal and spiral pipe mills and in pressure vessel production.

In (DOUMANIDIS, CHARALABOS; KWAK, 2002) two simultaneous but independent control loops are used. One senses the temperature with infrared camera and controls the torch trajectory. The other senses the geometric profile with laser stripe and controls the welding speed and wire feed speed. One variable delay Smith predictor is used for reducing the dead time effect of laser strip sensor. The author tested a SISO closed loop with PI controller and a MIMO GOSA. The last one obtains the best result.

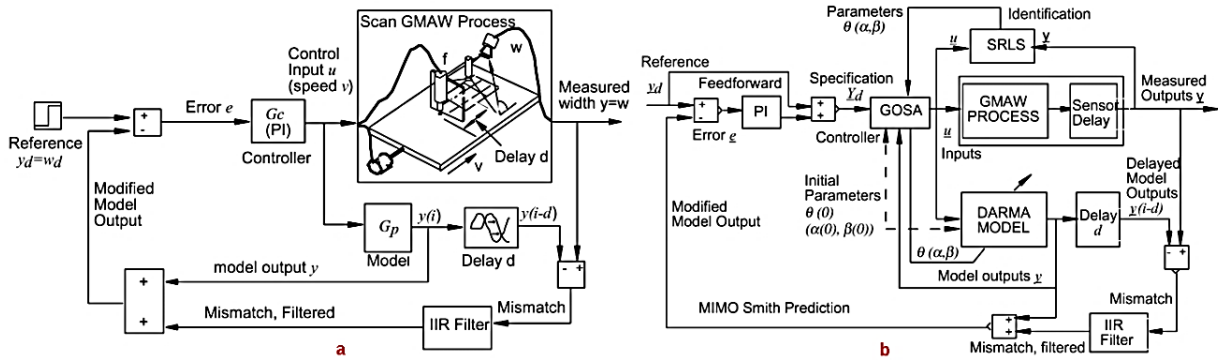


Figure 27 SISO (a) and DIDO (b) control loops that employ infrared information.  
Adapted from (DOUMANIDIS, CHARALABOS; KWAK, 2002)

A H-Infinity robust control system is proposed in (JOU, 2002) to control the length and width of the weld pool, regulating the welding current and the weld speed. The simulation shows an effective robust control method that is capable of controlling the processes with large uncertainties in the dynamics. However, the complexity of the H-infinity control algorithm can make the implementation in embedded devices difficult. Also, it needs an effective description of the uncertainties of the welding process dynamics and this is difficult under conditions of the real process.

A weld pool imaging system employing a LaserStrobe high shutter speed camera is used in (LUO, H *et al.*, 2002) to obtain contrasting images and eliminate arcing interference. Two image processing tools based on edge detection and connectivity analysis extract online information about the weld pool length and width. A neuro-fuzzy controller, based in human experience and experimental results, has been developed to control the welding feed speed in real time. Closed loop control of welding speed is used to achieve desirable weld pool geometry. The control results are satisfactory, but the response time was somewhat slow because the time required for the image processing and fuzzy calculation.

Similarly, in (MOORE; NAIDU; OZCELIK, 2003) the difficult to tune PI parameters to get desired performance in the whole range of the process operation is shown. Therefore, design and implementation of more complex controllers are required to obtain higher welding process control.

The Casalino method (CASALINO; HU; HOU, 2003) defines an automated methodology for selecting weld process parameters based on the artificial intelligence. Though many methods are available to improve the reliability of the traditional “open loop” type control schemes, they can only be applicable to use with a particular welding power source and a specific welding arrangement.

Lu *et al.* (LU, WEI *et al.*, 2005) developed a non-transferred plasma charge sensor based vision system for measuring the depth of the weld pool surface in the orbital GTAW process. The sensor measures the arc voltage when the arc current is off and obtains the arc distance by a linear inversely relation. An isolated gate bipolar transistor (IGBT) power module is utilized to temporarily switch off the main power supply. During this period, the large arc pressure associated with the main arc is not present so that the depth of the weld pool surface decreases and the sensor output increases. When the main arc is off, only the measurement arc is present and the sensing can be done automatically. An adaptive interval algorithm controls the depth of the weld pool surface, regulating the main-arc-on period. Four experiments were executed under different conditions and show good response.

Smith et al. (Smith & Balfour 2005) uses two independent PI to control a pulsed TIG process in horizontal position. Both controllers have the top face weld pool width error as input. The independent outputs are the welding current and the wire feed speed. Active adjustment of the current and wire feed rate allows a drift or variation in the weld pool size to be compensated for. A camera and the use of image processing algorithm, measures the top face weld pool width. A step change in plate thickness was used to test the controller. The result produced welds with a more consistent profile if variations in the process conditions occur.

In (YANG, SANG-MIN *et al.*, 2007) a three-dimensional vision system is used for obtaining the geometrical parameters of weld joint. A closed-loop neuronal-network controller is developed to control the width and depth of the weld joint, by regulating the welding voltage, welding speed and wire feed speed. The neuronal model has two hidden layers with 6 and 4 neurons respectively as shown in Figure 28. The validation results applied to the welding using the neural-network learning data and the error range of width and depth is within 3%.

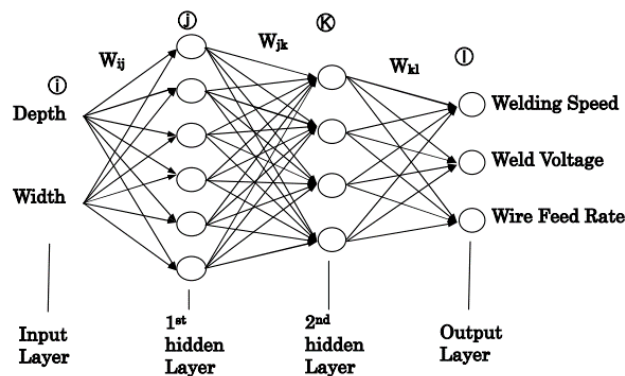


Figure 28 Neural network for determining weld parameters (YANG, SANG-MIN *et al.*, 2007)

A fuzzy and PID controllers are employed in (SHEN *et al.*, 2008) to control the geometry stability in a GTAW process, by regulating the welding current ( $\Delta I$ ) and wire feed rate ( $v$ ). A visual image analysis algorithm was developed for seam tracking and seam gap measuring. The control has been applied in the “teach and playback” robotic welding process, which helps the robot track the seam and chooses the corresponding welding procedures with the gap variation. The quality of the products has reached the standard of first-order welding seam in terms of dimensions and soundness as demonstrated by X-ray inspection. Figure 29 shows the block diagram.

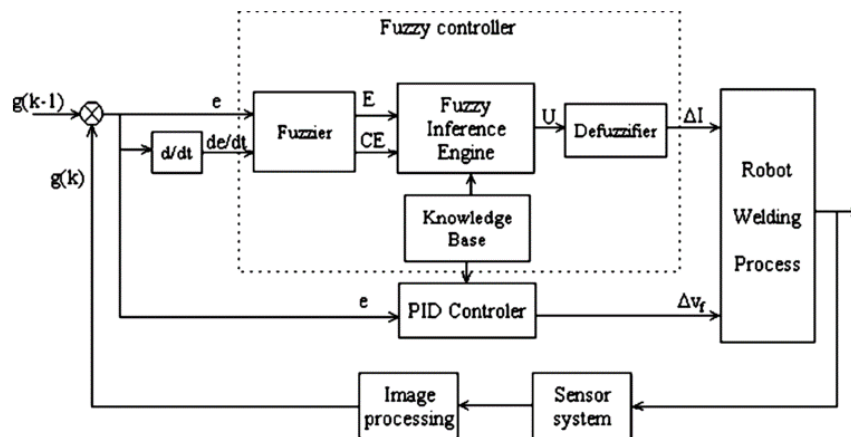


Figure 29 Block diagram of the weld pool controller (SHEN *et al.*, 2008).



In (LI; ZHANG, 2009) two SISO subsystems are developed to control the Double Electrode GMAW process. The control structure is selected for convenient implementation and design. One system controls the welding current of the main torch by manipulating its wire feed speed. The other controls the welding voltage of the bypass torch by manipulating its current. Two interval models have been obtained, based on experimental data from step-response experiments under different manufacturing conditions. These simple controllers show an acceptable behavior to control this relatively complex process.

Chen solved the full penetration detection, in orbital the GTAW process, with a vision system over the top-side pool and a neural network model for estimating the back-side weld bead width (CHEN, HUABIN *et al.*, 2009). The neural network has 17 neurons in the input layer, 40 in the hidden layer and 1 in the output. An adaptive controller receives the back-side weld bead width estimated by the neural network and regulates the peak current. A fuzzy controller received the gap state and controlled the wire feed speed. The experimental results, examined in X-ray, shown a uniform back-side weld bead width.

A adaptive inverse control based on support vector machine–fuzzy rules acquisition system is proposed by (HUANG, XIXIA *et al.*, 2009) for the pulsed GTAW process. The proposed adaptive inverse control method can automatically extract the control rules from the process data using an adaptive learning algorithm and a support vector machine to adjust the fuzzy rules. The controlled variable is the backside weld width and the control variable is the peak current of pulse. A double-side visual sensor system captures the topside and back-side images of the weld pool simultaneously. The data for model identifying is obtained experimentally. The control is simulated and shows satisfactory results.

Fenglin Lü and others (LÜ *et al.*, 2010) developed a MISO algorithm for the control of the width of the weld pool back side in the GTAW process. The vision sensing technology and model-free adaptive control (MFC) are used. The welding current and wire-feeding speed are selected as the control variable, and the backside width of weld pool is selected as the controlled variable. The main difficulty was the availability of computational resources to maintain the control period and the processing speed of the images within acceptable values. It has the disadvantage of using complex optical systems for obtaining the image of the back and front side of the weld pool. They propose the development of a MIMO system that adds the welding speed and reinforcement of welding bead.

In (MOUSAVI; HAERI, 2011) a space state model of the GMAW process is obtained to compare the behavior of three controllers: ARMarkov-PFC (based MPC controller), PI and feedback linearization based PID (FL-PID). The controller outputs are the wire feed motor voltage and the welding voltage. The controlled variables are the welding current and voltage. The simulation results show that the ARMarkov-PFC outperformed other controllers from the viewpoints of the transient response, desired output tracking, and robustness against the process parameters uncertainties, but require more computational resources. The FL-PID controller was sensitive to the process parameters variations, presence of noise and disturbance, and results in an improper performance. The PI controller produced inappropriate transient response and inadequate interaction reduction in spite of good tracking performance, low sensitivity to parameter variations and low computational resources requirements.

The main advantages of MPC over structured PID controllers are its ability to handle constraints, non-minimum phase processes, changes in system parameters (robust control) and its straightforward applicability to large, multivariable or multi-input multi-output (MIMO) processes. In spite of having many advantages, a noticeable drawback of an MPC is that it requires higher computation capability. (ABU-AYYAD; DUBAY, 2007).

The change in arc voltage during the peak current is used to estimate the weld penetration depth in a pulsed GMAW process (WANG, ZHIJIANG; ZHANG; WU, 2012). An adaptive interval model control system is implemented but, contrary to the author's comment, the control accuracy is not good.

Lui et al. (YU KANG LIU; YU MING ZHANG, 2014) developed a model-based predictive control for the orbital GTAW process. The control input is the backside weld bead width and the outputs are the welding current and welding speed. A nonlinear neuro-fuzzy (ANFIS) model is utilized to estimate the backside weld bead width (related with weld depth penetration) using the front-side weld pool characteristic. The Figure 30 shows a block diagram of this approach.

In (XIONG; ZHANG, 2014) the GMAW LAM process is modeled using the recursive least squares algorithm for system identification. An image processing algorithm is employed for obtaining the nozzle to top surface distance. An adaptive controller adjusts the deposition rate and keep the nozzle to top surface distance constant. The precision range of the control system is limited within  $\pm 0.5$  mm.

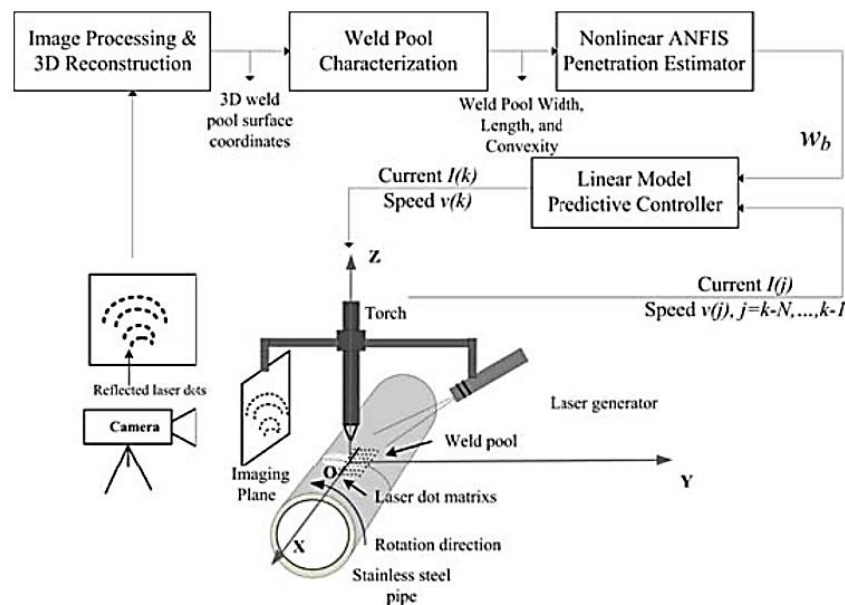


Figure 30 Model-based predictive control to orbital GTAW process (YU KANG LIU; YU MING ZHANG, 2014)

A segmented self-adaptive PID controller was developed in (LV *et al.*, 2014) to controlling the arc length and monitoring the arc sound signal in the pulsed GTAW process for flat and arched plate. The experiments show that the controller has an acceptable accuracy.

Lui and Zhang (LIU, YUKANG; ZHANG, 2015) developed a machine-human cooperative control scheme to perform welder teleoperation experiments in the orbital GTAW process. They developed an ANFIS model of the human welder's adjustment on the welding speed. The welder sees the weld pool image overlaid with an assistant visual signal, and moves the virtual welding torch accordingly. The robot follows the welder's movement and completes the welding task. The experimental data is used to obtain the model. Later, they transfer this model to the welding robot controller to perform automated welding. The controller receives the 3-D weld pool characteristic parameters (weld pool length, width, and convexity) and change the welding speed. In other similar work (LIU, YUKANG; ZHANG; ZHANG, 2015) a neuro-fuzzy-based human intelligence model is proposed for implementing an intelligent controller to maintain a full penetration by governing the welding current. These works establish a method to rapidly transform human welder intelligence into welding robots by using 3D weld pool surface sense, fitting the human

welder response to the information by a neuro-fuzzy model, and using the neuro-fuzzy model as a replacement for human intelligence in automated systems. In a previous work (LIU, Y. K.; ZHANG; KVIDAHL, 2014a, b) correlated the skilled human welder response to the fluctuating 3D weld pool surface and compared with a novice welder.

#### 2.4 Embedded devices in welding process control.

Embedded systems, especially the FPGA and System on Chip (SoC), are used in a multitude of technological processes in various industries, covering hazardous areas such as medical, aerospace and military, or even the most common household appliances.

With the increase in processing capabilities of these systems, based on microcontrollers and new processors generation, it is possible to obtain remarkably improved measurement and control systems with the use of advanced algorithms for processing information provided by the sensors. The parallel processing capabilities of the FPGA (into the SoC) allow execution times lower than in processors or microcontrollers. These capabilities are important to estimators based in neural networks (parallel execution) and to control systems in real time that needs attend several sensors and actuators.

The FPGA have numerous digital inputs and outputs, with the possibility of adding several analog and other peripherals. Many of them have a hard processor, with one or more cores and various peripherals for communication, video, sound and large Random Access Memory (RAM) capacity, where you can run a standard operating system interconnected with the FPGA. These features and small size, low power consumption, low heat dissipation and reconfigurable architecture, make it an ideal tool for monitoring and control systems with real time requirements.

The literature review does not show the application of FPGA to bead geometry control in arc welding process. But other works, related with welding, as the weld pool volume control (DAVE; COLA, 2013), the images processing (NEFEDYEV; GOMERA; SUDAKOV, 2014) , the wire feed control (YANG, FU; ZHANG; ZHANG, 2013), the defect detection (HURTADO; ALFARO; LLANOS, 2012; LLANOS; HURTADO; ALFARO, 2016; VELASCO, 2010) and the arc signal monitoring (MACHADO *et al.*, 2012; MILLÁN; QUERO; FRANQUELO, 1997), were found. This prove that the FPGA can be useful for this research and is a new field of application for this technology. A graphical summary is shown below.

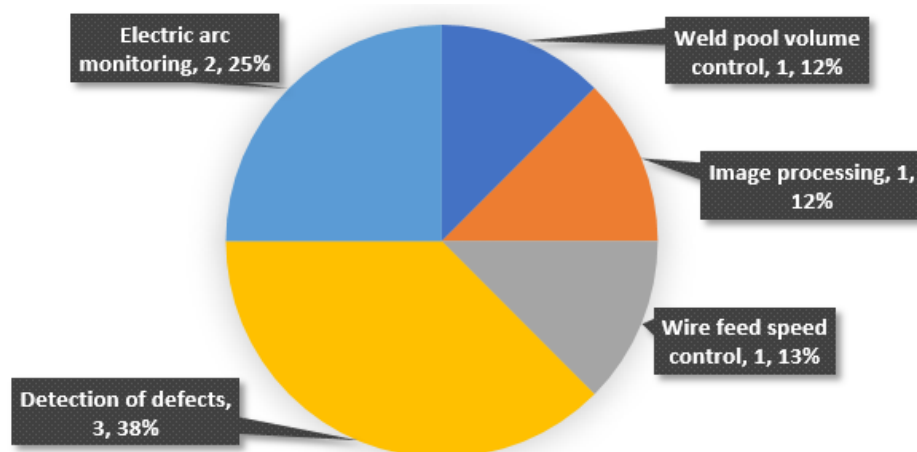


Figure 31 Embedded devices in welding process.

## 2.5 Chapter considerations.

Based on the literature review about measurement of welding bead geometry, this work selected the thermographic and arc welding variables to obtain the information for estimating the geometry of the weld bead.

The artificial neural network algorithm was selected to fusion the measurements and obtain the estimate values of depth and width of the weld bead.

### 3 Methods and tools.

In this work, an experimental system was developed to collect the values of the selected variables and to send stimulus to GMAW process, allowing the open loop control and data storage in a personal computer. The methods and tools used to data processing and estimate the depth and width of the weld bead are discussed in this chapter.

The general structure of a data acquisition and control system involves a measuring system, a control system and an actuator system. The measuring system collects and processes the sensor's measurements, estimates or predicts the not measurable variables values and saves the data. The control system calculates the control strategy and manipulates the process inputs, through the actuator system, to achieve the desired behavior in its output.

When the control strategy is based on the measurements received from the data acquisition system through any feedback channel, the control system operates in a closed loop (see Figure 32). When the controller does not receive information from the measurement system, the control system operates in an open loop (see Figure 33). In this case, the control strategy is defined by an operation sequence or a human operator.

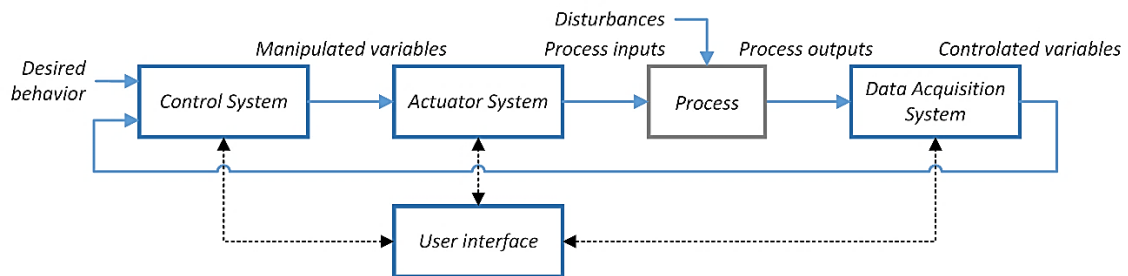


Figure 32 Block diagram of the data acquisition and closed loop control system architecture.

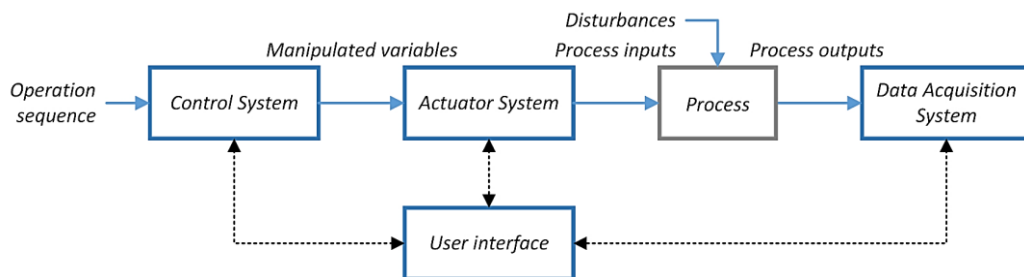


Figure 33 Block diagram of the data acquisition and open loop control system architecture.

Disturbances affect the behavior of the process and can cause instability and a significant control error in open-loop systems. These can be measurable or not measurable. Measurable disturbances can be compensated with anticipatory or feed-forward control systems.

A user-friendly interface is also required that allows the easy configuration of the controller operating parameters and monitor the state of the process. The complexity of each system fluctuates according to the number of variables involved as well as the quantity and complexity of control loops and the processing algorithms, among others.

The variables measured by the developed system are: welding voltage, welding current, infrared thermography and welding torch (or work piece) position. The system controls the welding speed and sends several set points to the welding power source such as the set point of welding voltage and the set point of the wire feed speed. Despite this, the control is in open loop because the system does not use the measurements to change the welding parameters and follows a sequence defined by the user.

The data acquisition and open loop control system has six main components: the welding power source, the welding table, the thermographic camera, the laser scanner, the data acquisition and control interface and the computer where a data acquisition and stimulus sequence design software are executed (BESTARD; ALFARO, 2017). The components, the data flow and a schematic side view are shown in Figure 34.

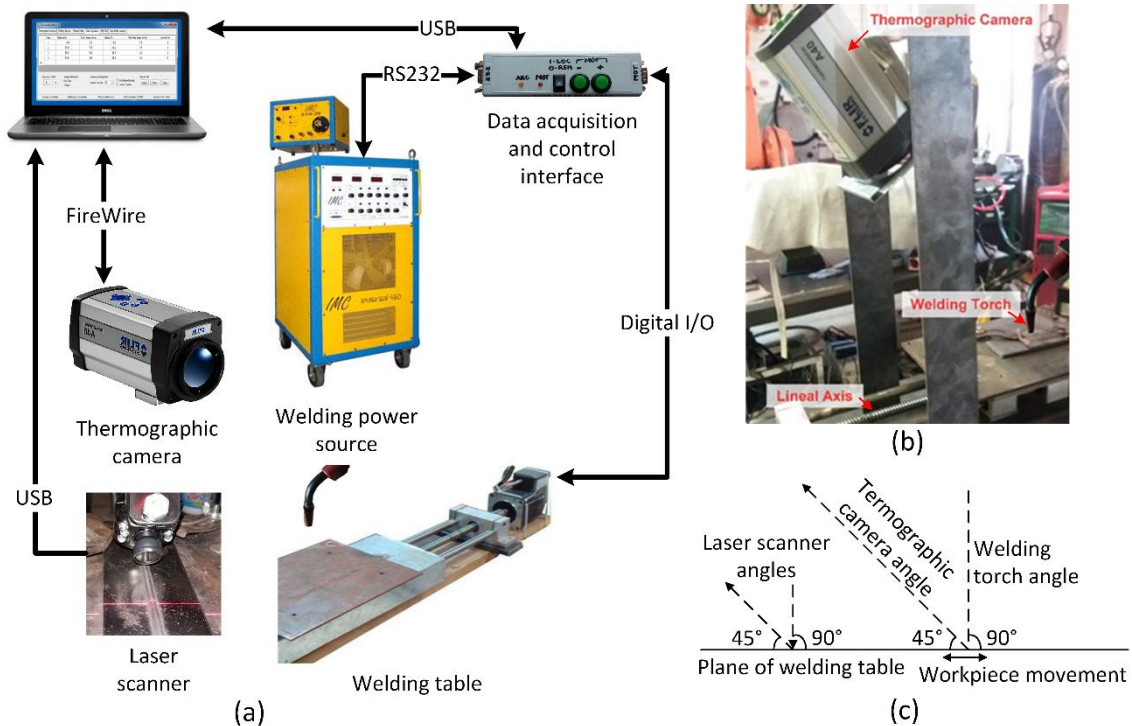


Figure 34 Data acquisition and open loop control system: (a) Main components and data flow; (b) Flat welding table and instruments support; (c) Schematic side view.

The main components, algorithms and software developed for the data acquisition and open loop control system are described below.

### 3.1 Data acquisition system

The measuring system for this work involves the measurement of the infrared data, weld bead profile and arc variables. It also provides the feature extraction of this data, the estimation of the depth and width of the weld bead, and others necessary calculations in the data processing algorithm. The next sections describe each subsystem of the measuring system.

#### 3.1.1 Measurement of the welding voltage and welding electric current.

The welding power source Inversal 450 has an RS232 interface to read the operation parameters (see section 3.2.1). This allows the acquisition of values of the effective welding voltage and the welding electric current with 2ms (or less) of sampling time.

The analog to digital converter of this measurement system has 10 bits. The input range (or span) for the welding voltage is 0 to 68V, obtaining 0.07V of resolution. The input range for the welding electric current is 0 to 450A, obtaining 0.44A of resolution (FRADEN, 2004; IMC-SOLDAGEM, 2005).

#### 3.1.2 Measurement of the welding speed.

The control interface (see section 3.3) has the control of the stepper motor driver that moves the workpiece. The welding speed is obtained directly from the registers in the interface.

### 3.1.3 Measurement of the weld bead profile.

The weld bead dimensions must be checked after finishing the welding process to verify the project requirements and the behavior of the model (see section 3.1.8).

A scanner or profilometer was developed to obtain a three-dimensional profile of the weld bead geometry after the completion of the welding process. Its operation is based on the triangulation technique and image processing algorithms was explained in section 2.2.3. The scanner uses a laser that draws a line on the weld bead, a low-resolution camera with USB communication (webcam of 600x400 pixels, 0.24 MP) and an optical filter adjusted to the laser emission frequency. This is shown in the Figure 35.

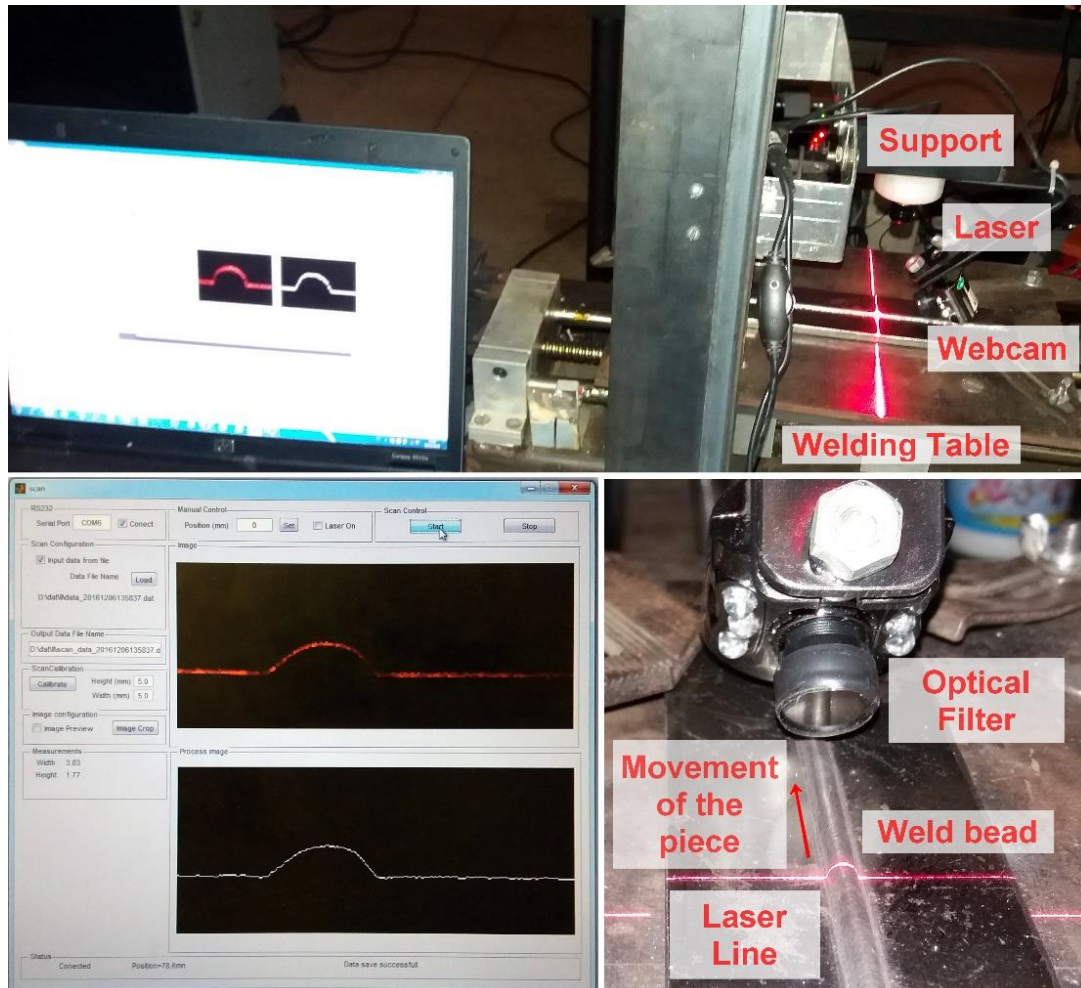


Figure 35 Low cost laser profilometer components.

The workpiece remains fixed on the welding table after the welding is finished and the control interface moves the workpiece to the position of the scanner. A program developed in Matlab/GUI, takes the image from the webcam and applies the image processing algorithm. The image is filtered and the missing data is completed. The algorithm rotates the image to find the base line corresponding to the surface of the base metal and thus calculates the reinforcement and width of the bead (see section 3.1.4). The procedure is valid only for flat parts. The Figure 35 (below-left) shows the image obtained by the camera for the current position in red and the calculated profile in white.





of the profile. The maximum reinforcement is obtained on the center segment. The dotted horizontal lines define this maximum value and the base line. The joint dimensions can be obtained using a similar analysis but flipping the profile in the  $y$  axis.

### 3.1.5 Infrared measurement.

The thermographic camera ThermoVision A40 (see Figure 34) is used to obtain the temperature values (based on infrared measurement) from the weld pool. It employs a semiconductor sensor of focal plane array uncooled microbolometer technology. It has a spectral range between 7.5 and 13  $\mu\text{m}$ , a temperature range between  $-40^\circ\text{C}$  and  $2000^\circ\text{C}$ , a sample frequency of 120 Hz (120 frames for second) and a maximum resolution of 16-bit monochrome and 8-bit color (FLIR-SYSTEMS, 2004). The data is obtained from a Firewire interface in matrix format, with the temperature of each pixel of the image. Among other notable features, it has automatic correction of the measurement by the effects of environmental reflection, temperature, distance, relative humidity and external optics that could have coupled.

The emissivity of the weld pool is not constant, so the temperature measurements of the weld pool using a thermographic camera should be considered approximate (see section 2.2.4). The accurate measuring of the absolute values of temperatures is not considered significant for the purposes of this work. In this work we used absolute values and not the calculated temperature values based in emissivity coefficient.

### 3.1.6 Feature extraction of the infrared image.

The infrared image is processed with a feature extraction algorithm developed to obtain the thermographic peak ( $T_p$ ), the base plane ( $T_b$ ), the curve width ( $T_w$ ), the area ( $T_a$ ) and the volume ( $T_v$ ) parameters. These values are used in the estimations of the depth and width of the weld bead explained in the section 3.1.8 . The block diagram is shown in the Figure 38.

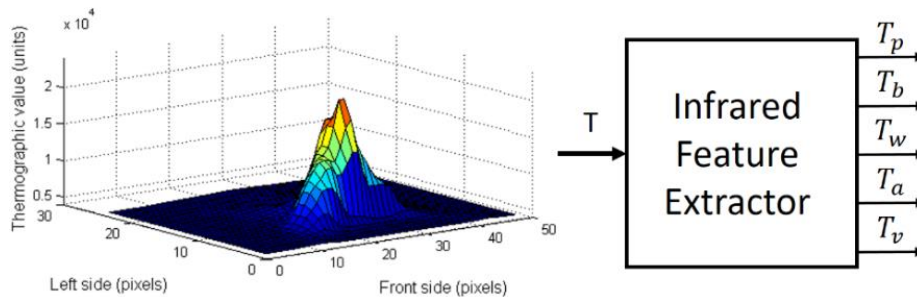


Figure 38 Infrared feature extraction block.

The thermographic matrix (supplied by the camera) is processed with a moving average filter of 3x3 pixels. The thermographic peak or maximum value of the matrix is calculated. The base plane is calculated as the average of 10% of the values in the left and right edges (left and right side, see Figure 39 down left). The boundary plane is 10% above the base plane.

The intersection plane between the thermographic surface and the boundary plane is the area and the maximum width in the front axis (front side in the Figure 39 down right) is the width. The sum of the thermographic values within the intersection plane is the thermographic volume.

In this image, it is possible to observe the two peaks present in several images of the thermographic profile and the difference with the Gaussian curve. This characteristic makes the first or second derivative analysis to determinate the width of the profile inaccurate.

This algorithm is very simple and can be implemented in an FPGA or microcontroller device.

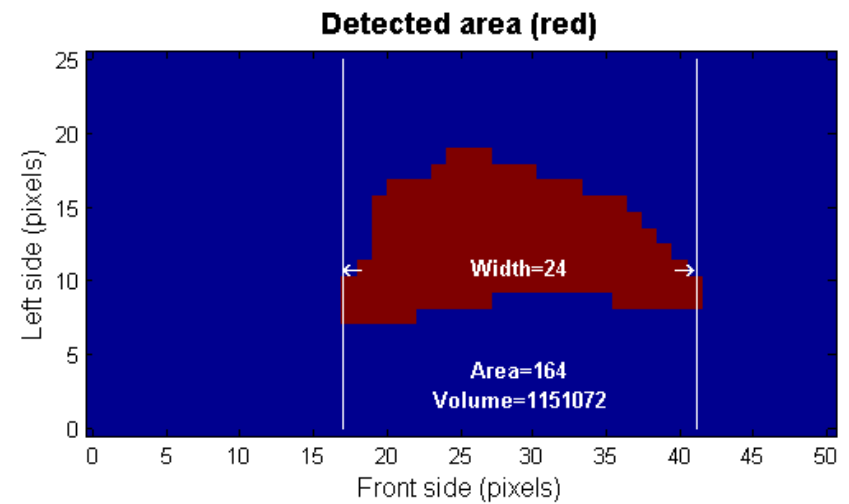
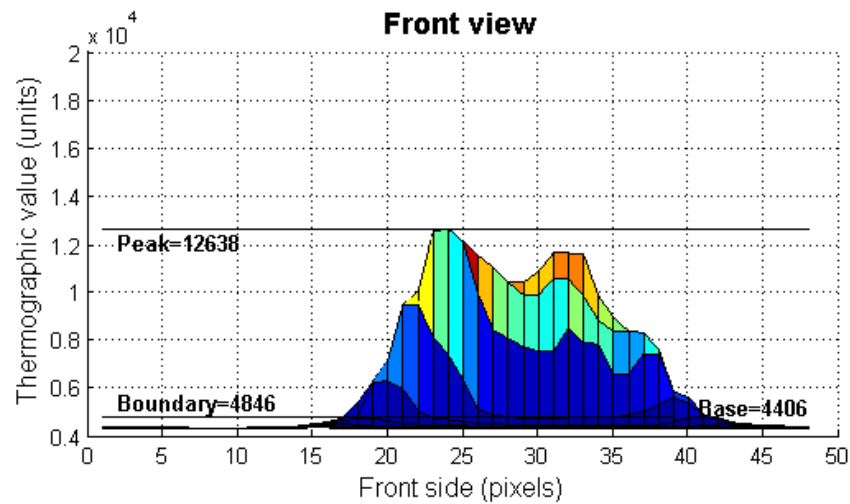
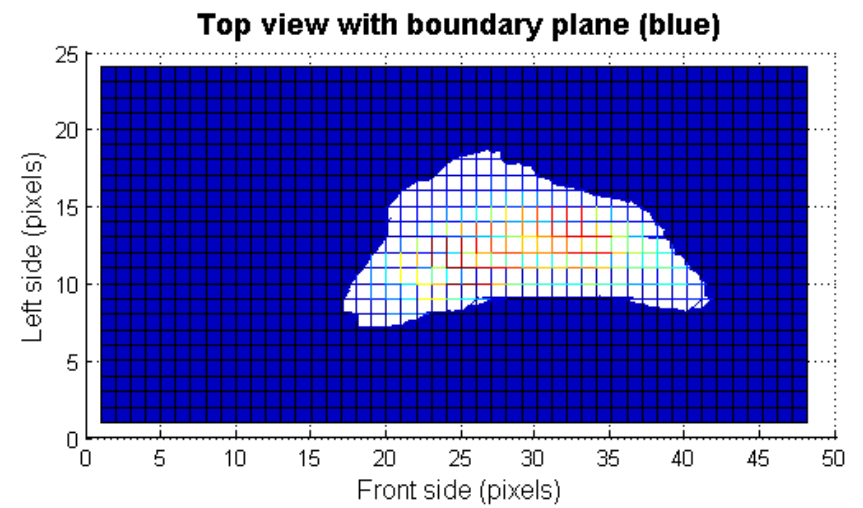
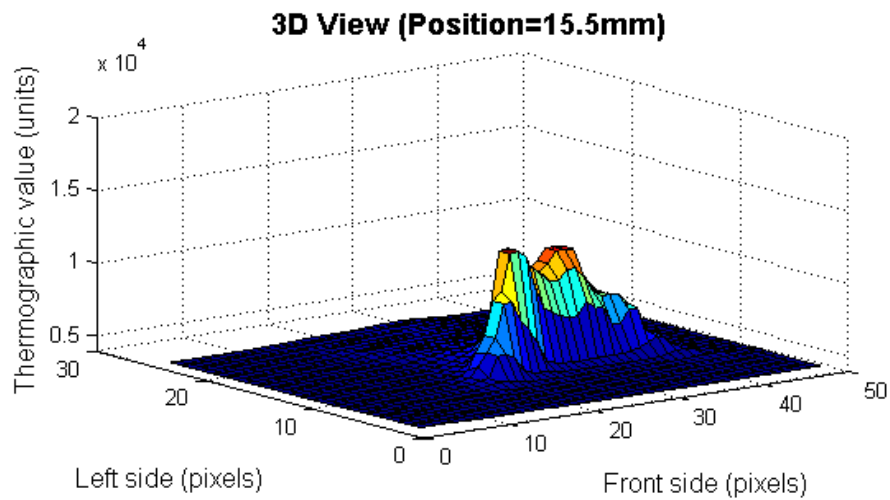


Figure 39 Features extracted of the infrared images.

### 3.1.7 Image processing for offline measuring of the weld bead depth.

The weld bead depth profile can be obtained from the macrographic analysis. For this, the cuts for the macrographic analysis are made in a longitudinal direction, this is in the direction of the torch movement. Could be necessary more than one cut due a bad alignment of the cut tool with the weld bead. In these cases, we take the maximum value in each measurement point.

In the processing, the specimen will be polished and etched using 2.5% nital solution (or it was etched by 3%  $\text{HNO}_3$  and 97%  $\text{H}_2\text{O}$  nital solution) to display the weld bead penetration. In similar position as shown in the Figure 40, a picture will be taken and analyzed with image processing algorithms.

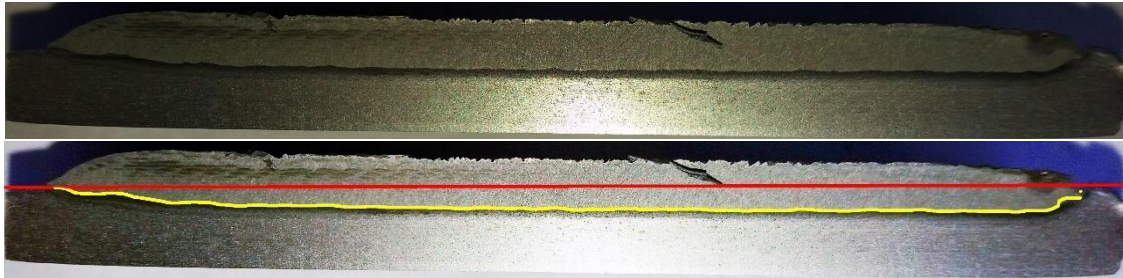


Figure 40 Longitudinal cut of the weld bead (above). Weld bead depth profile (yellow line) and base surface (red line) on the same picture (below), obtained using image processing algorithms.

The algorithm corrects image misalignment and filters the image for the border detection procedure. The base line (show by red color in the Figure 40) is detected. The piece thickness and length are known and used to calculate the scale coefficients. The penetration limit is detected (shown by the yellow color) and the difference between it and the base line produce the weld bead depth penetration profile. The profile is filtered and the missing values are repaired with the interpolation method. The algorithm was developed in Matlab scripts.

### 3.1.8 Sensor fusion for estimating the depth and width of the weld bead.

A cooperative, data-in/data-out and centralized sensor fusion [15] algorithm was developed based on a Multilayer Perceptron (MLP) artificial neural network to estimate two characteristics of the weld bead geometry. The same MLP structure is used to estimate both the weld bead depth ( $\hat{D}$ ) and the weld bead width ( $\hat{W}$ ), by changing the input parameters of the welding current ( $i$ ) to the welding voltage ( $u$ ). It is possible because both estimators have the same neural network structure and a selection signal is used to change the parameters (weights), the inputs and the output of the network. A controller performs the evaluation of two algorithms in sequence, updating the weights of the neural network for each case.

The artificial neural network has eight neurons in the input layer, twelve in the hidden layers and one in the output layer. The size of the hidden layer was selected by balancing the computational cost (neuron quantity) and the estimation error, by testing different configurations. The structure of neural network is shown in Figure 41.

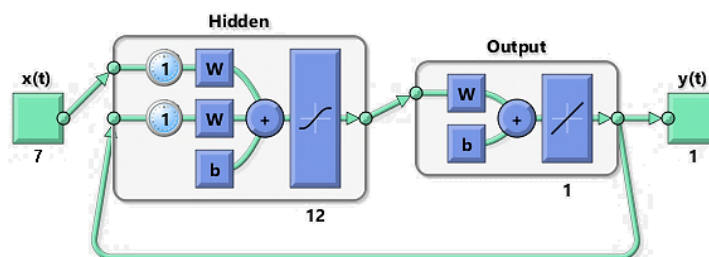


Figure 41 Neural network structure for estimate the depth and width of the weld bead.

The inputs variables are the thermographic peak ( $T_p$ ), the thermographic base ( $T_b$ ), the thermographic area ( $T_a$ ), the thermographic volume ( $T_v$ ), the thermographic width ( $T_w$ ), the measurements of welding current or voltage ( $iu$ ) in the actual ( $nT$ ) and previous sample ( $nT - T$ ), and the previous estimated value [ $\widehat{D}W(nT - T)$ ] for capturing the process dynamic. The symbol  $T$  is the sample time and  $n$  is the sample number. The activate function is the hyperbolic tangent sigmoid transfer function (MATHWORKS, 2017). The network training should be done with experimental measurements of the parameters of input and output, and using the backpropagation algorithm. The input data is normalized in the Matlab neural network tool. The Figure 42 shows the block diagram of the estimator.

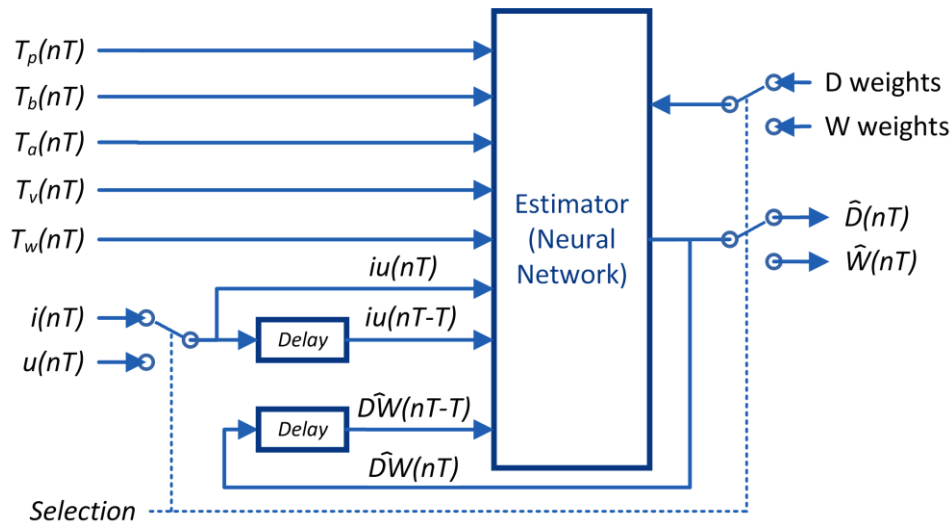


Figure 42 Estimator of depth and width of the weld bead that uses the thermographic features with welding current or voltage in cooperative mode.

The relation between inputs and outputs of the models is explained on the basis of the power density concept as proposed by Ponomarev and Scotti (SCOTTY; PONOMAREV, 2008). From the thermal point of view, it can be expected that the more concentrated (smaller diameter arcs) and intense (higher current) the heat is, the deeper the penetration of the molten metal.

The **Selection** signal allows the switching between the estimation of the weld bead depth or the weld bead width. To estimate the weld bead depth, this algorithm uses the features of the infrared image and measurements of the welding current as indicators of the energy delivered (welding energy) and the last value of the weld bead depth. The welding voltage and the last value of the weld bead width are used to estimate the weld bead width. The values of neural network weights are changed to by the selector.

For the training and validation of the neural network, the input values of the thermographic and arc variables are obtained from the data acquisition system and infrared feature extraction algorithm (see section 3.1.6). The real values of depth and width of the weld bead are obtained from the macrographic analysis (see section 3.1.7) and the laser scanner (see section 3.1.3) respectively.

These models of estimators are valid only for the current process conditions and must be updated if these change, such as electrode diameter and material, base material, gas type and flow rate, welding current or welding voltage range, among others.

Several programs were developed for data processing and data plot. All the curves, the statistical analysis, the image processing and the neural network training and testing were made in Matlab scripts.

We must emphasize the importance of simplifying the estimating algorithm due to real-time requirements. The use of the proposed parameters and not the complete infrared image, can help reduce the resources used and increase the speed of the estimation process. The same structure for the estimation of two parameters in sequential mode minimizes the hardware requirements, but increases the processing time. If less processing time is required and the hardware resource is not a problem, two equal neural networks can be used. The implementation and synthesis of the neural network can be done with the methodology and tools proposed in (AYALA, HELON *et al.*, 2016; AYALA, HELON VICENTE HULTMANN *et al.*, 2017). Ayala et. al shows a floating-point implementation in hardware for neural network architecture that guarantees low time rates.

### 3.2 Actuator system.

The actuator system is in charge of changing the process status. It is made up of the welding power source and the welding table. The first manipulates the arc conditions directly while the second does the movement of the torch or the piece. These two sub-systems will be described in the next sections.

#### 3.2.1 Welding power source

The welding power source selected is an Inversal 450 (see Figure 34), developed by Brazilian IMC-Soldagem company (IMC-SOLDAGEM, 2005). This power source is a multi-process machine, with digital control executed by a microcontroller device and IGBT for generating the electric arc. The principal advantage for this application, in contrast with the other welding power sources available in the GRACO Laboratory, is the open communication protocol over the standard serial RS232 interface.

With the available information and the serial interface, it is possible to remote control of the welding power source. The controller can modify all the operation parameters and obtain the measurements and status of the machine. For example, in the GMAW constant voltage process, it is possible to modify the welding voltage, the speed and direction of the wire feed, the pre-gas and post-gas time, the phase out time, the inductance and the open or close arc command. Also, the control system can read the real welding voltage and real welding electric current. The main characteristics of the welding power source are shown in Table 3.

*Table 3 Inversal 450 welding power source characteristics (IMC-SOLDAGEM, 2005).*

<b>Parameter</b>	<b>Value</b>
Alimentation voltage	220, 380 or 440 V Three-phasic
Open circuit voltage	68V
Nominal electric current	280 A
Maxima electric current	450 A
Electric current at 100% of duty cycle	280 A / 35 V
Nominal power	13 kVA
Power factor	0.95
Dimensions	0.5 x 0.6 x 1.2 m
Weight	170 kg
Cooling circuit	3.5 L of distilled water

The communication algorithm for remote control and data acquisition was developed based in the RS232 communication protocol. A state machine, implemented in the microcontroller of the control interface (see section 3.3), defines the operation parameters and obtains the measurements and status of the welding power source.

The operation sequence for controlling the welding power source and the data acquisition software was also developed as shown in Figure 43. This sequence uses a state machine and is repeated continuously into the main program of the microcontroller (see Figure 46).

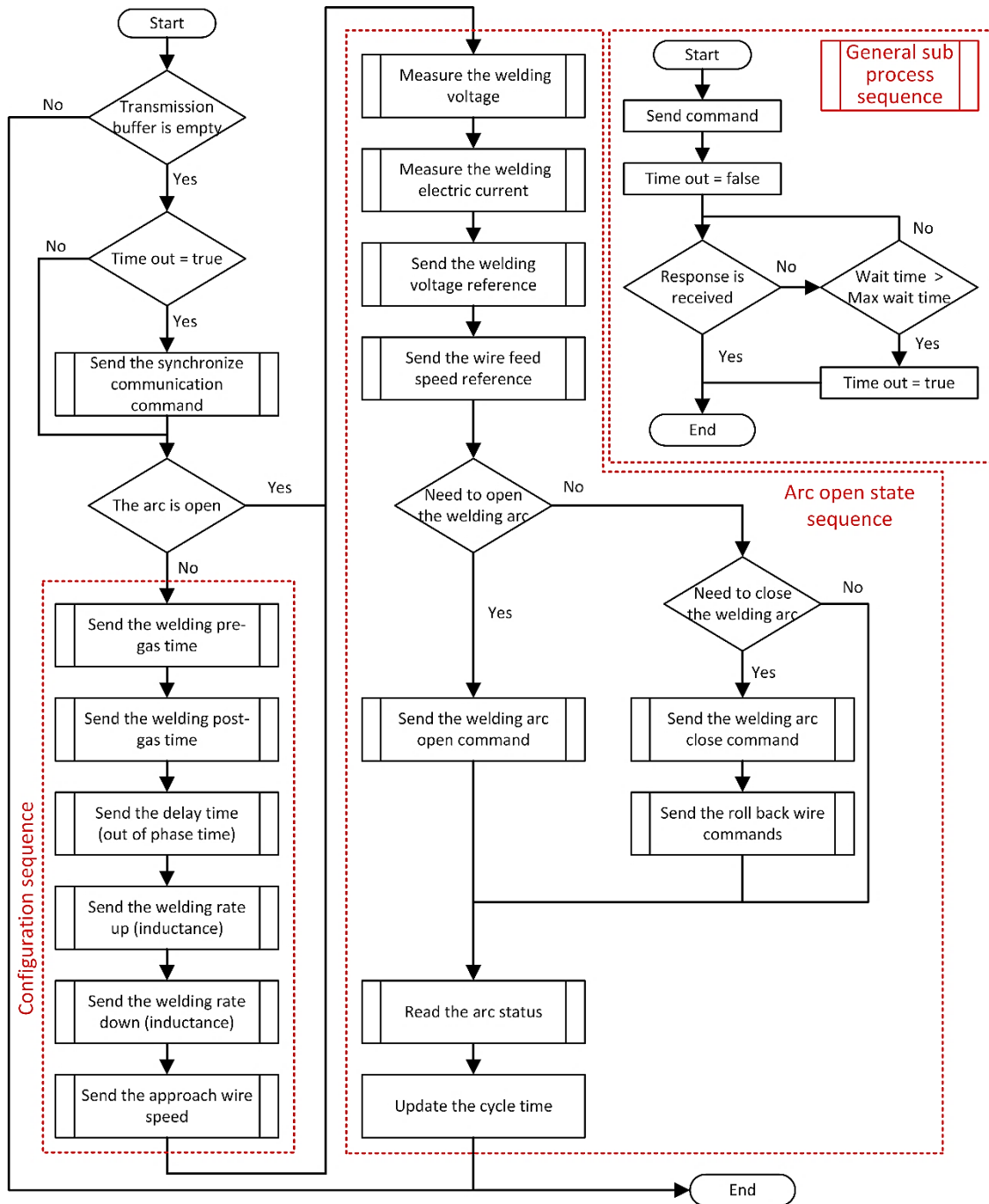


Figure 43 Welding power source operation sequence for the process control and data acquisition.

The sequence is started only if the RS232 transmission buffer is empty. When the interface sends a command, a timer is activated. If the value of the timer is greater than the maximum response time, the time out flag is activated and the program execution exits the sequence. In the next cycle, if the time out flag is true, the synchronization command is sent to the welding power source and the communication is reset.

The sequence has two blocks: the configuration and the arc open state sequence. To increase the data acquisition speed, the configuration parameters are sent to welding power source only

when the arc is closed. The necessary commands for process control are executed all the time, including the open and close arc sequence when necessary.

When the arc is closed, the wire feed direction is inverted and the wire feed speed is increased by a few milliseconds. This roll back wire prevents the trapping of the wire in the welding bead. Finally, in each cycle, the arc status is read and the cycle time is updated. In this algorithm, the measure unit conversion, the numerical formats conversion and the treatment of communication errors are necessary.

In the development of the communication algorithm and the operation sequence, the author received invaluable support from Professor PhD. Raul Gohr Jr, of the IMC-Soldagem company.

### 3.2.2 Flat welding table.

The electro-mechanical system, integrated for a linear axis of 5 mm of movement by revolution and a stepper motor of 1.8 grades by step, are used to move the piece, keeping the welding torch fixed. The support structure of the thermographic camera and the laser scanner were developed as shown in the Figure 34.

This system, development by GRACO students (FRANCO, 2008), has a stepper motor controller circuit with signals for modifying the stepper time (speed) and the direction. Other signals show the status of the system and protect against overload (GMBH, 2006). This structure supports 15 Kg of load and 15 mm/s of maximum speed.

### 3.3 Open loop control system.

The control system is mainly located in the data acquisition and control interface, but it has a close relationship with the Data Acquisition module of the data acquisition and stimulus sequence design software (see section 3.4).

The control interface synchronizes the movement of the workpiece with the welding power source operation and obtains the process measurements in real time. The interface is connected to the welding power source through an RS232 port, to a computer through an USB port and to the stepper motor driver circuit by digital signals, as shown in Figure 34a.

The simplicity and small size of the interface (since its larger complexity is in the firmware) as well as the low cost of its components are shown in Figure 44. In the figure one can also see the manual controls that move the welding table, the remote or manual operation selector, the motor on and open arc indicators, and the external connections. A small piezoelectric horn emits sounds indicating the start or the end of welding sequence or if an error occurs.



Figure 44 Data acquisition and control interface.

The electronic circuit developed for the interface is shown in Figure 45. The interface needs a power source between 7V and 24V, which plug in to the P1 connector. The USB and RS232 communication wires are connected to P2 and P5 respectively. The motor driver is plugged in P6. P3 gets the state of pushbutton and switch, and driver the light indicators in the panel. In P7 are plugged the limit detectors of the welding table. P4 is used for programming the microcontroller.

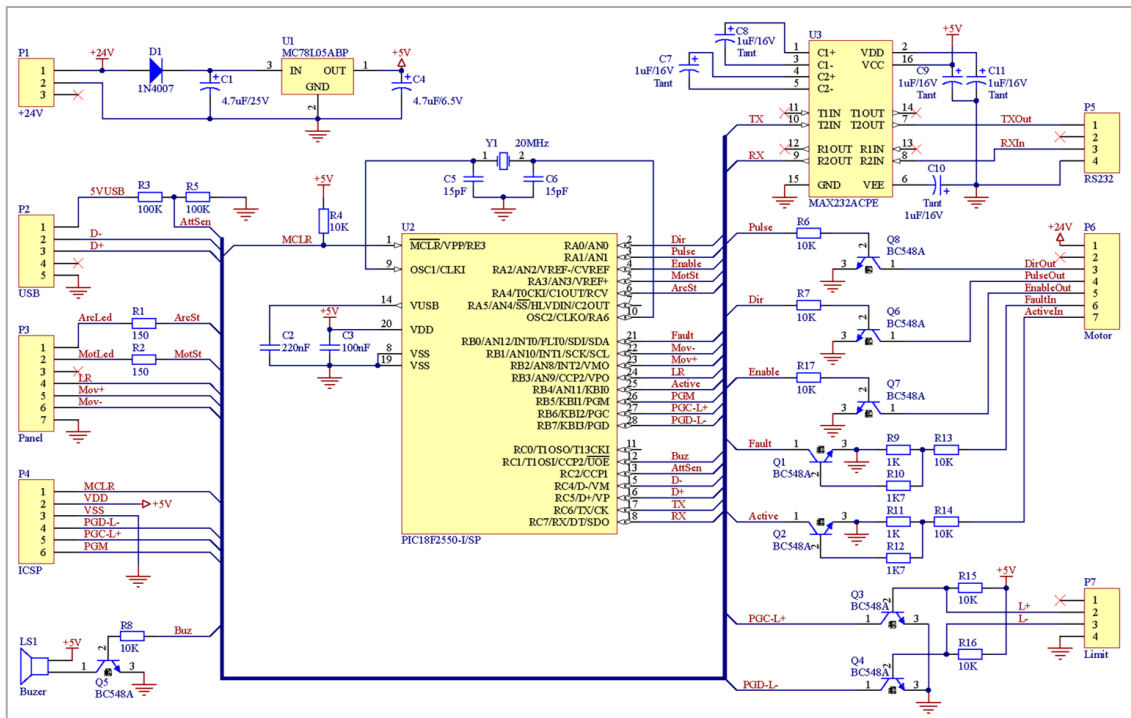


Figure 45. Electronic circuit of the data acquisition and control interface.

The operation is totally controlled by a microcontroller PIC18F2550. Before starting the welding, this microcontroller receives from the computer, the sequence of values to be sent to the welding power source in each position of the work piece. These values are fixed by the user in the data acquisition program (see section 3.4). The start and end point of the weld, the movement speed and the sampling period or the distance between samples are defined by the user according to the selected work mode.

Following that, the interface has an autonomous and independent operation and sends to the computer the measurements obtained in each position in real time. The acquisition program (synchronized with the interface) obtains the thermographic data regardless of the clock or priorities of the operating system. The main loop of the firmware is drawn in Figure 46.

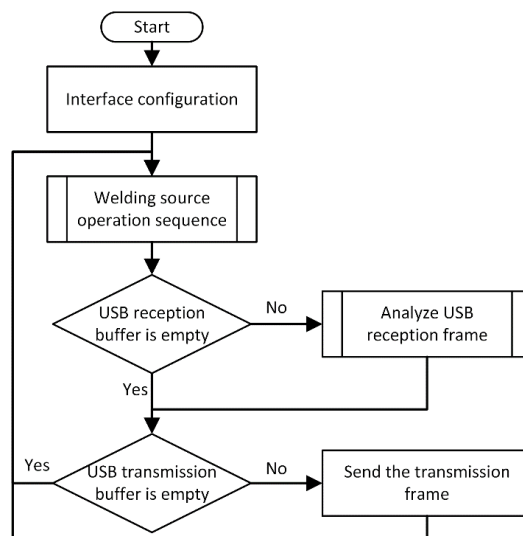


Figure 46 Main loop of the data acquisition and control interface.



The development of the interface requires a detailed study of the welding power source communication protocol and numerous tests. To control and sample the operation of the welding power source, a state machine was used, minimizing the communication time to ensure an acceptable sampling period (see section 3.2.1)

A communication protocol between the interface and the computer was created, based on ASCII characters. This allows the full control of the welding power source, the welding table, the interface and the operation sequence of the process. The interface controls the driver circuit of the stepper motor and verifies the occurrence of an error by the feedback signal. The processing of these signals is done by timer interruptions, which are adjusted by the step time.

Two modes of operation are available for data acquisition. One is based on a sampling time and is controlled by a timer interruption between 5 to 500 ms. In this mode, in each interruption a data set is sent to the computer. It has the disadvantage that by varying the speed of movement the distance between samples will vary.

The other mode is based on comparing the position increment with a steep value pre-set by the user. Once this increment is equal to the pre-set value, a new data set is sent to the computer. This is repeated in equal intervals of position, independently of the movement speed and provide equidistant measurements in the piece.

### 3.4 User interface.

The user interface is mainly placed in the data acquisition and stimulus sequence design software Thermo Data Welding (TDW) and the manual panel of the control interface.

TDW was developed in Visual Studio using the libraries provided by the thermographic camera manufacturer (FLIR-SYSTEMS, 2007). This program collects and stores the data of the welding process and the operation of the whole system in text files. The status bar continuously displays the status of the communication with the data acquisition interface, the welding power source and the thermographic camera. The main form is shown in Figure 47.

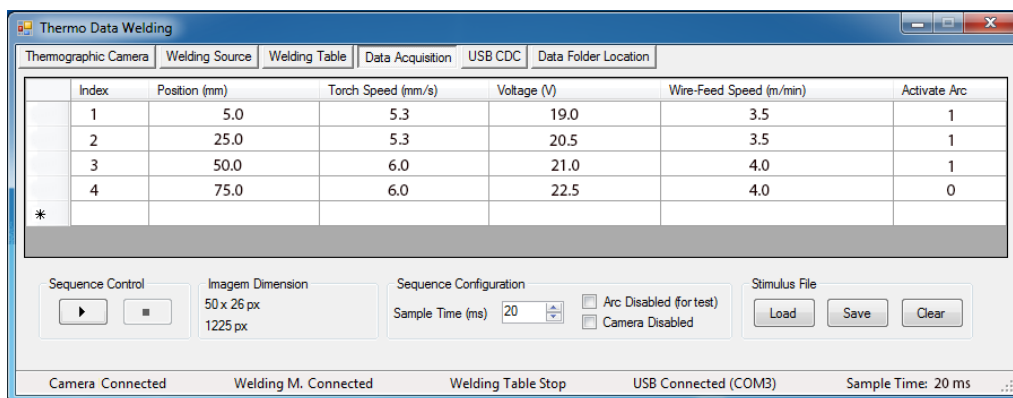
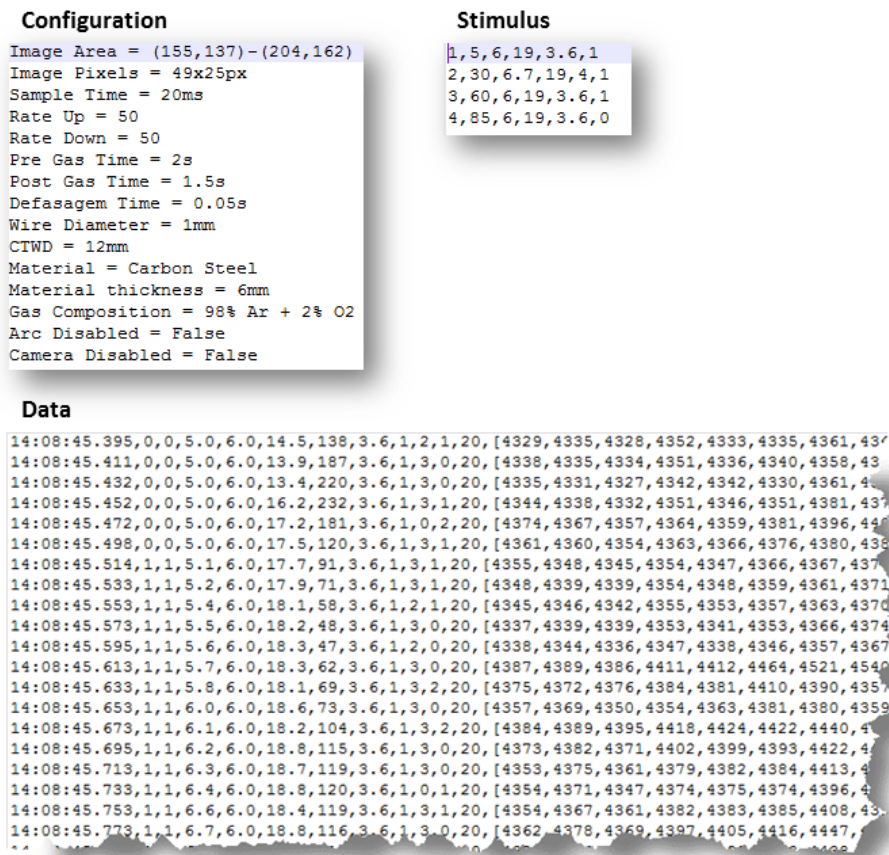


Figure 47. Data acquisition and stimulus sequence design software.

The TDW is divided in six modules oriented to specific functions that are discussed below:

- **Thermographic Camera:** It allows the configuration and verification of the camera. It shows the thermographic image, the maximum and minimum values, and a profile of the line that contains the maximum value.
- **Welding Power Source:** It sets the fixed welding parameters. This includes the inductance, pre-gas and post-gas times and gap wire-arc time. It also records the data for the experiment report such as: wire diameter, contact tip to work distance, type and thickness of the material, composition and flow rate of the shielding gas.

- **Welding Table:** It facilitates the adjustment of the initial position of the piece in the welding table and shows the state of the control interface.
- **Data Acquisition:** It provides a tool to create the welding sequence. This includes the start and end positions, the stimulus that will be sent to the welding power source and the sampling period. The user starts the process and it stops automatically when the sequence ends, or when the sequence is stopped manually. Three files are created in each experiment that store the system configuration, the stimulus sequence and the measurements collected. Figure 48 shows an example of these data files.
- **USB CDC:** Sets the communication port where the data acquisition interface is connected.
- **Data Folder Location:** Defines the folder where the configuration and measurements files will be stored.



## 4 Experimental results.

The main results of the work are shown and discussed in this chapter. Four welding experiments were made using carbon steel pieces with dimensions of 85x50x6mm on which welds were laid adopting the bead-on-plate technique (welding on top). The surfaces of the pieces were cleaned to eliminate any dirt and oxides. The piece was welded in a horizontal position, with the torch at 90° from the horizontal and 12 mm of contact tip to work distance.

In two experiments, a mixture of 98% argon and 2% oxygen was used as the shielding gas. The other two used 96% argon and 4% carbon dioxide as the shielding gas. In both the gas was applied with 15 psi of pressure. In each experiment a different stimulus sequence was used. These changes between experiments were carried out with the objective of testing the proposed methodology under different process conditions.

The selection of the welding electrode wire was based principally upon matching the mechanical properties and physical characteristics of the base metal, weld size and existing electrode inventory. Steel wires with a diameter of 1 mm (Product code CAJMERS6100S015W00 of Merit®S-6 Lincoln Electric) were used.

The welding power source was configured (through the interface) with a rate up and a rate down of 50, 2 s of pre-gas time, 1.5 s of post-gas time and 0.05 s of gap time. The sampling time was 20 ms. The dimensions of the thermographic image were 49x25 pixels.

The measurements were obtained using the data acquisition and control system described in section 3. The bead profile was obtained using the laser scanner (see section 3.1.3) and the weld bead depth profile was obtained using the longitudinal macrography and image processing algorithms described in section 3.1.7.

The validation of the data acquisition and control system shows a good behavior in real time with acceptable accuracy and performance. The data collected for process modeling, is shown as an example of the usefulness of the system for research activities that do not have many resources and equipment.

The neural network proposed in section 3.1.8, for estimating the depth and width of the weld bead, was trained and validated using the experimental data. Each experiment data set was divided in 70% to train, 15% to validate and 15% to test. Experiments 1 and 3 were used to model the weld bead depth due to the relationship between this variable and the welding current, which in this case it is modified by the wire feed speed. Experiments 2 and 4 were used to model the weld bead width due to the relationship between this variable and the welding voltage modified in these experiments.

In addition, the complete data set from experiments 2 and 4 were useful for testing the weld bead depth model under different process conditions. Similarly, the complete data set from experiment 1 and 3 were useful for testing the weld bead width model.

In the next sections, we will describe the results obtained. These results aim to demonstrate the feasibility of this project as far as possible with the available equipment and time.

### 4.1 Experiments with argon and oxygen as the shielding gas.

The following sections describe two experiments that use a mixture of 98% argon and 2% oxygen as the shielding gas. The first experiment makes variations in the welding speed and the wire feed speed. The second experiment makes variations in the welding voltage. The rest of parameters are constant.

#### 4.1.1 Experiment 1: Process response to the steps in the welding speed and wire feed speed using 98% argon and 2% oxygen as the shielding gas.

This experiment was carry out to research the behavior of the process with welding speed and wire feed speed variations. These variations were made while keeping constant the deposited volume by area unit by keeping constant the relation between the welding speed and wire feed speed. The CTWD and the voltage are constant. The step input sequence of the selected experiment is shown in Table 4.

*Table 4 Sequence of stimulus applied during the experiment 1 (shielding gas 98% argon and 2% oxygen and variations in the welding speed and wire feed speed)*

<b>Position (mm)</b>	<b>Welding speed (mm/s)</b>	<b>Welding voltage (V)</b>	<b>Wire feed speed (m/min)</b>	<b>Arc status</b>
5.0	6.0	20.0	3.0	On
30.0	8.0	20.0	4.0	On
60.0	6.0	20.0	3.0	On
85.0	6.0	20.0	3.0	Off

The data set was collected and calculated, used for training the neural network model, is shown in the figures below. Figure 49 shows the three-dimensional bead profile obtained with the scanner. Figure 50a shows the top side of the bead weld. Figure 50b shows the curves of the weld bead depth and baseline on the picture, obtained with the image processing algorithm.

Figure 51 shows the unfiltered data while the Figure 52 shows the filtered data. The data used for modeling are unfiltered but are filtered in the modeling algorithm if necessary. In these figures, it is possible to notice that although the wire feed speed is changed, the weld bead width and the bead reinforcement remain stable because of the constant relationship between wire feed speed and welding speed and the constant value of the welding voltage.

The correlation between the wire feed speed and the welding current is observed in the figures. When the wire feed speed is increased the welding current increases too. The relationship between the penetration and the welding current is clear but the penetration reaches a very small value, which makes us believe that the applied stimuli are not disturbing enough. This is observed in Figure 52. For this reason, the data set is not recommended for the final process model. Anyway, this data set was used for modeling because the current objective of the work is just to test the methodology and not for obtaining the final process model.

Figure 53 shows a sample of thermographic information and the feature extraction process explained in section 3.1.6.

The autocorrelation and cross-correlation analyses show high values, indicating a satisfactory sampling time and a delay of 11 sampling times between the weld bead depth and the stimulus.

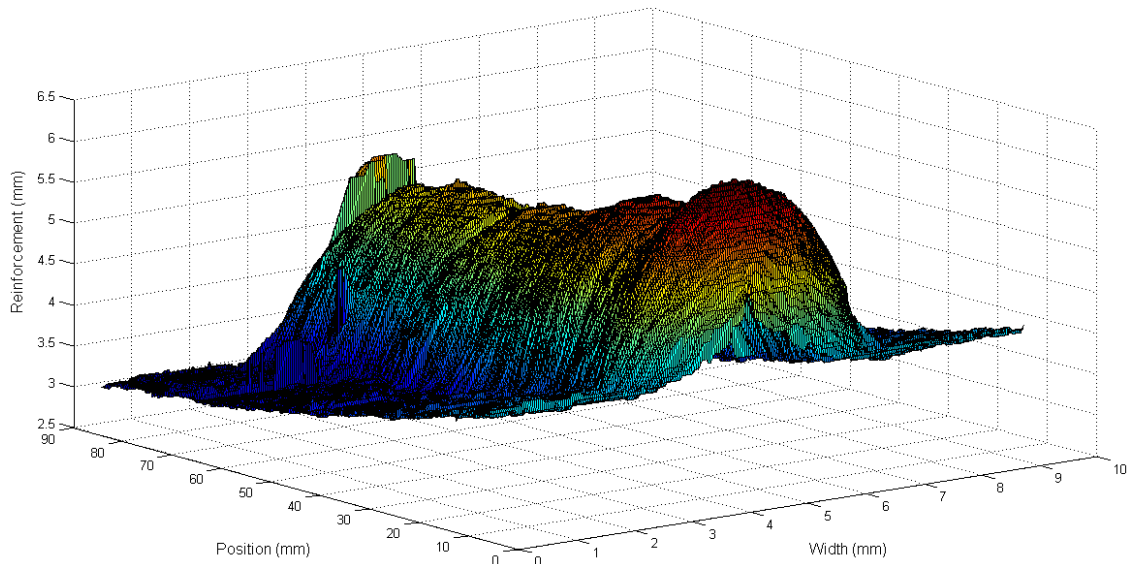


Figure 49 Three-dimensional reconstruction of the weld bead obtained with the low-cost laser scanner in the experiment 1.

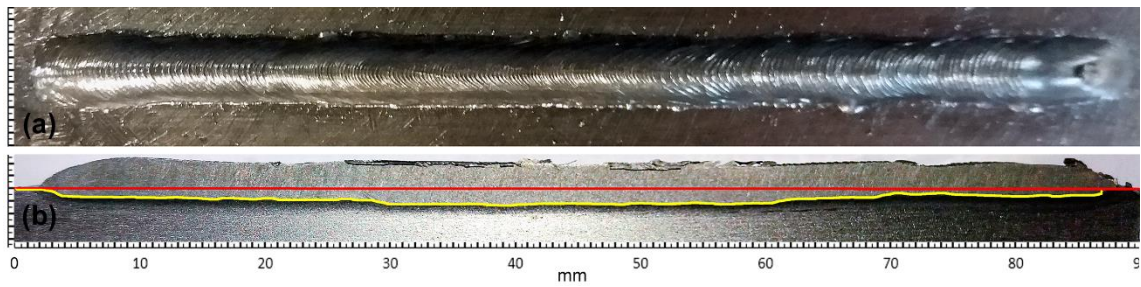


Figure 50 Weld bead obtained in the experiment 1: (a) Top view of the weld bead; (b) Weld bead depth profile (yellow line) and surface of the workpiece (red line) obtained by the macrographic analyses algorithm.

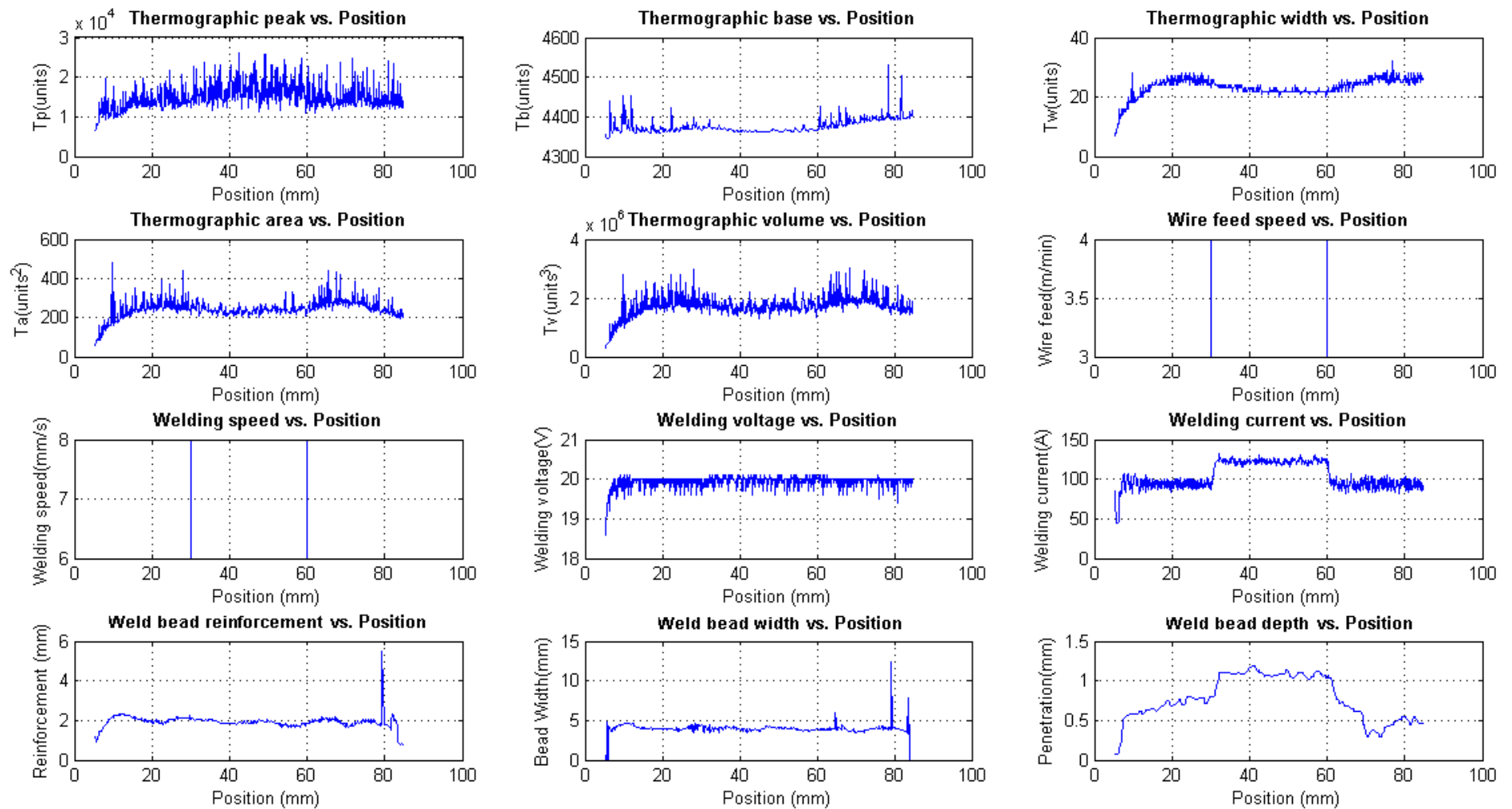


Figure 51 Unfiltered measurements obtained with the data acquisition and open-loop control system in the experiment 1.

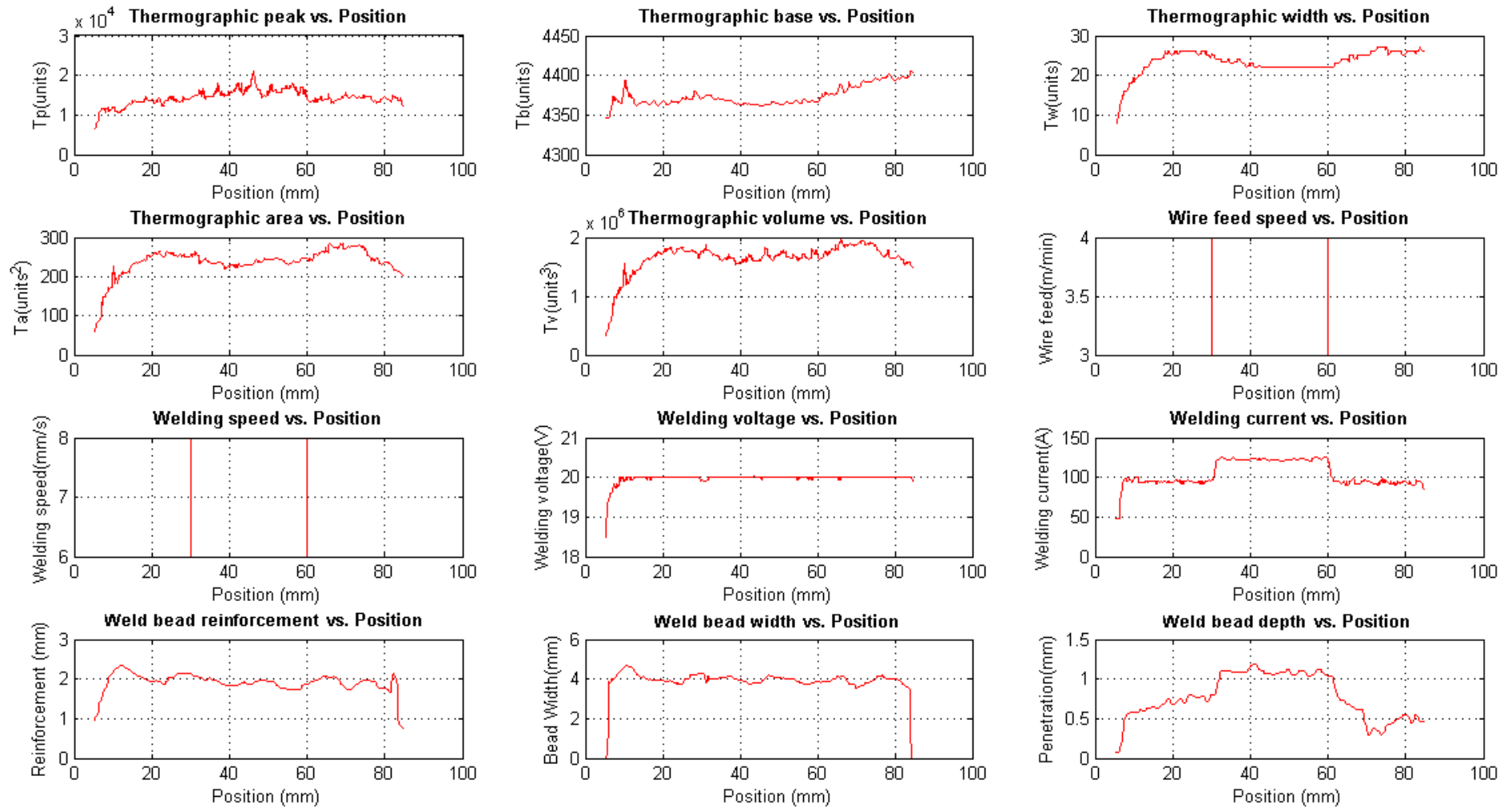


Figure 52 Filtered measurements obtained with the data acquisition and open-loop control system in the experiment 1.

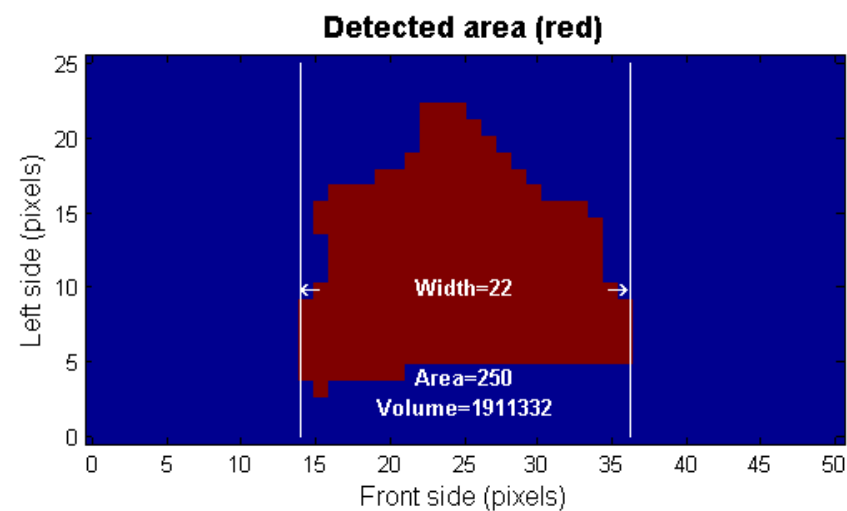
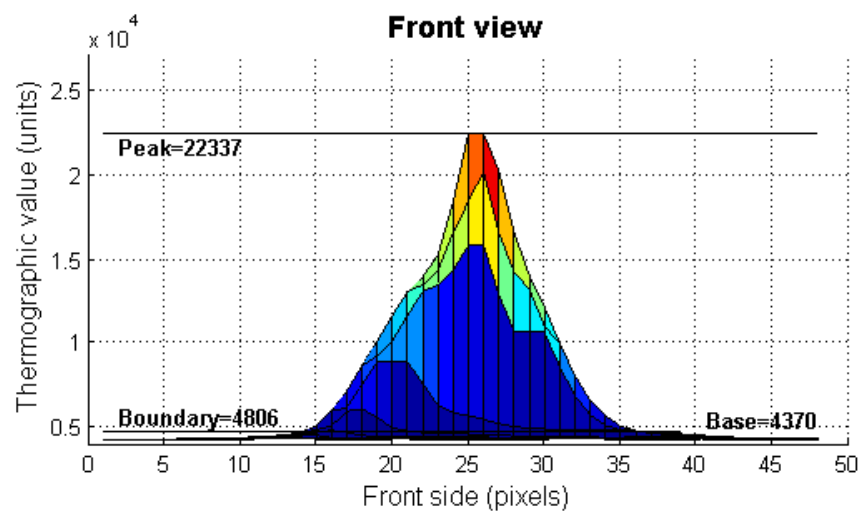
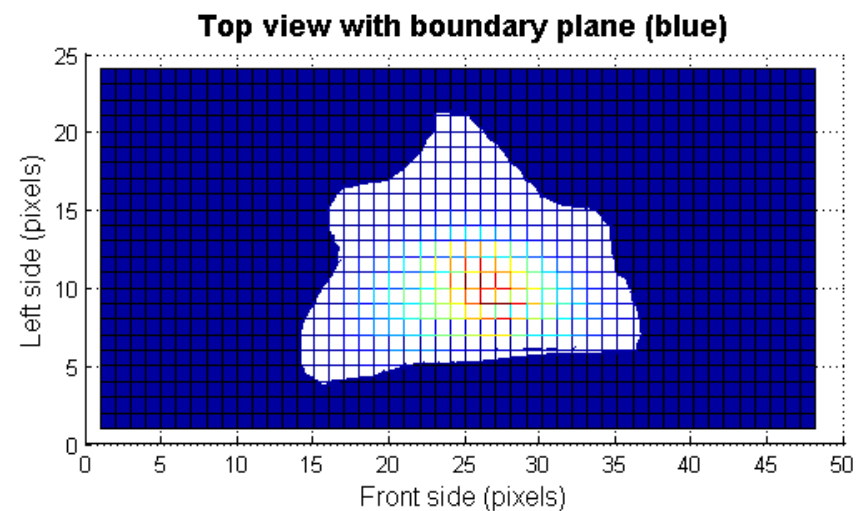
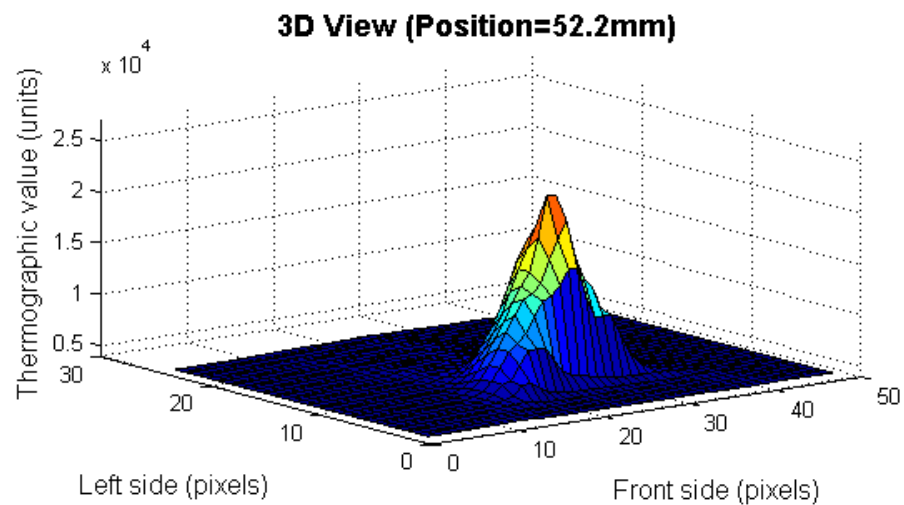


Figure 53 Sample of the thermographic data and feature extraction process in the experiment 1.



#### 4.1.2 Experiment 2: Process response to the steps in the welding voltage using 98% argon and 2% oxygen as the shielding gas.

This experiment was performed to research the behavior of the process with welding voltage variations. The CTWD, the wire feed speed and the welding speed are constant. The step input sequence of the selected experiment is shown in Table 5.

*Table 5 Sequence of stimulus applied during the experiment 2  
(shielding gas 98% argon and 2% oxygen and variations in the welding voltage)*

<b>Position (mm)</b>	<b>Welding speed (mm/s)</b>	<b>Welding voltage (V)</b>	<b>Wire feed speed (m/min)</b>	<b>Arc status</b>
5.0	6.0	19.0	3.5	On
30.0	6.0	21.0	3.5	On
60.0	6.0	19.0	3.5	On
85.0	6.0	19.0	3.5	Off

The data set collected and calculated, used for training the neural network model, is shown in the figures below. Figure 54 shows the three-dimensional bead profile obtained with the scanner. Figure 55a shows the top side of the bead weld. Figure 55b shows the curves of the weld bead depth and baseline on the picture, obtained with the image processing algorithm.

Figure 56 shows the unfiltered data and Figure 57 shows the filtered data. The data used for modeling are unfiltered but are filtered in the modeling algorithm if necessary. The correlation between the welding voltage and the thermographic parameters is observed in the figures. When the voltage is increased, the thermographic width increases too. As a consequence, the area and volume are increased. The thermographic peak does not change significantly but the base value is increased. This base change causes that the change in the width, the area and volume are less noticeable.

The relation between the weld bead width and reinforcement and the voltage is clear too, but the applied stimuli are not disturbing enough. This is observed in Figure 56, where the weld bead width variation is very low. In this case, the data set is not recommended for modeling.

Again, this data set was used for modeling because the current objective of the work is just to test the methodology and not for obtaining the final model of the process.

The complex relation between the welding parameters and the disturbances effect is noted when the weld bead depth changes for no apparent reason, although a small variation of the welding current in position 55 mm is observed.

The autocorrelation and cross-correlation analyses show high values, indicating a satisfactory sampling time and a no dead time between the weld bead width and the stimulus.

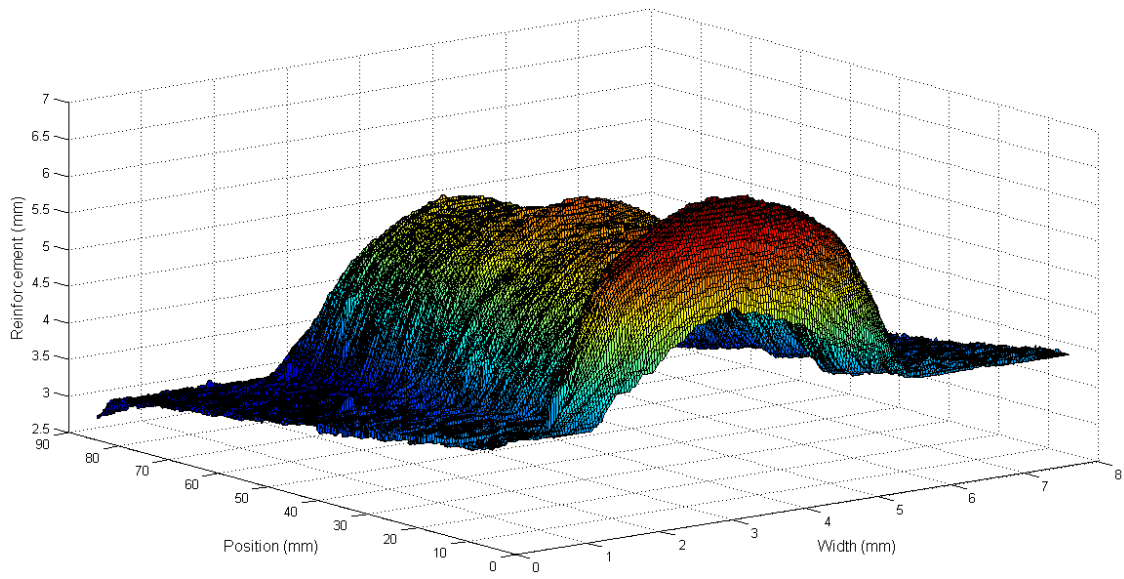


Figure 54 Three-dimensional reconstruction of the weld bead obtained with the low-cost laser scanner in the experiment 2.

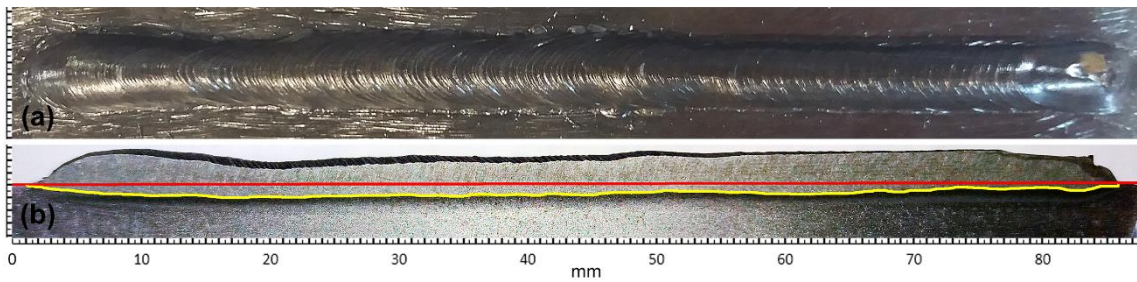


Figure 55 Weld bead obtained in the experiment 2: (a) Top view of the weld bead; (b) Weld bead depth profile (yellow line) and surface of the workpiece (red line) obtained by the macrographic analyses algorithm.

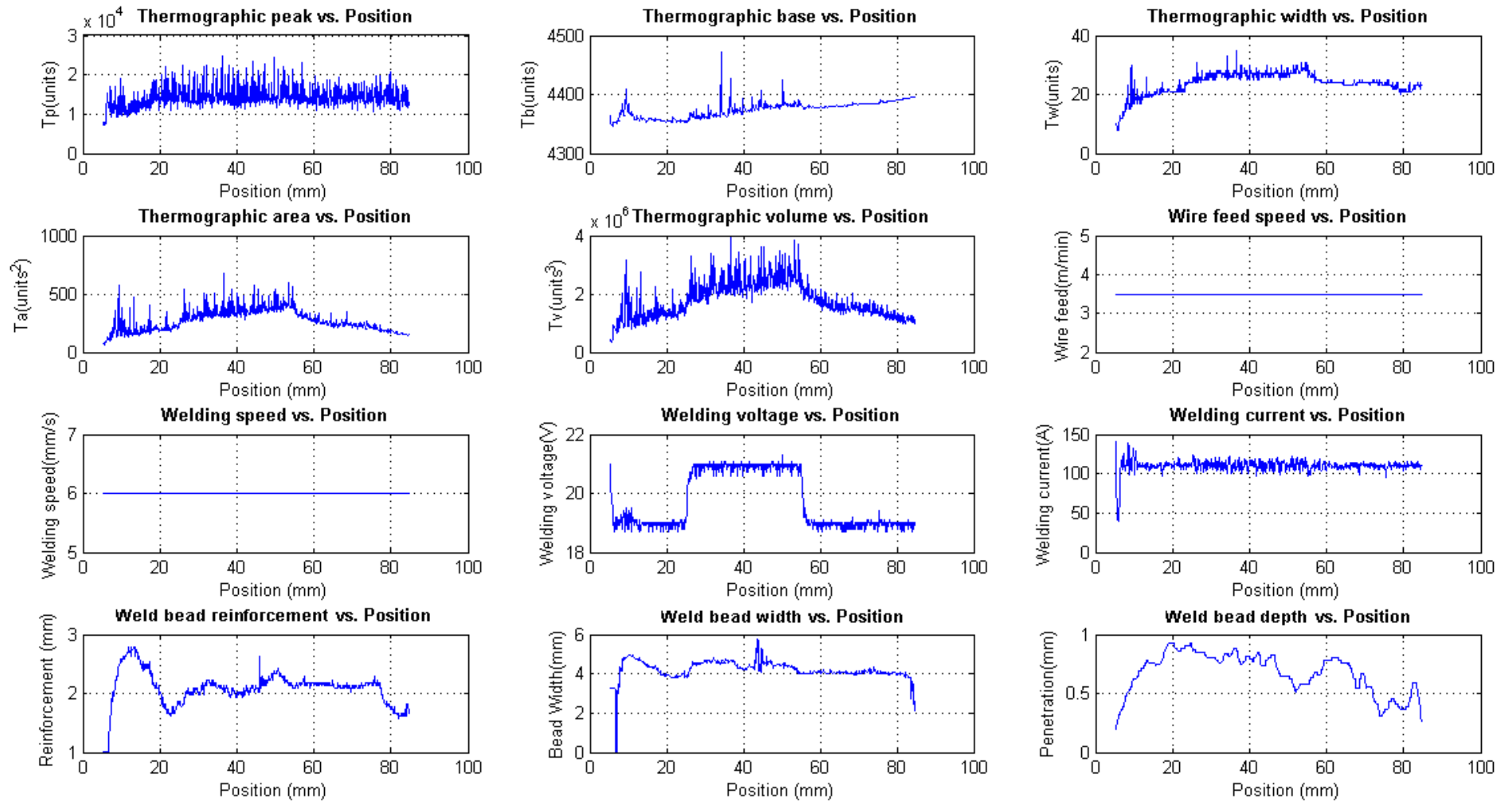


Figure 56 Unfiltered measurements obtained with the data acquisition and open-loop control system in the experiment 2.

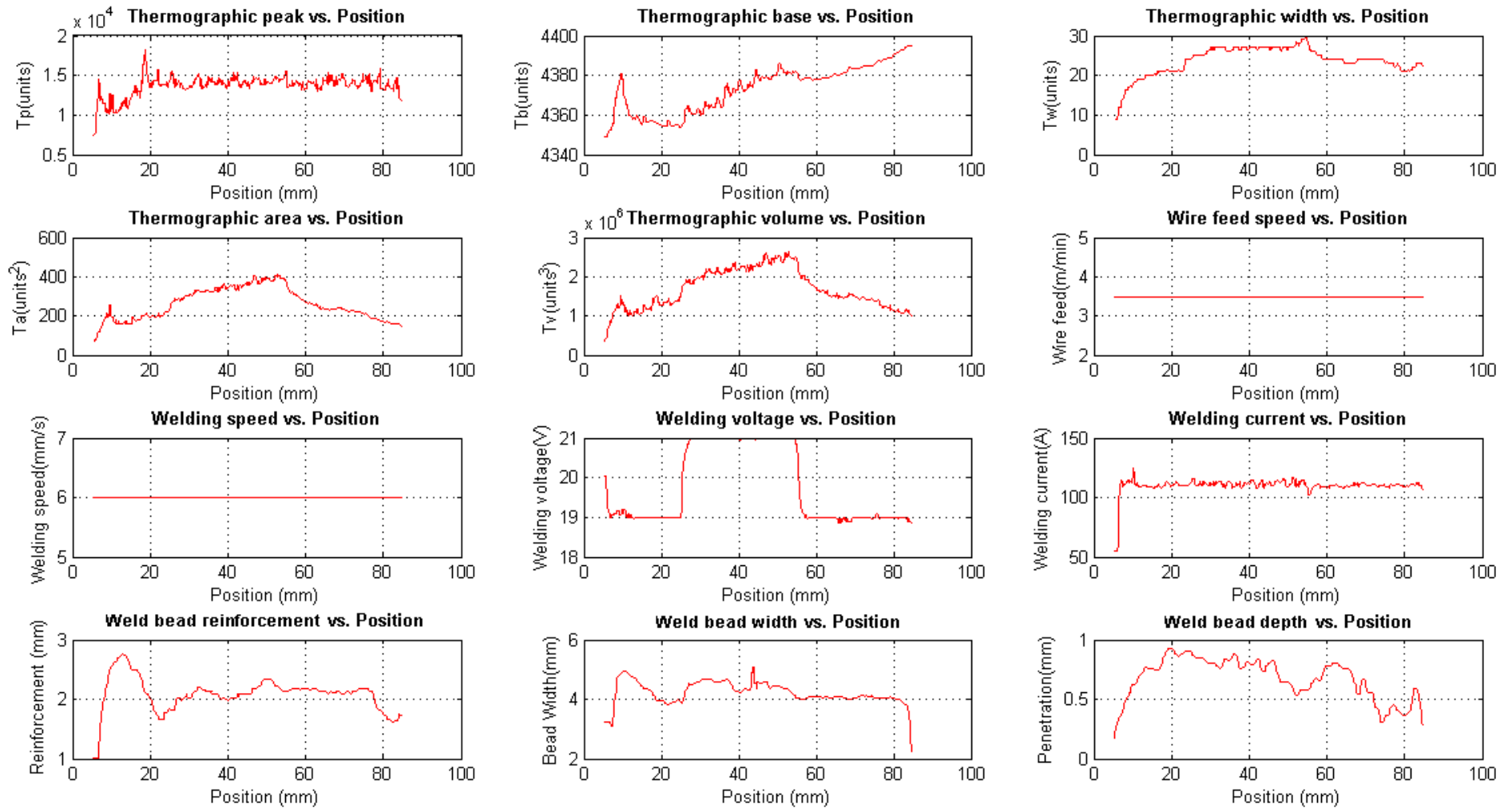


Figure 57 Filtered measurements obtained with the data acquisition and open-loop control system in the experiment 2.

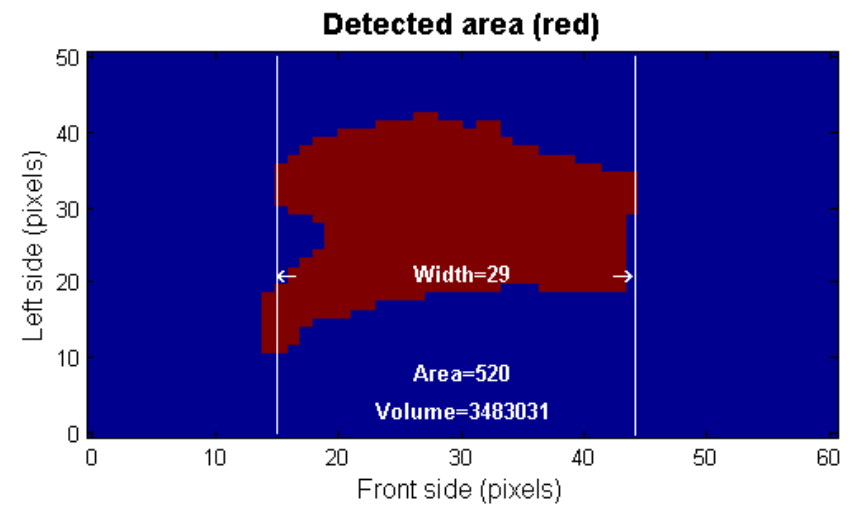
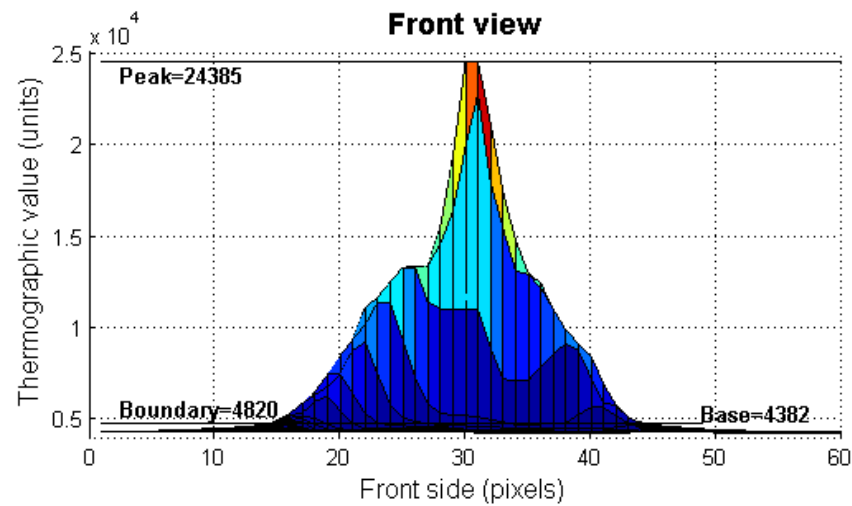
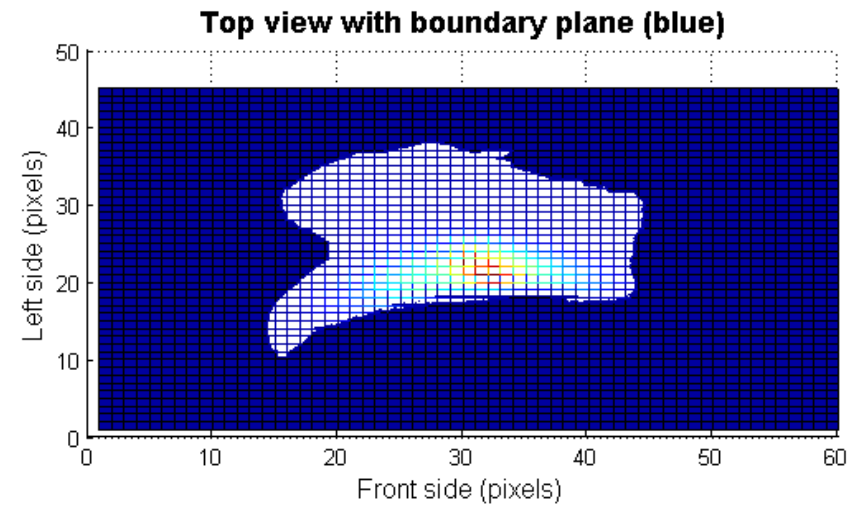
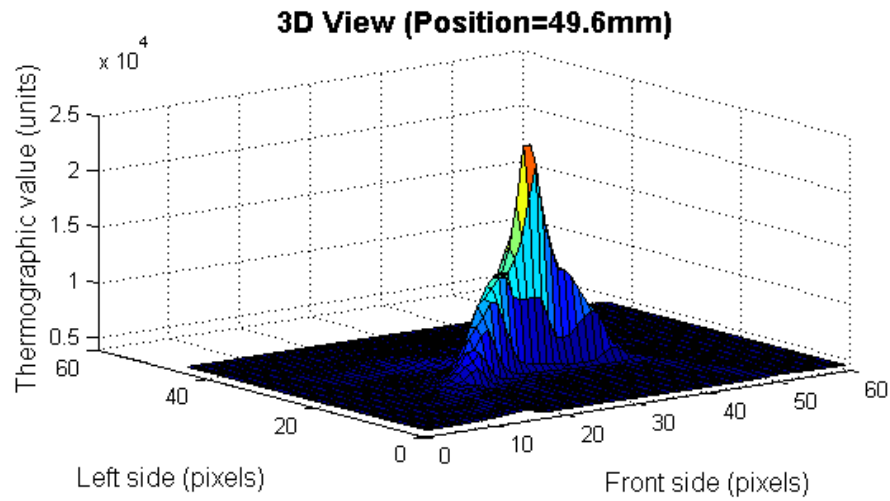


Figure 58 Example of the thermographic data and feature extraction process in the experiment 2.

#### 4.1.3 Modeling and validation of the weld bead depth estimator with data from experiments with argon and oxygen as the shielding gas.

The model obtained from the weld bead depth, with data from experiment 1, has a fit of 0.99844, a performance or median square error (MSE) of  $7.61 \times 10^{-4}$  at epoch 6, a closed loop performance of  $6.4 \times 10^{-3}$  and the network response is very good. The best result was obtained without filtering. These results are discussed below.

Figure 59a represents the regression plot between the model outputs and the targets (in this case is the real weld bead depth). The dashed line represents the perfect result (outputs = targets) and the solid line represents the best fit linear regression line. The R value is an indication of the relationship between the outputs and targets. If  $R = 1$ , this indicates that there is an exact linear relationship between outputs and targets. The regression plot for this model, achieves an excellent value across the range of measurements.

The performance curve (see Figure 59b) does not show indications of overfitting and defines the best performance value in epoch 6. This performance is obtained in open loop and the input  $\hat{D}(nT - T)$  is substituted by the corresponding target value in the input data set. The performance value shows that the estimation error is very low.

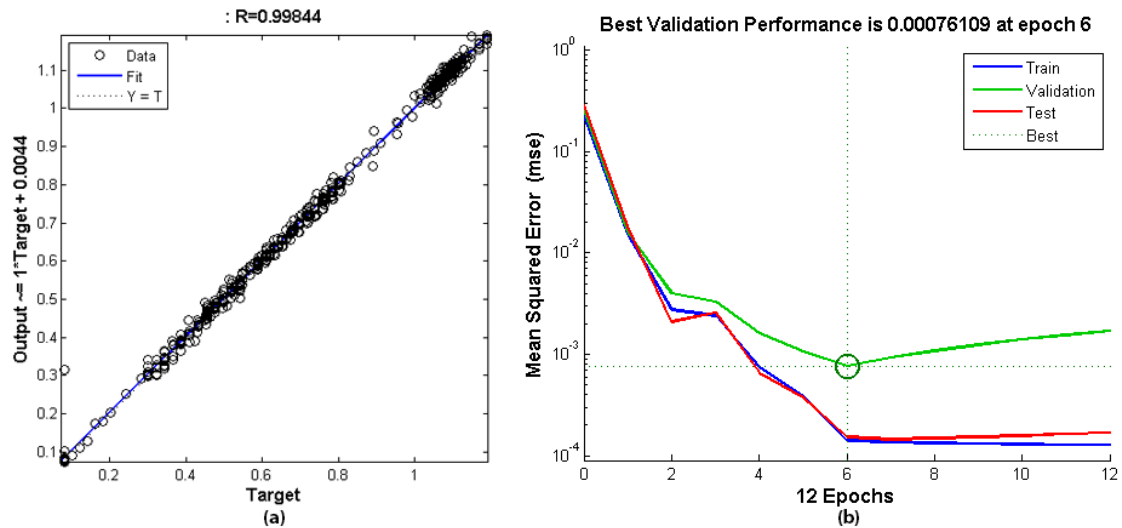


Figure 59. Results in the training of the weld bead depth model for experiments with argon and oxygen: (a) Regression curve between the model output and the real depth (target); (b) Performance curve in training, validation and test.

The closed loop performance is obtained with the feedback activated, such as when the model is used as an estimator in real time. It is natural that it is larger than the previous performance value because the model error is also fed back. For this model, the closed loop performance value predicts a good behavior in a closed loop.

The response curve (see Figure 60) shows that the model is able to reproduce the behavior of the process with great accuracy. The estimation error is very low (less than 0.05mm) in all the curve.

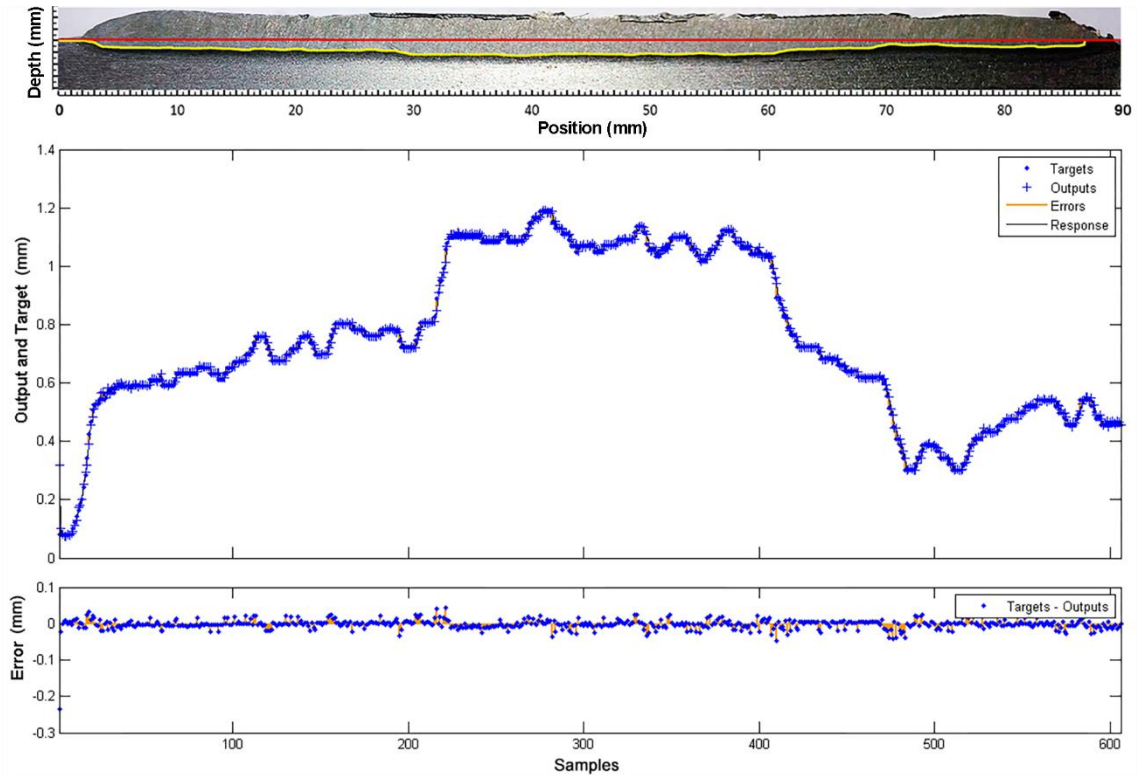


Figure 60 Comparison between the response of the weld bead depth model (outputs) and the measurements obtained in the experiment 1 (targets). In the time axis, each time value corresponds with a position in the piece.

The test of the model, with a different data set obtained from experiment 2, had a fit of 0.9901 and the performance was  $8.076 \times 10^{-4}$ . The closed loop performance was 0.244 and the network response was very good with an estimation error less than 0.1 mm. These results are shown in Figure 61 and Figure 62.

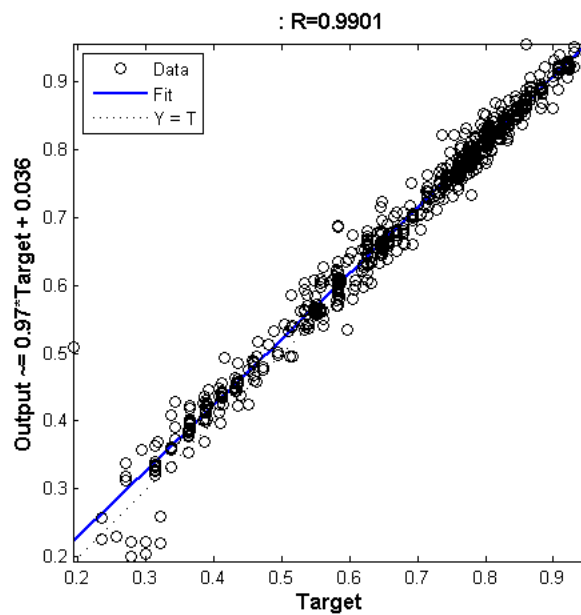


Figure 61 Regression curve between the measurements of the weld bead depth (target) obtained in experiment 2 and the output of the weld bead depth model obtained from the data of experiment 1.

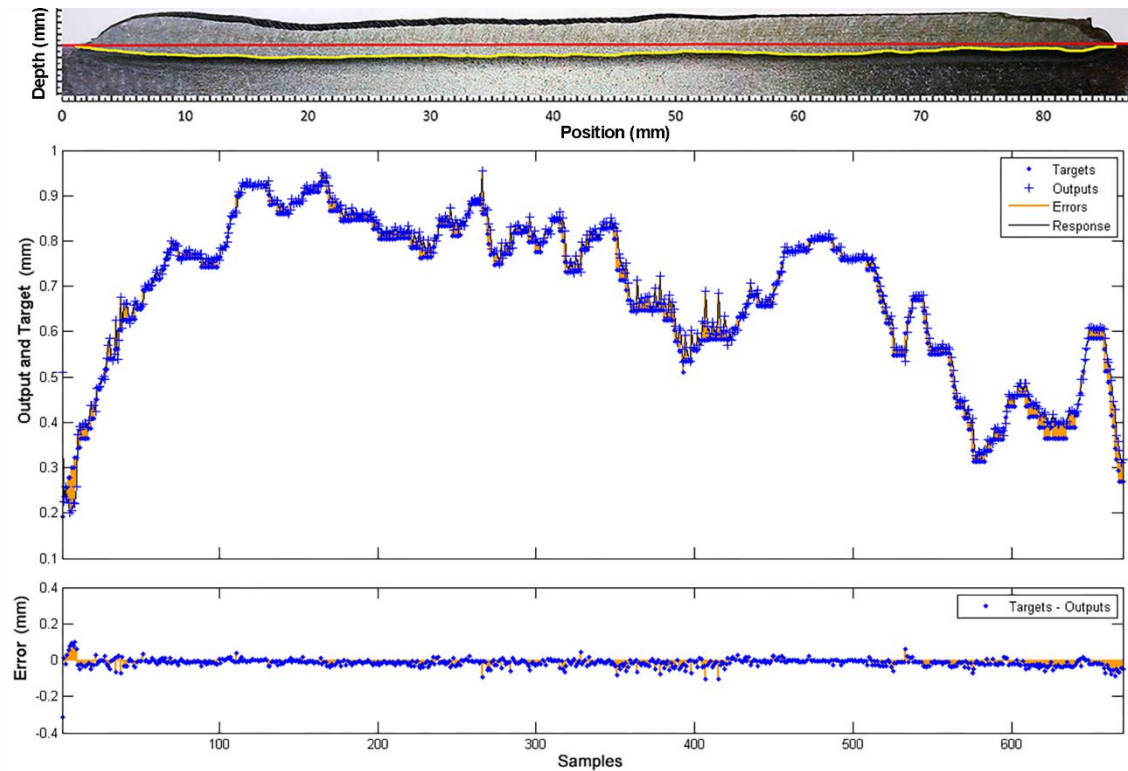


Figure 62 Comparison between the measurements of the weld bead depth (target) obtained in experiment 2 and the output of the weld bead depth model obtained from the data of experiment 1. In the time axis, each time value corresponds with a position in the piece.

#### 4.1.4 Modeling and validation of the weld bead width estimator with data from experiments with argon and oxygen as the shielding gas.

The weld bead width estimator model was obtained with data from experiment 2. Several tests were performed with different filter values applied to inputs and targets values. The best result was obtained filtering the targets with a median filtering of a 10-element window.

The model has a fit of 0.9957, a performance or median square error (MSE) of  $3.1 \times 10^{-3}$  at epoch 11, a closed loop performance of 0.094 and the network response is good. These results are discussed below.

The regression plot for this model shown in Figure 63a achieves an excellent value across the range of measurements. The performance curve (see Figure 63b) does not show indications of overfitting and defines the best performance value in epoch 11. This performance is obtained in open loop and the input  $\widehat{W}(nT - T)$  is substituted by the corresponding target value in the input data set. The performance value shows that the estimation error is acceptable.



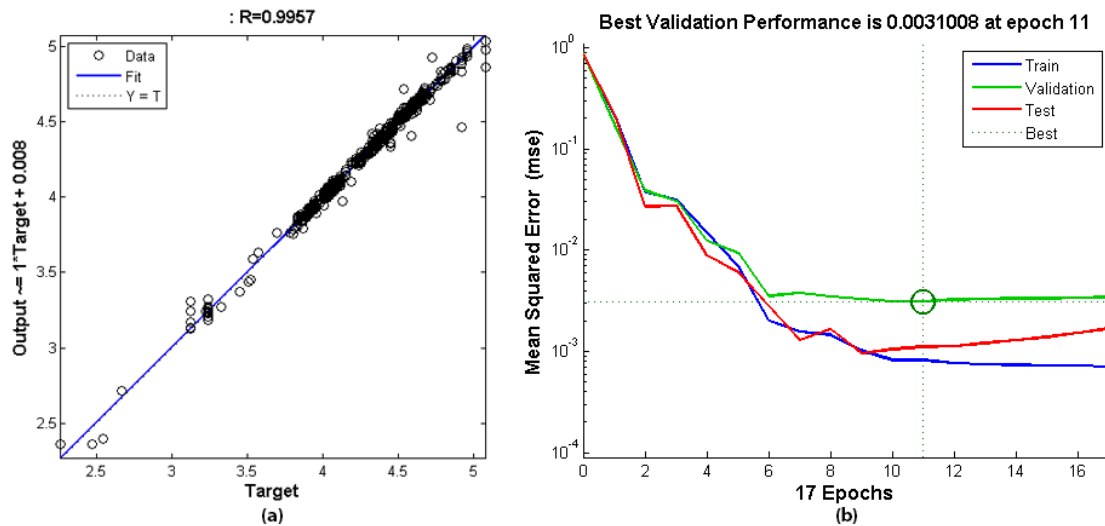


Figure 63. Results in the training of the weld bead width model for experiments with argon and oxygen: (a) Regression curve between the model output and the real depth (target); (b) Performance curve in training, validation and test.

The response curve (see Figure 64) shows that the model is able to reproduce the behavior of the process with acceptable accuracy. The estimation error was acceptable in most of the curve (less than 0.1 mm).

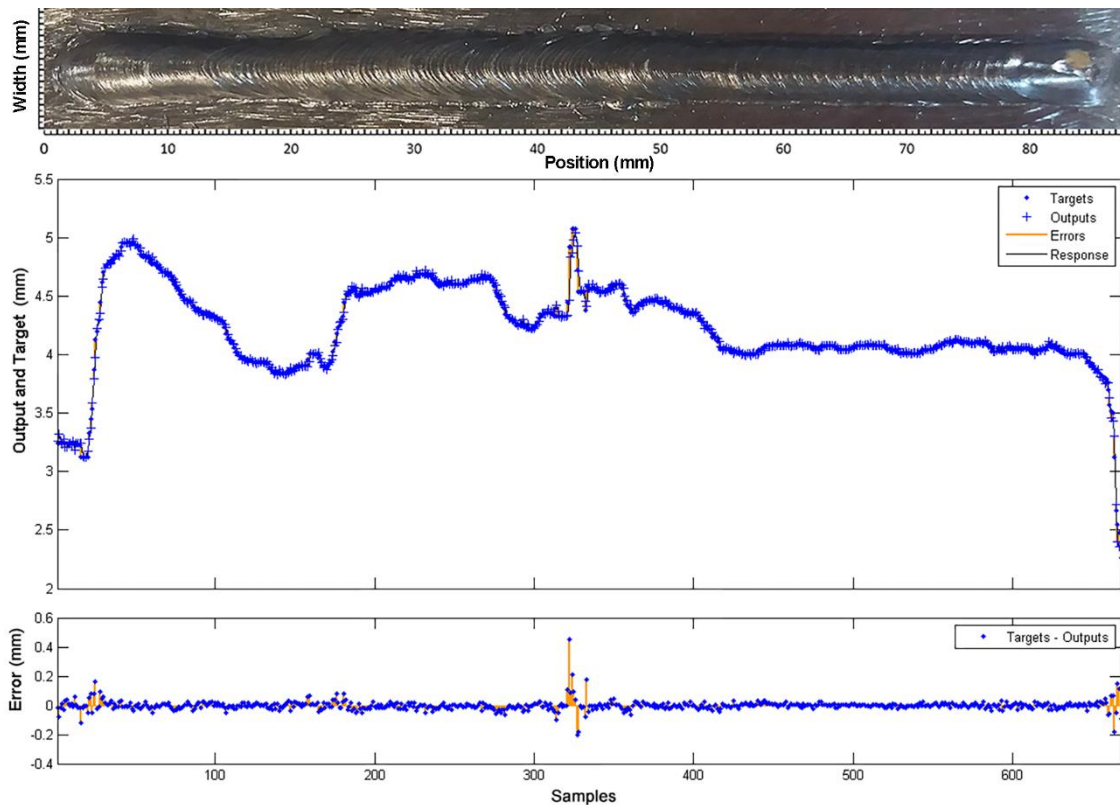


Figure 64 Comparison between the response of the weld bead width model (outputs) and the measurements obtained in the experiment 2 (targets). In the time axis, each time value corresponds with a position in the piece.

The test of the model, with a different data set obtained from experiment 1, had a fit of 0.852 and the performance was 0.128. The closed loop performance was 0.67 and the network response was acceptable with an estimating error less than 0.3mm in the curve. These results are shown below.

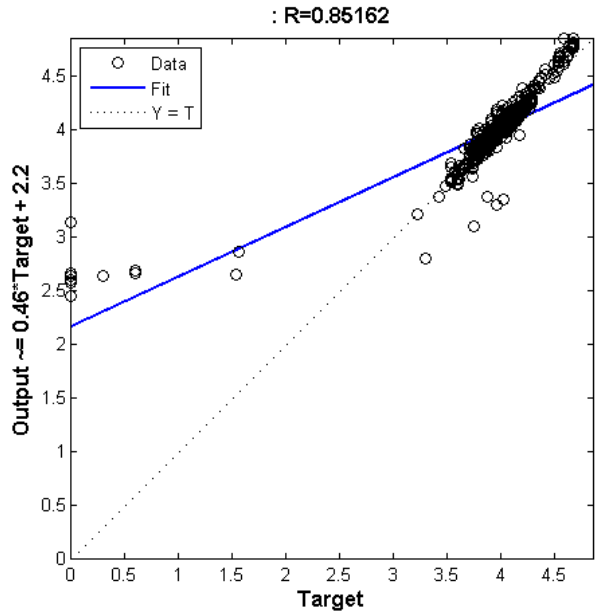


Figure 65 Regression curve between the measurements of the weld bead width (target) obtained in experiment 1 and the output of the weld bead depth model obtained from the data of experiment 2.

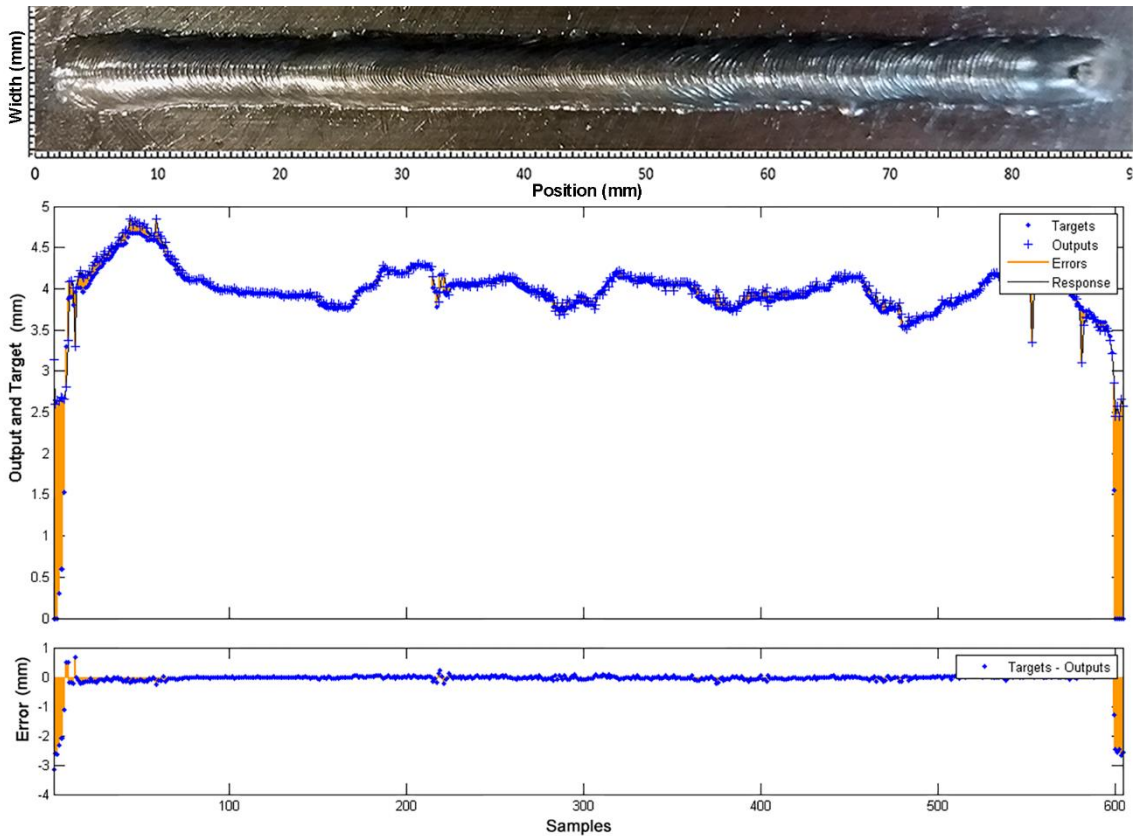


Figure 66 Comparison between the measurements of the weld bead width (target) obtained in experiment 1 and the output of the weld bead width model obtained from the data of experiment 2. In the time axis, each time value corresponds with a position in the piece.

On the other hand, it is necessary to emphasize that the greater errors of the model are at the beginning and the end of the weld bead. These intervals correspond to the opening and closing of the arc, which are very unstable moments of the process and do not respond to the same dynamic, so they do not represent a threat to the quality of the model.

## 4.2 Experiments with argon and carbon dioxide as the shielding gas.

The following sections describe two experiments that use a mixture of 96% argon and 4% carbon dioxide as the shielding gas. The first experiment makes variations in the welding speed and the wire feed speed. The second experiment makes variations in the welding voltage. The rest of parameters are constant.

### 4.2.1 Experiment 3: Process response to the steps in the welding speed and wire feed speed using 96% argon and 4% carbon dioxide as the shielding gas.

This experiment was performed to research the behavior of the process with welding speed and wire feed speed variations. These variations were made keeping constant the deposited volume by area unit by keeping constant the relation between the welding speed and wire feed speed. The CTWD and the voltage are constant. The step input sequence of the selected experiment is shown in Table 6.

Table 6 Sequence of stimulus applied during the experiment 3  
(shielding gas 96% argon and 4% carbon dioxide and variations in the welding speed and wire feed speed)

Position (mm)	Welding speed (mm/s)	Welding voltage (V)	Wire feed speed (m/min)	Arc status
5.0	6.0	19.0	3.6	On
30.0	6.7	19.0	4.0	On
60.0	6.0	19.0	3.6	On
85.0	6.0	19.0	3.6	Off

The data set collected and calculated, used for training the neural network model, is shown in the figures below. Figure 67 shows the three-dimensional bead profile obtained with the scanner. Figure 68a shows the top side of the bead weld. Figure 68b shows the curves of the weld bead depth and baseline on the picture, obtained with the image processing algorithm.

Figure 69 shows the unfiltered data and Figure 70 shows the filtered data. The data used for modeling are unfiltered but are filtered in the modeling algorithm if necessary. In these figures, it is possible to notice that although the wire feed speed is changed, the weld bead width and the bead reinforcement remain stable because of the constant relationship between wire feed speed and welding speed and the constant value of the welding voltage.

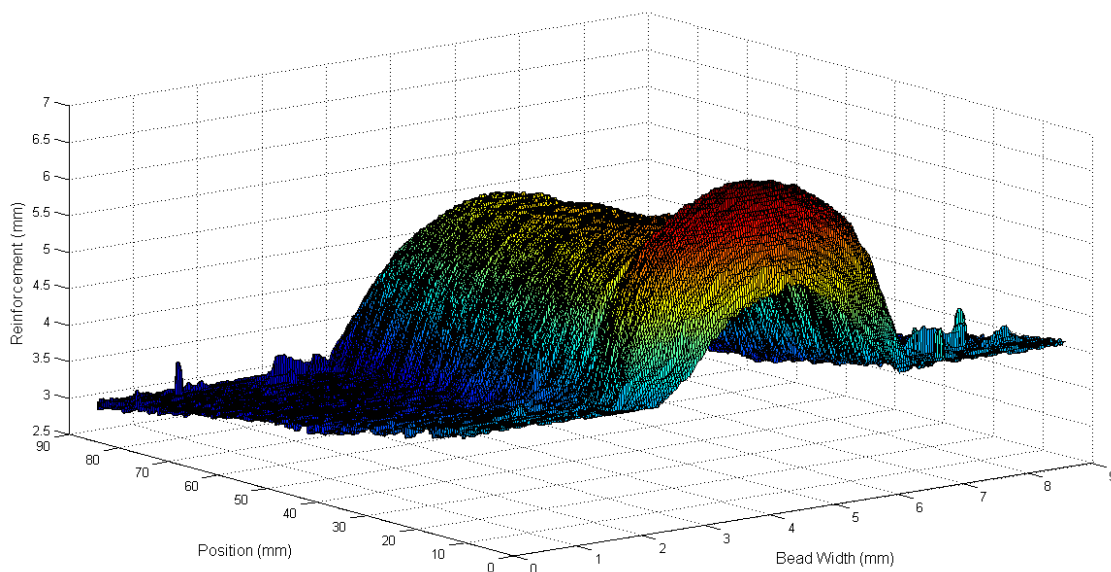


Figure 67 Three-dimensional reconstruction of the weld bead obtained with the low-cost laser scanner in the experiment 3.

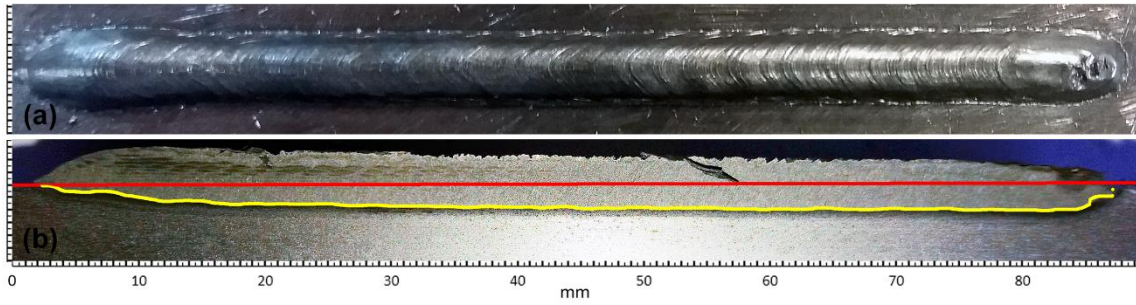


Figure 68 Weld bead obtained in the experiment 3: (a) Top view of the weld bead; (b) Weld bead depth profile (yellow line) and surface of the workpiece (red line) obtained by the macrographic analyses algorithm.

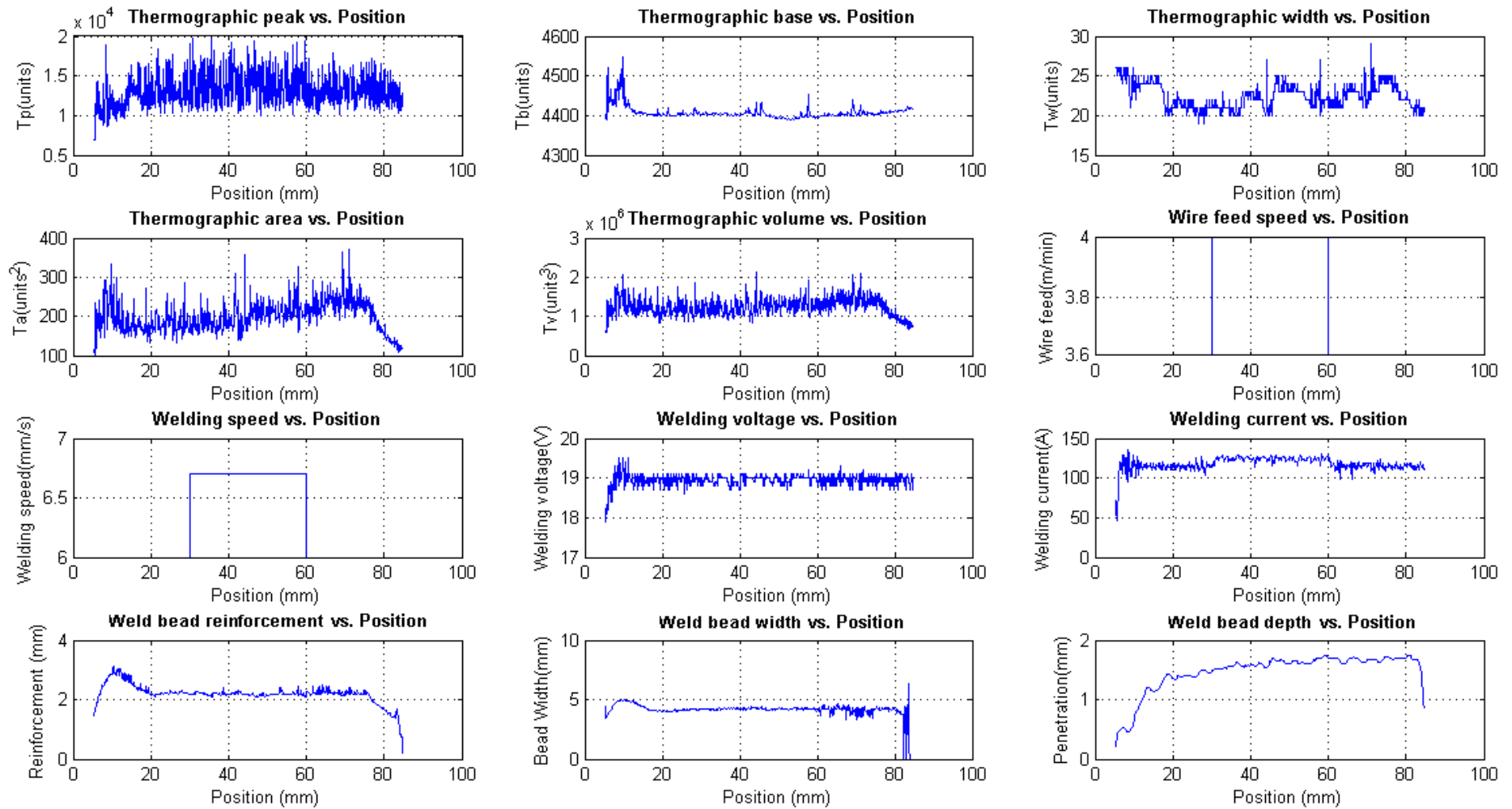


Figure 69 Unfiltered measurements obtained with the data acquisition and open loop control system in the experiment 3.

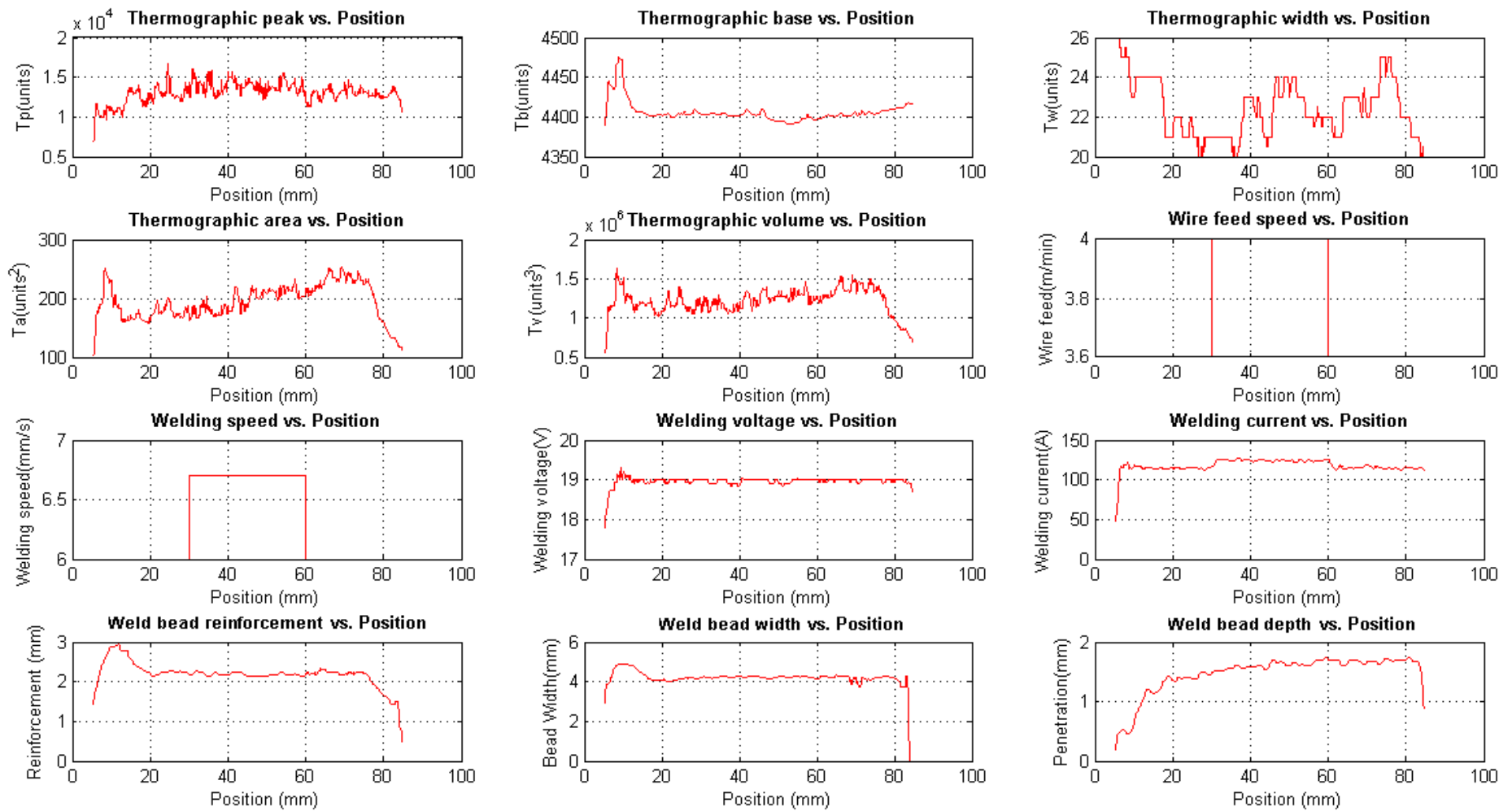


Figure 70 Filtered measurements obtained with the data acquisition and open loop control system in the experiment 3.

#### 4.2.2 Experiment 4: Process response to the steps in the welding voltage using 96% argon and 4% carbon dioxide as the shielding gas.

This experiment was performed to research the behavior of the process with welding voltage variations. The CTWD, the wire feed speed and the welding speed are constant. The step input sequence of the selected experiment is shown in Table 7.

*Table 7 Sequence of stimulus applied during the experiment 4 (shielding gas 96% argon and 4% carbon dioxide and variations in the welding voltage)*

Position (mm)	Welding speed (mm/s)	Welding voltage (V)	Wire feed speed (m/min)	Arc status
5.0	6.0	19.0	3.5	On
30.0	6.0	20.0	3.5	On
60.0	6.0	19.0	3.5	On
85.0	6.0	19.0	3.5	Off

The data set collected and calculated, used for training the neural network model, is shown in the figures below. Figure 71 shows the three-dimensional bead profile obtained with the scanner. Figure 72a shows the top side of the bead weld. Figure 72b shows the curves of the weld bead depth and baseline on the picture, obtained with the image processing algorithm.

Figure 73 shows the unfiltered data while Figure 74 shows the filtered data. The correlation between the welding voltage and the thermographic parameters is observed in the figures. When the voltage is increased, the thermographic width increases too. As a result, the area and volume are increased.

The relation between the weld bead width and reinforcement and the voltage is not clear. This is observed in Figure 56.

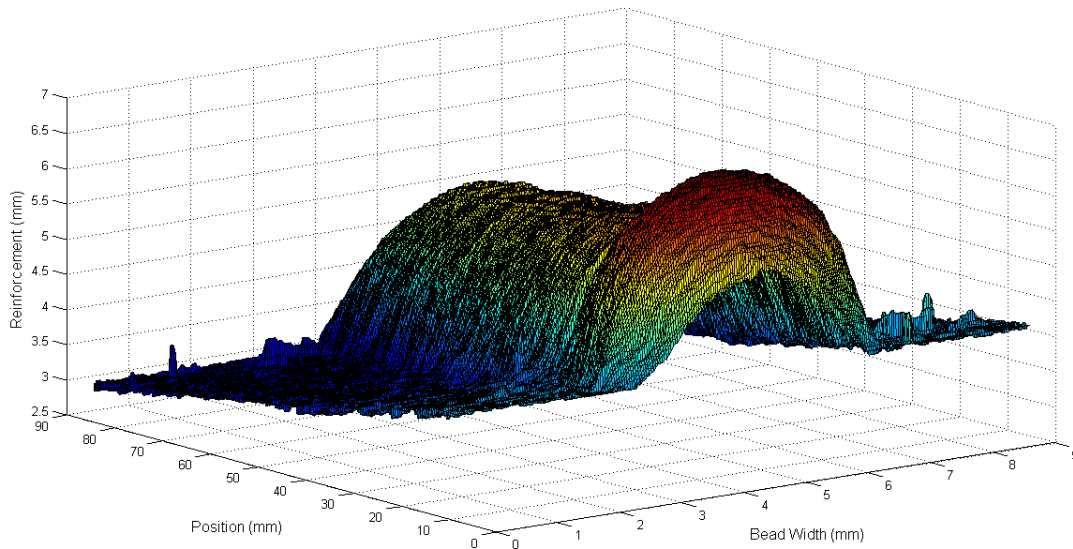


*Figure 71 Three-dimensional reconstruction of the weld bead obtained with the low-cost laser scanner in the experiment 4.*

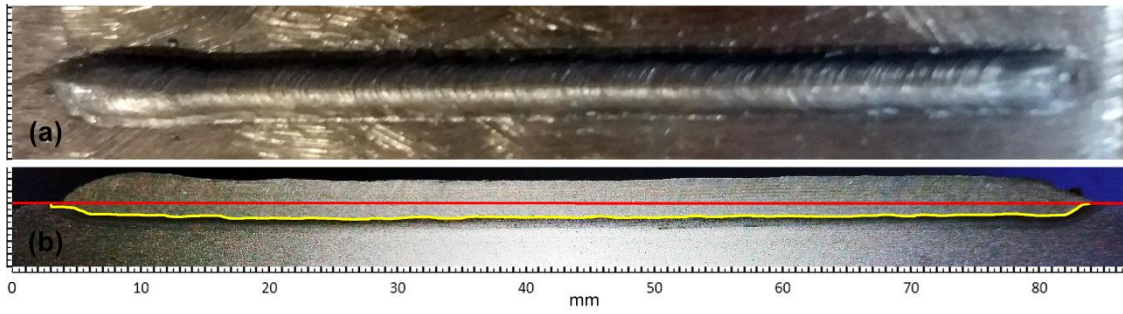


Figure 72 Weld bead obtained in the experiment 4: (a) Top view of the weld bead; (b) Weld bead depth profile (yellow line) and surface of the workpiece (red line) obtained by the macrographic analyses algorithm.



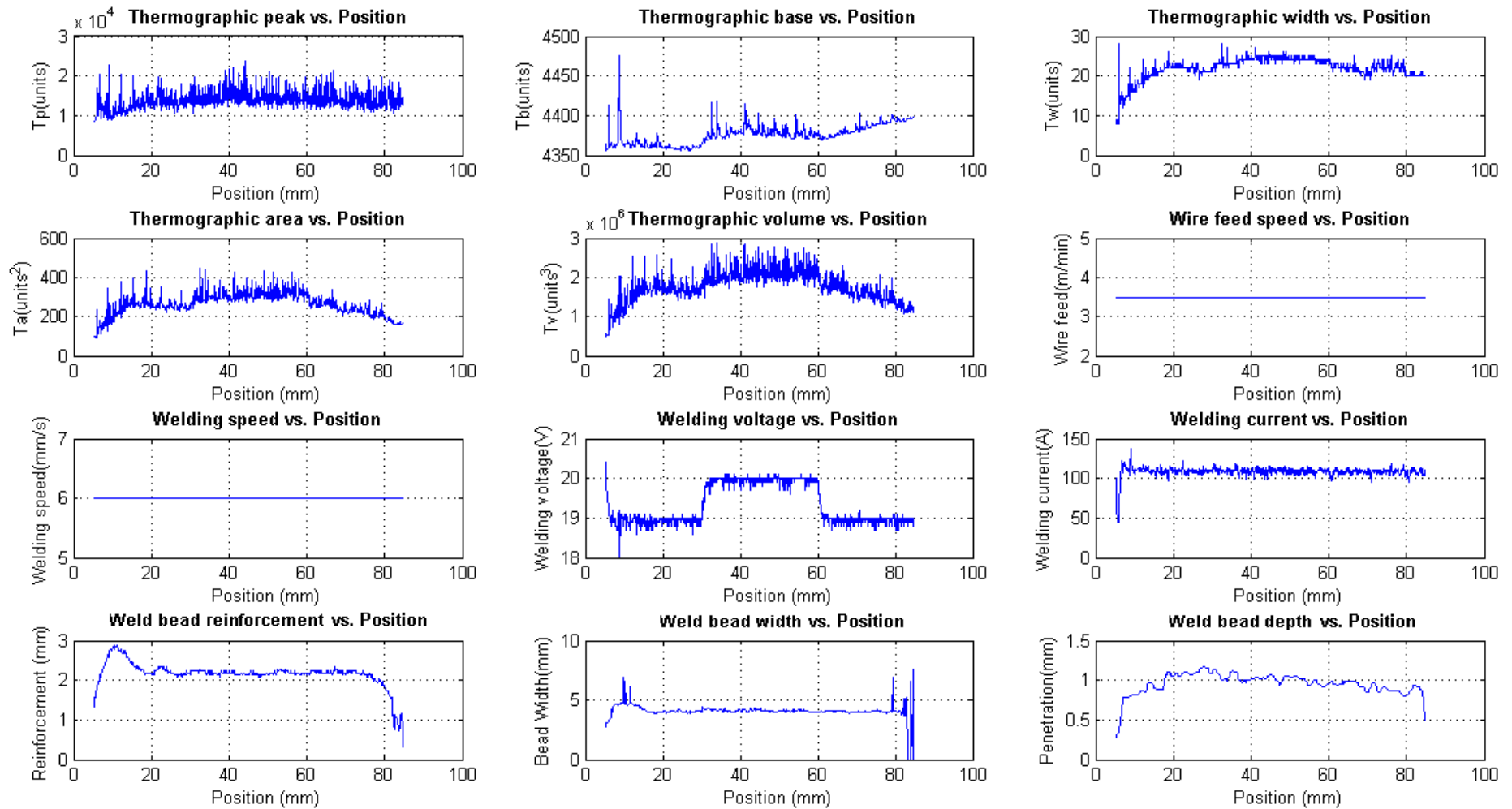


Figure 73 Unfiltered measurements obtained with the data acquisition and open-loop control system in the experiment 4.

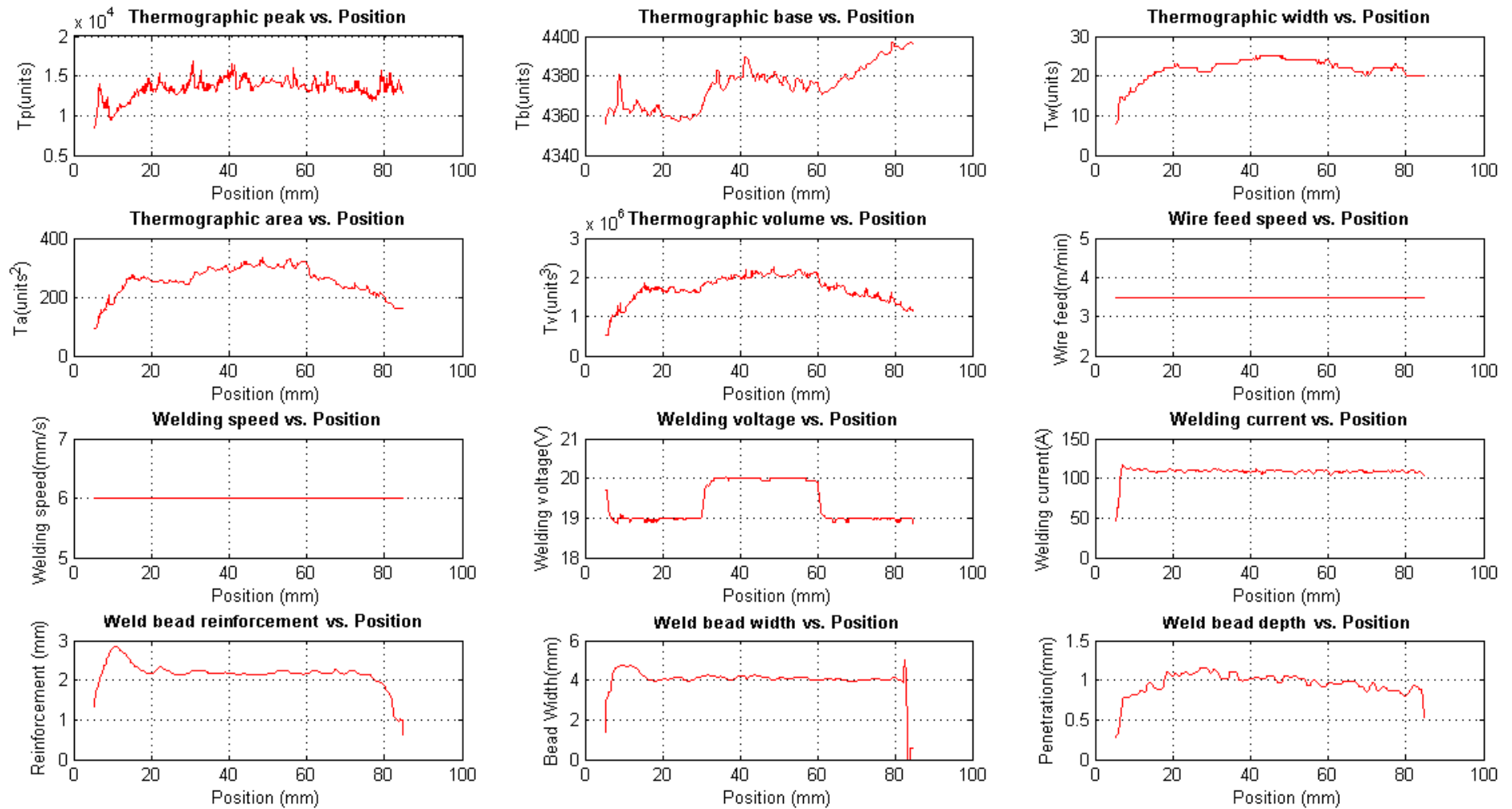


Figure 74 Filtered measurements obtained with the data acquisition and open-loop control system in the experiment 4.

#### 4.2.3 Modeling and validation of the weld bead depth estimator with data from experiments with argon and carbon dioxide as the shielding gas.

The model is obtained from the weld bead depth, with data from experiment 3. Several tests were performed with different filter values applied to inputs and targets values. The best result was obtained filtering the targets with a median filtering of a 10-element window.

The model has a fit of 0.9993 (see Figure 75a), a performance or median square error (MSE) of  $7.16 \times 10^{-5}$  at epoch 14 (see Figure 75b), a closed loop performance of 0.8122 and the network response is good.

The performance curve (see Figure 75b) does not show indications of overfitting. This performance is obtained in open loop and the input  $\hat{D}(nT - T)$  is substituted by the corresponding target value in the input data set. The performance value shows that the estimation error is very low.

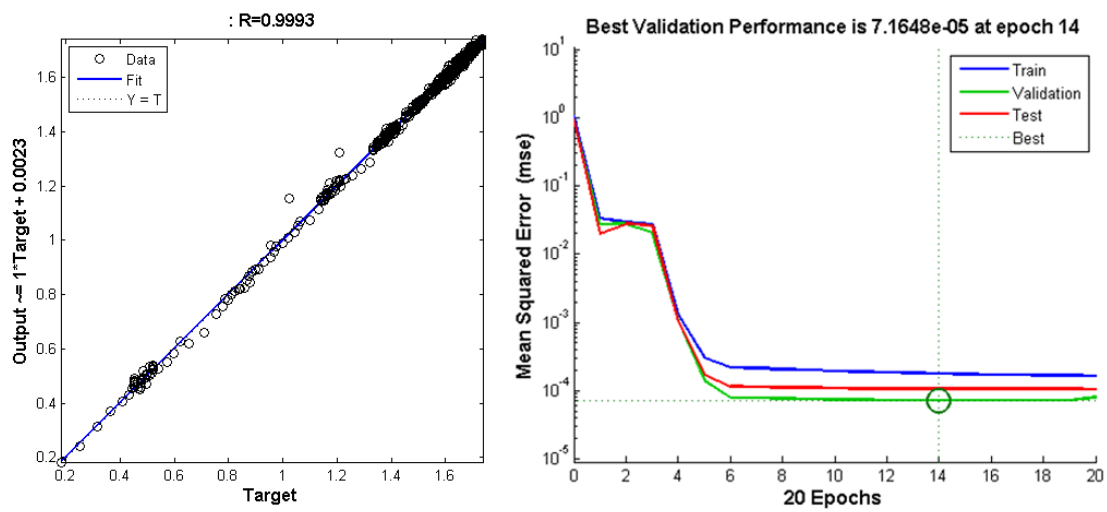


Figure 75. Results in the training of the weld bead depth model for experiments with argon and carbon dioxide: (a) Regression curve between the model output and the real depth (target); (b) Performance curve in training, validation and test.

The response curve (see Figure 76) shows that the model is able to reproduce the behavior of the process with great accuracy. The estimation error is very low (less than 0.05mm) in all the curve.

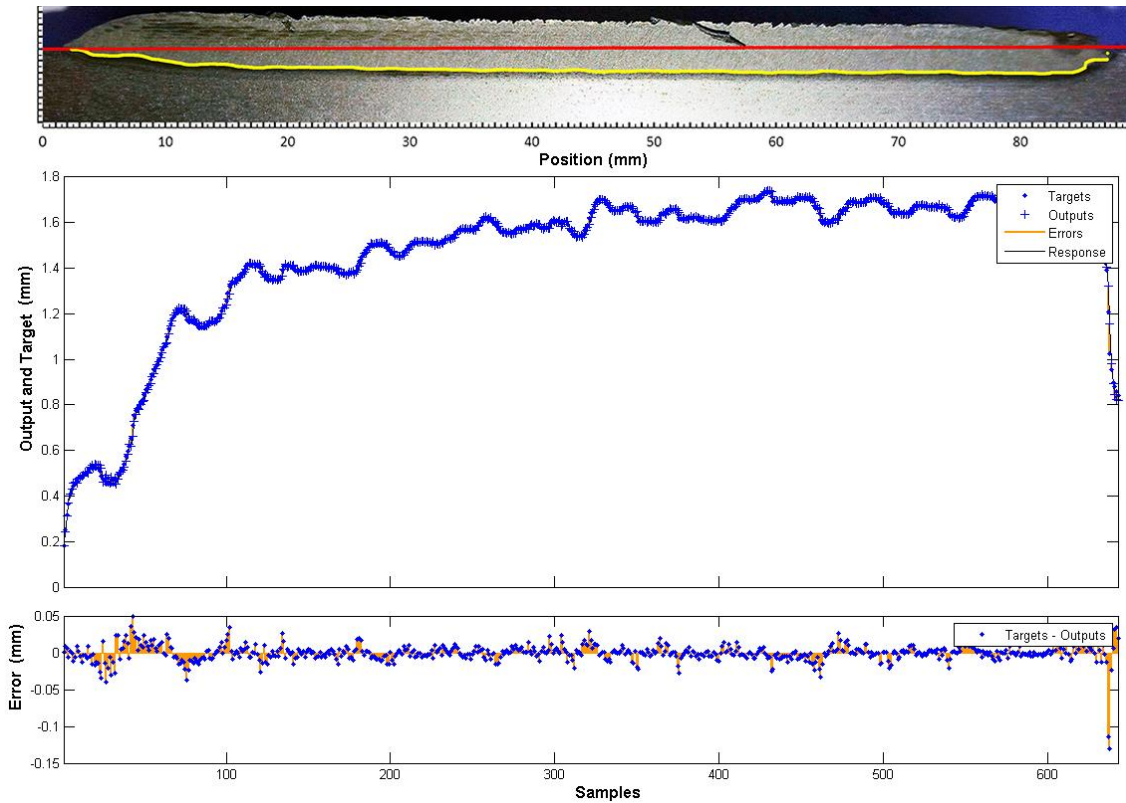


Figure 76 Comparison between the response of the weld bead depth model (outputs) and the measurements obtained in the experiment 3 (targets). In the time axis, each time value corresponds with a position in the piece.

The test of the model, with a different data set obtained from experiment 4, had a fit of 0.99196 and the performance was  $3.65 \times 10^{-4}$ . The closed loop performance was 0.8157 and the network response was very good with an estimation error less than 0.05 mm. These results are shown in Figure 77 and Figure 78.

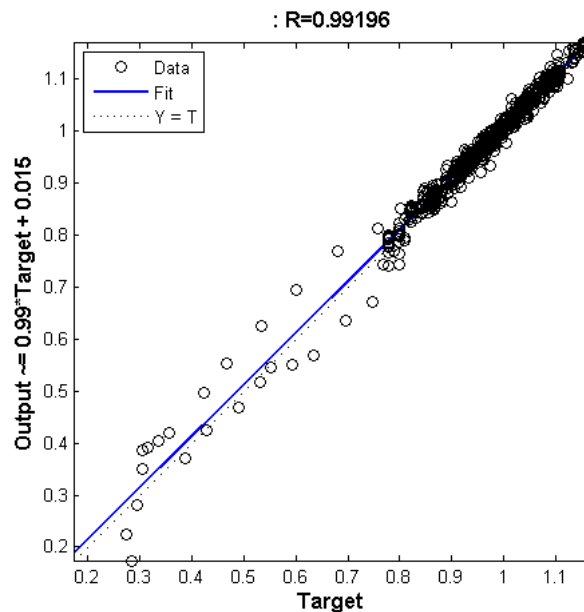


Figure 77 Regression curve between the measurements of the weld bead depth (target) obtained in experiment 4 and the output of the weld bead depth model obtained from the data of experiment 3.

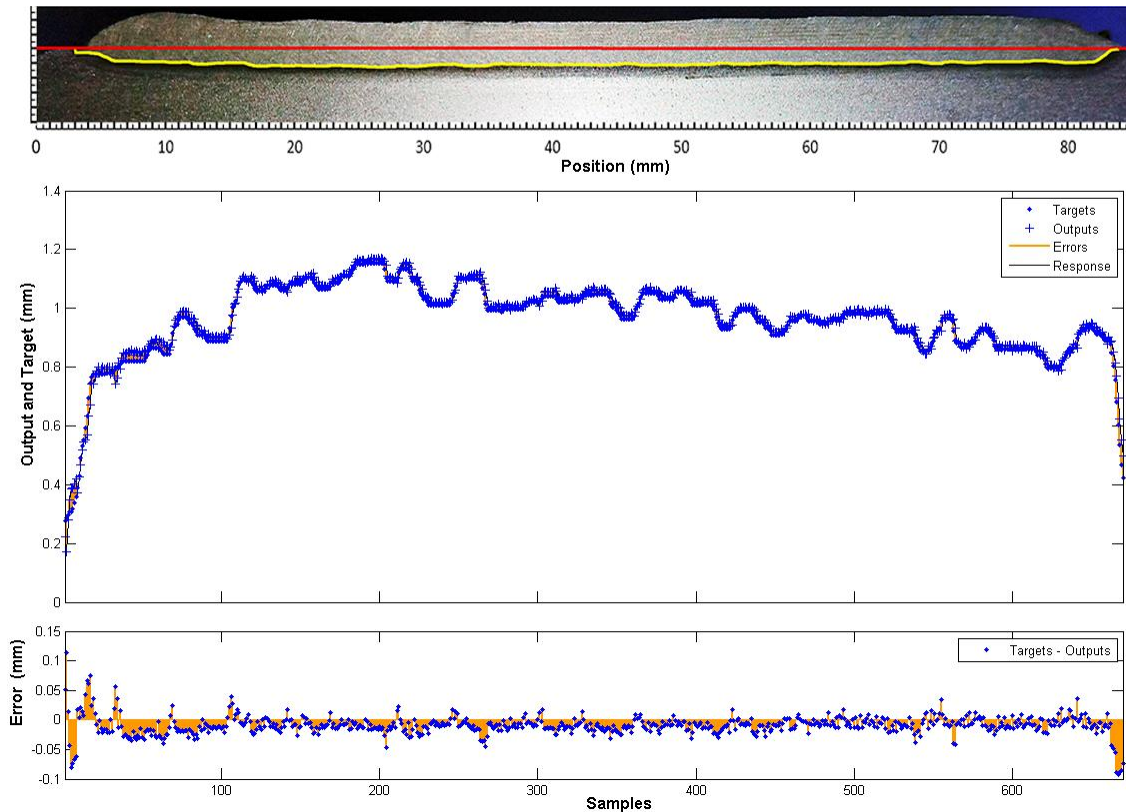


Figure 78 Comparison between the measurements of the weld bead depth (target) obtained in experiment 4 and the output of the weld bead depth model obtained from the data of experiment 3. In the time axis, each time value corresponds with a position in the piece.

#### 4.2.4 Modeling and validation of the weld bead width estimator with data from experiments with argon and carbon dioxide as the shielding gas.

The weld bead width estimator model was obtained with data from experiment 4. Several tests were performed with different filter values applied to inputs and targets values. The best result was obtained filtering the targets with a median filtering of a 15-element window.

The model has a fit of 0.96433, a performance or median square error (MSE) of 0.125 at epoch 5, a closed loop performance of 1.6.

The regression plot for this model shown in Figure 79a achieves an excellent value across the range of measurements. The performance curve (see Figure 79b) does not show indications of overfitting and defines the best performance value in epoch 5. This performance is obtained in open loop and the input  $\widehat{W}(nT - T)$  is substituted by the corresponding target value in the input data set. The performance value is larger than in previous models, but still acceptable.

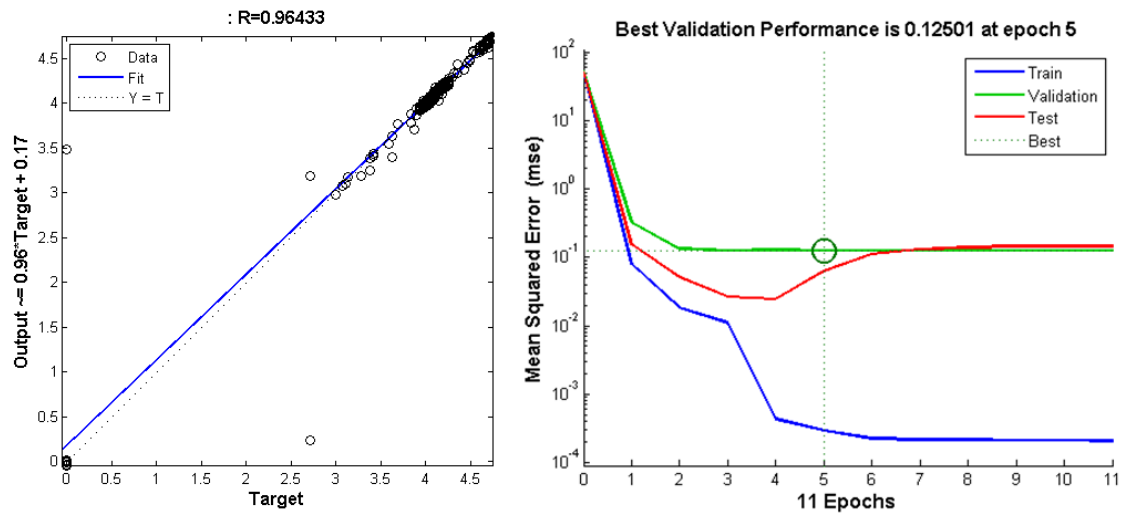


Figure 79. Results in the training of the weld bead width model for experiments with argon and oxygen:  
 (a) Regression curve between the model output and the real depth (target); (b) Performance curve in training, validation and test.

The response curve (see Figure 80) shows that the model is able to reproduce the behavior of the process with good accuracy. The estimation error was very good throughout the curve.

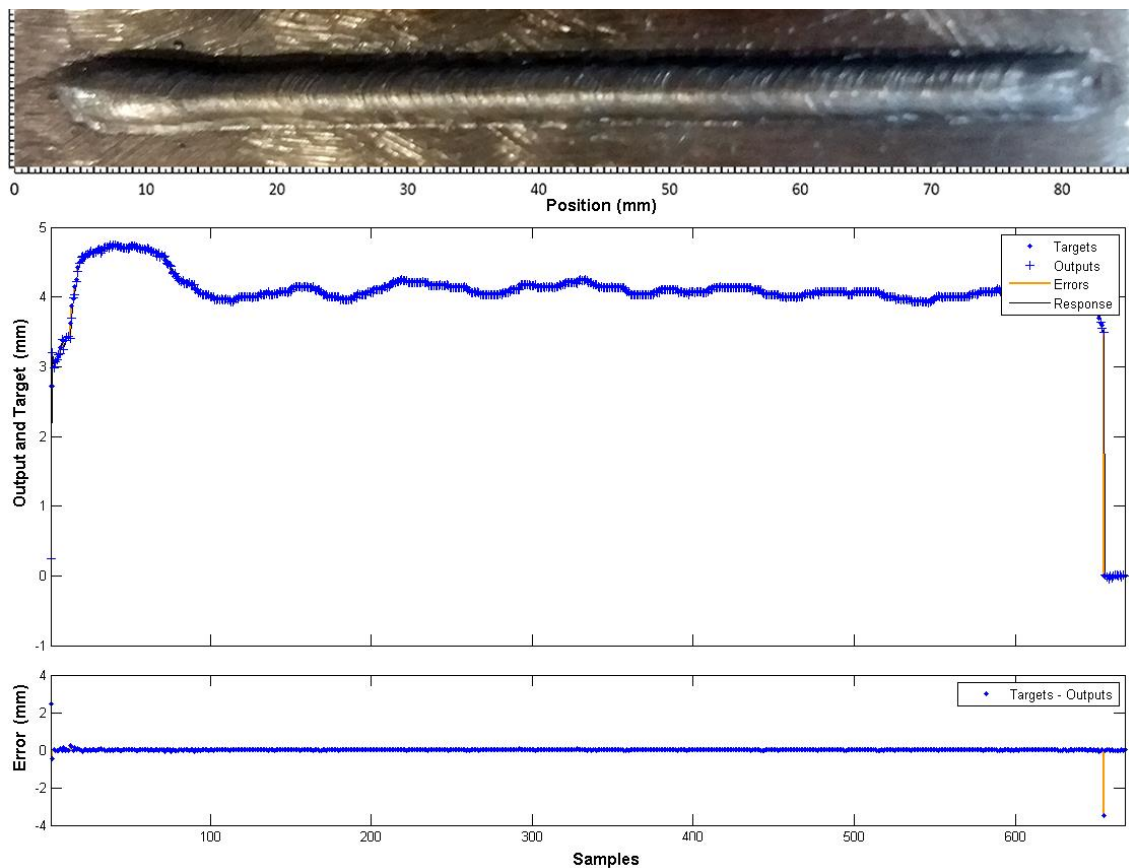


Figure 80 Comparison between the response of the weld bead width model (outputs) and the measurements obtained in the experiment 4 (targets). In the time axis, each time value corresponds with a position in the piece.

The test of the model, with a different data set obtained from experiment 3, had a fit of 0.97287 and the performance was 0.0174. The closed loop performance was 1.8 and the network response was acceptable with an estimating error less than 0.5 mm throughout the curve. These results are shown below.

It is important to note that even with sharp variations in the measured variables (see Figure 82 data near time 530), it was possible to obtain correct estimates without a considerable delay.

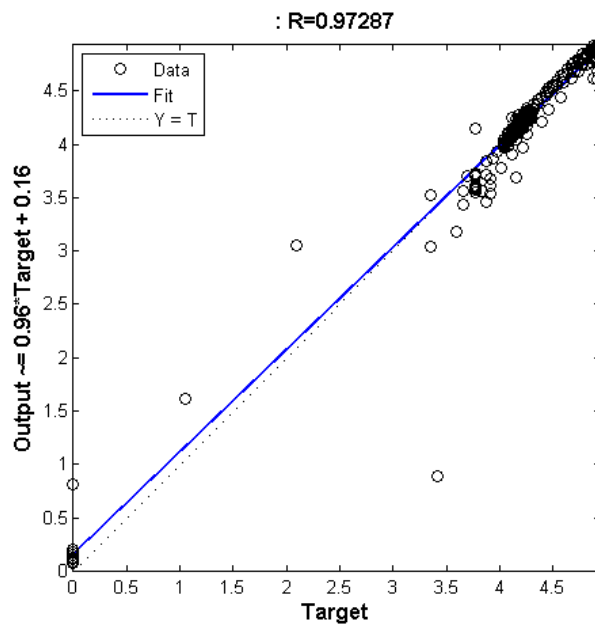


Figure 81 Regression curve between the measurements of the weld bead width (target) obtained in experiment 3 and the output of the weld bead depth model obtained from the data of experiment 4.

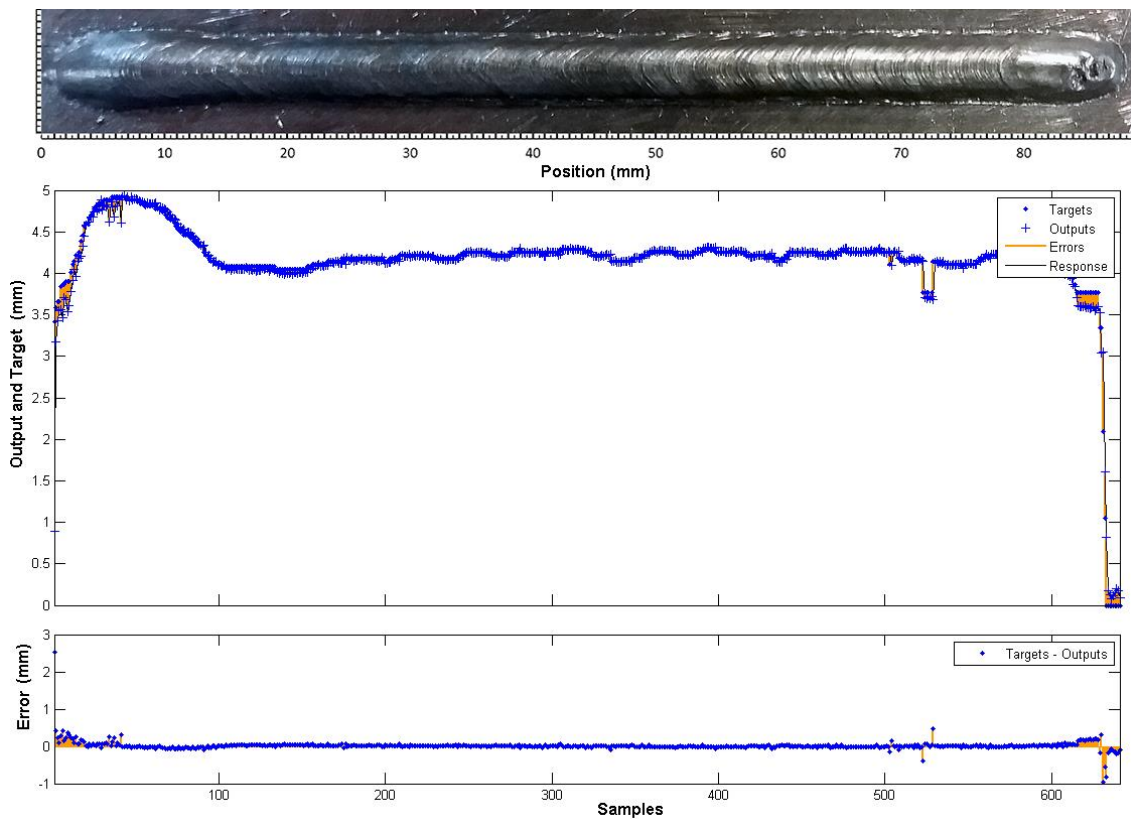


Figure 82 Comparison between the measurements of the weld bead width (target) obtained in experiment 3 and the output of the weld bead width model obtained from the data of experiment 4. In the time axis, each time value corresponds with a position in the piece.

### 4.3 Chapter considerations.

Four experiments were performed for this work. Two experiments use argon and oxygen as the shielding gas and two use argon and carbon dioxide to make two groups under different process conditions and process models.

These changes between groups were carried out with the objective of testing the proposed modeling methodology. In this sense, the results confirm that the methodology can be successfully applied under different process conditions. Proof of this are the results obtained in the modeling of the process for different shielding gases.

In each group two models were obtained: **weld bead depth estimator model** and **weld bead width estimator model**. For this, we send stimuli to the process to cause changes in the selected variables and capture the dynamics of their behavior. The stimuli were selected based on a basic knowledge about the relationships between the input and output variables of the process. The summary of main results as shown in Table 8 and Table 9.

Table 8 Results obtained in train and test of estimators with argon and oxygen as protection gas.

Estimator of	Depth		Width	
	Train	Test	Train	Test
Fit (R)	0.9984	0.9901	0.9957	0.8516
Epoch	6	-	11	-
MSE open loop	7.6109e-4	8.076e-4	31.008e-4	0.128
MSE closed loop	6.4 e-3	0.224	0.094	0.67

Table 9 Results obtained in train and test of estimators with argon and carbon oxide as protection gas.

Estimator of	Depth		Width	
	Train	Test	Train	Test
Fit (R)	0.9993	0.99196	0.96433	0.97287
Epoch	14	-	5	-
MSE open loop	7.16e-5	3.65e-4	0.125	0.0174
MSE closed loop	0.8122	0.8157	1.6	1.8

The methodology proposed to estimate the depth and width of the weld bead, tries to offer a tool that can be used in industry by operators and technicians without a high scientific level.

In the estimator validation is possible to notice that the initial and final instability of the arc welding process causes considerable errors in the estimates. This is an important aspect to take into account in automatic control systems of weld bead geometry. These estimation errors can cause the controller to respond abruptly and unacceptably, generating more instability in the process. Algorithms to reduce or cancel the action of the controllers must be applied in these intervals.

On the other hand, once the welding arc is opened, the models behave satisfactorily, offering an accurate estimate. Even with sharp variations in the measured variables, it was possible to obtain correct estimates without a considerable delay.

A problem, which we consider important but which was not possible to verify, is the cumulative error due to the feedback of the weld bead depth estimated value. This can cause the estimation error to increase in very long weld beads. This is because it is not possible to measure the real value of the weld bead depth on-line and therefore it is not possible to correct the estimation



error during welding. This problem also exists in the case of weld bead width estimates, but it can be corrected by applying the solution proposed in section **Error! Reference source not found.**

The results obtained show that the proposed methodology has a good performance and precision. In addition, its use can be simple if it is applied as part of a package of tools developed for this purpose.

## 5 Conclusions.

Sensory fusion techniques have been developed for the estimation of depth and width of the weld bead using a new approach to process data processing.

The estimators, based in the fusion of thermographic information and arc welding variables, were implemented and tested with satisfactory results.

For the modeling of the estimators, a data acquisition and open loop control system was developed, which showed good performance to capture the dynamics of the welding process.

An image processing algorithm was developed to measure the depth of the weld bead over its entire length and that guarantees the data to obtain the dynamic model of this magnitude.

The models of depth and width of the weld bead are valid only in the working conditions of the identification experiments. In case of change in operating conditions the model must be updated.

Based on the developed estimators, was made a proposal of multivariate control of the orbital welding process in real-time, which includes a robotic emulator of the orbital welding process.

The work offers a non-contact measuring tool for use in the industry by operators, technicians and unskilled labor.

## 6 Future works.

Continue the test of the methodology to obtain the penetration and weld bead width estimators under other operating conditions and other welding processes.

Continue the development of the multivariate control of the orbital welding process within the framework of the approved CNPQ project.

## Bibliographic references.

- ABU-AYYAD, M.; DUBAY, R. Real-time comparison of a number of predictive controllers. *ISA Transactions*, v. 46, n. 3, p. 411–418, 2007.
- ACUITY L. *AccuRange 200™ Laser Measurement Sensor User's Manual*. . [S.l: s.n.]. Disponível em: <[www.acuitylaser.com](http://www.acuitylaser.com)>. , 2014
- AENDENROOMER, A.J.R.; DEN OUDEN, G. Weld Pool Oscillation as a Tool for Penetration Sensing during Pulsed GTA Welding. *Welding Journal*, n. May, p. 181–187, 1998.
- AKKAS, Nuri *et al.* Modeling and Analysis of the Weld Bead Geometry in Submerged Arc Welding by Using Adaptive Neurofuzzy Inference System. *Mathematical Problems in Engineering*, v. 2013, p. 1–10, 2013.
- ALFARO, Sadek C. A; DREWS, Paul. Intelligent systems for welding process automation. *Journal of the Brazilian Society of Mechanical Sciences and Engineering*, v. 28, n. 1, p. 25–29, mar. 2006. Disponível em: <[http://www.scielo.br/scielo.php?pid=S1678-58782006000100002&script=sci\\_arttext%5Chttp://www.scielo.br/scielo.php?script=sci\\_arttext&pid=S1678-58782006000100002&lng=en&nrm=iso&tlng=en](http://www.scielo.br/scielo.php?pid=S1678-58782006000100002&script=sci_arttext%5Chttp://www.scielo.br/scielo.php?script=sci_arttext&pid=S1678-58782006000100002&lng=en&nrm=iso&tlng=en)>.
- ALFARO, Sadek C Absi *et al.* Characterization of “Humping” in the GTA welding process using infrared images. *Journal of Materials Processing Technology*, v. 223, p. 216–224, 2015.
- ALFARO, Sadek Crisóstomo Absi. Sensors for quality control in welding. *Soldagem & Inspeção*, v. 17, n. 3, p. 192–200, set. 2012. Disponível em: <[http://www.scielo.br/scielo.php?script=sci\\_arttext&pid=S0104-92242012000300003&lng=en&tlng=en](http://www.scielo.br/scielo.php?script=sci_arttext&pid=S0104-92242012000300003&lng=en&tlng=en)>.
- ALFARO, Sadek Crisóstomo Absi. *Uso de técnicas de sensoriamento (fusão de sensores) para monitoração e controle “on-line” da qualidade em processos de soldagem. Processo 401073/2016-5, Chamada Universal 01/2016 - Faixa C*. . Brasília, DF, Brazil: [s.n.], 2016.
- ALFARO, Sadek Crisóstomo Absi; CAYO, Eber Huanca. Sensing fusion data from the optic and acoustic emissions of electric arcs in the GMAW-S process for welding quality assessment. *Sensors (Switzerland)*, v. 12, n. 6, p. 6953–6966, 2012.
- AMERICAN WELDING SOCIETY STAFF. *Welding science and technology*. 9th. ed. [S.l.]: American Welding Society, 2002. v. 1.
- ANDERSEN, K. *et al.* Artificial Neural Networks Applied to Arc Welding Process Modeling and Control. *IEEE Transactions on Industry Applications*, v. 26, n. 5, p. 824–830, 1990.
- ÅSTRÖM, K. J.; HÄGGLUND, T. The future of PID control. *Control Engineering Practice*, v. 9, n. 11, p. 1163–1175, 2001.
- AYALA, Helon *et al.* Nonlinear Model Predictive Control Hardware Implementation with Custom-precision Floating Point Operations. 2016.
- AYALA, Helon Vicente Hultmann *et al.* Efficient hardware implementation of radial basis function neural network with customized-precision floating-point operations. *Control Engineering Practice*, v. 60, n. December 2016, p. 124–132, 2017. Disponível em: <<http://linkinghub.elsevier.com/retrieve/pii/S0967066116302921>>.
- BAE, K.Y.; LEE, T.H.; AHN, K.C. An optical sensing system for seam tracking and weld pool control in gas metal arc welding of steel pipe. *J.Mater. Process. Technol.*, v. 120, n. 2, p. 458–465, 2002.
- BANERJEE, P.; CHIN, B.A. Front side sensor based dynamic weld penetration control in robotic GTAW. 1992, [S.l: s.n.], 1992.

- BANGS, Edmund R.; LONGINOW, Nicholas E.; BLAHA, James R. *Using infrared image to monitor and control welding*. . Unites States: [s.n.]. Disponível em: <<http://illinois.patentlibrary.us/us-4877940.html>>. , 1989
- BARRON ADAME, J. M. *Modelado de un sistema de supervisión de la calidad del aire usando técnicas de fusión de sensores y redes neuronales. PhD thesis*. 2010. Universidad Politécnica de Madrid, 2010. Disponível em: <[http://oa.upm.es/4839/1/JOSE\\_MIGUEL\\_BARRON\\_ADAME.pdf](http://oa.upm.es/4839/1/JOSE_MIGUEL_BARRON_ADAME.pdf)>.
- BATES, B.E.; HARDT, D.E. A real-time calibrated thermal model for closed-loop weld bead geometry control. *Trans. ASME J. Dyn. Syst., Meas. Control*, p. 25–33, 1985.
- BEARDSLEY, H.E.; ZHANG, Y.M. M.; KOVACEVIC, R. Infrared sensing of full penetration state in gas tungsten arc welding. *International Journal of Machine Tool and Manufacturing*, v. 34, n. 8, p. 1079–1090, nov. 1994. Disponível em: <<http://linkinghub.elsevier.com/retrieve/pii/0890695594900140>>. Acesso em: 17 mar. 2017.
- BEHAR, Alberto Aguado. *Identificación y Control Adaptativo*. [S.l: s.n.], 2003.
- BENNETT, Stuart. Development of the PID Controller. *IEEE Control Systems*, v. 13, n. 6, p. 58–62, 1993.
- BESTARD, Guillermo Alvarez; ALFARO, Sadek C Absi. Propuesta de diseño de un sistema de control de la geometría del cordón en procesos de soldadura orbital. *Revista Control, Cibernética y Automatización*, v. IV, n. 1, 2016.
- BESTARD, Guillermo Alvarez; ALFARO, Sadek C Absi. Sistema de adquisición de datos y control en lazo abierto para procesos de soldadura GMAW. 2017, La Habana: [s.n.], 2017. p. 1–7.
- BESTARD, Guillermo Alvarez; ALFARO, Sadek Crisóstomo Absi. Sensor fusion: theory review and applications. 2015, Rio de Janeiro, Brazil: [s.n.], 2015. Disponível em: <<http://www.swge.inf.br/proceedings/paper/?P=COB-2015-0365>>.
- BHARATHI, M; SELVAKUMAR, C. Interaction reducer for closed-loop control of multivariable systems. *International Journal of Engineering Trends and Technology*, v. 4, 2012. Disponível em: <<http://www.ijettjournal.org>>. Acesso em: 12 abr. 2017.
- BOUGHTON, P.; RIDER, G.; SMITH, E.J. Feedback of weld penetration in 1978. *Adisances Weld. Proc.*, p. 203–209, 1978.
- BRISTOL, Edgar H. On a new measure of interaction for multivariable process control. *IEEE Transactions on Automatic Control*, v. 11, n. 1, p. 133–134, 1966.
- BROSED, Francisco Javier *et al.* 3D geometrical inspection of complex geometry parts using a novel laser triangulation sensor and a robot. *Sensors*, v. 11, n. 1, p. 90–110, 2011.
- BROWN, Lyndon J.; MEYN, Sean P.; WEBER, Robert A. Adaptive dead-time compensation with application to a robotic welding system. *IEEE Transactions on Control Systems Technology*, v. 6, n. 3, p. 335–349, 1998.
- CARLSON, N.M. et al. Ultrasonic NDT methods for weld sensing. *Materials Evaluation*, v. 50, n. 11, p. 1338–1343, 1992.
- CARLSON, N.M.; JOHNSON, J.A. Ultrasonic sensing of weld pool penetration. *Welding Journal*, v. 67, n. 11, p. 239–246, 1988.
- CARVAJAL, James; CHEN, Guanrong; OGMEN, Haluk. Fuzzy PID controller: Design, performance evaluation, and stability analysis. *Information sciences*, v. 123, n. 3, p. 249–270, 2000.
- CASALINO, G.; HU, S. J.; HOU, W. Deformation prediction and quality evaluation of the gas metal arc welding butt weld. *Inst. Mech. Eng., B J. Eng. Manuf.*, v. 217, n. 11, p. 1615–1622, 2003.

CASTANEDO SOTELA, F. *Fusión de Datos Distribuida en Redes de Sensores Visuales Utilizando Sistemas Multi-Agente*. PhD Thesis. 2010. Universidad Carlos III de Madrid, 2010.

CAYO, Eber H.; ALFARO, Sadek C. A. A Non-Intrusive GMA Welding Process Quality Monitoring System Using Acoustic Sensing. *Sensors (Basel, Switzerland)*, v. 9, n. 9, p. 7150–66, 2009. Disponible em: <<http://www.pubmedcentral.nih.gov/articlerender.fcgi?artid=3290464&tool=pmcentrez&rendertype=abstract>>.

CAYO, Eber Huanca; ALFARO, Sadek Crisóstomo Absi. Aplicabilidad del monitoreo de emisiones del arco eléctrico para el control de calidad en el proceso MAG-S. *Soldagem & Inspeção*, v. 16, n. 4, p. 341–349, dez. 2011. Disponible em: <[http://www.scielo.br/scielo.php?script=sci\\_arttext&pid=S0104-92242011000400005&lng=es&tlng=es](http://www.scielo.br/scielo.php?script=sci_arttext&pid=S0104-92242011000400005&lng=es&tlng=es)>.

CAYO, EH. Weld transference modes identification through sound pressure level in GMAW process. *Journal of Achievements in Materials and*, v. 29, n. 1, p. 57–62, 2008. Disponible em: <[http://www.journalamme.org/papers\\_vol29\\_1/2918.pdf](http://www.journalamme.org/papers_vol29_1/2918.pdf)>.

CHANDRASEKHAR, N. *et al.* Intelligent modeling for estimating weld bead width and depth of penetration from infra-red thermal images of the weld pool. *J IntellManuf*, v. 26, p. 59–71, 2015.

CHANG, Doyoung *et al.* A new seam-tracking algorithm through characteristic-point detection for a portable welding robot. *Robotics and Computer Integrated Manufacturing*, v. 28, n. 1, p. 1–13, 2012. Disponible em: <<http://dx.doi.org/10.1016/j.rcim.2011.06.001>>.

CHEN, Bo; CHEN, Shanben; FENG, Jicai. A study of multisensor information fusion in welding process by using fuzzy integral method. *The International Journal of Advanced Manufacturing Technology*, v. 74, n. 1–4, p. 413–422, 4 set. 2014. Disponible em: <<http://link.springer.com/10.1007/s00170-014-6001-6>>.

CHEN, Bo; FENG, Jicai. Multisensor information fusion of pulsed GTAW based on improved D-S evidence theory. *The International Journal of Advanced Manufacturing Technology*, v. 71, n. 1–4, p. 91–99, 20 mar. 2014. Disponible em: <<http://link.springer.com/10.1007/s00170-013-5288-z>>.

CHEN, Bo; WANG, Jifeng; CHEN, Shanben. Modeling of pulsed GTAW based on multi-sensor fusion. *Sensor Review*, v. 29, n. 3, p. 223–232, 26 jun. 2009. Disponible em: <<http://www.emeraldinsight.com/doi/10.1108/02602280910967639>>.

CHEN, Bo; WANG, Jifeng; CHEN, Shanben. Prediction of pulsed GTAW penetration status based on BP neural network and D-S evidence theory information fusion. *The International Journal of Advanced Manufacturing Technology*, v. 48, n. 1–4, p. 83–94, 25 abr. 2010. Disponible em: <<http://link.springer.com/10.1007/s00170-009-2258-6>>.

CHEN, Huabin *et al.* Closed-loop control of robotic arc welding system with full-penetration monitoring. *Journal of Intelligent and Robotic Systems: Theory and Applications*, v. 56, n. 5, p. 565–578, 2009.

CHEN, S.B. *et al.* Intelligent Methodology for Sensing, Modeling and Control of Pulsed GTAW Part 2 Butt Joint Welding. *Welding Research Supplement*, n. June, p. 164s–174s, 2000.

CHEN, S B *et al.* Robotic Welding Systems with Vision-Sensing and Self-learning Neuron Control of Arc Welding Dynamic Process. *Journal of Intelligent and Robotic Systems*, v. 36, p. 191–208, 2003.

CHEN, S B; WU, J. *Intelligentized methodology for arc welding dynamical processes: visual information acquiring, knowledge modeling and intelligent control*. Springer ed. Berlin: [s.n.], 2008.

CHEN, Shang-Ben; WU, Jing. *Lecture notes in electrical engineering. Intelligentized methodology for arc welding dynamical process. Visual information acquiring, knowledge modeling and intelligent control*. [S.l.]: Springer, 2009.

CHEN, W.; CHIN, B. A. Monitoring joint penetration using infrared sensing techniques. *Welding Journal*, v. 69, n. 4, p. 18–85, 1990.

CHEN, W. H.; NAGARAJAN, S.; CHIN, B. A. Weld penetration sensing and control. *Infrared Technology*, v. 972, n. XIV, p. 268–272, 1988.

CHEN, Ziqin; GAO, Xiangdong. Detection of weld pool width using infrared imaging during high-power fiber laser welding of type 304 austenitic stainless steel. *Int J AdvManuf Technol*, v. 74, p. 1247–1254, 2014.

CHENG, S B *et al.* Welding robotic systems with visual sensing and real - time control of dynamic weld pool during pulsed GTAW. *International Journal of Robotics and Automation*, v. 19, n. 1, p. 28–35, 2004.

CHI, Y.; YIN, D.; GAO, Y. Closed-loop control of weld penetration in pulsed plasma arc welding. *Weld. Prod.*, v. 1, p. 11–17, 1980.

CHIN, Bryan A. *Welding GAP Control Using Infrared Sensing*. . [S.l: s.n.], 2001. Disponível em: <<http://oai.dtic.mil/oai/oai?verb=getRecord&metadataPrefix=html&identifier=ADA392828>>. Acesso em: 17 mar. 2017.

CHO, H.S. Application of AI to welding process automation. 1992, [S.l: s.n.], 1992. p. 303–308.

CHOKKALINGHAM, S.; CHANDRASEKHAR, N.; VASUDEVAN, M. Predicting the depth of penetration and weld bead width from the infra red thermal image of the weld pool using artificial neural network modeling. *Journal of Intelligent Manufacturing*, v. 23, n. 5, p. 1995–2001, 2012.

CLARKE, D. W.; MOHTADI, C. Properties of generalized predictive control. *Automatica*, v. 25, n. 6, p. 859–875, 1989.

CLARKE, D. W.; MOHTADI, C.; TUFFS, P. S. Generalized predictive control-Part I. The basic algorithm. *Automatica*, v. 23, n. 2, p. 137–148, 1987a.

CLARKE, D. W.; MOHTADI, C.; TUFFS, P. S. Generalized Predictive Control-Part II Extensions and interpretations. *Automatica*, v. 23, n. 2, p. 149–160, 1987b.

CNM. *Xfuzzy Fuzzy logic design tools*. . [S.l: s.n.]. Disponível em: <<http://www2.imse-cnm.csic.es/Xfuzzy/>>. , 2012

COOK, G.E. Feedback and adaptive control to process variables in arc welding. *Mech. Auto. Robot. Weld.*, p. 321–329, 1980.

COOK, George E; BARNETT, Robert Joel; STRAUSS, Alvin M. *Neural Network Systems Techniques in Weld Modeling and Control*. [S.l: s.n.], 1999.

CRUZ, Jorge Andrés Girón. *Uma metodologia para modelagem e controle da altura do reforço e da largura do cordão de solda no processo gmaw*. *Master Thesis in Mechatronic Systems*. 2014. Universidade de Brasília, 2014.

CUIURI, Dominic. *Control of the short-circuit gas metal arc welding process using instantaneous current regulation*. *PhD Thesis*. 2000. University of Wollongong, 2000.

CULLEN, J D *et al.* Multisensor fusion for on line monitoring of the quality of spot welding in automotive industry. *Measurement*, v. 41, p. 412–423, 2008.

DAVE, Vivek R; COLA, Mark J. *Methods for control of fudion welding process by maintaining a controller weld pool volume*. . [S.l: s.n.]. , 2013

- DE, A.; PARLE, D. Real time seam tracking system for automated fusion arc welding. *Science and Technology of Welding and Joining*, v. 8, n. 5, p. 340–346, 2003.
- DE GARCIA, José A Orłowski *et al.* Advances of orbital gas tungsten arc welding for Brazilian space applications - Experimental setup. *Journal of Aerospace Technology and Management*, v. 2, n. 2, p. 203–210, 2010.
- DI, Li *et al.* Neural-network-based self-organized fuzzy logic control for arc welding. *Engineering Applications of Artificial Intelligence*, v. 14, n. 2, p. 115–124, 2001.
- DOMFELD, D.A.; TOMIZUKA, M.; LANGARI, G. Modelling and adaptive control of arc welding processes. *Meas. Control Batch Manufact.*, p. 53–64, 1982.
- DOUMANIDIS, C.C.; HARDT, D.E. Simultaneous in-process control of heat affected zone and cooling rate during arc welding. *Welding Journal*, v. 69/5, p. 186s–196s, 1990.
- DOUMANIDIS, Charalabos C. Multiplexed and Distributed Control of Automated Welding. *IEEE Control Systems*, v. 14, n. 4, p. 13–24, 1994.
- DOUMANIDIS, Charalabos; KWAK, Yong M. Multivariable adaptive control of the bead profile geometry in gas metal arc welding with thermal scanning. *International Journal of Pressure Vessels and Piping*, v. 79, n. 4, p. 251–262, 2002.
- DUBOUÉ, Ramón Carrasco; BESTARD, Guillermo Alvarez. Diseño e implementación de un PID Profesional y un PID Difuso utilizando un microcontrolador PIC18F4550. 2014, [S.l: s.n.], 2014. Disponible em: [http://www.researchgate.net/profile/Ramon\\_Carrasco\\_Duboue/publication/273439309\\_Diseño\\_e\\_implementación\\_de\\_un\\_PID\\_Profesional\\_y\\_un\\_PID\\_Difuso\\_utilizando\\_un\\_microcontrolador\\_PIC18F4550/links/5500823a0cf2aee14b54f6b8.pdf](http://www.researchgate.net/profile/Ramon_Carrasco_Duboue/publication/273439309_Diseño_e_implementación_de_un_PID_Profesional_y_un_PID_Difuso_utilizando_un_microcontrolador_PIC18F4550/links/5500823a0cf2aee14b54f6b8.pdf).
- EINERSON, C.J. *et al.* Development of an intelligent system for cooling rate and fill control in GMAW. *Proc. ASME Japan/USA Symp. Flex. Auto.*, 1992.
- FAN, Haibo *et al.* Low-cost infrared sensing system for monitoring the welding process in the presence of plate inclination angle. *Journal of Materials Processing Technology*, v. 140, p. 668–675, 2003.
- FENN, R. Ultrasonic monitoring and control during arc welding. *Welding Journal*, v. 64, n. 9, p. 18–24, 1985.
- FLIR-SYSTEMS. *ThermoVision™ A40 M Manual del usuario*. . [S.l: s.n.]. , 2004
- FLIR-SYSTEMS. *ThermoVision™ SDK User 's manual*. . [S.l: s.n.]. , 2007
- FONT COMAS, Tomas *et al.* A Passive Imaging System for Geometry Measurement for the Plasma Arc Welding Process. *IEEE Transactions on Industrial Electronics*, v. 64, n. 9, p. 7201–7209, set. 2017. Disponible em: <http://ieeexplore.ieee.org/document/7884932/>.
- FRADEN, Jacob. *Handbook of modern sensors. Physics, designs, and applications*. 3. ed. [S.l.]: Springer-Verlag NewYork Berlin Heidelberg, 2004.
- FRANCO, Fernando Díaz. *Monitorização e localização de defeitos na soldagem TIG através do sensoriamento infravermelho. Master Thesis*. 2008. 124 f. Universidad de Brasília, 2008.
- FRANCOIS, Nadeau *et al.* *Method and apparatus for controlling root pass weld penetration in open butt joints*. . Unites States: [s.n.]. Disponible em: <http://illinois.patentlibrary.us/us-4733051.html>. , 1988
- FRONIUS. *Rob 4000 / 5000 Operating Instructions*. . [S.l.]: Fronius International GmbH. , 2001
- GARRIDO, J; VÁZQUEZ, F; MORILLA, F. Diseño de Sistemas de Control Multivariable por Desacoplo con Controladores PID. 2012, [S.l: s.n.], 2012. p. 64–71. Disponible em:

<<http://www.researchgate.net/publication/265806776>>.

GHANTY, P. *et al.* Artificial neural network approach for estimating weld bead width and depth of penetration from infrared thermal image of weld pool. *Science and Technology of Welding and Joining*, v. 13, n. 4, p. 395–401, 2008. Disponível em: <<http://www.tandfonline.com/doi/full/10.1179/174329308X300118>>.

GLADKOV, E.A. *et al.* An automatic stabilizer of penetration in plasma welding with a penetrating arc. *Weld. Prod. U.S.S.R.*, v. 24, p. 26–27, 1974.

GMBH, Berger Lahr. *Product manual. Intelligent Compact Drive Pulse/direction stepper motor IclA IDS*. . [S.l: s.n.]. , 2006

GRAD, Ladislav *et al.* Feasibility study of acoustic signals for on-line monitoring in short circuit gas metal arc welding. *International Journal of Machine Tools & Manufacture*, v. 44, p. 555–561, 2004.

GUU, A.C.; ROKHLIN, S.I. Computerized radiographic weld penetration control with feedback on weld pool depression. *Material Evaluation*, v. 47, n. 1204–1210, 1989.

GWEON, Dae-gab. In-Process Joint Strength Estimation in Pulsed Laser Spot Welding Using Artificial Neural Networks. *Journal of Manufacturing Processes*, v. 1, n. 1, p. 31–42, 1999.

HALE, M. Multivariable geometry control of welding. 1990, [S.l: s.n.], 1990.

HARDT, D. E.; KATZ, J. M. Ultrasonic measurement of weld penetration. *Welding Journal*, v. 63, n. 9, p. 273–281, 1984.

HARDT, D.E.; GARLOW, D.A.; WEINERT, J.B. A model of full penetration arc welding for control system design. *Trans. ASME J. Dyn. Sysf., Meas. Control*, v. 107, p. 40–46, 1985.

HENDERSON, D E *et al.* Adaptive Control of an Arc Welding Process. *IEEE Control Sysytems*, p. 49–53, 1993.

HENDERSON, Thomas C. *et al.* Sensor Fusion. *Control Problems in Robotic and Automation (Lectures Notes in Control and Information Science)*, v. 230, p. 193–207, 1998.

HIRAI, Akira *et al.* Sensing and Control of Weld Pool by Fuzzy-Neural Network in Robotic Welding System. 2001, [S.l: s.n.], 2001. p. 238–242.

HKS PROZESSTECHNIK. *ThermoProfilScanner*. Disponível em: <<http://www.hks-prozesstechnik.de/produkte/thermoprofilscanner/>>. Acesso em: 18 mar. 2017.

HUANG, Wei; KOVACEVIC, R. Development of a real-time laser-based machine vision system to monitor and control welding processes. *International Journal of Advanced Manufacturing Technology*, v. 63, n. 1–4, p. 235–248, 2012.

HUANG, Xixia *et al.* An adaptive inverse control method based on SVM-fuzzy rules acquisition system for pulsed GTAW process. *International Journal of Advanced Manufacturing Technology*, v. 44, n. 7–8, p. 686–694, 2009.

HUNTER, J.J.; BRYCE, G.W.; DOHERTY, J. On-line control of the arc welding process. *Dev. Mech. Auto. Robot. Weld.*, p. 37–49, 1980.

HURTADO, Ronald H; ALFARO, Sadek C A; LLANOS, Carlos H. Discontinuity welding detection using an embedded hardware system. 2012, [S.l: s.n.], 2012. p. 879–888.

ICELAND, William F.; MARTIN E. O'DOR. *Weld penetration control*. . Unites States: [s.n.]. , 1971

IMC-SOLDAGEM. *Manual de Instruções Inversal 450/600*. . [S.l: s.n.]. , 2005

INVENSENSE. *MPU-6000/6050: World's First Integrated 3-Axis Gyro, 3-Axis Accel and 9-Axis MotionFusion*. Disponível em: <[www.invensense.com](http://www.invensense.com)>.



JANTZEN, Jan. Tuning Of Fuzzy PID Controllers. *Technical University of Denmark, Department of Automation*, v. 871, n. 98-H, p. 1–22, 1998. Disponível em: <<http://www.automa.altervista.org/Documenti/fpid.pdf>>.

JOU, Min. A study on development of an H-infinity robust control system for arc welding. *Journal of Manufacturing Systems*, v. 21, n. 2, p. 140–150, 2002. Disponível em: <<http://www.sciencedirect.com/science/article/pii/S0278612502800073>>.

KARADENIZ, Erdal. The effect of process parameters on penetration in gas metal arc welding processes. *Materials and Design*, v. 28, p. 649–656, 2007.

KARASAKAL, Onur *et al.* Online tuning of fuzzy PID controllers via rule weighing based on normalized acceleration. *Engineering Applications of Artificial Intelligence*, v. 26, n. 1, p. 184–197, 2013.

KAZEMIAN, Hassan B. Comparative study of a learning fuzzy PID controller and a self-tuning controller. *ISA Transactions*, v. 40, n. 3, p. 245–253, 2001.

KIELHORN, W. H. *et al.* *Survey of Joining, Cutting and Allied Processes*. [S.l.: s.n.], 2002.

KIM, I. S.; BASU, A.; SIORES, E. Mathematical models for control of weld bead penetration in the GMAW process. *International Journal of Advanced Manufacturing Technology*, v. 12, n. 6, p. 393–401, 1996.

KIM, I S *et al.* An investigation into an intelligent system for predicting bead geometry in GMA welding process. *Journal of Materials Processing Technology*, v. 159, p. 113–118, 2005.

KIM, Ill-Soo *et al.* A Study on Development of a New Algorithm for Predicting the Process Variables in GMA Welding Processes. *JSME International Journal*, v. 44, n. 2, p. 561–566, 2001.

KO, C N; WU, C J. A PSO-tuning method for design of fuzzy PID controllers. *Journal of Vibration and Control*, v. 14, n. 3, p. 375–395, 2008.

KOVACEVIC, R.; ZHANG, Y. M. Real-time image processing for monitoring of free weld pool surface. *J. Manuf. Sci. Eng.*, v. 119, n. 5, p. 161–169, 1997. Disponível em: <<http://manufacturingscience.asmedigitalcollection.asme.org/article.aspx?articleid=1433169>> . Acesso em: 17 mar. 2017.

KOVACEVIC, R.; ZHANG, Y. M. Sensing free surface of arc weld pool using specular reflection: principle and analysis. *Proc Instn Mech Engrs*, v. 210, 1996.

KOVACEVIC, R.; ZHANG, Y. M.; RUAN, S. Sensing and Control of Weld Pool Geometry for Automated GTA Welding. *Journal of Engineering for Industry*, v. 117, n. 2, p. 210, 1995. Disponível em: <<http://manufacturingscience.asmedigitalcollection.asme.org/article.aspx?articleid=1447976>> . Acesso em: 17 mar. 2017.

KOVACEVIC, R.; ZHANG, Y M; LI, L. Monitoring of Weld Joint Penetration Based on Weld Pool Geometrical Appearance. *Welding Journal*, v. Welding re, p. 317–329, 1996.

KUMAR, Vineet; NAKRA, B. C.; MITTAL, A. P. A review on classical and fuzzy pid controllers. *International Journal of Intelligent Control Systems*, v. 16, n. 3, p. 170–181, 2011. Disponível em: <<http://www.ezconf.net/newfiles/IJICS/232/IJICS-2011-03-02-Final-1.pdf>>.

LAP LASER. *Laser sensors*. Disponível em: <<https://www.lap-laser.com/pt/general-industries/products/measurement/laser-sensors/>>. Acesso em: 1 jan. 2017.

LI, Kehai Li Kehai; ZHANG, YuMing Zhang YuMing. Interval Model Control of Consumable Double-Electrode Gas Metal Arc Welding Process. *IEEE Transactions on Automation Science and Engineering*, v. 7, n. 4, p. 1–14, 2009. Disponível em:

<<http://ieeexplore.ieee.org/lpdocs/epic03/wrapper.htm?arnumber=5325790>>.

LIM, T. G.; CHO, H. S. Estimation of weld pool sizes in GMA welding process using neural networks. *J. Syst. Control Eng.*, v. 207, n. 1, p. 15–26, 1993.

LIN, M.; EAGAR, T. W. Influence of Arc Pressure on Weld Pool Geometry. *Welding Journal*, p. 163–169, 1985.

LIN, M. L.; EAGAR, T. W. Influence of surface depression and convection on arc weld pool geometry. 1984, New York: [s.n.], 1984. p. 63–69.

LINCOLN ELECTRIC. *Gas Metal Arc Welding Product and Procedure Selection*. . [S.l: s.n.]. Disponível em: <[www.lincolnelectric.com](http://www.lincolnelectric.com)>. , 2017

LIU, Wen hong; XIE, Zhi. Design and Simulation Test of Advanced Secondary Cooling Control System of Continuous Casting Based on Fuzzy Self-Adaptive PID. *Journal of Iron and Steel Research International*, v. 18, n. 1, p. 26–30, 2011.

LIU, Y. K.; ZHANG, Y M; KVIDAHL, L. Skilled Human Welder Intelligence Modeling and Control : Part II — Analysis and Control Applications. *The welding journal*, v. 93, n. May, p. 162–170, 2014a.

LIU, Y. K.; ZHANG, Y M; KVIDAHL, L. Skilled Human Welder Intelligence Modeling and Control: Part 1 — Modeling. *The welding journal*, v. 93, n. February, p. 46s–52s, 2014b.

LIU, Yukang; ZHANG, Weijie; ZHANG, Yuming. Dynamic neuro-fuzzy-based human intelligence modeling and control in GTAW. *IEEE Transactions on Automation Science and Engineering*, v. 12, n. 1, p. 324–335, 2015.

LIU, Yukang; ZHANG, Yuming. Iterative local ANFIS-based human welder intelligence modeling and control in pipe GTAW process: A data-driven approach. *IEEE/ASME Transactions on Mechatronics*, v. 20, n. 3, p. 1079–1088, 2015.

LLANOS, Carlos H.; HURTADO, Ronald H.; ALFARO, Sadek C. Absi. FPGA-based approach for change detection in GTAW welding process. *Journal of the Brazilian Society of Mechanical Sciences and Engineering*, v. 38, n. 3, p. 913–929, 2016. Disponível em: <<http://link.springer.com/10.1007/s40430-015-0371-z>>.

LOTT, L.A. Ultrasonic detection of molten solid interface of weld pools. *Materials Evaluation*, v. 42, n. 3, p. 337–341, 1984.

LÜ, Fenglin *et al.* A novel control algorithm for weld pool control. *Industrial Robot: An International Journal*, v. 37, n. 1, p. 89–96, 2010.

LU, J L; CHEN, G R; YING, H. Predictive fuzzy PID control: theory, design and simulation. *Information Sciences*, v. 137, n. 1–4, p. 157–187, 2001. Disponível em: <[http://ac.els-cdn.com/S0020025501001190/1-s2.0-S0020025501001190-main.pdf?\\_tid=b233020e-e547-11e5-8339-00000aacb361&acdnat=1457453360\\_67e3233e675a81227ababf9565cf7047](http://ac.els-cdn.com/S0020025501001190/1-s2.0-S0020025501001190-main.pdf?_tid=b233020e-e547-11e5-8339-00000aacb361&acdnat=1457453360_67e3233e675a81227ababf9565cf7047)>.

LU, Wei *et al.* Robust sensing and control of weld pool surface. *IFAC Proceedings Volumes (IFAC-PapersOnline)*, v. 16, p. 301–306, 2005.

LUKENS, William E.; DENALE, Robert; ZANIS, Charles A. *System for control of weld arc development*. . Unites States: [s.n.]. Disponível em: <<http://illinois.patentlibrary.us/us-4975558.html>>. , 1990

LUO, H *et al.* Vision based neurofuzzy logic control of weld pool geometry. *Science and Technology of Welding and Joining*, v. 7, n. 5, p. 321–325, 2002.

LUO, Hong; CHEN, Xiaoqi. Laser visual sensing for seam tracking in robotic arc welding of titanium alloys. *Int J Adv Manuf Technol*, v. 26, p. 1012–1017, 2005.

- LV, Na *et al.* Real-time control of welding penetration during robotic GTAW dynamical process by audio sensing of arc length. *International Journal of Advanced Manufacturing Technology*, v. 74, n. 1–4, p. 235–249, 2014.
- LV, Na *et al.* Research on detection of welding penetration state during robotic GTAW process based on audible arc sound. *Industrial Robot: An International Journal*, v. 40, n. 5, p. 474–493, 16 ago. 2013. Disponível em: <<http://www.emeraldinsight.com/doi/10.1108/IR-09-2012-417>>.
- MACHADO, Marcus Vinícius Ribeiro *et al.* Sistema Embarcado para Monitoramento Sem Fio de Sinais em Soldagem a Arco Elétrico com Abordagem Tecnológica. *Soldag. Insp.*, v. 17, n. 2, p. 147–157, 2012.
- MALDON, H. Tracking Pitches for Broadcast Television. *Computer*, v. 5, 2002.
- MASUMUDI, R.; HARDT, D.E. Multivariable control of geometric and thermal properties in GTAW. 1992, Gatlinburg: [s.n.], 1992.
- MATHWORKS. *Hyperbolic tangent sigmoid transfer function - MATLAB tansig*. Disponível em: <<https://www.mathworks.com/help/nnet/ref/tansig.html>>. Acesso em: 19 jul. 2017.
- MICRO-EPSILON. *Laser line triangulation*. Disponível em: <<http://www.micro-epsilon.com/service/glossar/Laser-Linien-Triangulation.html>>. Acesso em: 1 jan. 2017a.
- MICRO-EPSILON. *optoNCDT ILR Laser distance sensors*. . [S.l.: s.n.]. Disponível em: <<http://www.micro-epsilon.com/download/products/cat--optoNCDT-ILR--en-us.pdf>>. , 2017b
- MIGUEL, V. *et al.* Optimización del proceso de soldadura GMAW de uniones a tope de la aleación AA 6063-T5 basada en la metodología de superficie de respuesta y en la geometría del cordón de soldadura. *Revista de Metalurgia*, v. 48, n. 5, p. 333–350, 2012.
- MILLÁN, R.; QUERO, J. M.; FRANQUELO, L. G. Welding data acquisition based on FPGA. *IC's for instrumentation and control*, p. 2–6, 1997. Disponível em: <<http://hdl.handle.net/11441/23596>>. Acesso em: 21 mar. 2017.
- MILLER, Matthew *et al.* Development of automated real-time data acquisition system for robotic weld quality monitoring. *Mechatronics*, v. 12, n. 9–10, p. 1259–1269, 2002.
- MILLER ELECTRIC MFG. CO. *Guidelines For Gas Metal Arc Welding (GMAW)*. [S.l.: s.n.], 2012. Disponível em: <[www.MillerWelds.com%0AGuidelines](http://www.MillerWelds.com%0AGuidelines)>.
- MIYACHI, H. *In-process control of root-gap changes during butt welding*. 1989. M.I.T., 1989.
- MOON, H.; BEATTIE, R. J. Development of Adaptive Fill Control for Multitorch Multipass Submerged Arc Welding. *International Journal of Advanced Manufacturing Technology*, v. 19, n. 2002, p. 867–872, 2002.
- MOON, H S; KIM, Y B; BEATTIE, R J. Multi sensor data fusion for improving performance and reliability of fully automatic welding system. *International Journal of Advanced Manufacturing Technology*, v. 28, n. 3–4, p. 286–293, 2006.
- MOORE, K. L.; NAIDU, D. S.; OZCELIK, S. *Modeling, sensing and control of gas metal arc welding*. [S.l.]: Elsevier, 2003. Disponível em: <[https://books.google.com.br/books?id=5GyYjNMcnxAC&lpg=PR7&ots=\\_H5Mjfp3Uv&dq=Modeling%2C sensing and control of gas metal arc welding moore&pg=PR7#v=onepage&q=Modeling, sensing and control of gas metal arc welding moore&f=true](https://books.google.com.br/books?id=5GyYjNMcnxAC&lpg=PR7&ots=_H5Mjfp3Uv&dq=Modeling%2C%20sensing%20and%20control%20of%20gas%20metal%20arc%20welding%20moore&pg=PR7#v=onepage&q=Modeling,%20sensing%20and%20control%20of%20gas%20metal%20arc%20welding%20moore&f=true)>.
- MOTA, Carolina Pimenta *et al.* Estudo da emissão de raios infravermelho próximo em processos de soldagem a arco. *Soldagem e Inspecao*, v. 16, n. 1, p. 44–52, 2011.
- MOTA, Carolina Pimenta *et al.* Sistema de visão por infravermelho próximo para monitoramento

de processos de soldagem a arco. *Soldagem & Inspeção*, v. 18, n. 1, p. 19–30, mar. 2013. Disponível em: <[http://www.scielo.br/scielo.php?script=sci\\_arttext&pid=S0104-92242013000100004&lng=pt&tlng=pt](http://www.scielo.br/scielo.php?script=sci_arttext&pid=S0104-92242013000100004&lng=pt&tlng=pt)>.

MOTA, Carolina Pimento *et al.* Sistema de visão por infravermelho próximo para monitoramento de processos de soldagem a arco. *Soldagem e Inspeção*, v. 18, n. 1, p. 19–30, mar. 2013. Disponível em: <[http://www.scielo.br/scielo.php?script=sci\\_arttext&pid=S0104-92242013000100004&lng=pt&tlng=pt](http://www.scielo.br/scielo.php?script=sci_arttext&pid=S0104-92242013000100004&lng=pt&tlng=pt)>.

MOUSAVI, Mohammad Anzehaee; HAERI, Mohammad. Welding current and arc voltage control in a GMAW process using ARMarkov based MPC. *Control Engineering Practice*, v. 19, n. 12, p. 1408–1422, 2011. Disponível em: <<http://dx.doi.org/10.1016/j.conengprac.2011.07.015>>.

MTI INSTRUMENTS. *Laser triangulation principle*. Disponível em: <<http://www.mtiinstruments.com/technology-principles/laser-triangulation-sensors>>. Acesso em: 1 jan. 2017.

MURATA MANUFACTURING CO., Ltd. *SCC1300 Combined Gyro Sensor and Accelerometer*. Disponível em: <<http://www.murata.com/products/sensor/gyro/scc1300>>. Acesso em: 1 jan. 2017.

MURUGAN, N; GUNARAJ, V. Prediction and control of weld bead geometry and shape relationships in submerged arc welding of pipes. *Journal of Materials Processing Technology*, v. 168, p. 478–487, 2005.

NAGARAJAN, S. *et al.* Weld pool size and position control using IR sensors. 1990, Arizona State University: [s.n.], 1990.

NAGARAJAN, S.; CHEN H., W.; CHIN, B. A. Infrared sensing for adaptive arc welding. *Welding Journal*, v. 68, n. 11, p. 462–466, 1989.

NAGESH, D S; DATTA, G L. Genetic algorithm for optimization of welding variables for height to width ratio and application of ANN for prediction of bead geometry for TIG welding process. *Applied Soft Computing Journal*, v. 10, n. 3, p. 897–907, 2010. Disponível em: <<http://dx.doi.org/10.1016/j.asoc.2009.10.007>>.

NAGESH, D S; DATTA, G L. Prediction of weld bead geometry and penetration in shielded metal-arc welding using artificial neural networks. *Journal of Materials Processing Technology*, v. 123, p. 303–312, 2002.

NEFEDYEV, Evgeny; GOMERA, Victor; SUDAKOV, Alexander. Application of Acoustic Emission Method for Control of Manual Arc Welding, Submerged Arc Welding. 2014, Dresden, Germany: [s.n.], 2014. p. 1–9.

NELE, L.; SARNO, E.; KESHARI, A. Modeling of multiple characteristics of an arc weld joint. *International Journal of Advanced Manufacturing Technology*, v. 69, n. 5–8, p. 1331–1341, 2013.

NIED, Herman A.; BAHETI, Radhakisan S. *Arc welding adaptive process control system*. . Unites States: [s.n.], 1986

NIT. *Infrared sensor system for arc welding process monitoring*. Disponível em: <[www.niteurope.com](http://www.niteurope.com)>.

NIT. *TACHYON 1024 microCORE*. . [S.l: s.n.]. Disponível em: <[www.niteurope.com](http://www.niteurope.com)>. , 2014

NOMURA, H. *et al.* Arc light intensity controls current in SA welding system. *I. Welding Metal Fab.*, p. 457–463, 1980.

NOMURA, Hirokazu; SUGITANI, Yuji; TAMAOKI, Naohiro. *Method of automatically controlling height of a weld bead*. . Unites States: [s.n.]. Disponível em: <<http://illinois.patentlibrary.us/us>>.

4608481.html>. , 1986

OZCELIK, S.; MOORE, K. L.; NAIDU, S. D. Application of MIMO direct adaptive control to gas metal arc welding. 1998, [S.l: s.n.], 1998. p. 1762–1766.

PAL, Kamal; PAL, Surjya K. Monitoring of Weld Penetration Using Arc Acoustics. *Materials and Manufacturing Processes*, v. 26, n. 5, p. 684–693, maio 2011. Disponível em: <<http://www.tandfonline.com/doi/abs/10.1080/10426910903496813>>.

PALACÍOS, Ana María Guzmán. *Uso de técnicas de termografía para detección de discontinuidades no processo GTAW através do monitoramento da poça de fusão. Master Thesis in Mechatronic Systems*. 2010. Universidad de Brasília, 2010.

PEÑA SANTOS, Deyci Yamile. *Evaluación de la técnica de termografía para la detección de defectos en soldaduras*. 2012. 96 f. Universidad Libre, 2012.

PINTO-LOPERA, Jesús; S. T. MOTTA, José; ABSI ALFARO, Sadek. Real-Time Measurement of Width and Height of Weld Beads in GMAW Processes. *Sensors*, v. 16, n. 9, p. 1500, 15 set. 2016. Disponível em: <<http://www.mdpi.com/1424-8220/16/9/1500>>. Acesso em: 17 mar. 2017.

R. S. PARMAR. *Welding processes and thecnologia*. 2. ed. [S.l.]: Romesh Chander Khanna, 1997.

REAL TIME ENGINEERS LTD. *The FreeRTOS™ Reference Manual*. . [S.l: s.n.]. Disponível em: <<http://www.freertos.org/>>. , 2016

REGUEIRO, Manuel A. *et al*. Semantic mediation of observation datasets through Sensor Observation Services. *Future Generation Computer Systems*, v. 67, p. 47–56, fev. 2017. Disponível em: <<http://linkinghub.elsevier.com/retrieve/pii/S0167739X16302722>>.

RENWICK, R. J.; RICHARDSON, R. W. Experimental investigation of GTA weld pool oscillations. *Welding Reasearch Supplement to the Welding Journal*, p. 29–35, 1983.

RICHARDSN, R.W.; CONRARDY, C. Coaxial vison-based control of GMAW. *Proc. ASME Japan/USA Symp. Flex. Auto.* ASME Japa, 1992.

RIFTEK. *Laser Scanners RF625 Series*. . [S.l: s.n.]. Disponível em: <[https://riftek.com/media/documents/rf625/manual/2D\\_Laser\\_Scanners\\_RF625\\_Series\\_eng.pdf](https://riftek.com/media/documents/rf625/manual/2D_Laser_Scanners_RF625_Series_eng.pdf)>. , 2015

RODRIGUEZ-COBO, L. *et al*. Fiber Bragg Grating sensors for on-line welding diagnostics. 2013, [S.l: s.n.], 2013. p. 1–4.

RODRÍGUEZ MUÑOZ, P. *Aplicación del filtro de Kalman al seguimiento de objetos en secuencias de imágenes*. 2003. Universidad Rey Juan Carlos, 2003.

ROGALSKI, Antoni. Infrared detectors: status and trends. *Progress in Quantum Electronics*, v. 27, n. 2–3, p. 59–210, jan. 2003. Disponível em: <<http://linkinghub.elsevier.com/retrieve/pii/S0079672702000241>>.

ROKHLIN, S. I.; GUU, A. C. A study of arc force, pool depression, and weld penetration during gas tungsten arc welding. *Welding Journal*, v. 72, n. 8, p. 381–390, 1993.

ROKHLIN, S.I.; CHO, K.; GUU, A.C. Closed-loop process control of weld penetration using real-time radiography. *Material Evaluation*, v. 47, p. 363–369, 1989.

S. NAGARAJAN; CHIN, B.A.; CHEN., W. Control of the welding process using infrared sensors. *IEEE Transactions on Robotics and Automation*, v. 8, n. 1, p. 86–93, 1992.

SAEED, G.; ZHANG, Y. M.; JAYNES, C. Weld pool surface monitoring and depth extraction using a calibrated CCD sensor. 2005, [S.l: s.n.], 2005. p. 665–670.

SANTIAGO MARTÍNEZ, R. S. *Control y Comportamiento de Robots Omnidireccionales*.

- Posicionamiento y Sensor Data Fusion. PhD Thesis.* 2009. Universidad de la República de Montevideo, 2009.
- SCHLICHTING, J *et al.* Thermographic testing of spot welds. *NDT and E International*, v. 48, p. 23–29, 2012. Disponível em: <<http://dx.doi.org/10.1016/j.ndteint.2012.02.003>>.
- SCOTTY, Américo; PONOMAREV, Vladimir. *Soldagem MIG-MAG: melhor entendimento, melhor desempenho.* [S.l.]: Artibler Editora Ltda., 2008.
- SFORZA, Patrizia; BLASIIS, Dario De. On-line optical monitoring system for arc welding. *NDT&International*, v. 35, p. 37–43, 2002.
- SHEN, Hong-yuan *et al.* Arc welding robot system with seam tracking and weld pool control based on passive vision. *Int J Adv Manuf Technol*, v. 39, p. 669–678, 2008.
- SHI, Y *et al.* Laser-Vision-Based Measurement and Analysis of Weld Pool Oscillation Frequency in GTAW-P. *Welding Journal*, v. 94, n. 5, p. 176–187, 2015.
- SMITH, C.J. Self-adaptive control of penetration in tungsten inert gas weld. *Advances Weld. Proc*, p. 272–282, 1974.
- SMITH, Carlos A.; CORRIPIO, Armando B. *Principles and practice of a automatic process control.* Second Edi ed. [S.l.]: John Wiley, 1997.
- SMITH, Jeremy S.; BALFOUR, Chris. Real-time top-face vision based control of weld pool size. *Industrial Robot: An International Journal*, v. 32, n. 4, p. 334–340, 2005. Disponível em: <<http://www.emeraldinsight.com/10.1108/01439910510600209>>.
- SONG, J.B.; HARDT, D.E. Closed-loop control of weld pool depth using a thermally based depth estimate. *Welding Journal*, v. 72, n. 10, p. 471s–478s, 1993.
- SONG, J.B.; HARDT, D.E. Multivariable adaptive control of bead geometry in GMA welding. 1991, [S.l.: s.n.], 1991.
- SOYGUDER, Servet; KARAKOSE, Mehmet; ALLI, Hasan. Design and simulation of self-tuning PID-type fuzzy adaptive control for an expert HVAC system. *Expert Systems with Applications*, v. 36, n. 3 PART 1, p. 4566–4573, 2009. Disponível em: <<http://dx.doi.org/10.1016/j.eswa.2008.05.031>>.
- SREEDHAR, U *et al.* Automatic defect identification using thermal image analysis for online weld quality monitoring. *Journal of Materials Processing Tech.*, v. 212, n. 7, p. 1557–1566, 2012. Disponível em: <<http://dx.doi.org/10.1016/j.jmatprotec.2012.03.002>>.
- SUBASHINI, L.; VASUDEVAN, M. Adaptive Neuro-Fuzzy Inference System (ANFIS)-Based Models for Predicting the Weld Bead Width and Depth of Penetration from the Infrared Thermal Image of the Weld Pool. *Metallurgical and Materials Transactions B*, v. 43, n. 1, p. 145–154, 8 fev. 2012. Disponível em: <<http://link.springer.com/10.1007/s11663-011-9570-x>>.
- SUDHAKARAN, R *et al.* Prediction and optimization of depth of penetration for stainless steel gas tungsten arc welded plates using artificial neural networks and simulated annealing algorithm. *Neural Comput & Applic*, 2011.
- SUGITANI, Yuji; NISHI, Yasuhiko. *Automatic arc-welding method.* . Unites States: [s.n.]. Disponível em: <<http://illinois.patentlibrary.us/us-4816641.html>>. , 1989
- SUNG, B. S *et al.* Fuzzy regression model to predict the bead geometry in the robotic welding process. *ACTA METALLURGICA SINICA (ENGLISH LETTERS)*, v. 20, n. 6, p. 391–397, 2007.
- SUZUKI, A.; HARDT, D.E.; VALAVANI, L. Application of adaptive control theory to on-line GTA weld geometry regulation. *Trans. ASME .I. Dyn. Syst., Meas. Conrrol*, p. 93–103, 1991.
- TAKAHASHI, Youichi *et al.* *Image processing welding control method.* . United States: [s.n.].

Disponível em: <<http://illinois.patentlibrary.us/us-4594497.html>>. , 1986

TORRES, Edna Margarita Moncayo. *Uma metodologia para modelagem e controle da largura do cordão de solda no processo GMAW*. Master Thesis in Mechatronic Systems. 2013. Universidade de Brasília, 2013.

VAN BOHEMEN, S. M. C.; HERMANS, M. J. M.; DEN OUDEN, G. Monitoring of martensite formation during welding by means of acoustic emission. *Journal of Physics D: Applied Physics*, v. 34, n. 22, p. 3312–3317, 2001.

VELASCO, Ronald Hernan Hurtado. *Detecção on-line de descontinuidades no processo de soldagem GTAW usando sensoriamento infravermelho e FPGAs*. Master Thesis in Mechatronic Systems. 2010. Universidade de Brasília, 2010.

VORMAN, A.R.; BRANDT, H. Feedback control of GTA welding using puddle width measurement. *Welding Journal*, p. 742–746, 1978.

WANG, Q. L.; YANG, C. L.; GENG, Z. Separately excited resonance phenomenon of the weld pool and its application. *Welding Research Supplement of Welding Journal*, v. 72, n. 9, p. 455–462, 1993.

WANG, Xuewu. Three-dimensional vision-based sensing of GTAW : a review. *Int J AdvManuf Technol*, v. 72, p. 333–345, 2014.

WANG, Zhijiang; ZHANG, Yuming; WU, Lin. Adaptive interval model control of weld pool surface in pulsed gas metal arc welding. *Automatica*, v. 48, n. 1, p. 233–238, 2012. Disponível em: <<http://dx.doi.org/10.1016/j.automatica.2011.09.052>>.

WEI, Shanchun *et al.* Three-dimensional weld seam tracking for robotic welding by composite sensing technology. *Industrial Robot: An International Journal*, v. 38, n. 5, p. 500–508, 2011.

WIKLE III, H. C. *et al.* Infrared Sensing Techniques for Penetration Depth Control of the Submerged Arc Welding Process. *Journal of Materials Processing Technology*, v. 113, p. 228–233, 2001.

WIKLEIII, H C; ZEE, R H; CHIN, B A. A sensing system for weld process control. *Journal of Materials Processing Technology*, v. 90, p. 254–259, 1999.

WU, CS; GAO, JQ. Vision-based neuro-fuzzy control of weld penetration in gas tungsten arc welding of thin sheets. *Int J Model Identif Control*, v. 1, n. 2, p. 126–132, 2006.

WU, Ying; JIANG, Hang; ZOU, Min. The Research on Fuzzy PID Control of the Permanent Magnet Linear Synchronous Motor. *Physics Procedia*, v. 24, p. 1311–1318, 2012.

XIAO, Y. H.; OUDEN, G. A study of GTA weld pool oscillation. *Welding Research Supplement of Welding Journal*, v. 69, n. 8, p. 289–293, 1990.

XIAO, Y. H.; OUDEN, G. Weld pool oscillation during GTA welding of mild steel. *Welding Research Supplement of Welding Journal*, v. 72, n. 8, p. 428–434, 1993.

XIONG, Jun; ZHANG, Guangjun. Adaptive control of deposited height in GMAW-based layer additive manufacturing. *Journal of Materials Processing Technology*, v. 214, n. 4, p. 962–968, 2014. Disponível em: <<http://dx.doi.org/10.1016/j.jmatprotec.2013.11.014>>.

XUE, Yu *et al.* Fuzzy regression method for prediction and control the bead width in the robotic arc-welding process. *Journal of Materials Processing Technology*, v. 165, p. 1134–1139, 2005.

YAN, Jun rong *et al.* H2/Hoo Robust controller of the arc welding inverter power. *Journal of Computers*, v. 6, n. 4, p. 705–710, 2011.

YAN, ZH; ZHANG, GJ; WU, L. Simulation and controlling for weld shape process in P-GMAW based on fuzzy logic. 2011, [S.l: s.n.], 2011. p. 2078–2082.

- YANG, Fu; ZHANG, Shu; ZHANG, Wen Ming. Design of GTAW Wire Feeder Control System Based on Nios II. *Applied Mechanics and Materials*, v. 397–400, p. 1909–1912, set. 2013. Disponível em: <<http://www.scientific.net/AMM.397-400.1909>>. Acesso em: 21 mar. 2017.
- YANG, Sang-Min *et al.* Weld line detection and process control for welding automation. *Measurement Science and Technology*, v. 18, n. 3, p. 819–826, 2007. Disponível em: <<http://stacks.iop.org/0957-0233/18/i=3/a=034?key=crossref.1d9e62c15260b1fcae542c4adfca1a08>>.
- YANG, J. *et al.* Ultrasonic weld penetration depth sensing with a laser phased array. Proceedings of 1994 ASME International Mechanical Engineering Congress. *Manufacturing Science and Engineering*, v. 68, n. 1, p. 245–254, 1994.
- YOO, C. D. *Effects of weld pool conditions on pool oscillation*. 1990. The Ohio State University, Columbus, Ohio., 1990.
- YOO, C. D. Experimental study on sensitivity and signal characteristics of weld pool oscillation. *Transactions of the Japan Welding Society*, v. 24, n. 2, p. 54–62, 1993.
- YU, Huanwei; YE, Zhen; CHEN, Shanben. Application of arc plasma spectral information in the monitor of Al–Mg alloy pulsed GTAW penetration status based on fuzzy logic system. *The International Journal of Advanced Manufacturing Technology*, v. 68, n. 9–12, p. 2713–2727, 23 out. 2013. Disponível em: <<http://link.springer.com/10.1007/s00170-013-4877-1>>.
- YU KANG LIU; YU MING ZHANG. Model-Based Predictive Control of Weld Penetration in Gas Tungsten Arc Welding. *IEEE Transactions on Control Systems Technology*, v. 22, n. 3, p. 955–966, maio 2014. Disponível em: <<http://ieeexplore.ieee.org/document/6547167/>>.
- ZACKSENHOUSE, M.; HARDT, D. E. Weld Pool Impedance Identification for Size Measurement and Control. *Journal of Dynamic Systems, Measurement, and Control*, v. 105, n. 3, p. 179, 1983. Disponível em: <<http://dynamicsystems.asmedigitalcollection.asme.org/article.aspx?articleid=1403448>>.
- ZHANG, G J; CHEN, S B; WU, L. Intelligent control of pulsed GTAW with filler metal. *Welding Journal*, v. 84, n. 1, p. 9S–16S, 2005.
- ZHANG, Y. M. *Real-time weld process monitoring*. Cambridge, England: [s.n.], 2008.
- ZHANG, Y. M.; KOVACEVIC, R.; WU, L. Dynamic analysis and identification of gas tungsten arc welding process for full penetration control. *Journal of Engineering for Industry*, v. 118, n. 1, p. 123–136, 1996.
- ZHANG, Y. M.; LIU, Y. C. Modeling and control of quasi-keyhole arc welding process. *Control Engineering Practice*, v. 11, n. 12, p. 1401–1411, 2003.
- ZHANG, YM; KOVACEVIC, R; WU, L. Dynamic analysis and identification of gas tungsten arc welding process for full penetration control. *J Eng Ind Trans ASME*, v. 118, n. 1, p. 123–136, 1996.
- ZHANG, YM Y.M.; KOVACEVIC, R. Neurofuzzy model-based predictive control of weld fusion zone geometry. *IEEE Transactions on Fuzzy Systems*, v. 6, n. 3, p. 389–401, 1998. Disponível em: <<http://ieeexplore.ieee.org/document/705507/>>. Acesso em: 17 mar. 2017.
- ZHANG, Yu. M.; KOVACEVIC, R.; LI, L. Adaptive control of full penetration gas tungsten arc welding. *IEEE Transactions on Control Systems Technology*, v. 4, n. 4, p. 394–403, 1996. Disponível em: <<http://ieeexplore.ieee.org/lpdocs/epic03/wrapper.htm?arnumber=508887>>.
- ZHAO, DB *et al.* Intelligent control for the shape of the weld pool in pulsed GTAW with filler metal. *Weld Res Suppl*, v. 80, n. 11, p. 253–260, 2001.
- ZI, Bin *et al.* The dynamics and sliding mode control of multiple cooperative welding robot



manipulators. *International Journal of Advanced Robotic Systems*, v. 9, p. 1–10, 2012.

Appendix 1 Representative information about measurement and estimation of the bead weld geometry found in literature.

Reference	Process	Estimation			Measure		Welding Position	Sample time	Hardware	Comment
		Estimated Variable	Model Type	Analysis Technique	Measured Variable	Sensor				
(ICELAND; MARTIN E. O'DOR, 1971)		weld bead depth				infrared thermograph				Patent weld penetration control
(NOMURA, H. <i>et al.</i> , 1980)		weld bead depth				infrared thermograph				
(RENWICK; RICHARDSON, 1983)	GTAW	weld bead depth				pool oscillation				An experimental investigation of the dynamics of molten weld pools was carried out for stationary, partial penetration. High speed films demonstrated that weld pool was oscillating at the same frequency as the arc voltage.
(ZACKSENHOUSE; HARDT, 1983)		back side bead width, penetration state			frequency of oscillation of the puddle-surface	pool oscillation	Flat			A method for determining this bead back side width in real-time is proposed that measures the natural frequency of pool motion when driven by a time varying arc plasma force. It requires that the frequency of oscillation of the puddle-surface tension system be identified in real-time and then regulated using the torch velocity as the control input.
(HARDT; KATZ, 1984)	GTAW	weld bead depth			P	contact ultrasound, contactless ultrasound	Flat		Electromagnetic acoustic transducer (Contactless ultrasound)	The use of pulse-echo techniques to determine weld pool dimensions is investigated
Lott LA		penetration state				contact ultrasound	Flat			
(LIN, M. L.; EAGAR, 1984)		weld bead depth		PM		vision	Flat			High speed photography was also used to investigate the fluid flow on the top surface of the liquid pool and to provide a clearer view of the sequence of formation of weld defects.

Reference	Process	Estimation			Measure		Welding Position	Sample time	Hardware	Comment
		Estimated Variable	Model Type	Analysis Technique	Measured Variable	Sensor				
(FENN, 1985)		weld bead depth				contact ultrasound	Flat			Ultrasonic sensing of the welding process and control
(LIN, M.; EAGAR, 1985)						vision	Flat			A new model of a compound vortex is proposed as a possible mechanism to explain the deep surface depression encountered at currents over 300 amperes
(CHEN, W. H.; NAGARAJAN; CHIN, 1988)	GTAW	weld bead depth	Static	ST, LSM	thermal pattern, minor axis and area of the thermal ellipse, thermal volume	infrared thermograph	Flat		PC, infrared camera, DAQ system	Off line analyses
(FRANCOIS <i>et al.</i> , 1988)						vision	Orbital		CCD	Patent of penetration and seam tracking control an open butt joint.
(CARLSON, N.M.; JOHNSON, 1988)	GMAW	weld bead depth		ES		contact ultrasound, contactless ultrasound	Flat			Ultrasonic sensing of the welding process has the potential to detect weld pool geometry and discontinuities in real time. Expert system.
(ROKHLIN; CHO; GUU, 1989)		defect detection				X-ray				
(GUU; ROKHLIN, 1989)		weld bead depth				X-ray				
(NAGARAJAN; CHEN H.; CHIN, 1989)		weld bead depth				infrared thermograph				
(BANGS; LONGINOW; BLAHA, 1989)		weld bead depth				infrared thermograph				Patent. The technique and arrangement of distributed, real time, intelligent control of welding including IR detection and measurement of process conditions.
(DOUMANIDIS, C.C.; HARDT, 1990)	GMAW	temperature	Dynamic	ST		infrared thermograph	Flat		infrared camera, PC, DAQ	Simultaneous regulation of both heat-affected zone and centerline cooling rate. Controlling the surface temperature field in-process, and using temperature feedback.

Reference	Process	Estimation			Measure		Welding Position	Sample time	Hardware	Comment
		Estimated Variable	Model Type	Analysis Technique	Measured Variable	Sensor				
(XIAO; OUDEN, 1990)	GTAW	penetration state			frequency of oscillation of the puddle-surface	pool oscillation	Flat			Monitoring oscillation frequency in the weld pool may offer a means of controlling joint penetration (full penetration)
(YOO, 1990)		weld bead depth				pool oscillation				
(NAGARAJAN <i>et al.</i> , 1990)		weld bead depth				infrared thermograph				
(CHEN, W.; CHIN, 1990)	GMAW	weld bead depth				infrared thermograph	Flat			
(SONG; HARDT, 1991)	GMAW					sensor fusion				Control
(CARLSON, N.M. ET AL., 1992)		weld bead depth				contact ultrasound				
(S. NAGARAJAN; CHIN; CHEN., 1992)	GMAW	weld bead depth				infrared thermograph	Flat			
(LIM; CHO, 1993)	GMAW	weld bead depth WPZ	Static	NN	Poll surface temperatures	infrared thermograph	Flat		Pyrometer	
(WANG, Q. L.; YANG; GENG, 1993)	GTAW	penetration state			resonance frequency, arc variables	pool oscillation	Flat			Resonance phenomenon of the weld pool is used for measurement and real-time control of full joint penetration.
(XIAO; OUDEN, 1993)	GTAW	penetration state			frequency of oscillation of the puddle-surface	pool oscillation	Flat			The oscillation behavior of the GTA weld pool depends on the welding conditions and can be used for in-process control of weld penetration (full penetration)
(YOO, 1993)		weld bead depth				pool oscillation				
(ROKHLIN; GUU, 1993)		weld bead depth				three-dimensional topography, X-ray	Flat			Experimentation with various welding currents establishes a relation between joint penetration and weld pool depression

Reference	Process	Estimation			Measure		Welding Position	Sample time	Hardware	Comment
		Estimated Variable	Model Type	Analysis Technique	Measured Variable	Sensor				
(SONG; HARDT, 1993)	GMAW	weld bead depth	Dy-namic	PM		infrared thermo-graphy, sensor fusion	Flat			A thermally based depth estimator provides accurate and fast estimates for real-time control of weld pool depth in gas metal arc welding. A closed- loop control system for weld pool depth using this thermally based depth estimator is also presented.
(DOUMANIDIS, CHARALABOS C., 1994)	GMAW, GTAW	weld bead depth	Static	MR, ST		infrared thermo-graph	Orbital			Review
(YANG, J. ET AL, 1994)		weld bead depth				contact ultra-sound				
(BEARDSLEY; ZHANG; KOVACEVIC, 1994)	GTAW	penetra-tion state	Dy-namic	RM, ST		infrared thermo-graph	Flat		PC, infrared camera, DAQ system	Present an applicable top-side infra-red sensing technique for the prospective closed-loop control of weld penetration in gas tungsten arc welding (GTAW). A
(KOVACEVIC; ZHANG; LI, 1996)	GTAW	penetra-tion state	Static	NN	Poll geome-try	vision	Flat	30ms+60ms (10Hz)	Pentium 90, DAQ board, high-shutter-speed video camera, Laser 7mW	Real time measure of geometry of weld pool. Measure the back-side width to determinate the full penetration.
(KIM, I. S.; BASU; SIORES, 1996)	GMAW	weld bead depth	Static	MR, ST	wire diame-ter, welding voltage, welding current, gas flow, weld-ing speed, penetration		Flat			Development of mathematical model (off line) for Control of Weld Bead Penetration
(ZHANG, Y. M.; KOVACEVIC; WU, 1996)	GTAW	weld bead width, weld de-pression	Dy-namic, MIMO	LSM, ST	welding current and arc length	vision	Flat		Camera, pc	Off-Line and on-line identification

Reference	Process	Estimation			Measure		Welding Position	Sample time	Hardware	Comment
		Estimated Variable	Model Type	Analysis Technique	Measured Variable	Sensor				
(KOVACEVIC; ZHANG, 1997)	GTAW	penetration state	-	IP		three-dimensional topography, vision	Flat	210ms(4Hz)	PC 486DX 100, 3D video camera	3D vision and laser strip to determine the weld pool boundaries and deformation in real time. They don't complete the penetration estimation, only talk about this.
(HENDERSON, THOMAS C. <i>et al.</i> , 1998)										
(ZHANG, YM Y.M.; KOVACEVIC, 1998)	GTAW	weld bead width, back side bead width	Dynamic	IP, NF		vision	Flat		Camera, PC	Closed-loop system is developed to control the weld fusion. Image processing algorithm and neuro-fuzzy model have been incorporated to measure and estimate the top-side and back-side weld bead widths based on an advanced top-side vision sensor.
(AENDENROOME R; DEN OUDEN, 1998)	GTAW-P	penetration state		FFT	arc voltage and arc current, pool oscillation frequency	pool oscillation	Flat			Measurement of the oscillation frequency of the weld pool during welding yields information about the penetration of the weld (Full penetration)
(GWEON, 1999)	Laser SPOT			NN		infrared thermograph	Flat			This paper introduces a method to estimate the joint strength of spot welds during the welding process. A point infrared sensor is used to measure temporal radiation on the top face of the spot weld. An artificial neural network (ANN) uses this feature to estimate joint strength.
(WIKLEIII; ZEE; CHIN, 1999)	GTAW	weld bead depth				infrared thermograph	Flat		PC, infrared camera, DAQ system	
(HIRAI <i>et al.</i> , 2001)		weld bead depth	Static	NN	pool width	vision	Flat	50ms	CCD, lens, pc	During the welding, a fuzzy controller adjusts the welding current so as to get the desired penetration depth.

Reference	Process	Estimation			Measure		Welding Position	Sample time	Hardware	Comment
		Estimated Variable	Model Type	Analysis Technique	Measured Variable	Sensor				
(KIM, ILL-SOO <i>et al.</i> , 2001)	GMAW	welding set points	Static	MR, LSM, ST			Flat			Development of inverse of mathematical model (off line) for Control of Weld Bead Penetration
(ZHAO <i>et al.</i> , 2001)	GTAW	back side bead width, weld bead reinforcement	Dynamic, MIMO	IP, NN	weld pool geometry	vision	Flat	Camera, PC		Neural network predictor of back side width and top side height . Multivariable Self-Adaptive Fuzzy Control
(VAN BOHEMEN; HERMANS; DEN OUDEN, 2001)		weld bead quality			sound	acoustic signal	Flat			
(WIKLE III <i>et al.</i> , 2001)	GTAW	weld bead depth				infrared thermography	Flat	pyrometer		
(MALDON, 2002)				KF, IP		vision				
(SFORZA; BLASIIS, 2002)	GMAW	weld bead quality, defect detection, penetration state		ST		sensor fusion, vision, infrared thermography, ultraviolet	Flat			
(BAE; LEE; AHN, 2002)	GMAW			IP		vision	Orbital	CCD, lens, PC		Seam tracking, control of root pass steel pipes
(NAGESH; DATTA, 2002)		weld bead depth	Static	NN	welding voltage, current, speeds		Flat			Off-line estimation
(DOUMANIDIS, CHARALABOS; KWAK, 2002)	GMAW, PAW	weld bead width, weld bead reinforcement	Dynamic, MIMO	ST, DARMA, SR		infrared thermograph	Orbital	laser profilometry, infrared pyrometry, PC		SISO control with fixed and variable delay Smith Predictor
(MILLER <i>et al.</i> , 2002)		weld bead depth				contactless ultrasound	Flat	Electromagnetic acoustic transducer (Contactless ultrasound)		
(RODRÍGUEZ MUÑOZ, 2003)				KF		sensor fusion				

Reference	Process	Estimation			Measure		Welding Position	Sample time	Hardware	Comment
		Estimated Variable	Model Type	Analysis Technique	Measured Variable	Sensor				
(ROGALSKI, 2003)										
(DE; PARLE, 2003)						infrared thermography				Seam tracking
(CHEN, S B <i>et al.</i> , 2003)	GTAW	back side bead width, weld bead width, weld pool half-length	Dynamic	NN, IP	peak current, pulse duty ratio, maximum weld pool width, weld pool half-length	vision	Flat		CCD camera with narrow-band composite light filter, PC, DAQ	Neuron self-learning PSD control. Backside weld bead width cannot be sensed and measured in real time, it is estimated with neural network
(FAN <i>et al.</i> , 2003)	SAW	weld bead depth				infrared thermography	Flat		pyrometer	Changes in the temperature distribution surrounding the weld pool were measured using a thermopile infrared detector and used to control weld penetration through changes of wire feed speed (welding current). Plate inclination angle on weld bead parameters was investigated. IR sensor signal variation was examined in the presence of plate inclination angles.
(CHENG <i>et al.</i> , 2004)	GTAW			NF		vision				
(GRAD <i>et al.</i> , 2004)	GMAW	defect detection			domain and frequency domain descriptors.	acoustic signal			microphone and PZT sensor	Results indicate that the arc sound exhibits distinct characteristics for each welding situation and that the main source of acoustic waves in short circuit metal transfer mode is arc reignition. From acoustic signals one can easily assess process stability and detect welding conditions resulting in weld defects.
(SAEED; ZHANG; JAYNES, 2005)		weld pool profile			depth (profile) of the weld pool surface	three-dimensional topography, vision	Flat		structured light system, CCD sensor, filter,	Welding current effect in weld pool profile



Reference	Process	Estimation			Measure		Welding Position	Sample time	Hardware	Comment
		Estimated Variable	Model Type	Analysis Technique	Measured Variable	Sensor				
(LUO, HONG; CHEN, 2005)						vision				Seam tracking
(KIM, I S <i>et al.</i> , 2005)	GMAW	welding set points	Static	MR, ST, NN			Flat			The developed system enables to input the desired weld dimensions and select the optimal welding parameters.
(MURUGAN; GUNARAJ, 2005)	SAW	weld bead depth, weld bead width, weld bead reinforcement	Static	FD		macrographie	Flat			Off-line estimation
(XUE <i>et al.</i> , 2005)	GMAW	weld bead width	Static	FL	welding voltage, current, welding speed		Flat			Regression method for prediction and control the weld bead width in the robotic arc-welding process
(ZHANG, G J; CHEN; WU, 2005)	GTAW	back side bead width, weld bead reinforcement	Dynamic, MIMO	IP, NN	weld pool geometry	vision	Flat		Camera, PC	Neural network predictor of back side width and top side reinforcement . Self-learning Fuzzy Neural Network Control of back side width
(MOON, H S; KIM; BEATTIE, 2006)	SAW, FCAW			IP	joint dimensions	sensor fusion, image processing, laser triangulation	Orbital		laser-based vision sensor	Seam tracking
(WU, CS; GAO, 2006)	GTAW	back side bead width	Dynamic	IP, NN	weld pool geometry	vision	Flat	1Hz	Camera, PC	Neural network predictor of back side width and neuro-fuzzy control
(ALFARO, SADEK C. A; DREWS, 2006)	GMAW			NN, FL, IP	width, voltage, current, torch velocity, weld pool geometry, weld	sensor fusion, vision, laser triangulation	Flat	20 Hz	CCD, profilometer, DAQ, PC, parallel processing system for manufacturing	Photogrammetry based computer vision. The sensor fusion concept employing Artificial Neural Networks pattern recognition and Fuzzy Logic supervision were implemented on specialized distributed processing units.

Reference	Process	Estimation			Measure		Welding Position	Sample time	Hardware	Comment
		Estimated Variable	Model Type	Analysis Technique	Measured Variable	Sensor				
					bead geometry					
(SUNG <i>et al.</i> , 2007)	GMAW	weld bead width	Static	FL	welding voltage, current, welding speed		Flat			Regression method for prediction and control the weld bead width in the robotic arc-welding process
(KARADENIZ, 2007)		weld bead depth					Flat			
(CULLEN <i>et al.</i> , 2008)	SPOT	weld bead quality		NN	current, infrared	sensor fusion, infrared thermography, contact ultrasound				
(CAYO, EH, 2008)	GMAW	transfer mode		ST	sound	acoustic signal	Flat			
(SANTIAGO MARTÍNEZ, 2009)						sensor fusion				
(CHEN, BO; WANG; CHEN, 2009)	GTAW	back side bead width	Dynamic	NN	voltage, current, wire feeding speed, topside length and topside width	sensor fusion, vision	Flat		CCD, PC, optic	Electronic and welding pool image information are, respectively, obtained by arc sensor and image sensor, then electronic signal processing and image processing algorithms are used to extract the features of the signals, the features are then fused by neural network to predict the backside width of weld pool.
(CHEN, HUABIN <i>et al.</i> , 2009)	GTAW	weld bead depth	Dynamic	NN, IP	weld pool geometry information, variation ratio of the topside weld bead width, welding voltage, current	vision	Orbital		CCD camera with narrow-band composite light filter, pc, DAQ	Fuzzy and adaptive controller for back-side weld bead width
(CAYO, EBER H.; ALFARO, 2009)	GMAW	defect detection				acoustic signal	Flat			Technique for defect detection based on acoustic of the process.

Reference	Process	Estimation			Measure		Welding Position	Sample time	Hardware	Comment
		Estimated Variable	Model Type	Analysis Technique	Measured Variable	Sensor				
(PALACÍOS, 2010)	GTAW	defect detection		ST		infrared thermograph	Flat			
(BARRON ADAME, 2010)				NN		sensor fusion				
(CASTANEDO SOTELA, 2010)						sensor fusion				
(NAGESH; DATTA, 2010)	GTAW	weld bead width, weld bead reinforcement	Static	NN	welding voltage, current, speeds		Flat			Off-line estimation
(CHEN, BO; WANG; CHEN, 2010)	GTAW -P	penetration state	Dynamic	NN, DSE, IP	back-side weld bead width, current, voltage, sound, wire feed speed, top side width, top side length	vision, sensor fusion	Flat		CCD, PC	Weld pool image feature extraction. Penetration status (incomplete penetration) estimation using D-S evidence theory and neural network to fusing the image, sound and arc measurements.
(MOTA, CAROLINA PIMENTA <i>et al.</i> , 2011)	GTAW, GMAW					luminosity sensor, infrared thermography, vision	Flat			
(BROSED <i>et al.</i> , 2011)										Laser triangulation
(WEI <i>et al.</i> , 2011)						vision				Seam tracking
(SUDHAKARAN <i>et al.</i> , 2011)	GTAW	weld bead depth	Static	NN	welding voltage, current, welding speed, gun angle		Flat			Off-line estimation
(YAN, ZH; ZHANG; WU, 2011)	P-GMAW	back side bead width	Dynamic	NN		vision	Flat		Camera, PC	Fuzzy controller of back side width, simulation and open loop experiment

Reference	Process	Estimation			Measure		Welding Position	Sample time	Hardware	Comment
		Estimated Variable	Model Type	Analysis Technique	Measured Variable	Sensor				
(PAL; PAL, 2011)	P-GMAW	weld bead depth	Static	ST, RM	temp, sound, current, voltage	acoustic signal, infrared thermography, sensor fusion	Flat	10 Hz (temp) / 40 Hz (voltage, current, sound)	pyrometer, sound sensor, hall effect sensor (arc current), DAQ, Pentium 4	The arc sound kurtosis, weld peak temperature along with arc power have been found to be correlated with weld penetration. The arc sound kurtosis was also found to be a better choice to monitor HAZ area.
(CAYO, EBERHUANCA; ALFARO, 2011)	GMAW-S	weld bead quality			voltage, sound, infrared,	infrared thermography, acoustic signal	Flat			
(CHOKKALINGHAM; CHANDRASEKHAR; VASUDEVAN, 2012)	GTAW	weld bead depth weld bead width	Static	NN		infrared thermograph	Flat		infrared camera, PC, DAQ	Same model structure to P and W
(PEÑA SANTOS, 2012)		defect detection, penetration state				infrared thermograph				
(SREEDHAR <i>et al.</i> , 2012)	GTAW	defect detection		IP		infrared thermograph	Orbital			
(SCHLICHTING <i>et al.</i> , 2012)	SPOT	defect detection				infrared thermograph	Flat			
(HURTADO; ALFARO; LLANOS, 2012)	GTAW	defect detection		KF		infrared thermograph	Flat		FPGA, pyrometer	
(ALFARO, SADEK CRISÓSTOMO ABSI, 2012)	GMAW-S	defect detection		KF		infrared thermography, acoustic signal, spectroscopy, sensor fusion				
(HUANG, WEI; KOVACEVIC, 2012)				IP	joint dimensions	laser triangulation, vision			laser-based vision sensor, multi-axis motion control module	Development of laser scanner

Reference	Process	Estimation			Measure		Welding Position	Sample time	Hardware	Comment
		Estimated Variable	Model Type	Analysis Technique	Measured Variable	Sensor				
(SUBASHINI; VASUDEVAN, 2012)	GTAW	weld bead depth	Static	FL, NF, AN-FIS		infrared thermograph	Flat		infrared camera, PC, DAQ	
(HURTADO; ALFARO; LLANOS, 2012)	GMAW-S	weld bead quality	Static	ST	sound, infrared	acoustic signal, infrared thermography, sensor fusion	Flat			Shows the relationship between welding quality and optical-acoustic emissions from electric arcs, during welding runs
(MOTA, CAROLINA PIMENTA <i>et al.</i> , 2013)	GTAW, GMAW					infrared thermography, vision	Flat			
(RODRIGUEZ-COBO <i>et al.</i> , 2013)	GTAW	defect detection				spectroscopy	Flat		Fiber Bragg Grating transducers (FBGs), CCD spectrometers	
(TORRES, 2013)	GMAW		Static	IP	weld bead width	vision	Flat			Control of weld bead width
(AKKAS <i>et al.</i> , 2013)	SAW	weld bead depth	Static	NF			Flat			Relationship between the values defining bead geometry and the welding parameters and also to select optimum welding parameters.
(NELE; SARNO; KESHARI, 2013)		Mechanical properties	Static	FL, NF, AN-FIS			Flat			Obtain the best mechanical properties, quality
(YU KANG LIU; YU MING ZHANG, 2014)	GTAW	back side bead width, penetration state	Static	FL	back-side weld bead width, current, voltage, Spectrometer,	spectroscopy, vision, sensor fusion	Flat		Spectrometer, CCD, DAQ, PC	Weld pool image feature extraction. Penetration status (incomplete penetration) estimation using D-S evidence theory and fuzzy logic to fusing the image, sound and arc measurements
(CHEN, ZIQIN; GAO, 2014)	Laser	weld bead width		IP		infrared thermograph				
(CHEN, BO; CHEN; FENG, 2014)	GTAW	penetration state		FL, IP	arc, sound, and visual	sensor fusion, vision, acoustic signal	Flat		CCD, PC, mic	

Reference	Process	Estimation			Measure		Welding Position	Sample time	Hardware	Comment
		Estimated Variable	Model Type	Analysis Technique	Measured Variable	Sensor				
(CRUZ, 2014)	GMAW		Static	IP	weld bead reinforcement	vision	Flat			Control of bead reinforcement
(YU KANG LIU; YU MING ZHANG, 2014)	GTAW	weld bead depth	Dy-namic	NF		three-dimensional topography, vision	Orbital			
(WANG, XUEWU, 2014)	GTAW	weld bead depth				contactless ultrasound, three-dimensional topography, vision				Review
(CHEN, BO; FENG, 2014)	GTAW	penetration state	Dy-namic	FL, DSE, IP	back-side weld bead width, current, voltage, sound, wire feed speed, top side width, top side length	vision, sensor fusion	Flat		CCD, PC	Weld pool image feature extraction. Penetration status (incomplete penetration) estimation using D-S evidence theory and fuzzy logic to fusing the image, sound and arc measurements
(LV <i>et al.</i> , 2014)	GTAW	weld bead depth	Dy-namic	ST	sound	acoustic signal	Flat	36 KHz		Arc sound signal can be used to predict the weld quality as the sag depression of weld pool is closely related to the weld penetration.
(CHANDRASEKHAR <i>et al.</i> , 2015)	GTAW	weld bead depth	Static	NF, ANFIS		infrared thermograph	Flat			
(ALFARO, SADEK C ABSI <i>et al.</i> , 2015)	GTAW	defect detection				infrared thermograph	Flat			
(LIU, YUKANG; ZHANG; ZHANG, 2015)	GTAW	weld bead width, Poll parameters (width, length, convexity)	Dy-namic	NF		three-dimensional topography, vision	Orbital	2 Hz	Laser, Camera, PC, DAQ	Control of Backside weld bead

Reference	Process	Estimation			Measure		Welding Position	Sample time	Hardware	Comment
		Estimated Variable	Model Type	Analysis Technique	Measured Variable	Sensor				
(SHI <i>et al.</i> , 2015)	GTAW-P	penetration state		IP, FFT	pool oscillation frequency	pool oscillation, vision, three-dimensional topography, laser triangulation	Flat			An image-processing algorithm was developed for extracting the pool oscillation frequency, and several experiments with varying weld joint penetration for traveling and stationary weld pools were conducted (partial and full penetration)
(LV <i>et al.</i> , 2013)	GTAW	penetration state		ST	sound	acoustic signal	Flat			Identify and classify the penetration state and welding quality through the features of arc sound signal during robotic GTAW process. This paper tried to make a foundation work to achieve on-line monitoring of penetration state to weld pool through arc sound signal. The statistic features of arc sound under different penetration states like partial penetration,
(LLANOS; HURTADO; ALFARO, 2016)	GTAW	defect detection		KF		infrared thermograph	Flat		FPGA, pyrometer	
(PINTO-LOPERA; S. T. MOTTA; ABSI ALFARO, 2016)	GMAW			IP	weld bead reinforcement, weld bead width	vision	Flat		high-speed camera	Measure of the width and reinforcement of weld beads in gas metal arc welding (GMAW) using a single high-speed camera and a long-pass optical filter in a passive vision system.
(HKS PROZESSTECHNIK, 2017)		weld bead depth				infrared thermograph				
(BESTARD; ALFARO, 2017)	GMAW			IP		vision, laser triangulation				
(FONT COMAS <i>et al.</i> , 2017)	Plasma			IP		Vision				

ANFIS: Adaptive Neuro-fuzzy Inference System.

ARMA: Auto-regressive Moving Average.

CCD: Charge coupled device.

DARMA: Deterministic Auto-regressive Moving Average.

DSE: D-S evidence

ES: Expert system

FCAW: Fluxed cored arc welding.

FD: Factorial design

FFT: Fast Fourier Transformer

FL: Fuzzy logic

GMAW: Gas Metal Arc Welding.

GTAW: Gas Tungsten Arc Welding.

IP: Image processing

KF: Kalman filter

LAM: Layer additive manufacturing.

LSM: Least square method

MIMO: Multiple Input, Multiple Output

MISO: Multiple Input, Single Output.

MPC: Model predictive control.

MR: Multiple regression

NF: Neuro-fuzzy

NN: Neural networks

PAW: Plasma Arc Welding.

PM: Physic modeling

RM: Regression model

SAW: Submerged Arc Welding.

SISO: Single Input, Single Output

SR: Step response

ST: Statistical

PC: Personal computer



## Appendix 2 Representative information about control systems found in welding research literature.

Reference	Process	Control System							Notes
		Model	Type	Inputs	Outputs	Sample time	Sensors	Hardware	
(ICELAND; MARTIN E. O'DOR, 1971)	Fusion welding	-	Proportional	Temperature of back side	Welding voltage or current, and flow of gas	-	Infrared (pyrometer)	Analogic circuit	United States Patent Number 3,567,899 Weld penetration control regulating the welding power and a flow of auxiliary gas.
(SMITH, C.J., 1974)	GTAW	-	On-off control (pulse-step)	Back bead radiation	Welding current	-	photoelectric	-	
(GLADKOV <i>et al.</i> , 1974)	PAW	-		Penetration estimate	Welding voltage	-	Back bead ion. voltage	Analogic circuit	Various materials
(VORMAN; BRANDT, 1978)	GTAW	-	P-PI	pool width @ fixed distance	Welding speed	-	Line scan camera	Analog computer	Problems with delays and phase not minima
(BOUGHTON; RIDER; SMITH, 1978)	Pulsed GTAW	2nd order	On-off, P	Back side and top side width	Welding current and speed	-	photocell	-	Full penetration, partial penetration
(CHI; YIN; GAO, 1980)	PAW	-	PWM	Back bead radiation	Welding voltage	-	photoelectric	-	Keyhole PAW
(COOK, G.E., 1980; HUNTER; BRYCE; DOHERTY, 1980)	GMAW	Static empirical	Open / closed loop	weld fillet, penetration	several	-	several	-	Estimated penetration
(NOMURA, H. <i>et al.</i> , 1980)	SAW	-	On-off	Back weld bead width	Welding current	-	Arc light intensity, 4 Infrared	-	Full penetration, disturbance rejection
(DOMFELD; TOMIZUKA; LANGARI, 1982)	GMAW	2nd order w/2 zeros	MRAC	Back bead temperature	Welding speed	-	Infrared	-	Measurability, causality, identification
(BATES; HARDT, 1985; HARDT;	GTAW	Nonlinear thermal	Linear PI	Pool cross section	Welding current and speed	-	Optical back bead temperature	-	Full penetration, identification

Reference	Process	Control System							Notes
		Model	Type	Inputs	Outputs	Sample time	Sensors	Hardware	
GARLOW; WEINERT, 1985)									
(NOMURA, HIROKAZU; SUGITANI; TAMAOKI, 1986)	Not defined	-	Not speci- fied	Arc voltage and current	Welding speed	-	-	Analogic circuit	United States Patent Number 4,608,481 The deviation of a groove line or variation of a groove width is de- tected by utilizing the character- istics of a welding arc itself with- out using a separate sensor.
(TAKAHASHI <i>et al.</i> , 1986)	Not defined	Isotherms patterns	Not speci- fied	Isotherms in infrared imagen	Torch posi- tion and welding cur- rent	-	Infrared camera	-	United States Patent Number 4,594,497 It calculates the centroid for the control algorithm.
(NIED; BAHETI, 1986)	TIG	-	Adaptive feedback control	Puddle ge- ometry er- ror and arc length	Welding cur- rent and voltage	-	Vision	-	United States Patent Number 4,613,743 Assure the full penetration
(FRANCOIS <i>et al.</i> , 1988)	Orbital	-	Not speci- fied	Weld pool penetration (equivalent signal)	Wire feed speed, weld- ing speed, welding volt- age and torch posi- tion	-	Vision	Computer and ex- ternal circuit	United States Patent Number 4,733,051 For controlling weld pool pene- tration during root pass welding in open butt joints. Analyzing the weld pool contour line to derive therefrom penetra- tion depth.
(MIYACHI, 1989)	GTAW	Numerical	Open-loop	Distortion, root gap	Lateral torch power	-	Stylus profilometer La- ser interferometer	-	Large process delays
(BANGS; LONGINOW; BLAHA, 1989)	GTAW, GMAW. PAW, FCAW, re- sistance or spot	-	Adaptive control, ex- pert system	Width of the puddle	Welding speed and current	-	Infrared camera	Four independent processors are in- terconnected for serial communica- tion to	United State Patented Number 4,877,940, assigned by IIT Re- search Institute

Reference	Process	Control System							Notes
		Model	Type	Inputs	Outputs	Sample time	Sensors	Hardware	
(SUGITANI; NISHI, 1989)	Not defined	Isotherms patterns	Not specified	Isotherms in infrared imagen	Welding current, welding speed, wire feed speed	-	Infrared camera	Computer and external circuit	United States Patent Number 4,816,641
(DOUMANI DIS, C.C.; HARDT, 1990)	GMAW	Analytical, FDM, expert system	Multivariable adaptive	Heat-affected zone and cooling rate	Double torch power	-	IR pyrometry camera	-	Timeshared multi-torch configuration
(HALE, 1990)	GMAW	2nd order empirical	Nonlinear sliding-mode	Weld bead width and reinforcement	Welding speed and wire feed speed	-	Active optical (Laser)	-	Partial penetration
(LUKENS; DENALE; ZANIS, 1990)	Not defined	Isotherms patterns	-	Isotherms in infrared imagen	Deflect of the welding arc	-	Infrared camera	-	United States Patent Number 4,975,558 The welding arc is deflected by magnetic actuator.
(ANDERSEN <i>et al.</i> , 1990)	GTAW	Neural network	PI	Weld bead width and depth penetration	Welding speed, current and arc length	-	-	-	A neural network set-point selector defined the start control parameters. Other neural network estimate the penetration. Two independently closed-loops PI adjust continuously the start parameters.
(SONG; HARDT, 1991)	GMAW	Analytical	Multivariable adaptive	Weld bead width and back bead temperature	Welding speed and wire feed speed	-	Optical and infrared pyrometer	-	On-line penetration estimator
(SUZUKI; HARDT; VALAVANI, 1991)	GTAW	2nd order empirical	Adaptive deadbeat	Back weld bead width	Welding current and speed	-	Optical	-	Full penetration
(MASMUDI; HARDT, 1992)	GTAW	Numerical	Multivariable adaptive	Weaving and welding current	Pool and HAZ width	-	Infrared pyrometer	-	Weaving amplitude modulation
(BANERJEE; CHIN, 1992; CHO, 1992;	GTAW and GMAW	Empirical, neural nets	linear, fuzzy logic	Weld bead width,	several	-	Infrared pyrometry, coaxial vision	-	

Reference	Process	Control System							Notes
		Model	Type	Inputs	Outputs	Sample time	Sensors	Hardware	
EINERSON <i>et al.</i> , 1992; RICHARDSN; CONRARDY, 1992)				penetration, cooling rate, fill					
(HENDERSO N, D E <i>et al.</i> , 1993)	GMAW	Transfer function	Pseudo gradient adaptive	Puddle width	Welding speed	-	-	-	The experiments shown a good behavior of the control.
(DOUMANI DIS, CHARALABO S C., 1994)	Orbital, GTAW and GMAW	Analytical and experimental first-order Autoregressive moving average (ARMA)	Adaptive control (internal loop) and PID (external loop)	Temperature in front and back side	Torch power, welding speed and wire feed speed	-	Thermal line scan	-	The weld bead width and reinforcement are measured on-line and the penetration is measured by off-line longitudinal sectioning. Multi-torch configuration.
(KOVACEVIC ; ZHANG; RUAN, 1995)	-	-	Robust adaptive	Pool area	-	-	High shutter speed camera and nitrogen laser	-	
(ZHANG, YU. M.; KOVACEVIC; LI, 1996)	Flat GMAW	Moving-average model with a predictive decoupling algorithm	Adaptive control (GPC)	Sag width and reinforcement	Welding current and arc length	500 ms	Vision system and laser strip	Computer and external circuit	Indirect control of full penetration
(OZCELIK; MOORE; NAIDU, 1998)	GMAW		Adaptive control						
(BROWN; MEYN; WEBER, 1998)	Flat, GMAW	ARMAX	PID with adaptive dead-time compensator	Weld pool width	Welding speed	-	-	-	Adaptive dead-time compensator. Simulation
(CHEN, S.B. <i>et al.</i> , 2000)	Pulsed GTAW	Neural network (DIDO, dynamic)	Self-Learning fuzzy neural network and	Weld pool width	Pulse duty ratio and welding speed	-	Vision	Computer and external circuit	

Reference	Process	Control System							Notes
		Model	Type	Inputs	Outputs	Sample time	Sensors	Hardware	
			expert system						
(DI <i>et al.</i> , 2001)	GTAW	-	Neuro-fuzzy	Width of the weld pool	Welding voltage	-	-	-	Simulation
(CHIN, 2001)	SAW	-	PID	Infrared emission	-	-	Infrared sensor	Computer and external circuit	
(WIKLE III <i>et al.</i> , 2001)	GTAW and SAW	-	PI	Infrared emission	Welding current (GTAW) Welding voltage and speed (SAW)	-	Infrared sensor (point)	Computer and external circuit	
(MOON, H.; BEATTIE, 2002)	Flat, SAW	-	Adaptive control	Joint geometry	Welding voltage, current and speed	-	Laser profilometer	Computer and external circuit	This technology has been used in longitudinal and spiral pipe mills and in pressure vessel production.
(JOU, 2002)	GTAW	State-space	H-Infinity robust	Length and width of the weld pool	Welding current and speed	-	-	-	Simulation
(DOUMANI DIS, CHARALABOS; KWAK, 2002)	Flat and orbital, PAW, GMAW	First order DARMA	SISO PI, MIMO GOSA and variable delay Smith predictor	Weld bead width and reinforcement	Welding speed and wire feed speed	1000 ms	Infrared camera, laser profilometer	Two computer and external circuit	Two simultaneous but independent control loops. One sense the temperature and control the torch trajectory. Other sense the profile geometry and control the welding speed and wire feed speed.
(LUO, H <i>et al.</i> , 2002)	Flat, GTAW	-	Neuro-fuzzy	Weld pool length and width	Welding feed speed	-	High shutter speed camera and laser system (LaserStrobe)	Computer and external circuit	
(CASALINO; HU; HOU, 2003)	GMAW	neural networks, finite element, fuzzy	-	Molten zone geometry	-	-	-	-	
(MOORE; NAIDU; OZCELIK, 2003)	GMAW	-	PI	-	-	-	-	-	

Reference	Process	Control System							Notes
		Model	Type	Inputs	Outputs	Sample time	Sensors	Hardware	
(ZHANG, Y. M.; LIU, 2003)	GMAW	-	Adaptive control	-	-	-	-	-	
(CHENG <i>et al.</i> , 2004)	Pulsed GTAW	-	PID and neuron self-learning PSD	Top side weld shape		-	Vision	-	
(LU, WEI <i>et al.</i> , 2005)	Orbital GTAW	Dynamic SISO in discrete time	Adaptive interval control	Depth of the weld pool surface	Main-arc-on period	1 ms	Analog to digital converter	Computer with and external circuit	Need modify the welding power source for switching the welding current.
(SMITH, JEREMY S.; BALFOUR, 2005)	Flat, Pulsed TIG	-	PI	Top face weld pool width	Welding current and wire feed speed	-	Vision (camera)	Computer with and external circuit	
(WU, CS; GAO, 2006)	GTAW	-	Neuro-fuzzy	Weld penetration	-	-	Vision	-	
(YANG, SANG-MIN <i>et al.</i> , 2007)	Flat GMAW	-	Neural network	Width and depth of the weld joint	Welding voltage, welding speed and wire feed speed	-	Three-dimensional vision system (laser stripe)	Computer with and external circuit	The adaptive Hough transformation is used for on-line imagen processing. The error range of width and depth is within 3%.
(SHEN <i>et al.</i> , 2008)	GTAW	-	Fuzzy and PID	Geometric parameters	Welding current and wire feed rate	-	Double- side visual sensor system (captures topside and backside)	Computer with and external circuit	
(LI; ZHANG, 2009)	Double Electrode GMAW	Interval model	Interval model control algorithm	Welding current (main), Welding voltage (bypass)	Wire feed speed (main), Welding current (bypass)	-	-	Computer with and external circuit	Two SISO systems are selected for convenient implementation and design.
(CHEN, HUABIN <i>et al.</i> , 2009)	Orbital GTAW	Neural network	Adaptive and fuzzy	Back-side weld bead width, gap	Welding peak current and wire feed speed	-	Vision (CCD camera)	-	An adaptive controller received the back-side weld bead width estimated for the neural network and regulate the peak current. A fuzzy controller received the gap

Reference	Process	Control System							Notes
		Model	Type	Inputs	Outputs	Sample time	Sensors	Hardware	
									state and control the wire feed speed.
(HUANG, XIXIA <i>et al.</i> , 2009)	Pulsed GTAW	Support vector machine–fuzzy rules	Adaptive inverse	Backside weld width	Peak current of pulse	-	Double- side visual sensor system (captures topside and backside)	-	The data for model identifying is obtained experimentally but the control is simulated.
(LÜ <i>et al.</i> , 2010)	GTAW	Discrete MISO nonlinear	Model-free adaptive (MFC) MISO	Width of the weld pool back side	Welding current and feed wire speed	-	Vision	Computer and external circuit	Used a complex optic in the front and back side of the weld pool. High computational resources to maintain the control period and the processing speed of the images.
(MOUSAVI; HAERI, 2011)	GMAW	State-space	ARMarkov-PFC (based MPC controller), PI and FL-PID.	Welding current and voltage	Wire feed motor voltage and welding voltage	-	-	-	Compare the behavior of three controllers in simulation.
(YAN, ZH; ZHANG; WU, 2011)	Pulsed GMAW	Neural networks	Fuzzy	Top and back side weld pool	-	-	-	-	
(WANG, ZHIJIANG; ZHANG; WU, 2012)	Pulsed GMAW	Static model	Adaptive interval model control system	Arc voltage during the peak current period	Welding voltage	1 ms	Analog to digital converter	Two computers and external circuit	The change in arc voltage during the peak current are related with the weld penetration depth. The control accuracy is not good.
(TORRES, 2013)	Flat, GMAW	Neural network (static)	Fuzzy	Weld bead width	Welding speed	-	Vision (camera)	Computer and external circuit	
(YU KANG LIU; YU MING ZHANG, 2014)	Orbital GTAW	Linear moving average and ANFIS	MPC	Backside weld bead width	Welding current and speed	500 ms	Vision (3D weld pool surface)	Computer and external circuit	A nonlinear neuro-fuzzy model estimate the weld depth penetration.
(XIONG; ZHANG, 2014)	GMAW LAM	First order, ARMA	Adaptive (generalized minimum variance)	Deposition rate	Nozzle to top surface distance	-	Passive vision sensor system	Computer and external circuit	The precision range of the control system is limited within $\pm 0.5$ mm.
(LV <i>et al.</i> , 2014)	Flat, Pulsed GTAW	Linear	Segmented self-adaptive PID	Arc sound pressure	Welding voltage	500 ms	Acoustic (Microphone)	Computer and external circuit	Indirect monitoring and control of arc length and penetration.

Reference	Process	Control System							Notes
		Model	Type	Inputs	Outputs	Sample time	Sensors	Hardware	
(LIU, Y. K.; ZHANG; KVIDAHL, 2014a, b)	Orbital GTAW	ANFIS	Neuro-fuzzy	Weld pool length, width, and convexity	Welding current	-	Vision (3D weld pool surface)	Computer and external circuit	Correlate a skilled human welder response to the fluctuating 3D weld pool surface. Compare with novice welder.
(CRUZ, 2014)	Flat, GMAW	Neural network (static)	Fuzzy	Weld bead width and reinforcement	Welding speed and wire feed speed	-	Vision (camera)	Computer and external circuit	
(LIU, YUKANG; ZHANG; ZHANG, 2015)	Orbital GTAW	ANFIS	Neuro-fuzzy	Weld pool length, width, and convexity	Welding current	500 ms	Vision (3D weld pool surface)	Computer and external circuit	Rapidly transform human welder intelligence into welding robots by using 3D weld pool surface sense.
(LIU, YUKANG; ZHANG, 2015)	Orbital GTAW	Linear and ANFIS	Cooperative control, Neuro-fuzzy	Weld pool length, width, and convexity	Welding speed	500 ms	Two cameras, 3-D weld pool sensing,	Computer and external circuit	Developed a machine–human cooperative control scheme to perform welder teleoperation experiments.

ANFIS: Adaptive Neuro-fuzzy Inference System.  
 ARMA: Auto-regressive Moving Average.  
 CCD: Charge coupled device.  
 DARMA: Deterministic Auto-regressive Moving Average.  
 DIDO: Double Input, Double Output  
 FCAW: Fluxed cored arc welding.  
 FL-PID: PI and feedback linearization based PID.  
 GMAW: Gas Metal Arc Welding.

GOSA: Generalized one step ahead algorithm.  
 GPC: Generalized Predictive Control.  
 GTAW: Gas Tungsten Arc Welding.  
 LAM: Layer additive manufacturing.  
 MFC: Model-free adaptive control.  
 MIMO: Multiple Input, Multiple Output  
 MISO: Multiple Input, Single Output.  
 MPC: Model predictive control.

PAW: Plasma Arc Welding.  
 PFC: Predictive functional controller.  
 PI: Proportional Integral.  
 PID: Proportional Integral Derivative.  
 SAW: Submerged Arc Welding.  
 SISO: Single Input, Single Output



## Apendix 3 Design proposal of a multivariable control system to GMAW orbital process.

The control of the welding bead geometry in orbital process is complex and involves several variables, closely related and with a non-linear behavior. This proposal takes advantage of the algorithms presented in chapter 3 and adds a multivariable control in real-time of the orbital welding process. A robotic emulator of orbital welding process is also proposed to test the control system and research works. This proposal is the basis for the CNPQ project “Use of sensing techniques (sensor fusion) for online monitoring and control of quality in welding processes”, process 401073/2016-5, called Universal 01/2016 - C range (ALFARO, SADEK CRISÓSTOMO ABSI, 2016)

The proposal to meet these requirements is shown in Figure 83 and consists of an embedded system SoC (System on Chip) of Altera, which has a FPGA Cyclone V, a HPS (Hard Processor System), a Gigabit Ethernet port, two USB ports, a connector for micro SD card, video input and output, numerous digital inputs and outputs, among other important features for our application. Two blocks are implemented in the FPGA, one NIOS II soft processor and a parallel processing block.

The Nios II processor is responsible for the welding data acquisition and processing by communicating with the welding power source through the RS232 protocol and the task sync and control loop sequence. The other block uses the parallel processing capability of the FPGA device to infrared matrix processing, bead profile processing, estimate the value of the weld penetration and weld bead width, control algorithms calculation and other peripheral functions as the pulse width modulation (PWM) generator and stepper motor control. Both blocks communicate with the HPS.

The HPS is a dual-core ARM Cortex-A9 800MHz processor and has 1GB of DDR3 SDRAM. The Ubuntu operating system, specially compiled for this architecture runs in it. It is responsible for reading the infrared data from the thermographic camera and the profile data from the profilometer sensor, storing the measurements, representing the state of the process and allowing the entry of parameters by the operator through the web interface.

This system meets the requirements of processing power and storage for our application, as well as the number of communication ports needed to interact with sensors, actuators, user interface and the network of the plant or lab.

Although Ubuntu is not a real-time operating system (RTOS), the distribution is optimized by Altera to operate with minimum requirements. With the use of FreeRTOS (REAL TIME ENGINEERS LTD., 2016), an optimized and distributed control strategy with the NIOS II processor, we believe that execution times can be met and assume that the system works in real time.

### A 3.1 The measuring system

The measuring system for this proposal incorporates some measurements and measure instruments, selected for this work, into the system discussed in the section 3. The following sections describe each subsystem added or modified in the proposed measurement system. The unmodified parts are not treated.

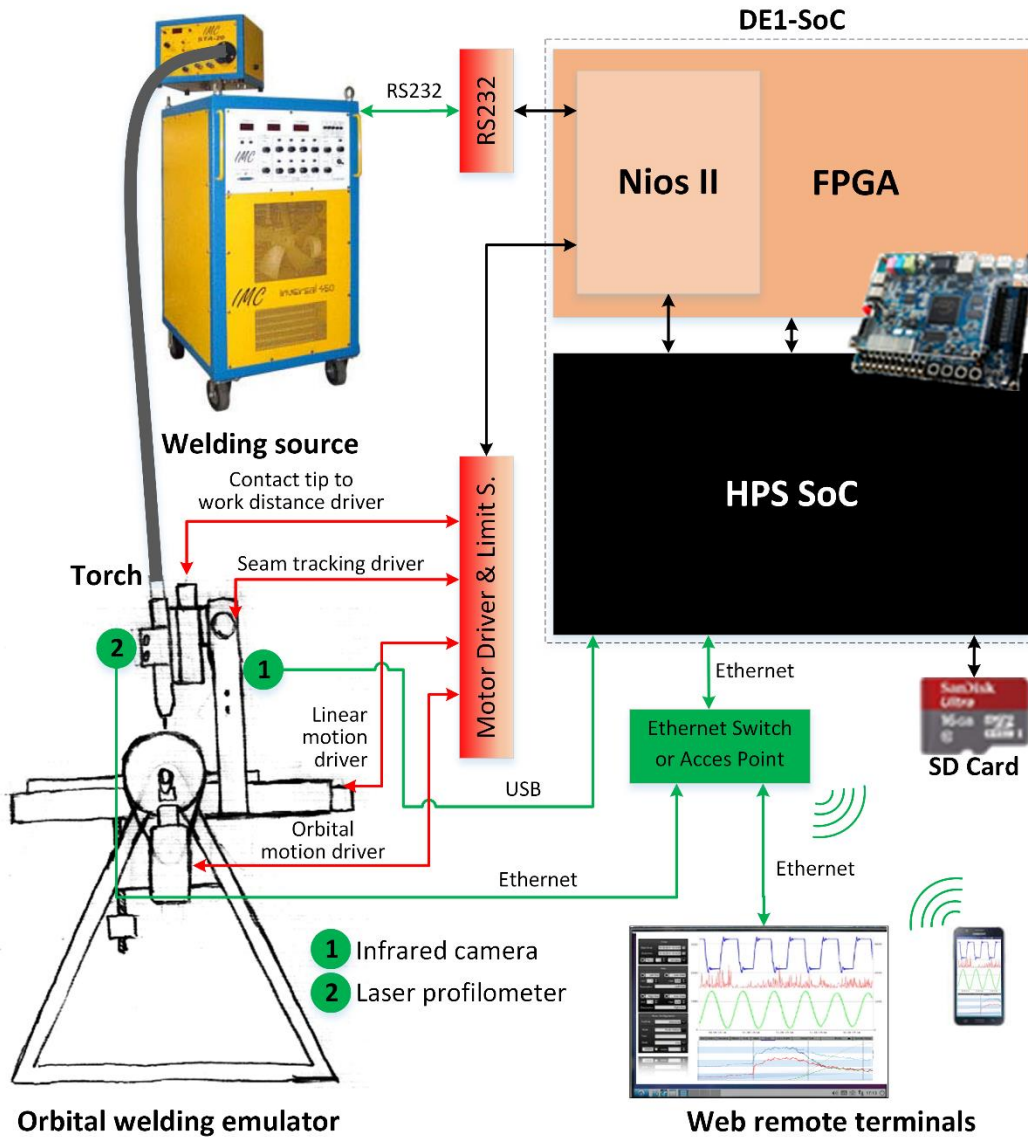


Figure 83 Data acquisition and control system proposed for the orbital welding process.

### A 3.1.1.1 Measurement of the orbital angle and the welding speed.

The control system of robotic emulator (see section A 3.2.1) has an encoder for measuring the orbital angle. This value is calculated by adding or subtracting (depending on the direction of movement) the encoder pulses from the start position. This initial position is detected by an optical sensor like the one shown in Figure 84b. The welding speed is obtained from the control registers of the X axis motor.

### A 3.1.1.2 Measurement of the joint profile and weld bead profile.

The measuring of the weld joint profile, before welding starts, is important in order to calculate the volume of material deposited and satisfies the bead reinforcement and width requirements. The seam joint center is necessary for the seam tracking algorithm and can be calculated using the joint profile. The profile can also be used for checking the alignment of the work pieces.

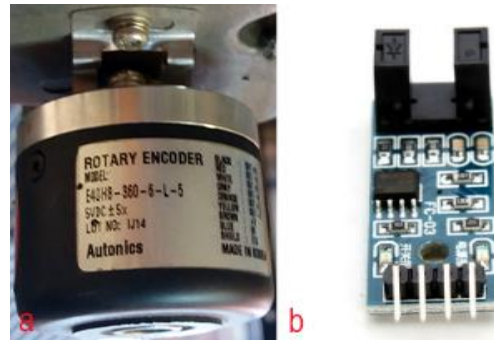


Figure 84 Sensors for measure the orbital angle and the welding speed (a) Encoder for welding angle measurement; (b) Optical sensor for detect the start position.

The weld bead dimensions must be checked afterwards finished the welding process, to verify the project requirements and the model behavior (see section 3.1.8). During the process, it is necessary to obtain this measurement to calculate the contact tip to work distance, on-line adjustment of the weld bead width estimator model and volume deposited parameter. The low-cost laser profilometer show in section 3.1.3 cannot be used for this purpose because it is slow and is affected by the electric arc.

For this task, we propose a RF625 laser profilometer (RIFTEK, 2015), of the RIFTEK company, which can take 491 scans per second (frequency of 2ms) with a resolution of  $8.6\mu\text{m}$ . The operation of the sensor is based on the optical triangulation principle (see section 2.2.3) and a blue laser beam of 405 or 450 nm wavelength is used (see Figure 23 left). The use of blue lasers instead of conventional red ones significantly enhances scanners capabilities, in particular, in controlling shiny materials and high temperature objects.

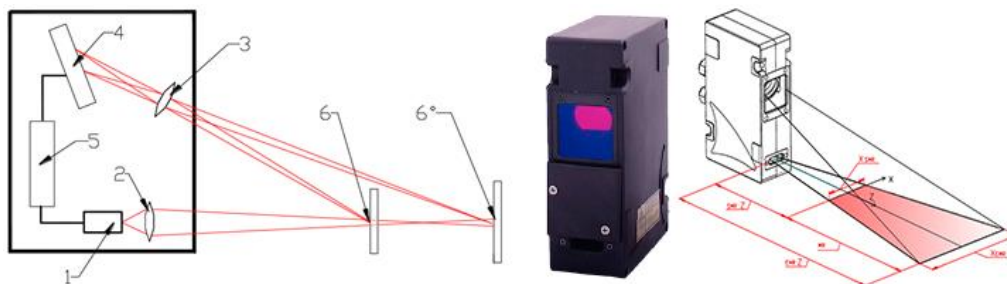


Figure 85 Profilometer laser. Adapted from (RIFTEK, 2015)

The radiation of a laser (1) is focused by a lens (2) onto an object (6). The radiation reflected by the object is collected by a lens (3) onto a linear CMOS array (4). A signal processor (5) calculates the distance to the object from the position of the light spot on the array (4). The communication with the instrument is via Ethernet and it sends an array with the distance ( $z$ ) for each point ( $x$ ). Each profile must be processed in real time by the data acquisition system, but note that, because of the distance between the electrode and laser stripe, the width and reinforcement of weld bead measurements have a dead time and is zero in the first moments. The dead time value depends on the welding speed. The solution proposed for this problem is a weld bead width estimator explained in the section 3.1.8 and a modified Smith predictor show in the section A 3.3.4.2

### A 3.1.3 Measuring the contact tip to work distance.

The contact tip to work distance ( $CTWD$ ) can be calculated with the same bead profile obtained from the laser profilometer described in the sections 3.1.3 and 3.1.4. The distance between the

torch contact tip to sensor reference is fixed and known. The *CTWD* is the difference between the base line value and this distance, as show in the figure below.

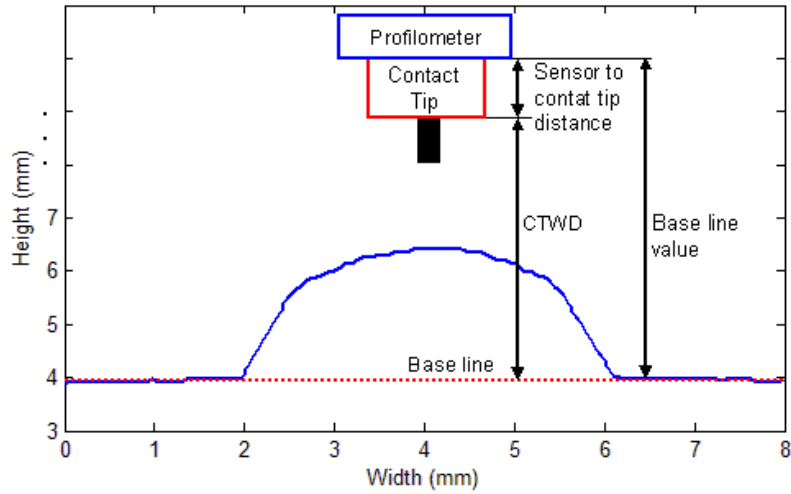


Figure 86 Calculus of the contact tip to work distance using the bead profile.

#### A 3.1.4 Calculation of the volume deposited by length unit.

The volume deposited by length unit (*VD*) can be defined as the rate between the volume of filler material (wire) melted over the base material in each length unit covered by the torch. It corresponds with the area of the weld bead (*A*) multiplied by the longitude of the torch step (*ts*), considered for this calculation. The figure below shows a typical weld joint and dimensions.

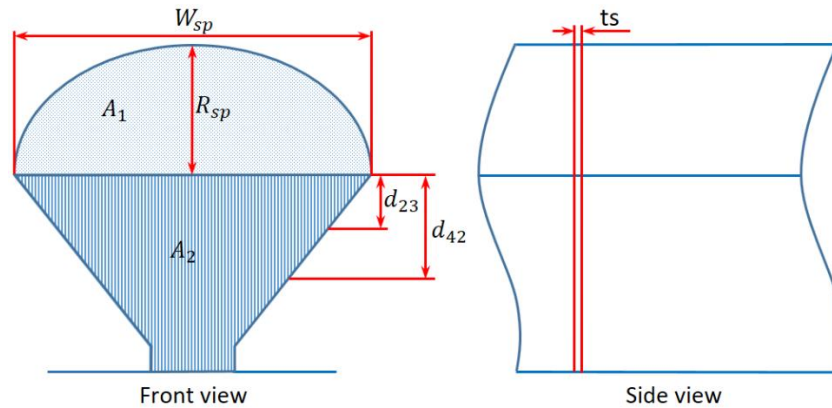


Figure 87 Area of the weld bead and joint.

If we make the rough approximation that the weld bead has a semi-ellipse profile, then the area ( $A_1$ ) can be estimated with the next equation, where  $W_{sp}$  is the weld bead width and  $R_{sp}$  is the weld bead reinforcement set points.

$$A_1 = \frac{\pi W_{sp} R_{sp}}{2} \quad (1)$$

The dimensions of the joint can be obtained by the laser scanner before the welding starts. The area of the joint ( $A_2$ ) can be calculated by the trapeziums method (numerical method) defined in equation below. The term  $d_i$  is the weld bead depth or weld bead reinforcement value supplied by the scanner profile and the  $r$  is the step or scanner resolution in the horizontal axis. The  $n$  term is the total measurements count in one scanner profile.

$$A_2 = r \sum_{i=1}^n (d_i) \quad (2)$$

The total area is the sum of both areas, as shown in the next equation.

$$A = A_1 + A_2 \quad (3)$$

Then the  $VD$  is expressed by equation below.

$$VD = A * ts \quad (4)$$

If the longitude unit is the millimeter (mm) then the term  $VD$  is expressed in  $mm^3$ .

These approximate calculations will be useful for the control loop explained in section A 3.3.3. The  $W_{sp}$  can be used to calculate the joint center for the seam tracking controller explained in the section A 3.3.1.

#### A 3.1.5 Infrared measurement.

The thermographic camera ThermoVision A40, used in this work, has a maximum sampling frequency of 120Hz and a Fireware link. This sampling frequency is not sufficient for the proposed system and the Fireware link is not compatible with the ports of the FPGA device. For this reason, we selected a new camera that meets the project requirements.

The 1024 TACHYON MicroCore infrared camera, developed by New Infrared Technologies (NIT, 2014), was selected for measuring the infrared emission of the weld pool. This instrument of small dimensions, is capable of sampling the interest area with a frequency of 1 kHz and 32x32 pixels resolution, using a USB2 port. An image of the instrument is shown in the figure below.



Figure 88 Infrared camera. Adapted from (NIT, 2014)

The emissivity of the weld pool is not constant, so the temperature measurements of the weld pool using a thermographic camera should be considered approximate (see section 2.2.4). The accurate measuring of the absolute values of temperatures is not considered significant for the purposes of this work. In this work are used absolute values and not the calculated temperature values based in emissivity coefficient.

The camera supplies the infrared image information in a matrix format. In the matrix each element  $(x,y)$  corresponds with the infrared value of the pixel  $(x,y)$  in the image.

#### A 3.1.6 Sensor fusion for estimating the depth and width of the weld bead in orbital welding position.

The estimator of depth and width of the weld bead explained in section 3.1.8, adds the welding angle input ( $\alpha$ ) to consider the effect of gravity force, as shows the Figure 89. The input layer of neural network has nine neurons.

#### A 3.1.7 Data acquisition.

The data collected by the measurement system, the values sent by the control system and relevant system parameters are saved as a text file in the SD card (see Figure 83). The files can be accessed and copied by the operator from the remote web terminal. The format of the file is fixed and can imported by any table processor, data base processor, statistic or scientific analysis software, as Microsoft Excel, Microsoft Access, SQL, Statgraphics, SPSS or Matlab.

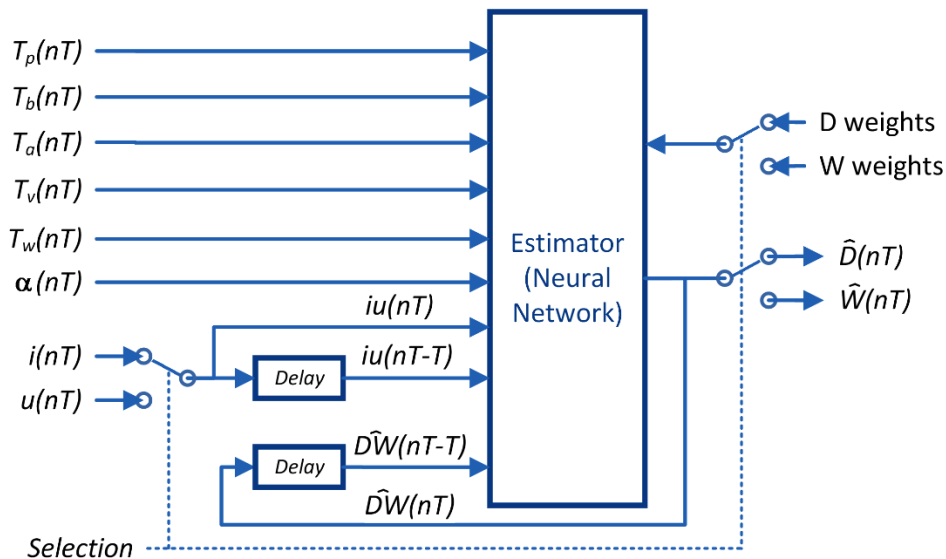


Figure 89 Estimator of depth and width of the weld bead for orbital welding position.

### A 3.2 The actuator system.

The actuator system in this proposal change only the welding table by a robotic emulator of orbital welding. The welding power source is the same described in section 3.2.1. In the next section, this emulator will be described.

#### A 3.2.1 Robotic emulator of orbital welding process

The installation of optical, video or common sensors on a welding robot is a difficult task, not only for the necessary mechanical and electrical coupling, but also because they can modify the robot kinematics (due to its weight and size) and lose focus during the its movement (due to variations in the CTWD).

Moreover, to evaluate the behavior of a control system and the weld quality by macrographic techniques, it's harder in orbital welding than on the flat welding. Also, the preparation and adjustment of position of flat pieces is less complex. Cutting the flat pieces for macrographic analysis is much simpler than in tubes, which generally have considerable dimensions. But for testing the control system in orbital welding, the torch and the work pieces need to take the all angles in the orbital route, so that the process is subject to the gravity effects.

For research purposes, we can combine the facilities of the flat welding and the orbital requirements in the same system. So, we've designed a robotic emulator that makes possible to move the piece linearly (movement relative to the torch) and simultaneously rotate all the system (orbital motion). Both movements are synchronized by the control system according to the desired welding speed and work piece or joint length. Both coordinated movements emulate the orbital movement of the welding torch with respect to the workpiece.

The system showed in the Figure 90 is a robotic emulator of an orbital welding process. This has a fixed base and a mobile table. The torch is fixed to the base and the work piece is fixed in the mobile table. To move orbitally without jumps it is necessary to balance it. A counterweight is used for this.

The system has one direct current (DC) motor for orbital movement and three stepper motors for linear movement, CTWD and seam tracking joint adjustment. With this the torch is moving with three degrees of freedom: orbital-linear, CTWD and seam tracking joint, as shown Figure 91.

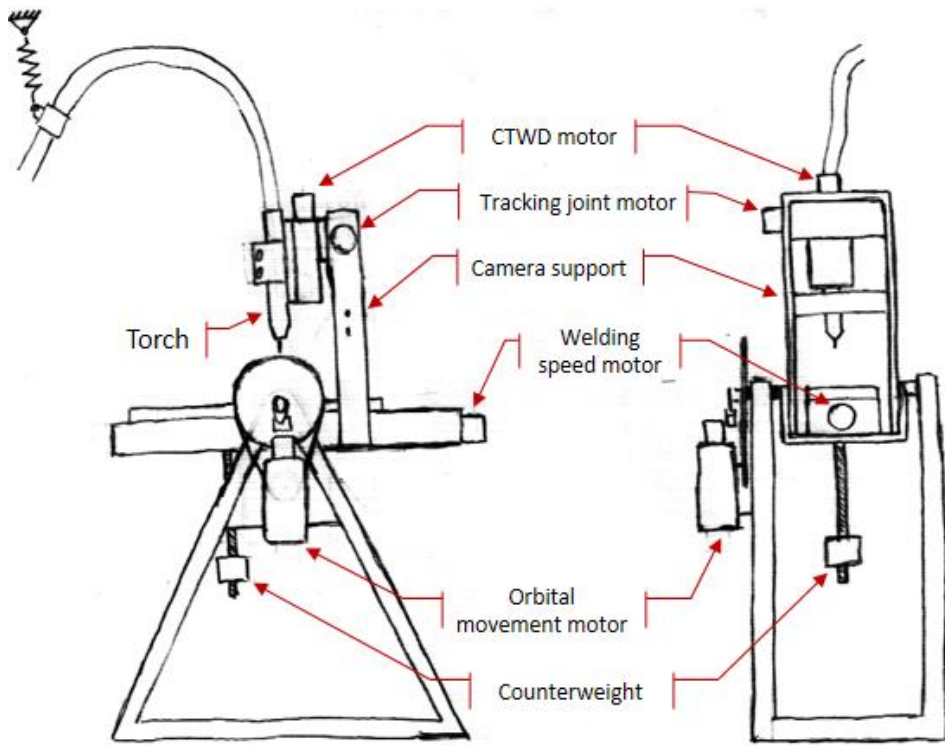


Figure 90 Mechanic structure for robotic emulator of orbital welding process.

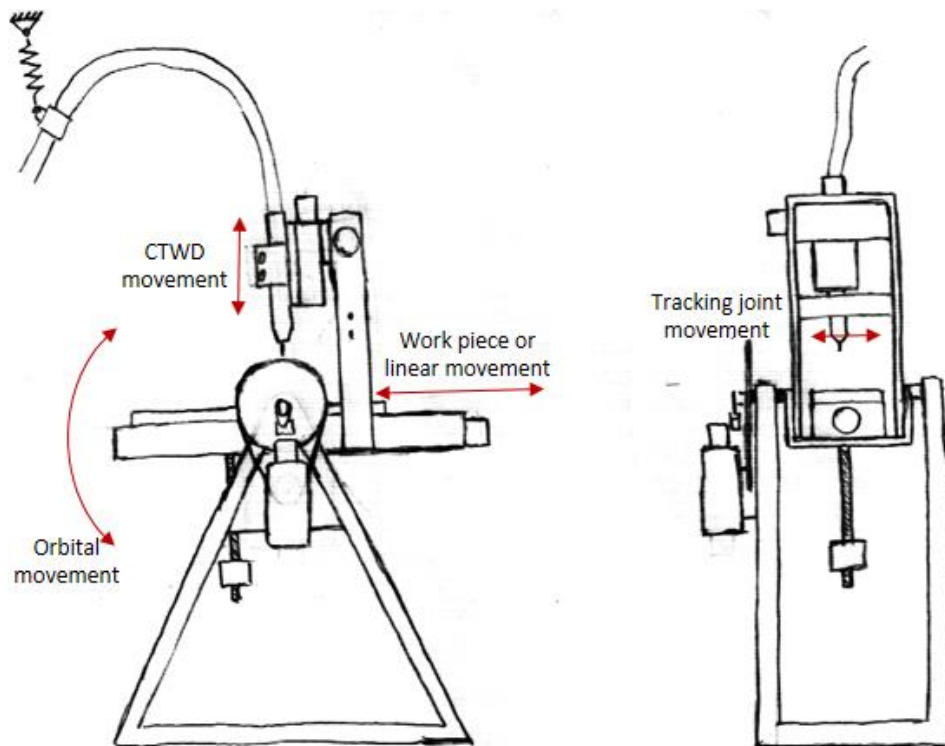


Figure 91 Degrees of freedom of the robotic emulator.

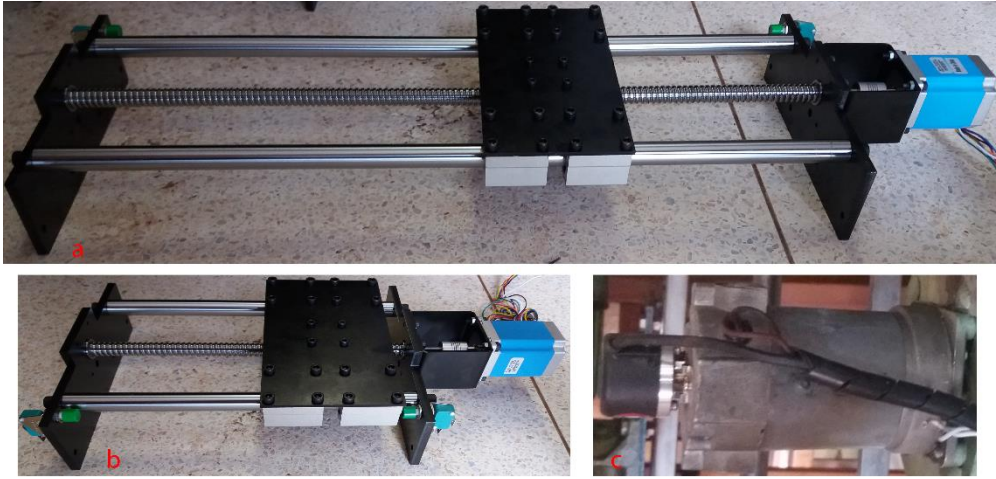


Figure 92 Motor and gearbox: (a) Stepper motor and gearbox to linear movement; (b) Stepper motor and gearbox to CTWD movement; (c) DC motor, encoder and gearbox to orbital movement.

The engines are coupled to gearboxes to achieve the necessary torque, as shown in the Figure 92. The stepper motors have optical detectors for sensing the end of travel and the DC motor is coupled with an encoder sensor.

#### A 3.2.1.1 Relationship between the torch speed and the base orbital movement.

The welding speed ( $WS$ ) or linear speed of the torch, can be expressed as:

$$WS = \frac{l}{t} \quad (5)$$

where  $l$  is the joint length and  $t$  is the time required to travel that distance.

The angular speed (orbital welding speed or  $WSO$ ) of the torch movement is defined by the orbital movement of the robotic emulator and can be expressed as:

$$WSO = \frac{\Delta\alpha}{t} \quad (6)$$

where  $\Delta\alpha$  is the difference between the end and start angles, and  $t$  is the time required to travel that distance.

Synchronize between the linear and angular speeds is possible if we consider that the time needed to travel both distances ( $t$ ) must be the same. Then, clearing  $t$  in 5 and substituting it in 6, you can define this relationship as:

$$WSO = \frac{\Delta\alpha}{l} WS \quad (7)$$

### A 3.3 The multivariable control system.

The proposed control system tries to control the width ( $W$ ) and depth ( $D$ ) of the weld bead. The control of the bead reinforcement ( $R$ ) is done indirectly by controlling of the deposited material volume ( $DV$ , see section A 3.1.4). The weld bead width and bead reinforcement are measured by a laser profilometer (see section A 3.1.2) with a dead time because of the sensor position, but it is not possible to measure the weld bead depth. The weld bead depth is estimated ( $\hat{D}$ ) based in infrared and welding arc measurements (see section 3.1.8). The weld bead width is predicted ( $\hat{W}$ ) by removing the dead time and the value is corrected by using the real value ( $W$ , see section A 3.3.4.2). The control strategy includes several control loops and different control algorithms. The Figure 93 shows the general diagram of the multivariable control system and it is described in the next sections.



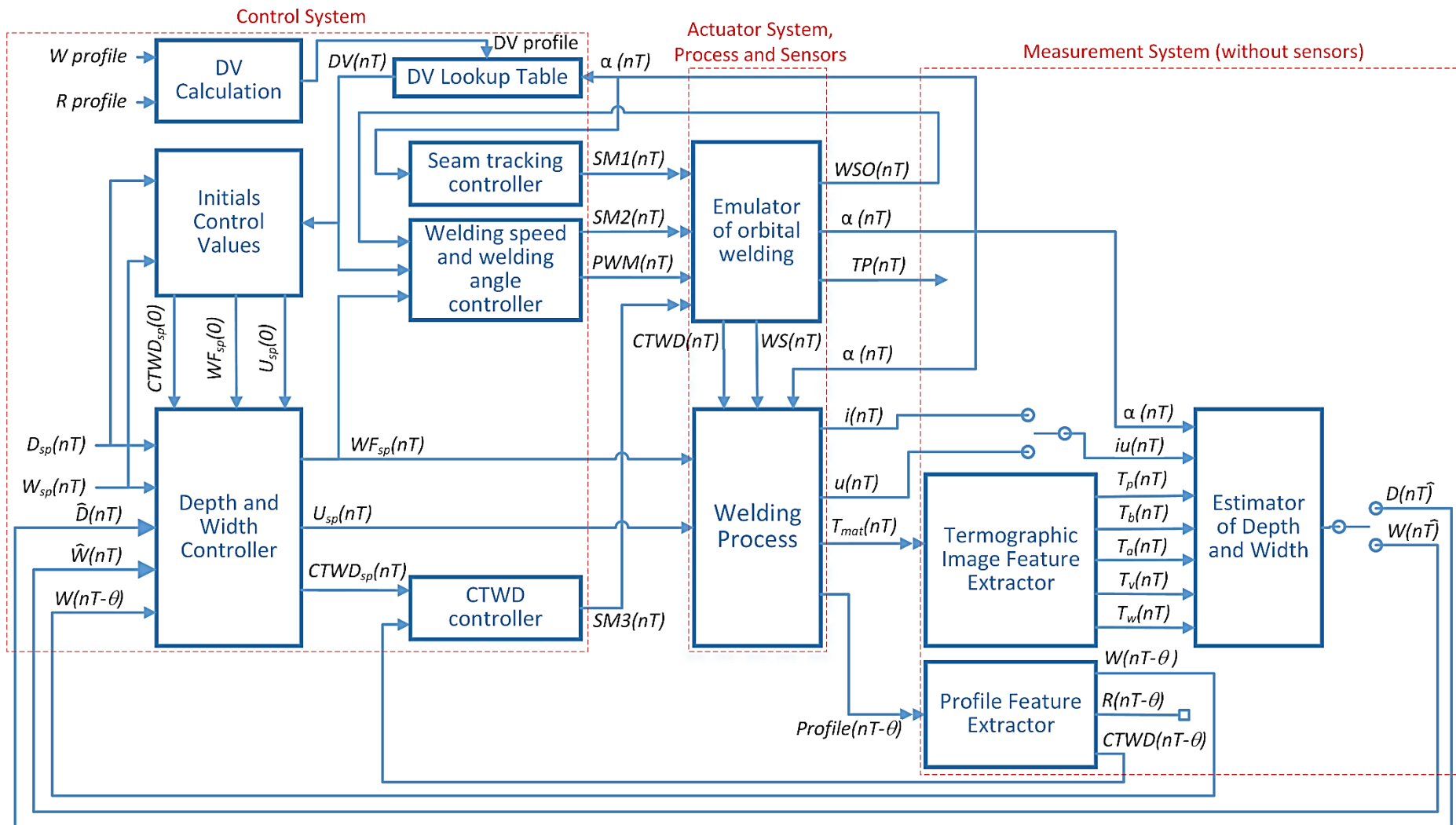


Figure 93 General diagram of the multivariable control system.

### A 3.3.1 Control of seam tracking.

The weld joint is scanned before welding process starts and the center joint is calculated in all the points of the torch trajectory, for the seam tracking algorithm. With this data, it is possible to define the correct trajectory for the torch and move the seam tracking stepper motor accordingly.

The seam tracking open control loop (show in the figure below) receives the welding angle and finds the correct torch position ( $TP_{SP}$ ) in the lookup table, obtained from the weld joint profile. Then, the controller moves the stepper motor to this position, regulating the step time and step count (embedded in the  $SM1$  signal). The  $nT$  parameter is the time of the sample, made up of by the sample time ( $T$ ) and the sample number ( $n$ ).



Figure 94 Blocks diagram of the seam tracking control loop.

To reduce the amount of data in the lookup table it is possible to save only the significant changes of trajectory and hold the last value of  $TP_{SP}$  in the output until the new value is found. Online analysis is possible. The same control strategy can be used substituting the lookup table by the algorithm that analyzes the profilometer data, but more calculation resources are needed.

### A 3.3.2 Control of contact tip to work distance.

The contact tip to work distance ( $CTWD$ ) is controlled in a closed loop by a professional Proportional Integral Derivative (P-PID) controller (see section A 3.3.4.1) The  $CTWD$  is measured with a laser profilometer and calculated with the algorithm described in the section A 3.1.3. The controller manipulates the step time and the step counter (embedded in the  $SM3$  signal) of the stepper motor associated with the  $CTWD$  movement in the robotic emulator of orbital welding (see section 0). The  $nT$  parameter is the time of the sample, composed by the sample time ( $T$ ) and the sample number ( $n$ ). The figure below shows this closed control loop.

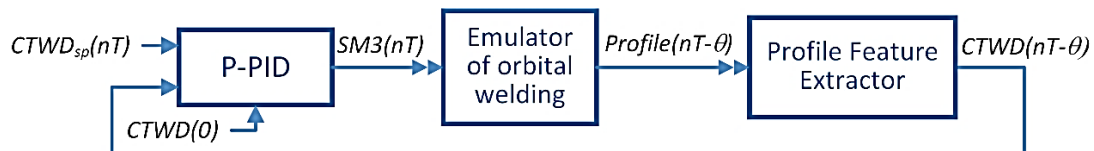


Figure 95 Blocks diagram of the contact tip to work distance control loop.

The measure of the  $CTWD$  has a dead time ( $\theta$ ) because the position of the sensor. This delay can be neglected in the especial conditions of the robotic emulator because the variation of the  $CTWD$ , in the dead time, is null or very small. The linear movement of the piece and the use of flat pieces guarantee these conditions.

### A 3.3.3 Control of welding speed and welding angle.

The linear welding speed ( $WS$ ) or the linear movement of the work piece, is controlled in an open loop with a stepper motor controller through of the step time and the step counter (embedded in the  $SM2$  signal) of the stepper motor associated to  $WS$  movement.

The speed of rotation or orbital welding speed ( $WSO$ ) is controlled in a closed loop. The professional Proportional Integral Derivative (P-PID) controller delivers to the driver of the direct current motor a pulse width modulation (PWM) signal. The feedback incorporates an encoder (see

section 3.1.2), which delivers pulses whose duration is inversely proportional to  $WSO$ . The position ( $\alpha$ ) is obtained by the count of the pulses in a positive direction or discounted in the negative direction, started in the index position.

The wire feed speed ( $WF$ ) and the volume deposited by length unit ( $VD$ , defined by the equation 4) are the inputs of the relationship control loop. The parameters  $VD$  and  $WF$  are used for calculating the  $WS$  set point, as shown in the figure below. This relationship defines the deposition volume of the material in the weld joint.

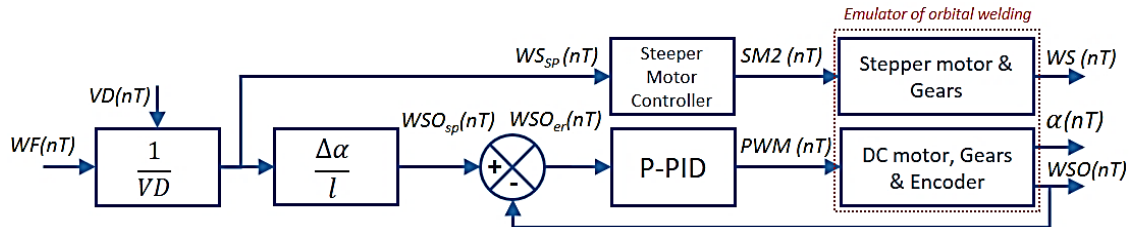


Figure 96 Blocks diagram of welding speed and orbital welding control loop.

The gain  $\frac{\Delta\alpha}{l}$ , defined by the equation 7, is used to calculate the set point of the orbital speed control loop and maintain the corresponding relationship between  $WS$  and  $WSO$ .

#### A 3.3.4 Control of depth and width of weld bead.

The welding process is represented in this work as a multiple input-multiple output (MIMO) process with three inputs and two outputs, as shown in the figure below. The pairing of controlled and manipulated variables is shown too. Other variables shown in Figure 97 are considered as disturbances or controlled by others control loops. This selection is based on the bibliographic review and requires the relative gains analysis (BRISTOL, 1966) and experimental test to confirm the hypothesis.

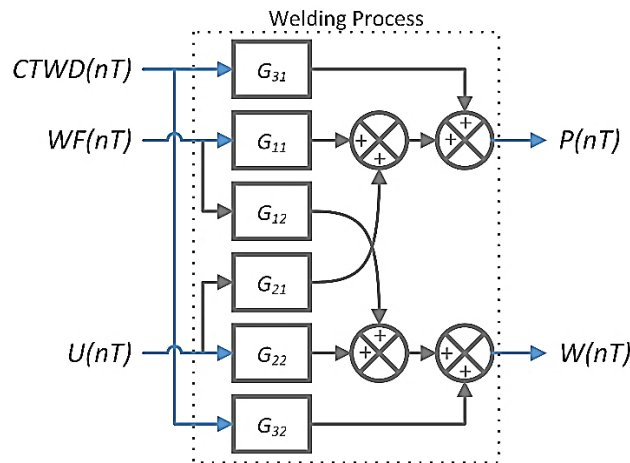


Figure 97 Welding process represented as a multiple input-multiple output process.

The principal variables that affect the bead geometry are the welding voltage ( $U$ ), the wire feed speed ( $WF$ ), the contact tip to work distance ( $CTWD$ ) and the welding speed ( $WSO$ ).

Increasing the electric current (increasing the  $WF$ ) for the same welding speed results in a greater weld bead depth and welding pools with greater volume. This can be achieved to fill a larger volume of the joint (greater production) and ensure the integrity of the same by the full penetration (good quality) simultaneously (SCOTTY; PONOMAREV, 2008).

An increase in electric current, accompanied by a proportional increase of the welding speed (wire feed speed / welding speed = constant) also results in greater penetration, but the welding

pool keeps the same volume. Then, the same welding joint volume can be filled (maintaining production) and ensure its integrity by full penetration (good quality) at the same time (SCOTTY; PONOMAREV, 2008).

Following this idea, in the control strategy the  $WSO$  depends on the  $WF$  by the welding speed and welding angle control loop. It allows the control of the volume deposited ( $DV$ ) in the bead join. The  $DV$  needed to create a weld bead with the width and reinforcement defined in the welding project is known.

The  $U$  and  $WF$  are manipulated by the multivariable control loop that controls the weld bead width ( $W$ ) and the weld bead depth ( $D$ ). The  $CTWD$  can be considered a disturbance or a manipulate variable, depending on the control strategy. The  $CTWD$  control loop, is an internal cascade loop. Then, if  $W$  and  $DV$  are controlled, the bead reinforcement ( $R$ ) is indirectly controlled too. The general block diagram of this control strategy is shown in Figure 93 and partially shown below.

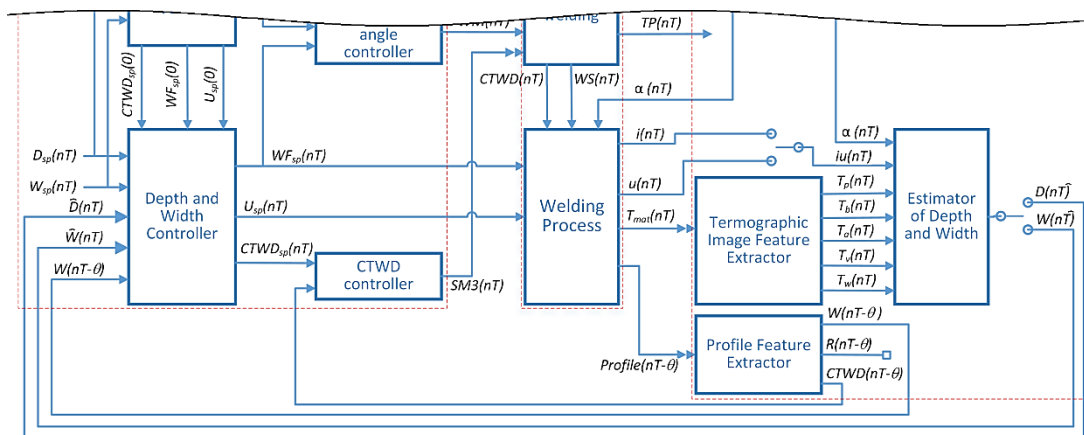


Figure 98 Diagram of the weld bead width and depth control loops.

The thermographic image feature extractor gets the thermographic matrix ( $T_{mat}$ ) and obtains the features described in the section 3.1.4. These values are used by the estimators to obtain the weld bead depth estimated value ( $\hat{P}$ ) and the weld bead width estimated value ( $\hat{W}$ ). These values are fed back to the controller and the control errors are calculated, using the set point of weld bead depth ( $P_{SP}$ ) and width ( $W_{SP}$ ) values.

Note that the estimator and predictor are implemented in the same logical structure and are multiplexed by the switch to obtain the penetration using the welding current or the weld bead width using the welding voltage.

A laser profilometer obtains the profile of the bead and a feature extractor algorithm calculates the real weld width ( $W$ ) and reinforcement ( $R$ ) of the bead. Note that the measurements have a dead time ( $\theta$ ) and are zero during the first moments. The  $W(nT - \theta)$  is used in a modified Smith predictor implementation to adjust the predictor value.

The initial values of manipulated variables ( $U(0)$ ,  $WF(0)$  and  $CTWD(0)$  in fuzzy controller) are estimated by the Initial Control Values block, based in set point values. An accuracy value for the manipulated variables is not necessary because the controller changes these values based on the control error.

While many control algorithms have been proposed, which approaches are theoretically elegant, most of the industrial processes nowadays are still controlled by Proportional-Integral-Derivative (PID) controllers (ÅSTRÖM; HÄGGLUND, 2001; KO; WU, 2008; KUMAR; NAKRA;

MITTAL, 2011). Conventional PID controllers have been widely applied in industrial process control for about half a century because of their simple structure and convenience of implementation (BENNETT, 1993). However, a conventional PID controller can have poor control performance for nonlinear and complex systems for which there are no precise mathematical models. Numerous variants of conventional PID controller, such as self-tuning, auto-tuning and adaptive PID controllers have been developed to overcome these difficulties. Many on-line self-tuning or adaptive algorithms are based in fuzzy inference systems (JANTZEN, 1998; KARASAKAL *et al.*, 2013; KAZEMIAN, 2001; KO; WU, 2008; KUMAR; NAKRA; MITTAL, 2011; LIU, WEN HONG; XIE, 2011; SOYGUDER; KARAKOSE; ALLI, 2009; WU, YING; JIANG; ZOU, 2012).

Fuzzy logic controllers are intrinsically nonlinear, allow direct insight into their behavior and is widely used for controlling nonlinear systems whose plant models are unknown or imprecise (LU, J L; CHEN; YING, 2001). Unlike others methods, such as the neural networks, it is usually easy to determinate what action a fuzzy controller will take for a given situation, since generally they have analytic structures (CARVAJAL; CHEN; OGMEN, 2000).

The multivariable control strategies proposed are based in the professional version of PID controller, a fuzzy self-adaptive algorithm, decoupling methods and a fuzzy controller. These elements are discussed below.

#### A 3.3.4.1 Professional version of the PID controller.

The professional version of Proportional-Integral-Derivative (P-PID) controller included several characteristics of other versions of PID (BEHAR, 2003) such as:

- The input of derivative term is the controller variable, implementing a derivative kick protection mechanism.
- The integral wind up protection algorithm is implemented.
- The integral term can be initialized with the actuator value.
- The controlled variable is filtered to reduce the noise that is responsible for oscillator behavior.
- The range of the measurement system and actuator system is used to normalize the calculations in the controller.
- The measurements are filtered to reduce noise of low, middle and high frequency.
- The reference is filtered to avoid the abrupt variations in the control error.

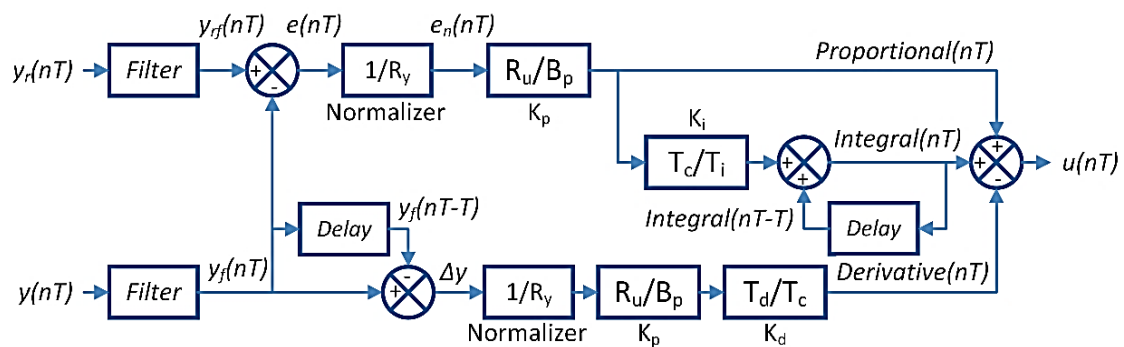


Figure 99 Professional version of the Proportional-Integral-Derivative controller.

The controller output is calculated with the equation

$$u(nT) = \frac{R_u}{B_p} \left[ e_n(nT) - \frac{T_d \Delta y(nT)}{T_c R_y} \right] + Int(nT) \quad (8)$$

where

$n$  is the sample number (integer and positive value)

$R_u$  is the actuator span and is expressed as

$$R_u = u_{max} - u_{min} \quad (9)$$

$B_p$  is the proportional band and is related to the gain in equation 10. The sign of  $B_p$  should be selected similarly to process gain (positive to direct action and negative to inverse action)

$$K_p = \frac{R_u}{B_p} \quad (10)$$

$T_d$  is the constant of derivative time

$T_c$  is the control time and is a multiple of the sample time ( $T_c = mT, m \geq n$ )

$R_y$  is the measurement system span and is expressed as

$$R_y = y_{max} - y_{min} \quad (11)$$

$e_n(t)$  is the normalized error in the sample time  $t$  and is expressed as

$$e_n(nT) = \frac{y_{rf}(nT) - y_f(nT)}{R_y} \quad (12)$$

$y_{rf}(nT)$  is the filtered set point value in the  $nT$  sample time.

$y_f(nT)$  is the filtered measurement in the  $nT$  sample time.

$\Delta y_f(nT)$  is the difference between the filtered measurement in the  $nT$  sample time and the previous sample time ( $nT - T$ ). Can be calculated by the equation

$$\Delta y_f(nT) = y_f(nT) - y_f(nT - T) \quad (13)$$

$Int(nT)$  is the integral term in the sample time  $t$  and is expressed as

$$Int(nT) = Int(nT - T) + \frac{T_c R_u}{T_i B_p} e_n(nT) \quad (14)$$

$Int(nT - T)$  is the integral term in the previous sample time. The initial value, when  $n = 1$ , is equal to  $u(0)$ .

The controller output is expressed in a range for 0 to 100% of the actuator span. The real value ( $u_{eu}$ ), expressed in engineer units, can be calculated in equation 15 for a normally closed actuator and 16 for a normally open.

$$u_{eu}(nT) = R_y \frac{u(nT)}{100} \quad (15)$$

$$u_{eu}(nT) = R_y \left(1 - \frac{u(nT)}{100}\right) \quad (16)$$

The first control strategy for the multivariable system included two professional PID controllers as shown in Figure 100.

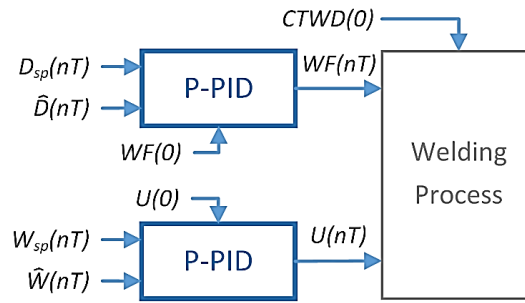


Figure 100 Controller of depth and width of the weld bead based on the Professional PID algorithm.

The first loop controls the weld bead depth ( $D$ ) and manipulates the wire feed speed ( $WF$ ). The second controls the weld bead width ( $W$ ) and manipulates the welding voltage. The  $CTWD$  is considered a measurable disturbance.

The design and synthesis of both professional PID in FPGA or microcontroller devices are possible and the resource consumption is very low (DUBOUÉ; BESTARD, 2014).

#### A 3.3.4.2 Smith Predictor variation for the weld bead width control loop.

The Smith Predictor control was developed for processes with a long and constant dead time. The block diagram of the control scheme is shown in Figure 101. The controller output ( $u$ ) goes to the process and to the first part of the process model. Everything that the controller does to the process is also done to the process model. The output of the first portion of the process model ( $\hat{y}(nT)$ ), without the dead time becomes a prediction of what the actual process measurement should be  $\theta$  seconds from now. This predicted output can be used as a feedback signal.

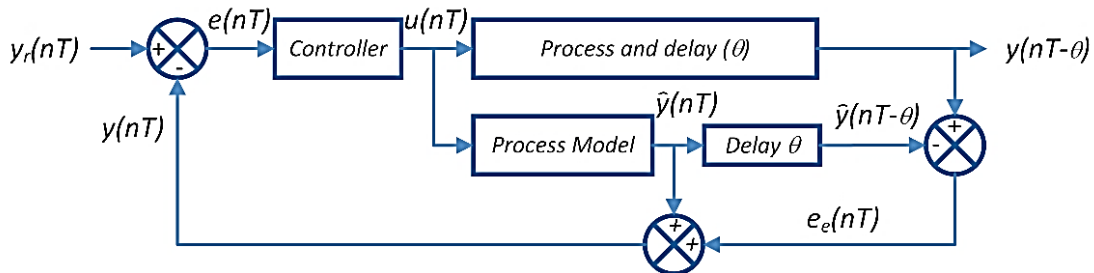


Figure 101 Typical control loop with Smith Predictor.

If the model contained a perfect representation of the nondead time portion of the process and if there were no other disturbances, this feedback is all that would be required. In the real world, neither of these two ideal conditions occur. Hence, the predicted future output is delayed by the time  $\theta$ , which itself is a prediction of the actual dead time in the process. The delayed signal  $\hat{y}(nT - \theta)$  is a prediction of what the measurement value should be at the present time. This can be compared with an actual measurement ( $y(nT)$ ) and the difference added to the feedback signal to compensate for the model error.

The proposed variation of the Smith Predictor only changes the predictor input. The weld bead width predictor output ( $\hat{W}(nT)$ ) is used as model output and the delayed process output is the weld bead width measurement ( $W(nT - \theta)$ ). The dead time  $\theta$  is not constant but is known. The block diagram show below describes the P-PID algorithm with the Smith Predictor (P-PID+SP).

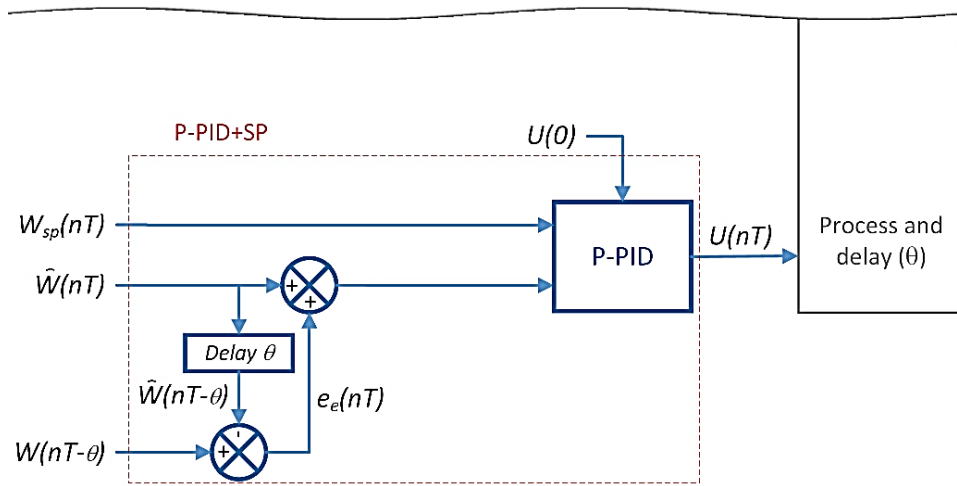


Figure 102 Weld bead width controller with modified Smith Predictor.

#### A 3.3.4.3 Fuzzy self-adaptive PID controller.

The fuzzy self-adaptive PID controller is an auto-adaptive controller that is designed by using an incremental fuzzy logic controller to tune the parameters of the PID controller on-line by fuzzy control rules. The controller uses the error ( $e$ ) and the rate of change of error ( $\Delta e$ ) as its inputs and can meet the desired of self-tuning parameters based on time-varying  $e$  and  $\Delta e$  (SOYGUDER; KARAKOSE; ALLI, 2009).

The proposed fuzzy self-adaptive algorithm improves the control performance of the PID controller in nonlinear and stochastic systems, but keeps the simple structure. According to the error of the controlled device response on the sampling time  $e(nT)$  and the change rate of the error  $\Delta e(nT)$ , the PID parameters ( $B_p$ ,  $T_i$  and  $T_d$ ) are determined. The static and dynamic performance of the process response are considered at the same time. The figure below shows the self-adaptive process.

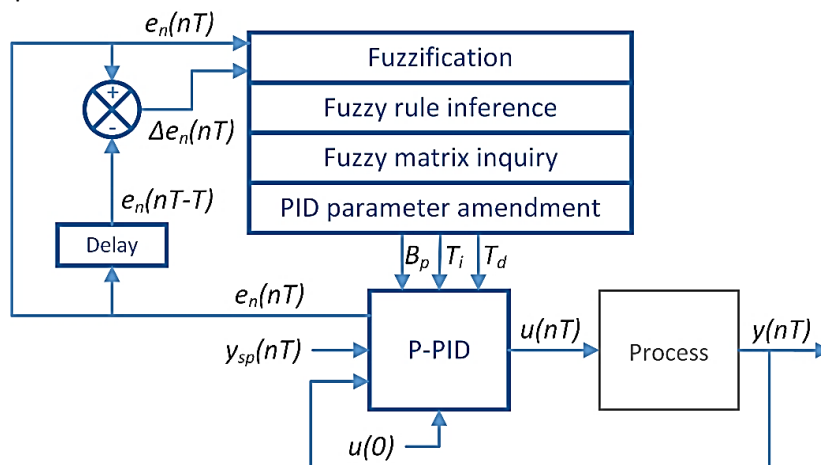


Figure 103 Fuzzy self-adaptive professional PID controller. Adapted from (LIU, WEN HONG; XIE, 2011)

The core of the design is to set up the proper fuzzy rules model for the controlled process by summing up expert experience and knowledge. According to the technology features and operating experiences of continuous casting, three sets of fuzzy rules are established.

The structure of fuzzy auto-tuning has two inputs ( $e$  and  $\Delta e$ ) and three outputs ( $\Delta B_p$ ,  $\Delta T_i$  and  $\Delta T_d$ ), but it can be changed to three subsystems of two inputs and one output. The rules and fuzzy matrix are defined in Table 10.



Table 10 Fuzzy matrix to  $B_p$ ,  $T_i$  and  $T_d$ .

		$\Delta e$				
		<b>NB</b>	<b>NS</b>	<b>Z</b>	<b>PS</b>	<b>PB</b>
$e$	<b>NB</b>	NB	NB	NS	NS	Z
	<b>NS</b>	NB	NS	NS	Z	PS
	<b>Z</b>	NS	NS	Z	PS	PS
	<b>PS</b>	NS	Z	PS	PS	PB
	<b>PB</b>	Z	PS	PS	PB	PB

		$\Delta e$				
		<b>NB</b>	<b>NS</b>	<b>Z</b>	<b>PS</b>	<b>PB</b>
$e$	<b>NB</b>	NB	NB	NS	Z	Z
	<b>NS</b>	NB	NS	NS	Z	Z
	<b>Z</b>	NS	NS	Z	PS	PS
	<b>PS</b>	Z	Z	PS	PS	PB
	<b>PB</b>	Z	Z	PS	PB	PB

		$\Delta e$				
		<b>NB</b>	<b>NS</b>	<b>Z</b>	<b>PS</b>	<b>PB</b>
$e$	<b>NB</b>	PS	NS	NB	NS	PS
	<b>NS</b>	Z	NS	NB	NS	Z
	<b>Z</b>	Z	NS	NS	NS	Z
	<b>PS</b>	Z	Z	Z	Z	Z
	<b>PB</b>	PB	PS	PS	PS	PB

The membership function is a curve that defines how each point in the input space is mapped to a membership value (on degree of membership) between 0 and 1. In this case, the triangular membership functions are used for input and outputs variables. These are defined by Negative Big (NB), Negative Small (NS), Zero (Z), Positive Small (PS), Positive Big (PB). The physical domain is selected based on a trial and error method. The membership functions picture is show below.

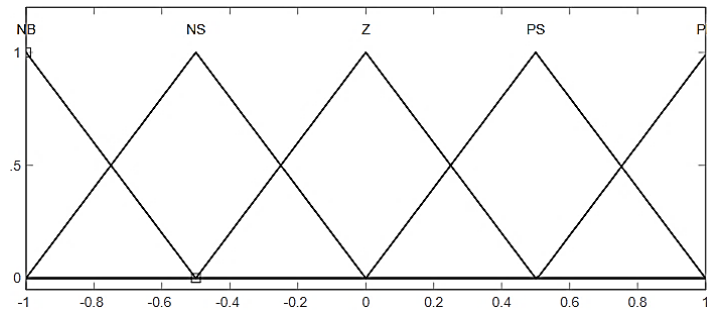


Figure 104 The membership functions for the inputs ( $e$  and  $\Delta e$ ) and outputs ( $B_p$ ,  $T_i$  and  $T_d$ ) of the fuzzy system.

Applying the fuzzy rules, the PID parameters are self-correcting. Firstly,  $e$  and  $\Delta e$  are fuzziness and the membership grades of the relevant fuzzy subsets are determined. Secondly, the adjusting process of the PID parameters is expressed by the fuzzy self-regulation model. Lastly, the fuzzy matrix tables are inferred by fuzzy fusion (LIU, WEN HONG; XIE, 2011).

After the three self-regulation models are evaluated, the corresponding control tables are determined, which are changed to the homologous values. The above values are substituted into the next equations and the final results are calculated.

$$B_p(nT) = B_p(nT - T) + \Delta B_p(nT) \quad (17)$$

$$T_i(nT) = T_i(nT - T) + \Delta T_i(nT) \quad (18)$$

$$T_d(nT) = T_d(nT - T) + \Delta T_d(nT) \quad (19)$$

The initial values for  $B_p$ ,  $T_i$  and  $T_d$  (when  $n = 1$ ) are defined in the system configuration or are loaded from the last saved tuning.

The design and synthesis of fuzzy inference system in the FPGA device is can be done using the X-Fuzzy software (CNM, 2012). The block diagram of the proposed fuzzy self-adaptive controllers is shown below.

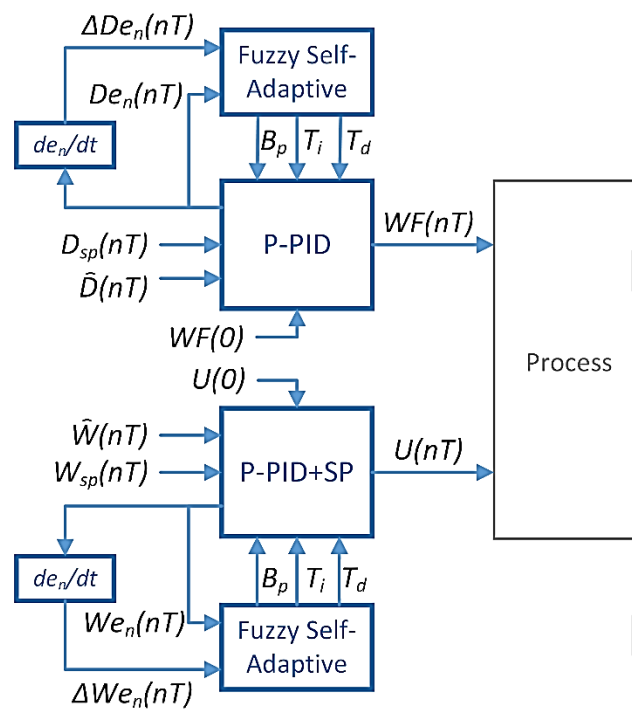


Figure 105 Weld bead width and depth controller with Fuzzy Self-Adaptive Professional PID algorithm.

#### A 3.3.4.4 Decoupling the control loops.

To improve the controller behavior the decoupling structures can be incorporated in the control loops for reducing the interaction between the loops. The decoupling used in this work is based in feedforward control and is discussed below.

The feedforward control is useful when the process is affected by strong measurable disturbances. This strategy can help improve the behavior of the controller in the face of this disturbance, but it cannot replace the feedback control (BEHAR, 2003). The typical feedforward control is shown in the next figure.

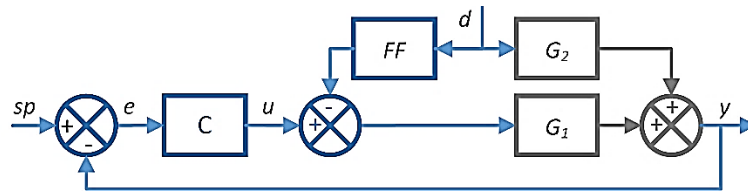


Figure 106 Typical feed forward control in a single control loop.

The feedforward control tries to anticipate the effect of the disturbance ( $d$ ). The control action is applied directly to the control loop drive element, before the disturbance can affect the controlled variable (BEHAR, 2003; SMITH, CARLOS A.; CORRIPIO, 1997). The equations 20 and 21 usually define the necessary conditions to it while the feedforward model is obtained in equation 22.

$$\frac{\Delta y}{\Delta v} = \frac{G_2(z^{-1})}{1+CG_1(z^{-1})} + \frac{FFG_1(z^{-1})}{1+CG_1(z^{-1})} = 0 \quad (20)$$

$$\frac{\Delta y}{\Delta v} = \frac{G_2(z^{-1})+FFG_1(z^{-1})}{1+CG_1(z^{-1})} = 0 \quad (21)$$

$$FF = -\frac{G_2(z^{-1})}{G_1(z^{-1})} \quad (22)$$

If  $G_1(z^{-1})$  and  $G_2(z^{-1})$  are quite close to first order transfer function with delay, as it is shown in

$$G_1(z^{-1}) = \frac{K_1 z^{-p_1}}{1 - \alpha_1 z^{-1}} \quad (23)$$

$$G_2(z^{-1}) = \frac{K_2 z^{-p_2}}{1 - \alpha_2 z^{-1}} \quad (24)$$

where the terms  $\alpha_1$  and  $\alpha_2$  are related with the sample time ( $T_s$ ) and process time constants ( $T_1$  and  $T_2$ ), as shown the next equations.

$$\alpha_1 = e^{-T_s/T_1} \quad (25)$$

$$\alpha_2 = e^{-T_s/T_2} \quad (26)$$

Then the feedforward transfer function is

$$\frac{\Delta u}{\Delta v} = FF(z^{-1}) = -\frac{K_2 z^{-p_2} (1 - \alpha_1 z^{-1})}{K_1 z^{-p_1} (1 - \alpha_2 z^{-1})} \quad (27)$$

$$\frac{\Delta u}{\Delta v} = FF(z^{-1}) = -K_{FF} z^{(p_1 - p_2)} \frac{1 - \alpha_1 z^{-1}}{1 - \alpha_2 z^{-1}} \quad (28)$$

where

$$K_{FF} = \frac{K_2}{K_1} \quad (29)$$

Sometimes only the steady value is compensated and the dynamic is depreciated in which case the transfer function of the feedforward block is  $K_{FF}$ .

It is important to note that the delay in the principal channel must be less or equal than the disturbance channel ( $p_1 \leq p_2$ ) for the dynamic compensation to be effective.

If the interactions between loops are considered as disturbances, the same feedforward scheme can be used to decoupling the weld bead width and penetration control loop in our welding process. The next figure shows the block diagram.

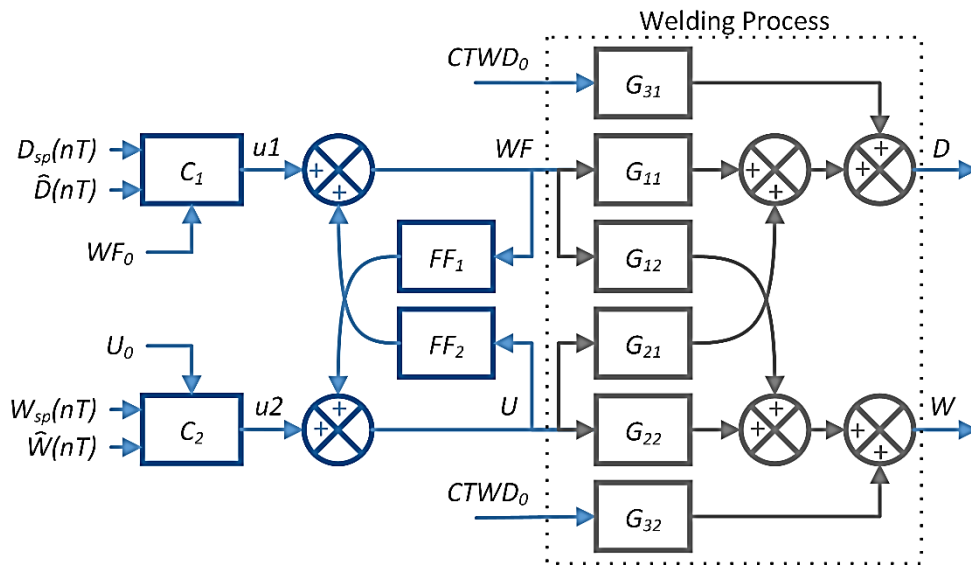


Figure 107 Weld bead width and depth penetration controller with decouples.

The decouples  $FF_1$  and  $FF_2$  are designed to minimize the interaction between loops and improve the controller behavior. The calculation of the transfer function of decouples is similar to what

is explain in the feedforward transfer function. This strategy is similar to inverse decoupling shown in (BHARATHI; SELVAKUMAR, 2012; GARRIDO; VÁZQUEZ; MORILLA, 2012).

#### A 3.3.4.5 Fuzzy logic for manipulated the CTWD.

The control strategy commented above is based in two professional Proportional-Integral-Derivative controllers and decoupler blocks. The process input  $CTWD$  is fixed by the estimation of the initial control parameters (see section A 3.3.5) and treated as a measurable disturbance. In this strategy, the control actions could be limited if the set points change or if other disturbances change the process conditions significantly. In others words, the control range of the  $WF$  and  $U$  could be insufficient for a fixed value of  $CTWD$ .

One solution for this problem is manipulating the  $CTWD$  based on the control error ( $e_n$ ) of the controlled variables and your variation ( $\Delta e_n$ ). For example, if the control error of  $W$  is positive big and the control error of  $P$  is negative big, the logical decision is to increment the  $CTWD$  because the arc resistance is incremented and the arc width too, while the welding voltage is kept the same and the welding current is slightly reduced. If we also take into account the error variation, the static and dynamic performance of the process response are considered at the same time.

Due to the non-linear nature of this relationship and the rules based in the process knowledge and experience, the selected algorithm is the fuzzy logic controller. The blocks diagram of the controller is shown in the next figure.

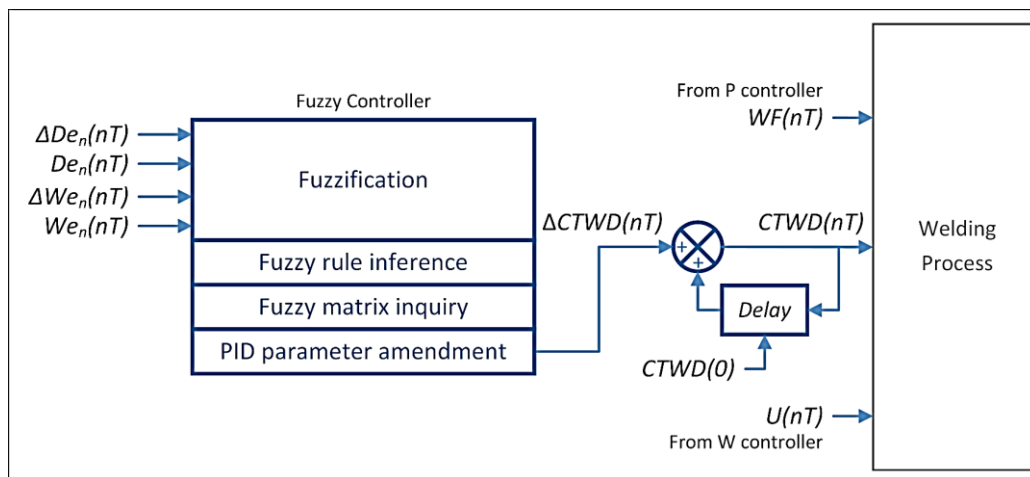


Figure 108 Weld bead width and depth penetration controller with Fuzzy and P-PID controllers.

The inputs for the fuzzy controller are the error and the error variation. When these parameters are big or tend to increase in large value, the controller outputs the corresponding  $\Delta CTWD$  value and moves the  $CTWD$ . When the errors are reduced, or tend to reduce, the  $CTWD$  change is stopped.

These variations must be slow so that the other loops can compensate for them. For this reason, the control period of this loop must be greater than that of the others and the error must be the average in this control period.

#### A 3.3.5 Estimation of the initials control parameters.

The initial output values of controllers can be estimated by the same neural network structure shown in the section 3.1.8, but with others parameters or weight coefficients. This procedure is executed only before starting the control system and it reduces the convergence time of the controlled variables to set point values and the control error in the initial time.

The neural network needs to be evaluated in three steps because it has only one output and it is necessary to estimate these three parameters: that are the contact tip to work distance ( $CTWD$ ), the wire feed speed ( $WF$ ) and the welding voltage ( $U$ ). This three steps algorithm concatenates three neural networks to obtain the initial control values and reduce the required FPGA resources. A block diagram is shown below.

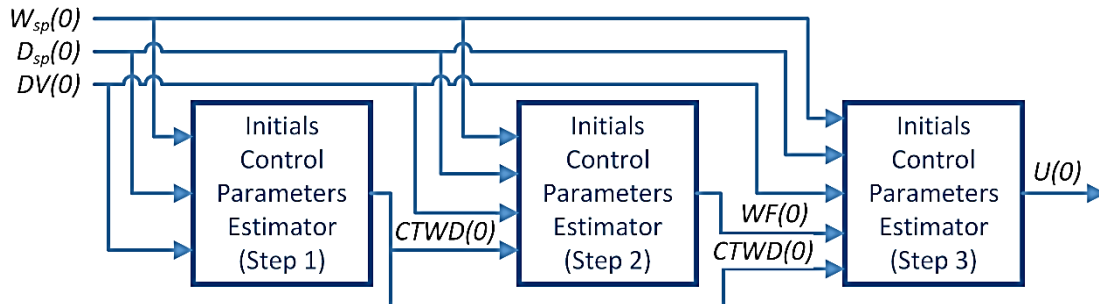


Figure 109 Estimator of the initials control parameters executed in three steps by the same neural network structure.

In the first step the system reads the set point values and configures the neural network to the  $CTWD$  estimation. The neural network input is the  $W_{sp}$  and bead depth penetration set point ( $P_{sp}$ ) and the volume deposited by length unit ( $DV$ ) calculated in section A 3.1.4. The output is the  $CTWD$  value.

In the second step, the neural network has the same inputs plus the  $CTWD$  value, calculated in the last step. The output is the  $WF$  value.

In the third step, the neural network has the same inputs plus the  $WF$  value, calculated in the last step. The output is the  $U$  value.

The appropriate weight coefficients for the specific model must be loaded in each step. The unused inputs and the associated weight coefficients are zero. The neural network can be trained with the experimental collected data.

### A 3.3.6 Sequential controller.

The sequential controller can be implemented in a finite state machine in the Nios II or FPGA. The controller is in charge of executing the following operation sequence:

1. Execute the initial sequence and verify the system status.
2. Read the set point operational sequence and configuration parameters defined by the operator
3. Scan the piece and save the three-dimensional profile.
4. Calculate the need deposited volume profile and save in the lookup table.
5. Configure and start the initial control values estimation
6. Get the initial control values and send to controllers.
7. Get the collected data from the sensors.
8. Start the features extraction algorithms (see sections 3.1.4 and 3.1.6).
9. Get the features values.
10. Configure and start the weld bead depth estimation algorithm (see section 3.1.8).
11. Get the weld bead depth value.
12. Configure and start the weld bead width estimation algorithm (see section 3.1.8).
13. Get the weld bead width value.
14. Send the set points values and controlled variable values to the controllers and start the manipulated variables calculation.
15. Send the manipulated variables values to the actuators.

16. Verify the system status. Check the alarm flags and trigger the emergency procedures if necessary.
17. Save the recollected data, controlled and manipulated variables and system status in an SD card.
18. Increment the pointer to the set point sequence and verify if it is the end position.
19. Return to step 6 if it is not the end position. Otherwise continue.
20. Execute the end sequence and verify the system status.

### A 3.3.7 Task distribution.

The general task distribution between the three logics components of the system is described in the table below. Note that the FPGA has a parallel architecture and can conduct several tasks at the same time.

Tasks 1 to 4 are executed only at the beginning of the work. The other tasks are executed in a loop. The estimated loop time delay is 1.251 ms. The hard-real-time execution is provided by the FPGA and NIOS II architecture. The FreeRTOS controls the real-time execution in the HPS.

*Table 11 Task distribution between the three logics components of the system.*

Task Number	HPS Soc	Nios II	FPGA		Estimated delay (ms)
1.	Web server initialization.	Execute the initial sequence and verify the system status			
2.	Web server tasks.				
3.	Read the set point operational sequence and configuration parameters and send to Nios II.				
4.	Scan the piece and save the three-dimensional profile.	Calculate the need deposited volume profile	Initial control values estimator.		
5.	Get the infrared matrix from the thermographic camera and send to FPGA (1ms)	Get the welding voltage and current of the welding power source (3ms)			1
6.	Get the profile from the profilometer and send to NIOS II (2ms)		Features extractor algorithm of thermographic data.		0.01
7.	Web server tasks.	Features extractor algorithm of bead profile data.	Weld bead depth estimator.		0.01
8.	Web server tasks.		Weld bead width predictor.		0.01
9.	Get the controlled variables values.	Send the set points values and controlled variable values to FPGA	Selft-adaptive P-PID and Fuzzy CTWD controller. Control loops of welding speed and seam tracking.		0.01
10.	Get the manipulated variables values.	Send the manipulated variables values to the actuators	Stepper motor drivers.	PWM driver.	0.01

Task Number	HPS Soc	Nios II	FPGA	Estimated delay (ms)
11.	Web server tasks.	Verify the system status.		0.1
12.	Get the system status.			0.001
13.	Save the data in SD card.			0.1

### A 3.4 Web user interface for process monitoring and parameter configuration.

The user has access to the system through a light web interface. The web interface can be viewed in any device with ethernet or Wifi connection in local network. This shows the process status, the control system status and the measurements collected. The control access is password restricted. The user level can view the status and data collected. The operator level can define set points and start or stop the process. The administrator level can change the configuration parameters. The total number of users connected to the system is restricted by the available memory.

The web server is implemented in the HPS (see section 3) and is saved in the SD card. The tools and methodology for developing of the web site are the same used in similar works. It is important to emphasize that the minimization of computational resources can improve the behavior of the user interface.